



---

# PROCEEDINGS OF THE 2022 ISEC

---

26-30 September Gothenburg, Sweden



## Table of content

### 1. Introduction

### 2. Analytical Chemistry

2.1 “Hrobonova, “Green Extraction Solvents and Selective Adsorbents in Analysis of Natural Bioactive compounds”

### 3. Environmental Applications

3.1 Llorente et al, “Feasibility studies in Extraction of Pharmaceuticals from aqueous Solutions using Terpenoids and Eutectic Solvents: Solvent Reuse and Countercurrent Extraction”

3.2 Hrouzkova et al, “Analysis of Bee Products as Environmental Pollution Bioindicators. Complex Approach to Various Extraction and Chromatographic Techniques”

3.2. Gutierrez-Sanchez et al,” Removal of Pharmaseuticals from Hospital Wastewater by Liquid-liquid Extraction with Natural Solvents”

3.2 Shariff et al, “Phosphorous Recovery from Sewage Sludge utilizing Reactive Extraction”

### 4. Fundamental, Theory and Modelling

3.1 Chaurasiya et al, “Conceptual Design of Process for Solvent Extraction of Uranium using Core-annular Flow in Microchannels”

3.2 Leleu et al, “Detailed Drop-based Simulation of Settling Behaviour”

### 5. Hydrometallurgy and Recycling

5.1 Kurniawan et al, “Extraction of Nickel from Ammonium Fluoride-based Electroplating Wastewater”

5.2 Mitshabu et al, “Management of the transfer of manganese impurity from the leach solution to the electrolyte at Ruashi Mining company in the Democratic Republic of Congo”

5.3 Bochevskaya et al, “Recovery of Rare-earth Metals from Nitrate Solutions by Extraction Method”

5.4 Nieto et al, “A Process Based on Ionic Liquids for Tungsten Valorization from Low Grade Scheelite Concentrates”

5.5 Onoberhie et al, “Zinc Recovery from Chloride Media by Applying the HALOMET Process”

5.6 Ocana et al, “Nickel and Copper Recovery from Sludge Waste Enhancing Circular Economy for the Galvanic Industry”

5.7 Percharroman et al, "ZINCEX Process applied on Manganese Bearing Materials"

5.8 Avsar et al, "Assessment of two Liquid-liquid Extraction Systems for Cr(VI) Extraction from Acidic Nitrate Media using  $^{51}\text{Cr}$  as Radiotracer"

5.9 Garg et al, "An Innovative Process for Simultaneous Production of High Purity Benzene and U:S: Grade Gasoline from C6Heart Cut of FCC Gasoline"

## 6. Nuclear Applications

6.1 Karim et al, "Kinetic Study of Uranium Extraction in a Microfluidic Channel"

6.2 Sarkar et al, "CFD Simulations of Pulsatile Two-phase Flow in Columnar Contactors: Effect of the Shape of the Internals on Dispersed Phase Holdup and Axial Dispersion"

6.3 Geist, "Distribution data for the extraction of Am(III), Ln(III) and  $\text{HNO}_3$  with 2,6-bis(1-(2-ethylhexyl)-1H-1,2,3-triazol-4-yl)pyridine"

6.4 Sakamoto et al, "Development of the Co-processing Process with the Centrifugal Contactor"

## 7. Plant equipment and Design

7.1 Sibirtsev et al, "Mask R-CNN Based Droplet Detection in Liquid-liquid Systems. Part 1: A Proof of Concept"

7.2 Glatz et al, "Optimal Mixing in Agitated Extraction Columns"

## 8. Posters

8.1 Boripun et al, "Electrical Separation for Biodiesel-glycerol Product Mixture"

# 1.

## Introduction

These are the proceedings of the 22<sup>nd</sup> ISEC (International Solvent Extraction Conference) in 2022 Göteborg, Sweden. Originally it was planned for 2020 but due to the raging pandemic it was postponed twice. It is a homecoming of the ISEC to its roots. It was in 1966 that a conference held in Gothenburg, Sweden concentrated on the chemistry of solvent extraction, which had a wider remit than the nuclear field. This was also probably the first truly international meeting held on the issue. The history is, however, somewhat longer. Prior to the first ISEC meeting, other conferences concerned with solvent extraction were held. The most significant in 1962 at Gatlinburg, USA and 1965 at Harwell, UK both of which were largely concerned with the nuclear application of the technology. At that time the main application for the technology was nuclear fuel processing.

ISEC comprise all aspects of solvent extraction ranging from the very fundamental molecular studies to industrial processing on the tonne scale. This is also reflected in the presentations and delegates attending ISEC making this the perfect foundation for cross fertilization between all the fields needed and used worldwide in this topic. In this way new topics and insights are found and discussed in an open and friendly way.

ISEC have been and continue to be a major gathering of scientists, engineers, operators and vendors from around the world, who present new findings since the last meeting, exchange ideas, make business contacts, and conduct collegial discussions.

In 2022 there were more than 150 delegates from all over the world. Sadly only a few of the excellent contributions were submitted as full papers and may be found within this volume.



## **2. Analytical Chemistry**

# Green Extraction Solvents and Selective Adsorbents in Analysis of Natural Bioactive Compounds

Katarína Hroboňová\*,<sup>a</sup>

**Abstract.** Analysis of complex samples requires the utilization of extraction techniques and analytical quantification methods that are characterized by high selectivity and sensitivity. The most widely used sample preparation techniques are liquid-solid and liquid-liquid extractions in many formats, microextractions, ultrasound- and microwave-assisted extractions, or conventional Soxhlet extraction and solvent extraction with stirring. Green extraction solvents, low transition temperature mixtures, consisting of choline chloride, L-lactic acid and 1,3-propanediol were involved in the extraction of phenolic substances, coumarins, from plant materials. Optimized conditions with low transition temperature mixture provided comparable or higher extraction yield than conventional solvents, water and methanol, respectively. Selective solid phase extraction with molecularly imprinted adsorbents was suitable for purification of primary extract, isolation of substances and/or their preconcentration. The adsorbent properties, such as adsorption capacity, kinetics, morphology, reusability and selectivity showed their applicability in real samples analysis. Developed extraction media are applicable in analytical scale, as well as, they have potential for isolation of phytochemicals from plant materials.

**Keywords:** extraction solvents, selective adsorbents, phenolic substances, green analytical method

## Introduction

Sample preparation is the most important step in process of chemical analysis. Detection of analyte signal at a low concentration level by the analytical instrument is sometimes problematic because of different interferences from real sample matrix. Accordingly, it is a necessary to develop an effective, fast, and simple sample preparation method to isolate and preconcentrate an analyte to a detectable limit.

Preparation of a plant sample for analysis for subsequent determination of active substances include mostly liquid extraction. Both traditional and advanced extraction techniques are used. The conventional widely used sample preparation techniques, such as liquid extraction, Soxhlet extraction, require large volumes of solvents and also additional operations to primary extract purification or analytes enrichment prior to their quantification by liquid chromatography methods. Extraction solvents cover a wide range, from greener ones such as water, ethanol, to more toxic ones. Organic solvents, commonly utilized in many extraction technique, are often flammable or their biodegradability is low. Low transition temperature mixtures (LTTMs) are also recently applied in analytical methods. LTTMs are a mixtures of hydrogen bond donor and hydrogen bond acceptor and thanks to their many advantages, such as biodegradability, properties variability based on type and ratio of the components are applicable in various extraction procedures and for extraction of a wide range of substances.<sup>i</sup> Plant extracts are very complex mixtures and additional operation, such as selective solid phase extraction, is suitable for extract purification, analyte isolation and/or their

---

<sup>a</sup> Slovak University of Technology in Bratislava, Faculty of Chemical and Food Technology, Institute of Analytical Chemistry, Radlinského 9, 812 37 Bratislava, Slovakia

preconcentration. For this purpose, selective adsorbents could be applied. Molecular imprinting technology allows preparing polymeric materials with predetermined selectivity and high affinity applicable for various analytical targets, e.g. adsorbent for extraction techniques. The fabrication process includes the creation of template- shaped binding sites (cavities) in polymer matrices, which allow selective recognition of the imprint species or structurally related compounds. The preparation of molecularly imprinted polymer (MIP) involves the formation of a complex between a target molecule (template) and functional monomer through covalent bonds or non-covalent interactions, afterwards polymerized to form an imprinted matrix. Finally, the template is removed, leaving a cavity complementary in size and shape to the template molecule.<sup>ii, iii</sup>

Recently, the development and application of green methods are growing, including reduction or replacement of toxic reagents and solvents, application of plan of experiments for optimization of conditions, utilization of low or medium energy instrumental consumption, and also decreasing of waste.<sup>iv</sup>

This work is focused on presentation of ecological approaches including in analytical method development and method applications. Presented methods for analysis of natural products include elements of miniaturization and utilize green extraction solvents, the chemometric approaches in method development and data evaluation.

## Experimental

Heat assisted solvent (extraction solvents: water, methanol, LTTMs based on choline chloride, L-lactic acid, 1,3-propanediol mol/mol/mol) and solid phase extraction utilizing MIP adsorbents were used for extraction of bioactive compounds (phenolic substances, coumarins) from plant materials. The extraction conditions were: liquid/solid ratio 40/1 mL/g, extraction time 15 min, rotation speed 20 rpm and temperature 60 °C. Finally, the mixture was centrifuged at 3000 rpm for 3 min.<sup>v</sup> MIP adsorbents were prepared by block polymerization (MIP A) or applying imprinting on surface of magnetite (MIP B) with a non-covalent approach (template- 7-hydroxycoumarin, monomer- methacrylic acid, crosslinker- ethyleneglycoldimethacrylate, initiator- 2,2'-azobisisobutyronitrile, porogen- chloroform) by procedure described in previous paper.<sup>vi</sup> Extraction conditions were as follows: conditioning with methanol and water, washing with water, and analytes eluting with methanol/acetic acid (9/1 v/v). Extracts were analyzed by reversed-phase high performance liquid chromatography method with fluorescence detection (stationary phase- Kinetex C18 (100 x 4.6 mm I.D., 5 µm) maintained at 23 °C.; mobile phase- methanol/acetic acid (99/1, v/v) and 1% aqueous solution of acetic acid with gradient elution and flow rate 1 mL/min; the detection wavelengths were set at 330 nm ( $\lambda_{ex}$ ) and 450 nm ( $\lambda_{em}$ )).

All chemicals used for preparation of LTTM mixtures and MIP adsorbents were per analysis grade. HPLC grade solvents were used for mobile phase preparation. A samples, dried plants were analyzed for coumarins content. Samples were stored in original bags at dark and dry places.

## Results and Discussion

Determination of analytes in complex samples is a challenging task, which requires analytical methods include effective and selective sample preparation and sensitive analyte quantification. Work was focused on the development of green analytical method for determination of coumarins applying the approaches of green analytical chemistry in several phases of analytical procedure, i) liquid extraction with ecological extraction solvents, ii) analytes purification and preconcentration on selective and reusable adsorbents, iii) miniaturization.

### *i) Liquid extraction with ecological solvents*

The type and ratio of the LTTM constituents are essential for extraction efficiency. Mixtures consisting of choline chloride-L-lactic acid 1/3 (mol/mol) and choline chloride-L-lactic acid-1,3-propanediol 1/2/1 (mol/mol/mol) were perspective for coumarins extraction providing recovery over 80 %. Extraction efficiency of three-component LTTM was higher in comparison with two-component LTTM under study. Addition of 1,3-propandiol (HBD agent) affect also viscosity (decreasing of viscosity in comparison with LTTM without 1,3-propandiol) and other physo-chemical characteristics of LTTMs.<sup>vii</sup> Higher extraction yields of monitored coumarins were obtained for LTTM in comparison with water or comparable to methanol as extraction solvents. The addition of water to the LTTM (25% for tested phenolic substances) had a positive effect on the extractability of substances (and also partially decrease viscosity of solvent affecting its penetration in the sample matrix).

The experimental parameters, temperature, time, rotation speed and liquid/solid ratio were investigated to obtain high extraction yields. To investigate the relationship between independent variables (experimental parameters) and the response value (extraction efficiency in %), the Taguchi orthogonal arrays design of experiment with five levels of variables was applied. Obtained optimal parameter values were liquid/solid ratio 40/1 mL/g, extraction time 15 min, rotation speed 20 rpm and temperature 60 °C. Temperature was the most important experimental parameter affecting extraction efficiency for both selected solvents. The extraction time influenced penetration of solvent in the sample matrix. The interacting parameters,  $T.V$  and  $Sp.V$ , indicated that the extraction temperature ( $T$ ) together with the solvent volume ( $V$ ), and more intensive mixing ( $Sp$ ) together with the solvent volume increased the extraction efficiency.

### *ii) Analytes purification and preconcentration on selective and reusable adsorbents*

Primary plant extracts are complex samples from the aspect of analysis and thus selective solid phase extraction is suitable technique for extract purification. For this purpose, selective adsorbents (MIPs), have been fabricated by molecularly imprinted technology. Adsorbents were prepared by block polymerization (MIP A) or by imprinting on surface of magnetite (MIP B) for template 7-hydroxycoumarin. The evaluation of MIP properties (adsorption capacity, morphology, kinetics) showed that adsorbents were selective for the extraction of the target substance and partially also for structural analogues (group selective adsorbents for simple coumarins). Table 1 summarizes important characteristics of adsorbents. MIP A was applied

in off-line solid phase extraction (SPE) as adsorbent in a column. Developed SPE procedure was optimal for maximal extraction efficiency with methanol and water as conditioning mixture and methanol/acetic acid (9/1 v/v) as elution solvent. The recovery values of more than 80 % were achieved for target coumarins (RSD < 6 %; Table 2). Another format of MIP application is batch extraction with core-shell type of MIP (MIP B) synthesized on the surface of magnetite particles. The advantage of magnetic extraction is separation of phases applying an external magnetic field. Comparing the mentioned extraction approaches, magnetic extraction is the most time-consuming (~ 60 min), however it is suitable for more viscous samples.

Table 1. Characteristics of adsorbents prepared by molecularly imprinted technology

	MIP A <sup>a</sup>	MIP B <sup>b</sup>
Adsorption capacity <sup>c</sup>	200 µg/g	80 µg/g
Adsorption kinetics	60 min	30 min
Selectivity <sup>d</sup>	4.1 for template	2.4 for template
	< 1.5 for structural analogues	< 1.5 for structural analogues
Reusability	10 cycles	10 cycles
	< 5.8% decrease of adsorption capacity	< 5.0% decrease of adsorption capacity

<sup>a</sup>MIP A - adsorbent prepared by block polymerization, <sup>b</sup>MIP B - adsorbent prepared by polymerization on surface of magnetite, <sup>c</sup>determined for template, <sup>d</sup>calculated as ratio of amount of analyte bound to imprinted polymer and amount of analyte bound to non-imprinted polymer

### *iii) Miniaturization in solid-phase extraction procedure*

Pipette tip SPE, a miniaturized format of SPE, is a popular technique in sample preparation, that uses the same procedure as conventional SPE, including conditioning, sample loading, washing, and elution. Pipette tip SPE has several advantages, simplicity, small bed volume and sorbent mass in the pipette tip significantly reduce solvent consumption. The extraction performances using the pipette tip SPE method and conventional SPE method with MIP adsorbent (MIP A) were compared and results are listed in Table 2. In general, the recoveries of methods with both SPE approaches were satisfactory. The good accuracy of the results can be obtained using the pipette tip MIP-SPE method with less sorbent and solvents consumptions.

Table 2. Comparison of pipette tip SPE and the conventional SPE with MIP A adsorbent for extraction of coumarins

	Pipette tip MIP-SPE	MIP-SPE
Adsorbent mass (mg)	20	100
Solvents (mL) <sup>a</sup>	1	4
Time (min) <sup>b</sup>	< 5	~ 15
Extraction efficiency (%) <sup>c</sup>	95.3	84.4

<sup>a</sup> only organic solvents are considered, including the solvents for conditioning and eluting, <sup>b</sup> time consumed per sample, <sup>c</sup> recovery values determined at concentration level 2 µg/mL (RSD < 6 %)

## Conclusions

LTTM and MIP were incorporated into extraction and miniaturized extraction techniques for sample preparation affecting their selectivity and extraction efficiency. LTTMs are green alternatives to conventional organic solvents, with unique physicochemical properties that offer possibility to design the solvents for specific purposes. LTTM extraction is frequently combined with mechanical agitation-extractions or ultrasound- and microwave-assisted techniques as innovative extraction technologies in term of reduction energy and required time, as well as in term of enhancing extraction yields. LTTM based extraction solvents applied for extraction of coumarins from plant materials provided higher extraction efficiency in comparison to the conventional organic solvents.

MIPs are an option for selective extraction of target compounds from complex matrices where other structurally related substances may coexist. Although MIPs exhibit the inherent qualities of polymers, such as stability, low cost of synthesis, when magnetic particles are introduced into their polymeric structure, new functions can be produced (e.g. simpler separation of phases during extraction procedure).

Obtained results are applicable in analytical scale, for sample pretreatment extraction techniques, as well as, they have potential for the application in scale-up production for isolation of compounds from plant materials.

## Acknowledgements

This work was supported by the Slovak Research and Development Agency under contract no. APVV-18-0155, Scientific Grant Agency of the Ministry of Education of the Slovak Republic and the Slovak Academy of Sciences (grants no. 1/0412/20 and 1/0159/20).

## References

- <sup>i</sup> M. Francisco, A. van den Bruinhorst, L.F. Zubeir, C.J. Peters, M.C. Kroon, *Fluid Phase Equilibrium*, 2013, **340**, 77.
- <sup>ii</sup> P.A.G. Cormack, K. Haupt, K. Mosbach, Imprint polymers, In I.D. Wilson, E.R. Adlard, M. Cooke, C.F. Poole (Eds.), *Encyclopedia of Separation*, Academic Press, 2000.
- <sup>iii</sup> K. Hroboňová, E. Brokešová, *Food Chemistry*, 2020, **332**, 127404.
- <sup>iv</sup> M. De la Guardia, S Garrigues, S. *Challenges in green analytical chemistry (2)*, Royal Society of Chemistry, 2020.
- <sup>v</sup> K. Hroboňová, M. Jablonský, P. Májek, *Journal of Molecular Liquids*, 2021, **338**, 116691
- <sup>vi</sup> A. Machyňáková, K. Hroboňová, *Analytical Methods*, 2017, **9**, 2168.
- <sup>vii</sup> M. Jablonský, V. Jančíková, J. Šíma, J. Jablonský, *Biointerface Research in Applied Chemistry*, 2023, **13**, 167.

### **3. Environmental Applications**

# Feasibility studies in extraction of pharmaceuticals from aqueous solutions using terpenoids and eutectic solvents: solvent reuse and countercurrent extraction.

Diego Rodríguez Llorente\*,<sup>a</sup> Pablo Gutiérrez-Sánchez,<sup>a</sup> Silvia Álvarez-Torrellas,<sup>a</sup> Juan García,<sup>a</sup> Marcos Larriba<sup>a</sup>

**Abstract.** In this work, the feasibility of using a liquid-liquid extraction technology to extract drugs from hospital water with terpenoids and eutectic solvents of natural origin has been studied. Drug removal process was simulated in a countercurrent extraction. The complete removal of pharmaceuticals from hospital wastewater could be achieved using carvacrol with an S/F of 2.00 at pH 4.00 in an extractor with six equilibrium stages.

**Keywords:** Terpenoids, Eutectic solvents, Pharmaceuticals, Hospital wastewater, Liquid-liquid extraction

## Introduction

The presence of pharmaceuticals in wastewater, mainly in hospital wastewater, is a serious environmental concern.<sup>i</sup> This work proposes extracting drugs from hospital wastewater using natural, renewable, and non-toxic solvents such as terpenes and eutectic solvents.

## Background

Pharmaceuticals can be frequently found in water due to the ineffectiveness of current treatment techniques in their removal, affecting aquatic organisms and accumulating in the trophic chain.<sup>ii</sup> Liquid-liquid extraction is proposed to remove these compounds. Using natural solvents such as terpenoids and eutectic solvents would improve sustainability and lower toxicity compared to the use of conventional solvents.<sup>iii,iv</sup>

## Experimental

The pharmaceutical compounds used are acetaminophen, atenolol, carbamazepine, ciprofloxacin, diclofenac, ibuprofen, naproxen, phenazone, sulfamethoxazole, tetracycline, trimethoprim. Pharmaceuticals were extracted using natural solvents, carvacrol, and eutectic solvent (thymol+C<sub>12</sub>OOH). Solvent reuse studies were performed using them in 5 stages. Extract phases after 5 solvent reuse cycles were regenerated through vacuum distillation. Distillates were employed in a new stage. ATR- FTIR spectra and TGAs were obtained to ensure the solvents' stability. Also, countercurrent extraction simulations were performed using experimental Batch Simulation of Multistage Countercurrent Extraction (BSMCE) at an S/F ratio of 0.25. Countercurrent extraction simulations were also performed using the Kremser method, where partition coefficients were obtained in a packed column.

---

<sup>a</sup> Catalysis and Separation Processes Research Group (CyPS), Department of Chemical Engineering and materials, Complutense University of Madrid, Avda. Complutense s/n, 28040 Madrid, Spain



## Results and Discussion

The results at an S/F ratio of 2.00 show no decrease in extraction yields after 5 reuse stages with (thymol+C<sub>12</sub>OOH). The global extraction yields in all 5 stages are higher than 99.00 %. The yields at an S/F of 0.50 improve extraction yields upon regeneration but are slightly lower than when using a fresh solvent. The global extraction yields decreased from 96.95 to 84.69 %. Concerning carvacrol, global extraction yields go from 90.95 % in the first stage to 81.15 % in stage 5. After the regeneration process, the yields increase for the previous stage but remain below the fresh solvent, reaching a global extraction yield of 87.40 %. FTIR and TGAs show that carvacrol and (thymol+C<sub>12</sub>OOH) are stable in the reuse process. Carvacrol is also stable in the regeneration process. In contrast, the eutectic solvent (thymol+C<sub>12</sub>OOH) changes in the distillation process, increasing the distillate's thymol composition. In the following stages of reuse and regeneration, C<sub>12</sub>OOH would be lost and would have to be replenished to avoid losing the composition of the eutectic point.

Countercurrent extraction experiments were then performed using carvacrol as solvent. The single-stage global extraction yield results are 77.59 % for BSMCE and 74.47 % for packed column extraction. This slight difference implies that there is a low mass transfer limitation in the extraction process. Global extraction yields with BSMCE increase from 77.59 to 85.50 % with 4 stages. The extraction yields with the Kremser method increase from 74.74 % with 1 stage to 87.51 % when using 6 stages.

## Conclusions

The results show that the solvents can be reused with high extraction yields. The solvent regeneration process does improve the extraction yields compared to the last stage but does not reach the extraction values of the fresh solvent. The countercurrent extraction shows a fast mass transfer of the drugs using carvacrol. The Kremser method is reliable for the performing of countercurrent extraction scenarios from single-stage distribution coefficients. Higher S/F ratios could almost eliminate the drugs when working in countercurrent mode.

## Acknowledgements

The authors are grateful to Comunidad Autónoma de Madrid for financial support of Projects P2018/EMT-4341 and PR65/19-22441 and to Ministerio de Ciencia, Innovación y Universidades for financial support of Project CTM2017-84033-R. This work has been supported by the Madrid Government (Comunidad de Madrid- Spain) under the Multiannual Agreement with Complutense University in the line Program to Stimulate Research for Young Doctors in the context of the V PRICIT (Regional Programme of Research and Technological Innovation). Diego Rodríguez-Llorente thanks Ministerio de Ciencia, Innovación y Universidades for awarding an FPU grant (FPU18/01536).

## References

---

<sup>i</sup> K. Kümmerer, *Journal of Environmental Management*, 2009, **90**, 2354–2366.

---

<sup>ii</sup> A.S. Adeleye, J. Xue, Y. Zhao, A.A. Taylor, J.E. Zenobio, Y. Sun, Z. Han, O.A. Salawu, Y. Zhu, *Journal of Hazardous Materials*, 2022, 424.

<sup>iii</sup> B.D. Ribeiro, C. Florindo, L.C. Iff, M.A.Z.Z. Coelho, I.M. Marrucho, *ACS Sustainable Chemistry & Engineering*, 2015, **3**, 2469–2477.

<sup>iv</sup> C. Boutekedjiret, M.A. Vian, F. Chemat, *Green Chemistry and Sustainable Technology*, 2014, 205–219.

# Analysis of Bee Products as Environmental Pollution Bioindicators. Complex Approach to Various Extraction and Chromatographic Techniques

Svetlana Hrouzková,<sup>\*a</sup> Ivana Blažková,<sup>a</sup> Ján Hrouzek,<sup>a</sup> Mária Rusnáková,<sup>a</sup> and Agneša Szarka<sup>a</sup>

## Abstract.

Honey bee (*Apis mellifera* L.) and bee products, such as beeswax, bee pollen and propolis commonly used in food, cosmetics and medicinal applications are well accepted as effective indicators of environmental pollution. The paper was focused to overview the new environmentally acceptable analytical methods used for detection of pesticide residues in various honeybee products employing miniaturized eco-friendly procedures. Matrix effects needs to be searched in details and combinations of sample preparation techniques are proposed. Search of various extraction approaches and their impact on analytical performance characteristics was done.

**Keywords:** bee pollen products, bioindication, environmental pollution, gas chromatography-mass spectrometry, sample preparation techniques

## Introduction

Environmental pollution bioindicator could be one living organisms or group of them providing the information based on the environment or some part of the environment's compartment state. There are different bioindicators reported in literature.<sup>1</sup>, e. g. bats, birds and fish, freshwater mussels, honey bee, various microorganisms, phytoplankton, lichens, and other animals, or plants, which are able under special environmental alterations produce certain molecular signals. Bioindication is the examination of some living organisms and this provides the possibility to monitor the large environment area which is the habitat of the living being serving as bioindicator. Honey bee is one of the most effective bioindicator for the environment pollution by toxic compounds. Among them, pesticides are large group of contaminants of environmental interest. Pesticides provide protection and also prevention against harmful influence in agrochemical procedures. Honey bees are also exposed to pesticides used for the treatment of parasites. Organic pollutants greatly affect the safety of honey bees, as they cause neurological disorders in bees and behavioural disturbances, also reduce susceptibility to sugars, reduce bee conditions and cause navigational capacity problems for bees. As a result of massive cases of bee mortality in recent years, beekeeping has increased concerns about the presence of pesticide residues in propolis, which is considered a health supporting product. Bee products that are produced in an environment with persistent organic pollutants (POPs) or come into contact with agricultural activities may be contaminated with these compounds. POPs are mainly lipophilic compounds that are relatively stable in the environment and are resistant to biological and chemical degradation.

---

<sup>a</sup> Slovak University of Technology in Bratislava, Faculty of Chemical and Food Technology, Institute of Analytical Chemistry, Radlinského 9, SK-812 37 Bratislava, Slovak Republic,

<sup>\*</sup>Corresponding author: E-mail: svetlana.hrouzkova@stuba.sk, Tel +421 915 396 928

They can cause developmental and reproductive toxicity, various types of cancer, central nervous system disorders and various other health problems.

Organic pollutants can enter bee products from two main sources, namely contamination from agricultural activities or contamination caused by the application of pesticides in hives to eradicate parasites.

This paper is aimed to overview the new environmentally acceptable analytical methods used for detection of pesticide residues in various honeybee products employing miniaturized eco-friendly procedures and to discuss various problems encountered in analysis of these multicomponent mixtures.

## **Background**

Honey bees and many bee products, such as beeswax, pollen and propolis which are used in food, cosmetics and medicinal applications are well accepted as effective indicators of environmental pollution. Analysis of said bee products is an opportunity to address the occurrence of wide range of various xenobiotics in the environment. Exposition to various insecticides, fungicides, and acaricides which are broadly applied in modern agriculture to enhance production and quality of agricultural crops is in many cases fatal to the bee population and may affect the honeybee health. Pesticides have been used worldwide for the protection of food crops against pests and diseases. It is common that residues of these pesticides occur in food products, especially agricultural commodities. Foodstuff as a sample for analysis represents a challenge to analytical chemists in their efforts to determine residues of pesticides at trace levels, as pesticides can represent a risk to the consumer and there are different adverse effects on human health if pesticide residues remain in food after they are applied to food crops. Even at ultratrace concentration levels, the contamination of bee products may lead to serious health problems, thus monitoring of xenobiotics in these samples is a matter of urgency. Positive findings of contaminants in honeybee and their products may indicate the contamination of a large monitored area as it is known, bees can operate in long distances. Advance in ecotoxicological research related to emerging pollutants such as pesticides, as well as treatment, occurrence, environmental dynamics, and the discovery of their ecological impacts, serves as a basis for introduction and improvement of technologies needed to determine these products in the environment. Pesticide residues analysis in honey bees and their products is a challenging task due to the low concentration levels of xenobiotics in environmental samples including the honey bee and its products brought to the beehive, such as bee pollen.<sup>ii</sup>

## **Sample extraction and clean-up**

Taking into account the ultratrace concentration levels of pesticide residues in environmental samples, the procedures for determination of these contaminants require complicated multistage sample preparation mainly including extraction and purification as well. Efficient sample preparation and subsequent instrumental analysis are required to determine pesticide residue levels. This usually consists of several steps and depend on the physicochemical properties of the investigated analytes and the matrix, as well as the chosen

analytical technique itself. All involved analytical steps (e.g., homogenization, derivatization, extraction, separation, detection) can affect the accuracy of the quantification. The sample preparation steps include the transfer of analytes from the primary matrix into the secondary one (an extract), with a concurrent removing of interfering substances, and increasing the analytes' concentrations to a desired level above the detection limit for an applied analytical technique. Investigating organic contaminants, sample preparation includes some steps which depend on the sample, the matrix, and the concentration level at which the analysis needs to be carried out. Extraction techniques most commonly involved in the analysis of pesticide residues in samples of bee products are the following: solid phase matrix dispersion (MSPD), solid phase extraction (SPE) and QuEChERS extraction procedure. Microextraction techniques based on both, liquid-based and sorption-based principle, are increasingly seeking. The recent approaches are focused to the elaboration of a comprehensive procedure applicable for a wide variety of analytes with a single extraction in various matrices or a solventless extraction technique at microscale level. Solid-phase microextraction (SPME) and stir-bar sorptive extraction (SBSE) are the most popular representatives of sorption-based microextraction techniques. For liquid samples, dispersive liquid-liquid microextraction, single drop microextraction and hollow-fibre microextraction are emerged in new research lines to develop environmentally acceptable sample preparation procedures. Owing to complicated matrices, very often combined techniques are elaborated. An overview of research outputs devoted to innovative analytical methods for toxic compounds in pollen samples was published recently<sup>iii</sup>.

The overview of most frequently applied techniques in apicultural samples analysis is shown in Figure 1.



Figure 1. Overview of sample preparation methods used in analysis of bee products

(DLLME – dispersive liquid-liquid extraction, SLE – supported liquid extraction, SPE – solid phase extraction, SAALLE – salt-assisted liquid-liquid extraction, DPX -disposable pipette extraction)

The most widespread technique is the QuEChERS based on liquid-liquid extraction followed by dispersive solid-phase extraction (dSPE) or disposable pipette extraction (DPX). After commonly applied pre-treatment (including, lyophilization or drying, homogenization, freezing-out), approximately 10 g of the sample is taken and extracted by solvents, e. g. acetonitrile or ethyl acetate, followed by salt-out partitioning using anhydrous  $\text{MgSO}_4$ , NaCl, and/or buffering agents, and further clean up using mentioned techniques. The flow diagram for illustration is shown in Figure 2.



Figure 2. Sample preparation of bee pollen by QuEChERS technique

## Detection of pesticide residues in bee products

The resulting extract is obviously the multicomponent solution which requires separation before detection and quantification. For determination of contaminating compounds, sensitive and effective instrumental analytical methods with sufficiently low limits of detection are unavoidable. As organic pollutants represent diverse classes of substances with various physico-chemical properties, highly efficient chromatographic methods must be applied for the separation of these mixtures. Multiresidual methods provide the capability of determining different pesticide residues in a single analysis<sup>iv</sup>. The multiresidue procedure deals with a wide variety of physicochemical properties of pesticides of different chemical families. The most efficient approach to pesticide residue separation involves the use of gas and/or liquid chromatographic methods combined with mass spectrometric detection employing various analyzers (quadrupole, triple quadrupole, time-of-flight, orbitrap, linear ion trap etc.).

## Matrix problems

Despite of great efforts in the research of pesticide residue analysis, the analysis might be substantially complicated by the co-injected matrix components responsible for the matrix-induced chromatographic response enhancement or the subsequent decrease of the response. Injecting a real sample extract, the matrix components are used to block active sites in the GC injector, column and /or other parts of the chromatographic system, thus reducing losses of susceptible analytes caused by adsorption or degradation on active sites. This phenomenon results in ordinarily higher analyte signals in matrix-containing versus matrix-

free solutions. Therefore, the detailed study of extract composition brings valuable information to suggest the efficient ways to remove interferences from the extract. Figure 3 demonstrates the search of various matrix components and the way to replace it by various combination of sorbents in sample clean-up step.

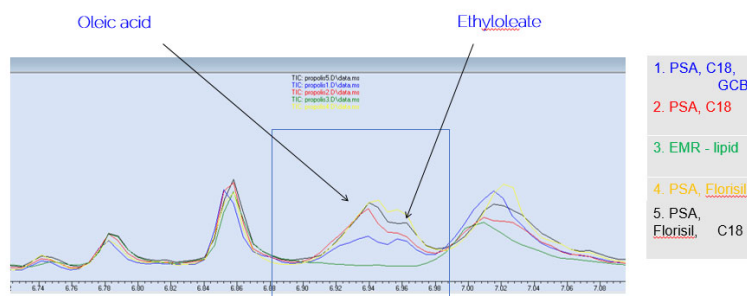


Figure 3. The study of matrix effects applying various combinations of sorbents (PSA – primary secondary amin. GCB – graphitized carbon black, EMR – enhanced matrix removal, C18 – silica gel modified by octadecylsiloxane)

## Conclusions

The paper was focused on the overviewing the analytical methods used for detection of organic contaminants in various honeybee products, including miniaturized eco-friendly sample preparation procedures. It was found that combinations of sample preparation techniques bring substantial positives to limit the matrix effects. Search of extract composition provides the valuable feedback to design the sample preparation in the clean-up step. Critical evaluation of various extraction approaches and their impact on analytical performance characteristics was done.

## Acknowledgements

This work was supported by the Slovak Research and Development Agency under the Contract No. APVV-19-0149. The work was supported by the Scientific Grant Agency of the Ministry of Education of the Slovak Republic (VEGA project No. 1/0412/20) and Tatra bank foundation.

## References

- <sup>i</sup> N. Asif, M. F. Malik, F. N. Chaudhry, *Pollution*, 2018, **4**(1), 111.
- <sup>ii</sup> I. Blažková, J. Hrouzek, A. Szarka, T. Pócsová, S. Hrouzková, *Acta Chimica Slovaca*, 2022, **15**(1), 103.
- <sup>iii</sup> M. Rusnáková, J. Hrouzek, S. Hrouzková, *Journal of Apicultural Research*, 2022, accepted.
- <sup>iv</sup> S. Hrouzková, Analytical methods for pesticides detection in foodstuffs. In: *Food analysis: Innovative analytical tools for safety and quality assessment*, Umile Gianfranco Spizzirri, Giuseppe Cirillo (Eds), John Wiley & Sons, 2022.

# Removal of pharmaceuticals from hospital wastewater by liquid-liquid extraction with natural solvents.

Pablo Gutiérrez-Sánchez,<sup>a\*</sup> Diego Rodríguez-Llorente,<sup>a</sup> Marcos Larriba,<sup>a</sup> Silvia Álvarez-Torrellas<sup>a</sup> and Juan García.<sup>a</sup>

**Abstract.** The increased consumption of pharmaceutical, and their further release into the aquatic environment due to an incomplete disposal in Wastewater Treatment Plants, has turned the spotlight on them. This research proposes the extraction of these pollutants from aqueous solutions by using carvacrol as natural extraction solvent. Not only high extraction yields were achieved, but also reuse and regeneration of carvacrol were technically feasible.

**Keywords:** Natural solvents, Continuous extraction, Carvacrol, Water treatment

## Introduction

The pharmaceutical industry has played a key role in developed and developing countries alike.<sup>i,ii</sup> Today, antibiotics are one of the most consumed pharmaceuticals worldwide, reaching values between 100,000 and 200,000 ton/year. This fact has led to an increased occurrence of this compounds in the environment, drawing the attention of several agencies and bodies around the world.<sup>iii,iv,v</sup>

All of the above is evidence of the need to find new technically feasible and environmentally-friendly methods to reduce the impact pharmaceuticals may have on the aquatic resources.

## Background

Pharmaceuticals are released into the environment mainly due to incomplete disposal in Wastewater Treatment Plants, in addition to other sources such as wastes from livestock and industry, hospital effluents or expired pharmaceutical products.<sup>vi,vii,viii</sup>

These compounds are considered as one of the main emerging pollutants in the aquatic environment. In particular, antibiotics such as trimethoprim, sulfamethoxazole, and ciprofloxacin have been included in the EU Watch Lists of pollutants of emerging concern under the Water Framework Directive.<sup>ix,x,xi</sup>

Several techniques related to the removal of pharmaceuticals from wastewater have been reported in the literature, including advanced oxidation processes, adsorption or membrane filtration. However, liquid-liquid extraction is generally applied to the purification of this compounds during their synthesis, rather than water treatment.<sup>xii</sup>

---

<sup>a</sup> Catalysis and Separation Processes Group, Chemical Engineering and Materials Department, Faculty of Chemistry, Complutense University, Avda. Complutense s/n, 28040, Madrid, Spain.

\* E-mail address: [pgutie03@ucm.es](mailto:pgutie03@ucm.es)



## Experimental

The continuous extraction process was performed on a packed column of 8 mm internal diameter and 80 mm length, filled with glass spheres of 2 mm diameter. The aqueous feed was prepared in a hospital wastewater matrix. Specifically, a multicomponent aqueous solution of trimethoprim, ciprofloxacin and sulfamethoxazole was made at a concentration of 50 mg/L of each compound. Carvacrol was selected as green extraction solvent. Experiments were carried out at 30°C and solvent/feed ratios of 2.00, 1.00 and 0.50.

In addition, solvent reuse was evaluated by performing five consecutive extraction steps in magnetically shaken flasks for 12 hours at 30 °C and an S/F ratio of 1.00. Fresh solvent was applied in the first extraction step and, for the rest, the extract from the previous step was used as the solvent for the following experiment. Finally, carvacrol was regenerated after step 5 by vacuum distillation at 20 mbar and 164 °C.

## Results and Discussion

The packed column extraction process exhibited yields above 98.7 % for any pharmaceutical when using a S/F ratio of 2.00. Furthermore, even with the lowest solvent amount tested (S/F of 0.50), yields of 99.3, 98.6 and 95.7 % were reached for trimethoprim, ciprofloxacin and sulfamethoxazole, respectively. From these results it could be concluded that carvacrol shows a higher affinity for trimethoprim, followed by ciprofloxacin.

Regarding the solvent reuse, a drop in yield is observed with increasing the number of cycles. This trend might be considered negligible for trimethoprim and very slight for ciprofloxacin. However, the extraction yield of sulfamethoxazole decreased from 96 to 84 % between stages 1 and 5. During the five stages, yields of around 83%, 98% and 96% for sulfamethoxazole, trimethoprim, and ciprofloxacin, respectively, were obtained. In addition, the recovered solvent showed results similar to those of the fresh solvent.

## Conclusions

The terpenoid carvacrol exhibited significantly high yields for the extraction of sulfamethoxazole, trimethoprim and ciprofloxacin. Therefore, the use of natural solvents, such as terpenoids, could be a potential alternative for the replacement of conventional solvents in the pharmaceutical extraction field. Moreover, the reuse and regeneration of carvacrol has been successfully tested.

## Acknowledgements

The authors are grateful to Comunidad Autónoma de Madrid for financial support of Project S2018/EMT-4341 and PR65/19-22441. This work has been supported by the Madrid Government under the Multiannual Agreement with Complutense University in the line Program to Stimulate Research for Young Doctors in the context of the V PRICIT (Regional Programme of Research and Technological Innovation).

## References

- 
- <sup>i</sup> Marić, S., Jocić, A., Krstić, A., Momčilović, M., Ignjatović, L., & Dimitrijević, A. (2021). Poloxamer-based aqueous biphasic systems in designing an integrated extraction platform for the valorization of pharmaceutical waste. *Separation and Purification Technology*, 275, 119101.
- <sup>ii</sup> Safari, H., Arab, M., Rashidian, A., Kebriaee-Zadeh, A., & Gorji, H. A. (2018). A comparative study on different pharmaceutical industries and proposing a model for the context of Iran. *Iranian Journal of Pharmaceutical Research*, 17(4), 1593–1603.
- <sup>iii</sup> Heberer, T. (2002). Occurrence, fate, and removal of pharmaceutical residues in the aquatic environment: A review of recent research data. *Toxicology Letters*, 131(1–2), 5–17.
- <sup>iv</sup> Liu, J. L., & Wong, M. H. (2013). Pharmaceuticals and personal care products (PPCPs): A review on environmental contamination in China. *Environment International*, 59, 208–224.
- <sup>v</sup> Tambosi, J. L., Yamanaka, L. Y., José, H. J., de Fátima Peralta Muniz Moreira, R., & Schröder, H. F. (2010). Recent research data on the removal of pharmaceuticals from sewage treatment plants (STP). *Quimica Nova*, 33(2), 411–420.
- <sup>vi</sup> Gezahegn, T., Tegegne, B., Zewge, F., & Chandravanshi, B. S. (2019). Salting-out assisted liquid-liquid extraction for the determination of ciprofloxacin residues in water samples by high performance liquid chromatography-diode array detector. *BMC Chemistry*, 13(28).
- <sup>vii</sup> Karungamye, P. N. (2020). Methods used for removal of pharmaceuticals from wastewater: A review. *Applied Journal of Environmental Engineering Science*, 6(4), 412–428.
- <sup>viii</sup> Mukimin, A., Vistanty, H., & Zen, N. (2020). Hybrid advanced oxidation process (HAOP) as highly efficient and powerful treatment for complete demineralization of antibiotics. *Separation and Purification Technology*, 241, 116728.
- <sup>ix</sup> European Commission. (2018). Decision (EU) 2018/840. Official Journal of the European Union, L 141.
- <sup>x</sup> European Commission. (2020). Decision (EU) 2020/1161. Official Journal of the European Union, L 257.
- <sup>xi</sup> O'Flynn, D., Lawler, J., Yusuf, A., Parle-Mcdermott, A., Harold, D., Mc Cloughlin, T., Holland, L., Regan, F., & White, B. (2021). A review of pharmaceutical occurrence and pathways in the aquatic environment in the context of a changing climate and the COVID-19 pandemic. *Analytical Methods*, 13(5), 575–594.
- <sup>xii</sup> Gutiérrez-Sánchez, P., Rodríguez-Llorente, D., Navarro, P., Águeda, V. I., Álvarez-Torrellas, S., García, J., & Larriba, M. (2022). Extraction of antibiotics identified in the EU Watch List 2020 from hospital wastewater using hydrophobic eutectic solvents and terpenoids. *Separation and Purification Technology*, 282, 120117.

# Phosphorous Recovery From Sewage Sludge Utilizing Reactive Extraction.

Zaheer Ahmed Shariff<sup>a</sup>, David Leleu<sup>a</sup>, Andreas Pfennig<sup>\*a</sup>

**Abstract** Phosphorus (P) is indispensable nutrient in agriculture, essential for nutrition of mankind. To close the P loop, P must be recovered during wastewater treatment in Germany by the end of this decade. Other EU countries will follow with similar regulations. As part of an Interreg NW-Europe project, several pilot-scale processes were tested by industrial and research partners to validate them in industrial settings. At the University of Liège, the PULSE (Phosphorus University of Liège Sludge Extraction) process was developed. It consists of sludge drying, which is essential for good process performance, leaching with hydrochloric acid, reactive extraction to remove unwanted metals such as iron and heavy metals, and fractional precipitation. Since sewage sludge changes properties during storage, the mobile pilot plant was operated at three different locations with fresh sewage sludge from wastewater treatment. To adapt the operating parameters of PULSE to the specifics of the respective sludges, they were optimized with the aid of simulations, based on cascaded option trees. A key point is the thermodynamic description of the aqueous speciation equilibria, of the reactive equilibria during extraction and of those describing precipitation. In particular, the model allows considering different models for the non-ideality of electrolyte solutions up to concentrated systems. The simulation tool can also be used to fit unknown parameters such as the equilibrium constants of reactive extraction. It was shown that the model is able to describe well all equilibria at the different process steps in the system. On the other hand, the optimal operating parameters could be confirmed experimentally. Finally, it was shown that the process can be operated well at pilot scale. The product obtained after precipitation was tested by the project partners and showed good performance as a fertilizer component in pot trials and could be easily incorporated into the granulation of a commercial fertilizer formulation.

**Keywords:** circular economy, equilibrium modelling, heavy metal, phosphorous recycling, reactive extraction, sewage sludge

## Introduction

At the University of Liège (ULiège), the PULSE (Phosphorus University of Liège Sludge Extraction) process was developed<sup>i</sup>. The concept of the PULSE process was developed based on the PASCH process<sup>ii</sup> and further adapted to treat dried sewage sludge to recover P. The scheme of the PULSE process developed at ULiège is depicted in Figure 1. The process shown produces calcium phosphate but can also be adapted to magnesium phosphate as final product.

The design and dimensioning of the PULSE demonstrator was carried out based on results of laboratory experiments that were established at ULiège and information from the PASCH process as well. While the equipment and parts for the PULSE demonstrator were ordered and procured, the optimization and evaluation of individual unit operations of the PULSE process was carried out at laboratory scale by making use of the cascaded option trees and equilibrium-speciation simulations. In order to carry out the equilibrium simulations for the

---

<sup>a</sup> Department of Chemical Engineering, University of Liège, Liège, Belgium

unit operations of the PULSE process a MATLAB tool has been developed for calculation of solid-liquid-liquid equilibria (SLLE).

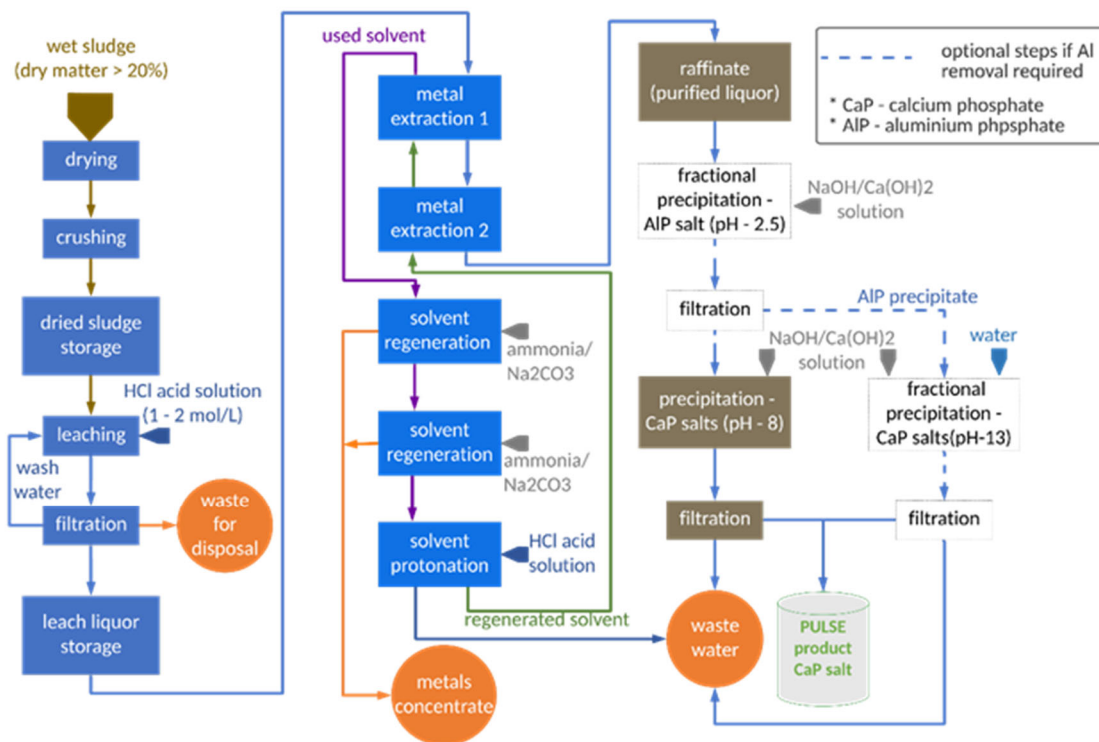


Figure 1: PULSE-process scheme.

## Methods

### Cascaded Option Trees

In order to find suitable operating options and to optimize the unit operations of the PULSE process, the cascaded option-tree methodology<sup>iii</sup> was used. In this method, the options are evaluated against a set of operation-relevant criteria. The option with the most positive evaluation is chosen for the process. The information for evaluation of the options is obtained from literature, laboratory experiments, and SLLE modelling.

### Solid Liquid Liquid equilibrium modelling tool

The chemical unit operations of the PULSE process, i.e. leaching, solvent extraction of metals and subsequent stripping of metals from the spent solvent for regeneration, and the precipitation of P salts are inter-dependent and sensitive to the *pH* of the respective operation among other operating parameters. As the characteristics of sludge can vary from day to day, it is imperative to understand the chemistry and reactions occurring as a function of *pH* in each of these operations. Therefore, a MATLAB tool for simulating SLLE was developed, which can be used to describe the chemical unit operations. With the help of this tool, it is possible to optimize the process for sludge with different characteristics minimizing experimental work.

The SLLE tool solves a set of nonlinear equations consisting of charge neutrality, mass balance and law of mass action constraints which describe the system<sup>iv</sup>, including appropriate quantification of thermodynamic non-idealities, where e.g. the Debye-Hückel and the Davies model can be selected<sup>v</sup>. The solution of the non-linear system of equations leads to the concentrations of all chemical species that exist in the aqueous phase and/or in the organic phase as well as the solids that can precipitate at equilibrium as shown in Figure 3. In that example, representing undigested dewatered sludge used for performing experiments to develop the PULSE process, contained calcium, iron, and aluminum as the predominant metals besides phosphorus. Analysis of ferric and ferrous iron leached from the dried sludge revealed that about 70% of the iron were present as ferric,  $\text{Fe}^{3+}$ . Depending on the molar concentration of iron, a major fraction of inorganic phosphorus in sludge can be present as ferric phosphate ( $\text{FePO}_4$ ). It can be seen from Figure 2,  $\text{FePO}_4$  can remain undissolved if the pH is greater than 0.3.

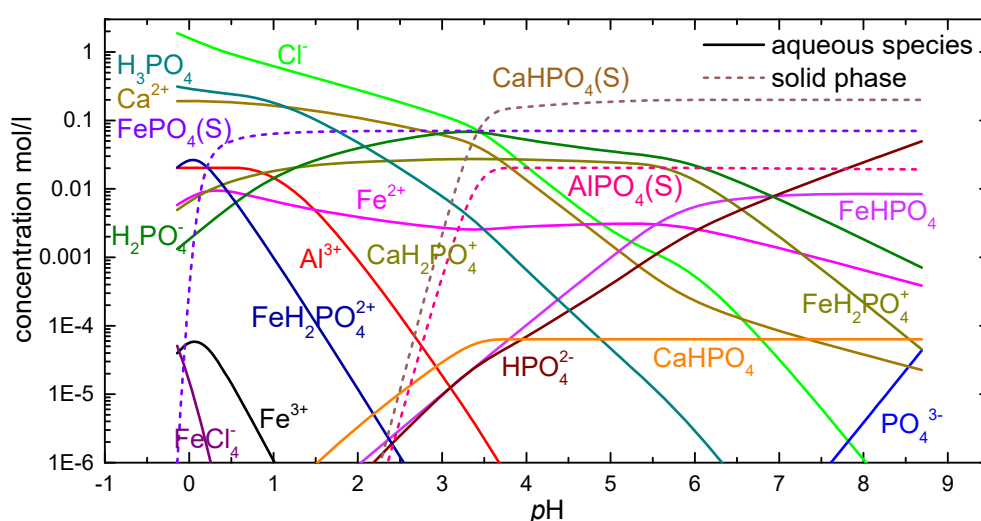


Figure 2: Speciation using the SLLE tool. Initial concentrations in [mol/L]:  $\text{Fe}^{3+}$ : 0.0703,  $\text{Al}^{3+}$ : 0.0203,  $\text{HCl}$ : varying,  $\text{PO}_4^{3-}$ : 0.348,  $\text{Ca}^{2+}$ : 0.2,  $\text{Fe}^{2+}$ : 0.03. The dashed curves show the precipitation equilibrium

Although extensive thermodynamic data are available for aqueous phase reactions and precipitation, it is not the case for solvent extraction or organic-phase reactions. Since the description of these equilibria is required to optimize the PULSE process, the chemical equilibrium constants and reaction stoichiometry are determined in this case by performing equilibrium experiments and fitting the parameters to experimental data using the tool.

### PULSE-process development and optimization with lab experiments

Lab-scale experiments for each unit operation of the PULSE process were established in order to obtain the necessary information for the design of the PULSE demonstrator and to develop and optimize the overall process. The materials and methods for these analyses are detailed in the project technical report<sup>i</sup>. Here, the general outcomes of the process development and optimization for the individual unit operations of the PULSE process are discussed below. All the laboratory experiments were carried out using undigested dewatered sludge from Oupeye wastewater-treatment plant (wwtp) in Liège, Belgium.

## The PULSE process

In the following the resulting conditions for the unit operations of the PULSE are presented.

### Sludge Drying

The P-leaching efficiency of dried sludge (DS) and dewatered sludge (DWS) was compared after leaching with hydrochloric acid (HCl) in order to select the optimal input material to the process. It turned out that the solid-liquid separation after leaching dewatered sludge directly was not possible as the solids were very fine and a sufficiently fine filter was blocked almost immediately. In contrast, for dried sludge the particle size could be controlled to a certain degree during crushing and removal of more than 80 % of the particles at 100 or 50  $\mu\text{m}$  was possible by filtration. Considering the reduction in acid consumption during leaching and the ease of solid-liquid separation after leaching in case of dried sludge, a drying step was included in the PULSE process.

### Leaching

The efficiency of overall P-recovery is largely dependent on the leaching operation. The results showed that the leaching of P depends only on the  $\text{pH}$  and not on the acid used. Also, the P leached is mainly stemming from the inorganic P while little or no organic P can be accessed around  $\text{pH}$  zero. The leaching of P estimated using the SLLE tool correlates well with the experimental data.

With respect to the different acids tested for leaching, HCl is one of the cheapest acids and it also provided better result with respect to solvent extraction of metals compared to sulfuric acid. Therefore, based on the cascaded option-tree evaluation of the different acids, it was decided to use HCl in the PULSE process. Further, based on the laboratory results, leaching time of 1 hour and an S/L ratio of 0.25 were chosen for the PULSE leaching.

### Reactive extraction

The metals that are co-leached with P are not desired in the final product as they may be detrimental when the recovered P product is used as a fertilizer or they may reduce the P availability to plants. Apart from P and Ca, Fe is the most predominant metal leached from Oupeye sludge and 70 % of Fe is present in the form of  $\text{Fe}^{3+}$ .  $\text{FePO}_4$  can precipitate even at a  $\text{pH}$  as low as 0.3, which would reduce the P availability to plants in the soil.

In the PULSE process, reactive extraction is used to remove Fe and other heavy metals from the leach liquor. Reactive extraction allows the selective extraction of metals as a function of  $\text{pH}$  and has a high capacity for metal loading. Based on the information obtained from the PASCH process and the mechanism of extraction, three extractants were evaluated, namely Alamine 336, which is an anion-exchange extractant, D2EHPA, which represents a cation-exchange extractant, and TBP, which is a complexing extractant. Ketrul-D80, which is a commercially available brand of desulfurized kerosene, was chosen as diluent. Kerosene is one of the most commonly used diluents due to the advantages it offers over other diluents such as low toxicity and high flash point. The extraction efficiencies of these extractants were evaluated using lab experiments.

The experimental results indicated that only the reactive extractant Alamine 336 provided a quantitative extraction of metals. The degree of extraction of iron is very low at a HCl concentration of 1 mol/l. It was found to increase with the concentration of HCl, as  $\text{Cl}^-$  is exchanged against negatively charged ferric-chloride complexes that are formed at low  $\text{pH}$ .

Based on the cascaded option tree evaluation, the solvent system containing Alamine 336, TBP and Exxal 10 dissolved in Ketrul D80 was chosen to be employed in the PULSE process. Exxal 10 is a modifier that is required to improve the solubility of Alamine 336 in the diluent and to prevent the formation of a third phase upon extraction.

In the PULSE demonstrator, a battery of four mixer settlers of 150 mm diameter and 1500 mm length is employed to carry out the different steps involved in extraction, i.e. protonation of solvent using acid, reactive extraction of metals in two counter-current stages and stripping of metals from solvent.

### **Precipitation**

In the PULSE process, it is possible to precipitate P either as calcium phosphate (CaP) or as magnesium phosphate (MP). Since precipitation of MP requires an additional step for the removal of calcium as calcium sulphate by fractional precipitation, it is preferred to precipitate P as calcium phosphate.

The different calcium-phosphate phases that could precipitate at different  $\text{pH}$  were evaluated based on the SLLE model considering the solubility-product constant of the various calcium-phosphate phases and the Ca/P ratio that was found in the precipitate. The precipitation of different phases is quite complex as at first a less stable phase such as di-calcium phosphate di-hydrate ( $\text{CaHPO}_4 \cdot 2\text{H}_2\text{O}$ ) or amorphous calcium phosphate ( $\text{Ca}_3(\text{PO}_4)_2$ ) is precipitated which transforms into the more stable hydroxyapatite (HAP) ( $\text{Ca}_5(\text{PO}_4)_3\text{OH}$ )<sup>vi</sup>. The time for transformation of the precursors to HAP depends on various factors such as temperature, saturation, presence of other ions such as magnesium and carbonates.

For the demonstrator tests, it has been decided to use a  $\text{pH}$  between 5 and 6 for the precipitation. As  $\text{Ca}(\text{OH})_2$  is cheaper compared to NaOH, it is more desirable to use  $\text{Ca}(\text{OH})_2$  compared to NaOH for the precipitation.

### **The PULSE Demonstrator**

The PULSE demonstrator was designed and built as a mobile pilot plant so that it could be transported in containers and tested at different locations within the Phos4You project. The PULSE demonstrator consists of two 20-feet containers which can be placed parallel and opened on the long side as well as the short side. A tent can be installed between the two containers in order to create an enclosed space where the mixer settlers (MS) for solvent extraction can be assembled as all the sites where the demonstrator was operated do not have an enclosed space.

The unit operations were dimensioned to realize a capacity of 100 kg of dewatered sludge per day. Considering a typical DM content of 20 % this relates to a daily capacity of 20 kg of dried sludge. The unit operations were realized in batch mode for leaching, filtering, and

precipitation. The extraction and stripping steps were operated in quasi-continuous mode, i.e. procedures were established that the continuous mixer-settler units could be switched off and restarted with only limited disturbance of their content. In Figure 3 the mixer-settler units are shown while being run in the technical hall during commissioning.

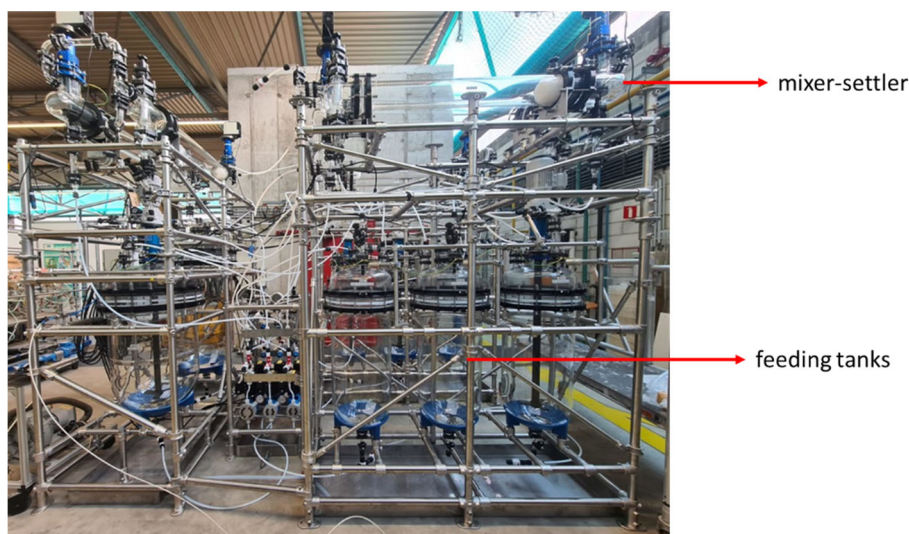


Figure 3: 5 stage mixer-settler equipment for solvent extraction tests in the PULSE demonstrator (Photo: ULiège/Z.A. Shariff)

The PULSE demonstrator was operated at ULiège with German sludge that had been shipped from Dortmund-Deusen wwtp, at Oupeye wwtp near Liège, and at the Waste-Water Development Centre of Scottish Water in Bo'ness.

## Results

Some results obtained with the demonstrator are presented in the following. A broader overview can be found in the technical report of the PhosForYou project<sup>1</sup>.

From 60 kg of dried sludge from the Dortmund-Deusen wwtp about 6.8 kg of product were obtained. The product concentrations are characterized in Figure 4 together with the reduction ratios that are required to reach EU legal limits for fertilizer ingredients. For the critical components these limits are clearly met. The only exception is Cr, the content is not reduced relative to P for the sludge from Oupeye wwtp. The high concentration of Cr is due to a specific industry present within the Oupeye wwtp catchment. The results with the German sludge indicate, that it is in principle possible to reduce the Cr content relative to that of P. The final product contains a rather high Cl concentration. This can be easily avoided by additional washing of the product before drying, which was not realized for this set of demonstrator runs.

## Conclusion

It has been shown that the PULSE process can efficiently recover P from sewage sludges of various origins. In particular, metallic impurities such as heavy metals can be sufficiently removed to meet the strict legal limits. The process can be easily adapted to the specific



conditions of a particular wastewater treatment plant using the SLLE tool. For example, it is possible to adjust the number of extraction stages depending on the metal concentrations, optimize the phase ratio, etc. to minimize process costs.

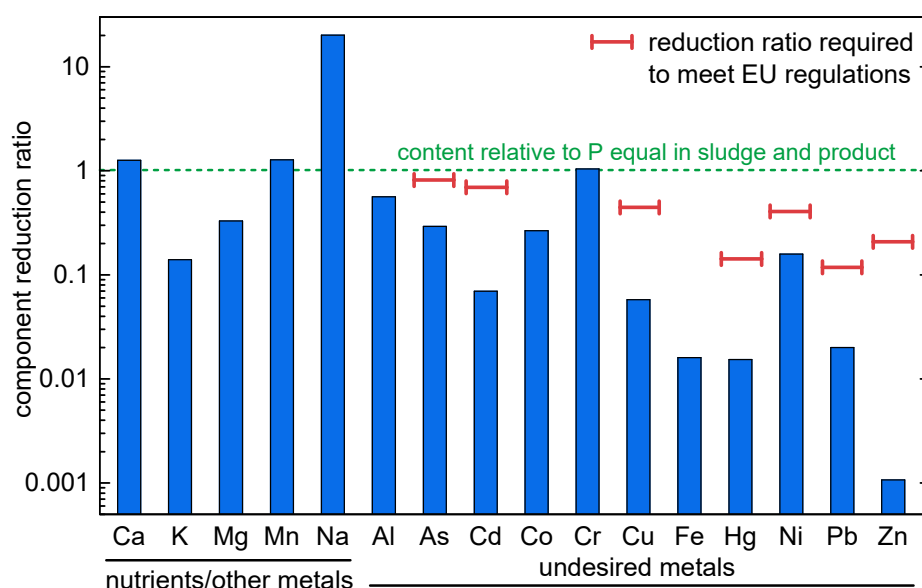


Figure 4: Reduction ratio relative to P (g/g P) between product and sludge and minimum reduction legally required for contaminants for the Oupeye sludge<sup>vii</sup>

## ACKNOWLEDGMENT

The research work was carried out as part of the PhosForYou project which was funded through the INTERREG VB North-West Europe Programme (2014-2020) under the grant NWE292. The matching funding for the work at ULiège was provided by Walloon Region.

## References

- <sup>i</sup> M.-E. Ploteau, A. Althoff, I. Nafo, B. Teichgräber (Eds.) (2021). Technical report of the Phos4You partnership on processes to recover phosphorus from wastewater. [Online]. Available: [https://duepublico2.uni-due.de/receive/duepublico\\_mods\\_00074788](https://duepublico2.uni-due.de/receive/duepublico_mods_00074788)
- <sup>ii</sup> P. Doetsch, J. Pinnekamp, D. Montag, W. Rath, (2010), Rückgewinnung von Pflanzennährstoffen, insbesondere Phosphor aus der Asche von Klärschlamm. v <https://hdl.handle.net/2268/183687>
- <sup>iii</sup> A. Bednarz, B. Rüngeler, A. Pfennig. Use of Cascaded Option Trees in Chemical-Engineering Process Development. *Chem. Ing. Technol.*, vol. 86, pp. 611-620, 2014.
- <sup>iv</sup> Z.A. Shariff, L. Fraikin, A. Léonard, A. Pfennig, (2020). Development of solid-liquid-liquid equilibrium speciation and data fitting tool and its application to phosphorus recovery process from sludge. In DECHEMA e.V. (Ed.). Jahrestreffen der ProcessNet-Fachgruppen Fluidverfahrenstechnik, Adsorption und Extraktion. Berchtesgaden, 26. - 28. Februar. [Online]. Available: <http://hdl.handle.net/2268/247818>.
- <sup>v</sup> C.W. Davies, *Ion Association*. London: Butterworths. pp. 37-53, 1962
- <sup>vi</sup> L. Montastruc, C. Azzaro-Pantel, B. Biscans, M. Cabassud, S. Domenech, A thermochemical approach for calcium phosphate precipitation modeling in a pellet reactor. *Chem. Eng. J.*, vol. 94, no. 1, pp. 41-50, 2003.
- <sup>vii</sup> European Parliament, Council of the European Union. (2019) Regulation (EU) 2019/1009 laying down rules on the making available on the market of EU fertilising products. [Online]. Available: <https://eur-lex.europa.eu/legal-content/EN/TXT/?uri=CELEX%3A32019R1009>

## **4. Fundamental, Theory and Modelling**

# Conceptual design of process for solvent extraction of uranium using core-annular flow in microchannels.

Rajnesh Kumar Chaurasiya,<sup>\*a,b</sup> K.K. Singh,<sup>a,b</sup> S. Chakraborty,<sup>a,c</sup> S. Mukhopadhyay<sup>a,b</sup>

**Abstract.** Core-Annular Flow (CAF), a non-dispersive mode of solvent extraction in microchannels is used in the conceptual design of process for solvent extraction to recover uranium from nitric acid medium. The conceptual design is based on a numerical model in which partial differential equations governing mass transfer of species are solved. The numerical model is used to have insights into the effect of different design variables on mass transfer. The results from the numerical model are used to estimate total extraction length and no. of stages required in cross-current cascade harnessing CAF in microchannels for targeted percentage recovery of uranium from aqueous feed at a desired throughput.

**Keywords:** Conceptual design, Core-annular flow, Extraction, Microchannel, Process-intensification

## Introduction

Microchannels are well known as a tools for achieving process intensification in solvent extraction due to high interfacial area for mass transfer, shorter diffusion lengths, low residence time etc. Different flow regimes are obtained when two immiscible liquid phases are contacted with each other at a microfluidic junction of the microchannel. Some of the flow regimes are slug flow, droplet flow, parallel flow, core-annular flow (CAF), etc.<sup>i</sup> These flow regimes can be categorized into dispersive (slug and droplet flow) in which two immiscible phases mix with each other and non-dispersive (parallel flow and CAF) in which two immiscible phases do not mix. The physical difference between slug flow and droplet flow is that length of slugs is more than the diameter of microchannel whereas droplets have size less than diameter of microchannel. Studies on extraction using the slug flow are ample as recirculations in slug flow greatly enhance extraction efficiency<sup>ii</sup>. Slug flow has been used for extraction of uranium in microchannel too<sup>iii</sup>. Studies on non-dispersive flow regime such as parallel flow have also been reported in the literature for extraction of uranium in microchannel.<sup>iv</sup> The non-dispersive flow regimes have the advantage of ease of phase separation as compared to dispersive flow regimes. It is reported that CAF, a non-dispersive flow regime, has higher volumetric mass transfer coefficient<sup>v</sup> and merit index<sup>vi</sup> too but the limitation is lower extraction efficiency due to less residence time owing to higher flowrates/velocities. CAF is obtained at higher flow-rates thus higher throughputs can be realized which is essential from industrial application point of view. Slug flow is obtained at lower flow-rates than CAF.<sup>vii</sup> The extraction efficiency is high in slug flow due to recirculations and equilibrium can be achieved in shorter length of microchannel as required residence time is available due to low flow-rate conditions. For higher throughput, it is obvious that slug flow requires large number of small length units whereas CAF requires lesser number of large length units.

---

<sup>a</sup> Homi Bhabha National Institute, Anushaktinagar, Mumbai 400094, India

<sup>b</sup> Chemical Engineering Division, Bhabha Atomic Research Centre, Trombay, Mumbai 400085, India

<sup>c</sup> Radiopharmaceuticals Division, Bhabha Atomic Research Centre, Trombay, Mumbai 400085, India

## Background

Though the design of the flow sheet for radionuclide separation using slug flow in microchannel is reported in the literature<sup>viii</sup>, despite of several above-mentioned advantages in CAF, the conceptual design of solvent extraction processes utilizing CAF has not been reported. Therefore, in this work we study quantitatively the effects of different parameters like flow-rate, diameter of microchannel, flow-rate ratio, microchannel length on the extraction of radionuclide species (uranium) using CAF with the help of a numerical model and subsequently use the findings from the numerical model for conceptual design of the flow sheet for desired throughputs. The numerical studies reported in this work provide the basic guidelines for the design of process for extraction of radionuclide species like uranium in microchannel using CAF.

## Numerical Model

In the numerical model, solvent extraction of uranium (VI) and nitric acid from an aqueous phase is considered using 30 % TBP (% v/v) in dodecane as the solvent. Isothermal conditions (25°C) are assumed. The schematic diagram of CAF is shown in Fig. 1.  $R_c$  represents the radius of the core and  $R_a$  represents the radius of the microchannel.

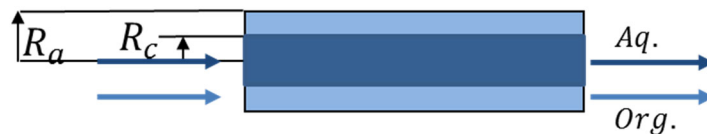
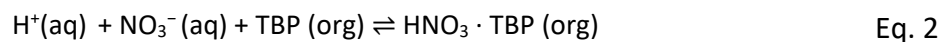
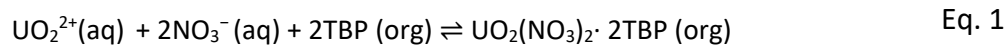


Figure 1 Schematic of core-annular flow

The reactions considered in extraction are:



It is to be noted that the system is assumed to be mass transfer controlled and the reactions (Eq. 1 & Eq. 2) are used only for estimating free TBP in organic stream.

The aqueous feed containing uranium in nitric acid flows through the core whereas organic stream containing extractant flows through the annulus in CAF. Thus mass transfer is taking place from core to annulus side. Mass transfer during initial contact of the phases at the microfluidic junction of the microchannel is not accounted in the model.

The radius of core ( $R_c$ ) in CAF depends on flowrate ratio (annulus to core) ( $Q_r$ ), viscosity ratio ( $\mu_r$ ) (annulus to core) and radius of microchannel ( $R_a$ ) as given by Eq. 3.

$$R_c = \frac{R_a}{((1 + Q_r) + ((1 + Q_r)^2 + Q_r\mu_r - 1 - 2Q_r)^{0.5})^{0.5}} \quad \text{Eq. 3}$$

Interfacial area per unit volume ( $A_{in}$ ) of microchannel is given by Eq. 4.

$$A_{in} = \frac{2\pi R_c L}{\pi R_a^2 L} = \frac{2R_c}{R_a^2} \quad \text{Eq. 4}$$

Velocity at the interface ( $V_{in}$ ) is given by Eq. 5.  $R_r$  is radius ratio (annulus to core).

$$V_{in} = \frac{2Q_a(R_a^2 - R_c^2)}{\pi(R_r^2 - 1)^2 R_c^4} \quad \text{Eq. 5}$$

Local mass transfer coefficient for aqueous phase side ( $K_{Laq,i}$ ) and organic phase side ( $K_{Lor,i}$ ) at local position ( $z$ ) are given by Eq. 6 and Eq. 7 respectively for  $i$ -th species.<sup>ix</sup>

$$i \in UO_2(NO_3), HNO_3$$

$$K_{Laq,i} = 1.0901 \left( \frac{D_{aq,i} V_{in}}{\pi z} \right)^{0.5053} \quad \text{Eq. 6}$$

$$K_{Lor,i} = 0.44 \left( \frac{D_{or,i} V_{in}}{\pi z} \right)^{0.4512} \quad \text{Eq. 7}$$

Overall mass transfer coefficient ( $K_{LO,i}$ ) is given by Eq. 9 where  $D_i$  is the distribution ratio for  $i$ -th species.

$$\frac{1}{K_{LO,i}} = \frac{1}{K_{Laq,i}} + \frac{1}{D_i K_{Lor,i}} \quad \text{Eq. 8}$$

Average velocity of aqueous phase in core ( $V_{aq.}$ ) is given by Eq. 9

$$V_{aq.} = \frac{Q_c}{\pi R_c^2} \quad \text{Eq. 9}$$

The partial differential equation for concentration variation of  $i$ -th species along the length  $z$  in aqueous phase is given by Eq.10.  $\varphi_{aq}$  is the holdup of aqueous phase in microcontactor which is equal to the square of radius ratio of core to microchannel ( $(R_c/R_a)^2$ ).

$$\frac{\partial C_{aq,i,z}}{\partial z} = \frac{-K_{LO,i} A_{in} (C_{aq,i,z} - C_{aq,i,z}^*)}{\varphi_{aq} V_{aq.}} \quad \text{Eq. 10}$$

The concentration in aqueous phase which is in equilibrium with the local concentration in the organic phase ( $C_{aq,i,z}^*$ ) is defined by Eq. 11.

$$C_{aq,i,z}^* = \frac{C_{or,i,z}}{D_i} \quad \text{Eq. 11}$$

The concentration of  $i$ -th species in the organic phase is obtained by mole balance of transferred species, as given by Eq. 12.

$$C_{or,i,z} = C_{or,i,z=0} + (1/Q_r)(C_{or,i,z=0} - C_{or,i,z}) \quad \text{Eq. 12}$$

The concentration of free TBP in organic phase is given by Eq. 13.

$$C_{or,TBP,z} = C_{or,TBP,z=0} - 2(1/Q_r)(C_{aq,U,z=0} - C_{aq,U,z}) - (1/Q_r)(C_{aq,H,z=0} - C_{aq,H,z}) \quad \text{Eq. 13}$$

The distribution ratio for U and nitric acid varies with nitrate ion concentration. The Richardson correlations are used for computing distribution ratios.<sup>x</sup> The partial differential equations (Eq. 10) for different species are solved numerically using finite difference with step size of 10 micron in Scilab 6.0. Table 1 provides the values of parameters which are kept constant in the numerical model.

**Table 1 Values of parameters used in the numerical solution**

Parameters	Values
Viscosity of aqueous phase (feed)	0.00091 Pa s
Viscosity of organic phase (solvent)	0.0017 Pa s

Concentration of uranyl nitrate in feed	1.05 M
Concentration of nitric acid in feed	3 M
Diffusivity of U(VI) in aqueous phase	$4.4 \times 10^{-10} \text{ m}^2\text{s}^{-1}$
Diffusivity of U(VI) in organic phase	$2.8 \times 10^{-10} \text{ m}^2\text{s}^{-1}$
Diffusivity of nitric acid in aqueous phase	$2.8 \times 10^{-9} \text{ m}^2\text{s}^{-1}$
Diffusivity of nitric acid in organic phase	$1.4 \times 10^{-9} \text{ m}^2\text{s}^{-1}$

## Results and Discussion

### Effect of microchannel diameter on concentration profile:

When diameter of microchannel is halved while keeping same mixture velocity, the concentration drop is more for a given length of microchannel which means lesser length will be required for desired extraction. It is to be noted that throughput also becomes lesser for the same mixture velocity when diameter of the microchannel is reduced. The smaller diameter microchannel has larger pressure gradient too which will increase the required pumping power. The concentration profiles for uranyl nitrate for microchannels of different diameter are shown in Figure 2. When diameter of microchannel is halved while keeping the same mixture velocity, the concentration drop is more for lesser diameter microchannel as specific interfacial area increases. When diameter of microchannel is halved while keeping the same flow-rate of each phase in channel then the concentration drop is not significant along the length due to the effect of reduction in residence time. Thus, the effect of microchannel diameter on the extraction length is significant for a given mixture velocity but insignificant for a given throughput.

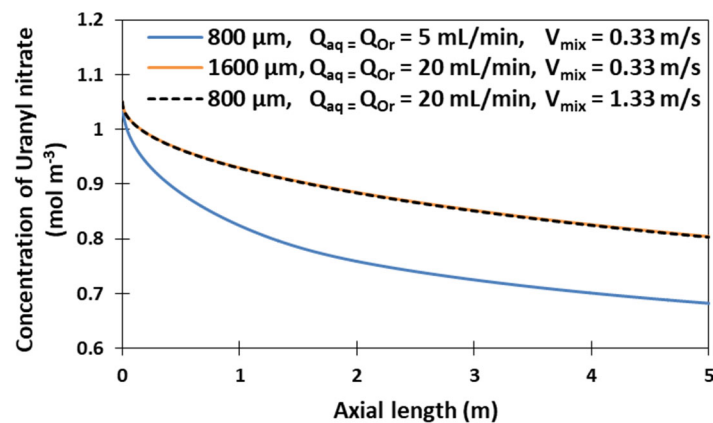
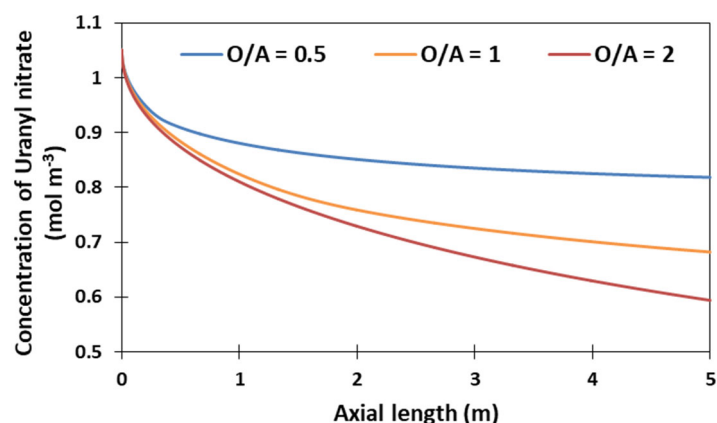


Figure 2 Concentration profile of uranyl nitrate along the length of microchannels of different diameters

### Effect of flow-rate ratio on concentration profile:

When flow-rate ratio of organic (annulus) to aqueous phase (core)(O/A) is increased while keeping aqueous phase flow-rate constant, the diameter of core shrinks which results in lesser interfacial area for mass transfer but interfacial velocity increases which will increase the local mass transfer coefficient. The effect of flow-rate ratio on the concentration profiles of uranyl nitrate along the length is shown in Figure 3. On increasing the O/A ratio, the concentration drop is more which means the effect of enhanced local mass transfer

coefficient is more pronounced than reduction in interfacial area. In the literature, it is found that CAF is more stable at  $O/A = 1$ , hence  $O/A = 1$  is chosen for subsequent analysis.



**Figure 3** Effect of flow-rate ratio on the concentration profile of uranyl nitrate (diameter of microchannel= 800  $\mu\text{m}$ , flow-rate of organic phase =5 mL/min)

#### Effect of stage efficiency on total extraction length and number of stages:

The length of the microchannel should not be either too large or too small. A large length will result in large pressure drop and hence large pumping cost. Also, seen in the figures given above, the concentration gradients at higher  $z$  reduces which means providing a very long length may not help much in mass transfer. On the other hand, a very small length will result in small percentage extraction in a single stage. It may be noted that a CAF in a single microchannel represents a single stage efficiency of which will depend on the length of the microchannel. 100% stage efficiency will be obtained only for a very long microchannel. Therefore, extraction is done in number of stages each having specific stage efficiency (<100%) to minimize the extraction length. The cross-current mode of extraction is considered in this study. For 99% extraction of uranium from feed having 1.05 M Uranium at 3 N acidity, the variation of total extraction length and no. of stages with desired stage efficiency is shown in Figure 4. As expected, selection of a higher stage efficiency reduces the requirement of no. of stages whereas increases the length required for extraction in each stage.

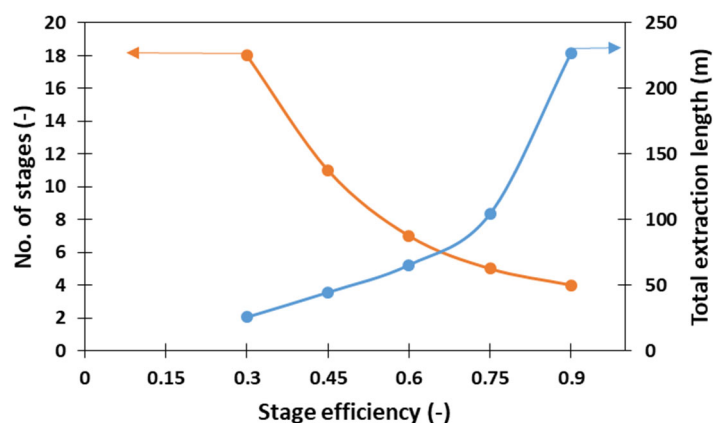


**Figure 4** Variation of total extraction length and no. of stages wrt stage efficiency (diameter of microchannel= 800  $\mu\text{m}$ , flow-rate of aqueous stream= flow-rate of organic stream = 5 mL/min)

It is to be noted that the maximum length in one stage is obtained at the last stage due to least driving force for mass transfer. The last stage will provide the maximum pressure drop. The variation of maximum extraction length in last stage with stage efficiency is shown in Fig. 5. For the stage efficiency of 0.6, pressure drop in last stage is less than 5 bar hence, stage efficiency of 0.6 is selected. In stages preceding the last stages, the extraction length will be smaller than that of the last stage and hence, pressure drop in them will be less than 5 bar.

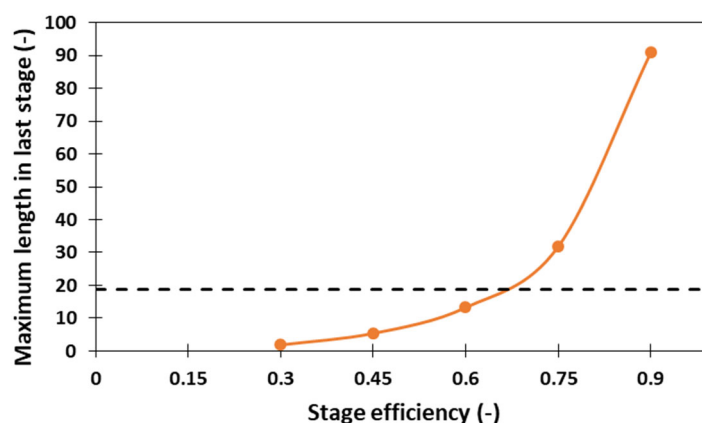


**Figure 5** Variation of length in the last stage with stage efficiency (diameter of microchannel= 800  $\mu\text{m}$ , flow-rate of aqueous stream= flow-rate of organic stream = 5 mL/min; dotted line shows the length corresponds to 5 bar pressure drop)

### Conceptual design of the process for uranium extraction

From preliminary experiments with nitric acid and 30% TBP-dodecane (not discussed here), it is found that stable CAF is achieved at equal flow-rate of organic and aqueous stream of 5 ml/min in 800  $\mu\text{m}$  channel diameter of microbore tube. Therefore, flow-rate of 5 mL/min and channel diameter of 800  $\mu\text{m}$  is selected for the design. From the results obtained from numerical model as discussed in previous sub-section, it is estimated that for a cross-current cascade of microchannels catering to a throughput of 500 MTHM (Metric Tonnes of Heavy Metal) per year with a feed containing 1.05 M of uranium at 3 N acidity, 752 parallel elements are required, each handling volumetric flow-rates of 5 ml/min of each phase. Each stage in the cascade is assumed to have stage efficiency of 0.6 which is selected based on consideration of pressure drop as discussed earlier. For 99 % extraction of uranium from the feed each of the parallel element will have total length of 66 m length distributed in seven cross-current stages (microchannels of 800  $\mu\text{m}$  diameter having CAF) having stage efficiency of 0.6. If instead of 99%, 95 % extraction of uranium from the same feed at the same throughput is considered, same number of parallel elements each having total length of 39 m distributed in five cross-current stages (microchannels of 800  $\mu\text{m}$  diameter having CAF) with stage efficiency of 0.6 will be required.

### Conclusions

A numerical model to simulate the process of extraction of uranium from nitric acid medium using TBP-dodecane as the solvent utilizing core annular flow (CAF) in microchannels is reported. The effects of microchannel diameter and flow-rate ratio on extraction and effect



of stage efficiency on extraction length for cross-current cascade are studied. Finally, the conceptual design of process of uranium extraction from feed of approximately 1.05 M uranium at 3 N acidity utilizing CAF in microchannels arranged in a cross-current cascade is carried out. The results show that throughput of 500 MTHM/year can be processed for recovery of 99% uranium by distributing it into 752 parallel elements each having 66 m long 800  $\mu\text{m}$  diameter microchannels distributed among seven cross-current stages each having stage efficiency of 0.6. However, if for the same processing rate and feed, desired percentage extraction of uranium is reduced to 95%, the length in each parallel element reduces to 39 m. Apparently larger length required in each element can be accommodated in a compact setup by coiling the microchannels in a relatively larger diameter helix such that stability of CAF is maintained. Coiling into relatively larger diameter helix may also help slightly enhance mass transfer due to Dean vortices generated due to coiling but with penalty in the form of slightly enhanced pressure drop. The extraction achieved during the first contact of the phases at microfluidic junction is not accounted in the model. Mass transfer achieved during the initial contact will further help in extraction. Number of parallel elements estimated in this study appear to be on higher side. This number will reduce significantly if the throughput considered is reduced. Therefore, it can be concluded that harnessing CAF in microchannels for uranium extraction processes is conceptually a promising solution.

## Acknowledgements

R.K.C would like to acknowledge the DAE (Dept. of Atomic Energy), India for providing the doctoral fellowship under DDFS-PhD scheme.

## References

- 
- <sup>i</sup> K. Wang & G. Luo, *Chemical Engineering Science*, 2017, 169, 18-33.
  - <sup>ii</sup> M. Sattari-Najafabadi, M. Nasr Esfahany, Z. Wu & B. Sunden, In *Chemical Engineering and Processing - Process Intensification*, 2018, 127, 213–237.
  - <sup>iii</sup> E. Garciadiego-Ortega, D. Tsaoulidis, M. Pineda, E. S. Fraga & P. Angeli, *Chemical Engineering and Processing - Process Intensification*, 2020, 153, 107921
  - <sup>iv</sup> H. Hotokezaka, *Progress in Nuclear Energy*, 2005, 47, 439-447.
  - <sup>v</sup> M. N. Kashid, A. Renken & L. Kiwi-Minsker, *Industrial and Engineering Chemistry Research*, 2011, 50(11), 6906–6914.
  - <sup>vi</sup> T. Y. Chen, P. Desir, M. Bracconi, B. Saha, M. Maestri, & D. G. Vlachos, *Industrial and Engineering Chemistry Research*, 2021, 60(9), 3723–3735.
  - <sup>vii</sup> J. Jovanovic, E. V. Rebrov, T.A. Nijhuis, M. T. Kreutzer, V. Hessel, & J. C. Schouten, *Industrial & Engineering Chemistry Research*, 2012, 51(2), 1015-1026.
  - <sup>viii</sup> D. Bascone, P. Angeli & E. S. Fraga, *Chemical Engineering and Processing-Process Intensification*, 2019, 143, 107618.
  - <sup>ix</sup> R. K. Chaurasiya, & K. K. Singh, *Chemical Engineering Science*, 2022, 249, 117295.
  - <sup>x</sup> S. B. Watson, & R. H. Rainey, *Modifications of SEPHIS Computer code for calculating the purex solvent extraction system*. (No. ORNL-TM-5123), 1975, Oak Ridge National Lab., Tenn. (USA).

# Detailed Drop-Based Simulation of Settling Behavior.

David Leleu<sup>a</sup>, Andreas Pfennig <sup>\*a</sup>

**Abstract.** Iso-optical systems were used to experimentally characterize the settling behavior of two liquid phase with high spatial and temporal resolution. These results were compared with drop-based detailed simulations. The comparison showed that lag time at the beginning of settling can be explained by very small initial drop size. The results also showed that a close-packed dispersion, where drops are in direct continuous contact, is hardly occurring.

**Keywords:** phase separation, settling, drop-based modelling, coalescence model, sedimentation model, close-packed dispersion

## Objectives

After solvent extraction steps in biotechnology, hydrometallurgy including urban mining, etc., the separation of the two liquid phases is often a major challenge. Impurities and minor components can strongly influence the settling behavior. Therefore, a tool is sought to provide a reliable description of the settling process as basis for process and equipment design. Here, a drop-based approach is adopted, where individual drops are tracked as they pass through the settler. To validate the applied models, it is not sufficient to consider only the sedimentation and coalescence curves. Rather, a detailed data set on local holdup as a function of time and position is required. Such data can be obtained with iso-optical systems, where the interfaces become invisible and thus the local phase ratio can be determined from the color intensity when one of the phases is colored with a dye.

## New Results

Settling experiments were performed in a standardized settling cell using the iso-optical system water + hexane + ethylene glycol, with methylene blue added to color the aqueous phase. The videos of the experiment were quantitatively evaluated based on the Lambert-Beer law to determine the local hold-up of the dispersed phase (see Figure 1). The initial drop-size distribution was determined using a SOPAT probe with slightly non-iso-optical systems, ensuring that these slight concentration shifts did not alter the drop-size distribution by varying the concentration in two directions.

In parallel, a simulation tool was developed that allows a drop-based simulation of the settling process. The individual drop effects are considered, such as drop sedimentation in a polydisperse drop swarm, drop-drop coalescence during sedimentation and in the densely packed zone, and drop-interface coalescence. This detailed modeling along with experimental validation provided new insights into the fundamentals of phase separation.

During settling in technical systems, a lag time is often observed during which essentially no sedimentation is observed. It was shown that this is due to the initially very small drops that are encountered. Only when the droplet size reaches a certain size around 200  $\mu\text{m}$  due to

---

<sup>a</sup> Department of Chemical Engineering, University of Liège, Liège, Belgium

drop-drop coalescence, does the sedimentation velocity become large enough for sedimentation to be observed visually. This also leads to the observation that the typical drop size determined from sedimentation experiments for a given material system is independent of the details of dispersion generation.

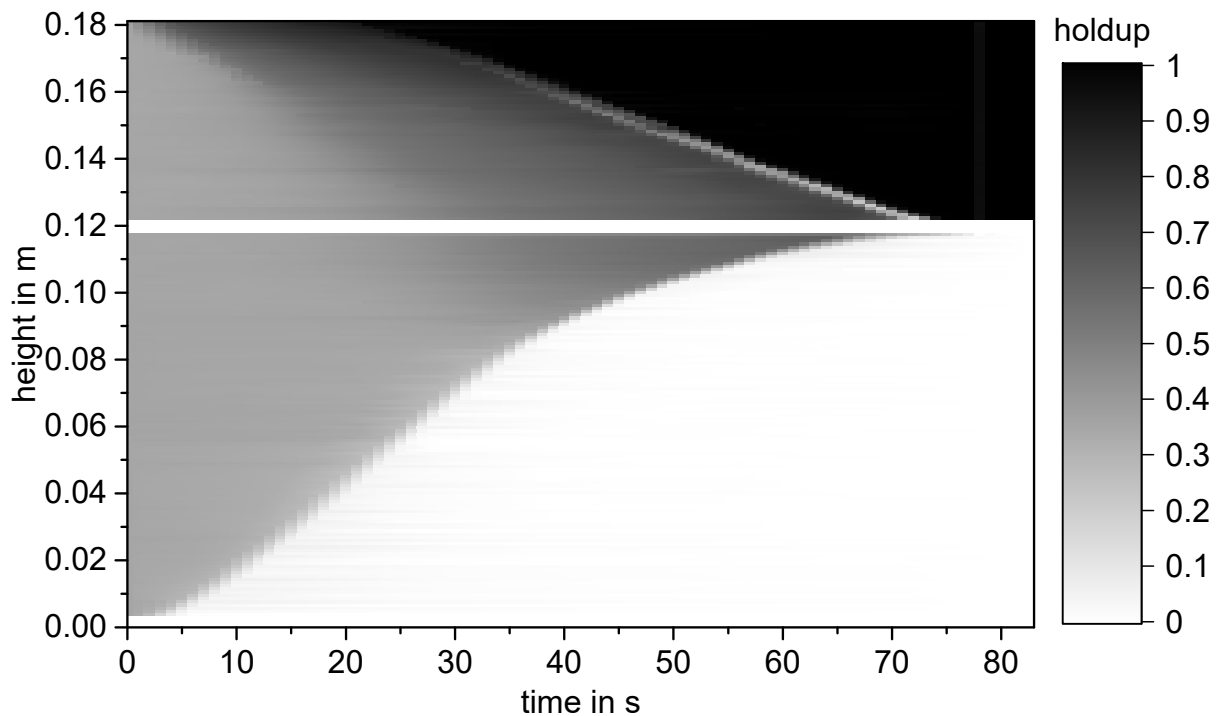


Figure 1: Result of the evaluation of an iso-optical settling experiment.

Previously, it was assumed that a zone of high hold-up in the settling experiments corresponds to a so-called close-packed zone, where the drops are in direct contact with several drops simultaneously. In that zone, sedimentation hardly occurs. Based on the hold-up data as well as in the simulations, it could be shown that a zone exists in which droplets sediment freely at high hold-up. The local holdup hardly at all reaches values that exceed the close-packing limit. This has a significant influence on the settler simulation. In this zone, the coalescence of two randomly colliding droplets must be considered, not the coalescence in a zone of closely stacked droplets, which transfer the hydrostatic pressure over the entire close-packed zone.

## Conclusions

Detailed modeling and validation with standardized settling tests based on iso-optical systems provided new insights that change the interpretation of settling experiments and that changes, which effects must be considered in drop-based settler design.

## **5. Hydrometallurgy and Recycling**

# Extraction of nickel from ammonium fluoride-based electroplating wastewater

Kurniawan Kurniawan<sup>a,b</sup>, \*Sookyung Kim<sup>a,b</sup>, Jae-chun Lee<sup>a,b</sup>, Ha Bich Trinh<sup>c</sup>, Young Ju Cho<sup>d</sup>

<sup>a</sup>Resources Recycling, Korea University of Science and Technology, Daejeon 34113, Republic of Korea

<sup>b</sup>Resources Utilization Division, Korea Institute of Geoscience and Mineral Resources (KIGAM), Daejeon 34132, Republic of Korea

<sup>c</sup>Department of Energy and Resources Engineering, Kangwon National University, Chuncheon-si, Republic of Korea

<sup>d</sup>eVLink, Daedeok-gu, Daejeon 34365, Republic of Korea

**Abstract.** This study describes the extraction of nickel from a synthetic solution of ammonium fluoride which corresponds to an electroplating wastewater using a solvent extraction (SX) process. LIX 84-I, an oxime-based extractant, was used as the extractant to extract and selectively separate nickel from the fluoride solution. Optimum extraction parameters were determined, and a quantitative extraction and separation of nickel was achieved in two extraction stages using 0.5 M LIX 84-I at an A/O phase ratio of 1.3. Nickel-loaded LIX 84-I was efficiently stripped with 2.0 M H<sub>2</sub>SO<sub>4</sub> solution in a three-stage process at an O/A ratio of 2. Nickel concentration in the strip solution was thus enriched 2.6 times the initial concentration in the working solution. The extraction mechanism was investigated, and it was found that two LIX 84-I molecules were required to extract Ni<sup>2+</sup> stoichiometrically. Recyclability test showed no loss in performance of LIX 84-I even after six extraction-stripping cycles.

**Keywords:** LIX 84-I, nickel, ammonium fluoride, extraction

## Introduction

Electroplating and other metal finishing processes are associated with the waste generation including that of wastewaters. Buffered oxide etching processes in the semiconductor industries, for instance, necessitate the use of high concentrations of ammonium fluoride solution in order to strip deposited nickel on the cell-tank and electrodes. The used solution containing high concentration of ammonia, fluoride and nickel eventually ends up as wastewater which may cause severe environmental problems if discharged as such into the water systems. Nickel, for example, can affect the growth of plants and organisms.<sup>1,2</sup> For human and animals, an uptake of too high quantities of nickel can be a danger to health with the consequences such as cancer, lung embolism, birth defects, heart disorders, etc. Therefore, it is of great importance to develop methods for treating nickel-containing electroplating wastewaters before discharging to the surface or water stream. Considering the high nickel content in the electroplating wastewater and its economic significance, the ultimate solution for the treatment of electroplating wastewater is to be worked out, particularly by extracting nickel and turning it into a valuable product.

A variety of physicochemical methods, including neutralization-precipitation,<sup>3</sup> crystallization,<sup>4</sup> dialysis/electrodialysis,<sup>5,6</sup> membrane-based processes,<sup>7</sup> ion exchange (IX)<sup>8</sup> and solvent extraction (SX),<sup>9</sup> have been used to treat electroplating wastewaters. Among the available options, the SX technique is highly favored, especially for the purpose of recovering metal product. The process has further advantages of excellent selectivity and rapid kinetics, with the

capacity to enrich the concentrations of the targeted constituents, besides the high recyclability of the organic extractants. Additionally, this process likewise employs relatively simple equipment and is suited to treat a large amount of aqueous solution.

Currently, various organic extractants are utilized to execute SX procedures. Specifically targeting the nickel, a variety of organic extractants, such as D2EHPA, PC88A, Cyanex 272, LIX 84-I, LIX 860, Versatic 10, etc. have demonstrated fairly good extraction capacity for the metal from various aqueous systems such as leach solutions, wastewaters, etc.<sup>10,11</sup> However, there seems to be no systematic study which has dealt with the extraction of nickel from ammonium fluoride system, particularly that of an electroplating wastewater.

In this work, a solvent extraction (SX)-based method with LIX 84-I as the organic extractant was used for the selective extraction of nickel from ammonium fluoride-based electroplating wastewater. The selection of LIX 84-I is based on its high affinity for nickel particularly from the ammonia systems, easier stripping potential and lower degradability compared to other extractants. It is important to achieve complete separation of nickel from fluoride; thus, extraction of both components serve as an indicator to judge the efficacy. Several parameters, such as extractant- and fluoride- concentration, pH value, temperature, and aqueous/organic (A/O) ratio were evaluated to determine the optimal conditions. The extraction mechanism is studied, and the recyclability of LIX 84-I is assessed through multiple extraction-stripping cycles. The possibility of enriching the nickel concentration is investigated further by varying the O/A ratio so as to recover a Ni-product.

## Experimental

### Materials

A synthetic solution containing nickel, ammonia and fluoride was prepared from NiSO<sub>4</sub>, NH<sub>4</sub>F and NH<sub>4</sub>OH (analytical grade), and used for the experimental work. The initial concentrations of Ni<sup>2+</sup>, NH<sub>3</sub> and F<sup>-</sup> were set at 6.9, 80 and 52 g/L, respectively, to simulate the actual electroplating wastewater. The reagent LIX 84-I (purity > 96%) supplied by BASF Germany and kerosene by Junsei Japan were used for preparing the organic solutions.

### Solvent extraction procedure

The extraction and stripping experiments were carried out in a 50 mL separating funnels under the conditions given in **Table 1**. The concentration of nickel in aqueous solutions was determined using an inductively coupled plasma optical emission spectrometer (ICP-OES, Model: iCAP6000 series, Thermo Scientific, USA). The content of fluoride was determined by a fluoride ion-selective electrode.<sup>12</sup> Distribution coefficient (*D*) and extraction percentage (%*E*) were calculated as follows:

$$D = \frac{[M]_{org}}{[M]_{raff}} \quad (1)$$

$$\%E = \frac{[M]_{org} \cdot V_{org}}{[M]_{init} \cdot V_{aq}} \quad (2)$$

where  $[M]_{org}$  represents metal ion concentration in the loaded organic solution,  $[M]_{raff}$  the metal ion concentrations in raffinate,  $[M]_{init}$  the metal concentration in the aqueous solution

before extraction,  $V_{org}$  the volume of organic solution and  $V_{init}$  being the volume of aqueous solution.

**Table 1.** Summary of solvent extraction experiments

Parameters	Varied value	Fixed value
Extraction		
Time (min)	–	5
LIX 84-I concentration (M)	0.1, 0.2, 0.3, 0.5, 0.7, 1.0	0.5
Fluoride concentration (g/L)	28, 32, 36, 40, 52, 60	52
pH	7.5, 7.75, 8.0, 8.71, 8.92, 9.64	8.0
Temperature (°C)	15, 25, 35, 45, 55	25
A/O ratio	4/1, 3/1, 2/1, 1/1, 1/2, 1/3	1/1
Stripping		
Time (min)	–	10
H <sub>2</sub> SO <sub>4</sub> concentration (M)	–	2.0
O/A ratio	4/1, 3/1, 2/1, 1/1, 1/2, 1/3, 1/4	1/1

## Results and discussion

### Solvent extraction results

#### Effect of extractant concentration

Different concentrations of LIX 84-I (0.1–1.0 M) was contacted with the aqueous solution under the aforementioned conditions and experimental procedures. Results presented in **Fig. 1** show that the Ni<sup>2+</sup> extraction increased from 27% to 97.6% as the LIX 84-I concentration was increased from 0.1 to 0.5 M, with only a slight change as a further increase of LIX 84-I to 1.0 M. No fluoride (F<sup>–</sup>) extraction was observed at all investigated LIX 84-I concentrations. As such a low extractant concentration leads to a low organic consumption and ease the stripping process. Consequently, 0.5 M LIX 84-I concentration was chosen for further study.

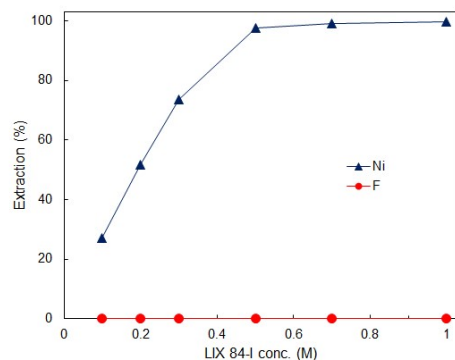


Figure 1. Effect of LIX 84-I concentration on the extraction and separation of nickel from fluoride

#### Effect of fluoride concentration

The effect of fluoride concentration on the selective extraction of Ni<sup>2+</sup> was carried out at the F<sup>–</sup> level ranging from 28 to 60 g/L (**Fig. 2**). The results demonstrated that the fluoride concentration had no effect on the Ni<sup>2+</sup> concentration, and the tendency towards complete

separation of  $\text{Ni}^{2+}$  from  $\text{F}^-$  remained intact. This result clearly indicates that the SX with LIX 84-I could be utilized in a variety of ammonium fluoride-based electroplating wastewaters without the need to control the fluoride concentration for the treatment.

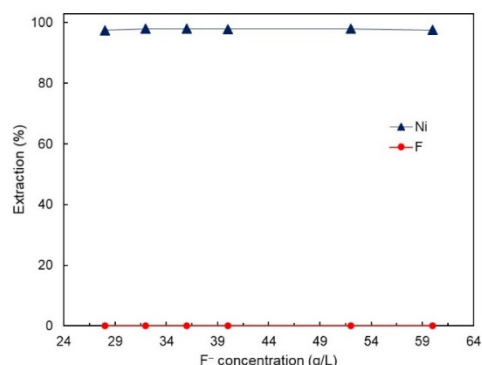


Figure 2. Effect of fluoride concentration on the extraction and separation of nickel from fluoride

### Effect of pH

Selective extraction of  $\text{Ni}^{2+}$  with the LIX 84-I as a function of initial pH was conducted by varying the pH of the working solution from 7.5 to 9.7 (at lower pH value, solid  $\text{Ni}(\text{OH})_2$  was formed). As shown in **Fig. 3**, only a negligible change in percentage  $\text{Ni}^{2+}$  extraction was observed in the pH range of 7.5–8.0. The nickel extraction however, decreased at higher pH values due to the formation of more stable  $\text{Ni}(\text{NH}_3)_6^{2+}$  species.<sup>13</sup>

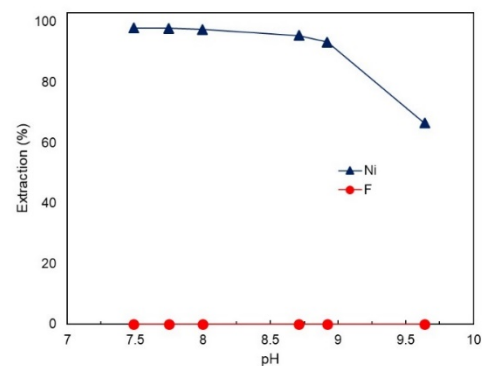


Figure 3. Effect of pH on the extraction and separation of nickel from fluoride

### Effect of temperature

Data on the effect of temperature was further used to determine the thermodynamic properties ( $\Delta G^0$ ,  $\Delta H^0$  and  $\Delta S^0$ ) of the extraction system. The thermodynamic properties can be calculated with the slope of the plots between temperature and  $\log D$  (**Fig. 4**) based on Van't Hoff equation (Eq. (3)) and Eq. (4).<sup>13</sup>

$$\log D = -\frac{\Delta H^0}{2.303RT} + \frac{\Delta S^0}{2.303R} + C \quad (3)$$

$$\Delta G^0 = \Delta H^0 - T\Delta S^0 \quad (4)$$



The results showed that the extraction reaction of  $\text{Ni}^{2+}$  from the ammonia fluoride system was endothermic in nature with  $\Delta H^0 = 60.58 \text{ kJ/mol}$  and  $\Delta S^0 = 226.99 \text{ J/(mol}\cdot\text{K)}$ . And the reaction was thermodynamically favorable in view of the negative standard Gibbs free energy calculated ( $-7.06 \text{ kJ/mol}$ ) for the system.

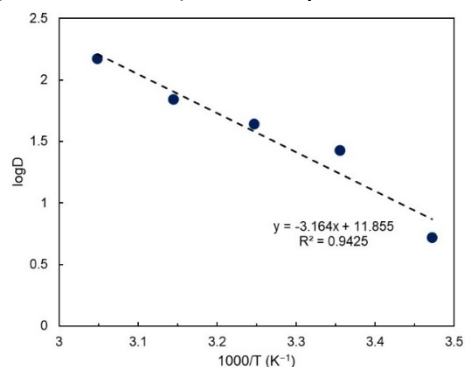


Figure 4. Plot of  $\log D$  as a function of temperature

### Effect of A/O phase ratio and McCabe-Thiele diagram

The aqueous/organic (A/O) phase ratio was varied while maintaining the total volume of 20 mL. The results were used to construct the McCabe-Thiele diagram of  $\text{Ni}^{2+}$  extraction (**Fig. 5(a)**), which demonstrates the possibility of complete extraction and enrichment of  $\text{Ni}^{2+}$  into the organic phase. A two-stage counter current extraction at an A/O ratio of 1.3 is required to quantitatively extract and enrich  $\text{Ni}^{2+}$  using 0.5 M LIX 84-I.

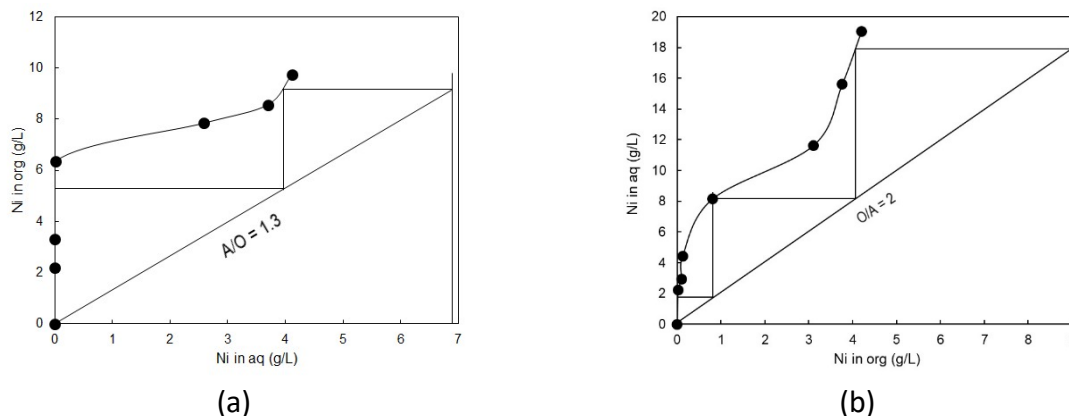


Figure 5. McCabe-Thiele diagram of (a) Ni extraction and (b) Ni stripping

### Stripping of extracted nickel

The nickel-loaded organic phase ( $\text{Ni}^{2+} = 8.96 \text{ g/L}$ ), after scrubbing was contacted with 2.0 M  $\text{H}_2\text{SO}_4$  solution at varied O/A ratio from 1/4 to 4/1. The results were then used to construct the McCabe-Thiele diagram of  $\text{Ni}^{2+}$  stripping (**Fig. 5(b)**). A three-stage counter current stripping at an O/A of 2 was found to be sufficient for quantitative stripping and enriching  $\text{Ni}^{2+}$ . A solution containing 17.92 g/L  $\text{Ni}^{2+}$  was obtained, giving a total enrichment factor of 2.6 times the initial  $\text{Ni}^{2+}$  concentration in the plating wastewater. From the strip solution Ni could be recovered in desired form.<sup>4,13</sup>

### Extraction mechanism

A series of SX experiments were performed to investigate the extraction mechanism using a solution containing 0.8 g/L  $\text{Ni}^{2+}$ , 20 g/L  $\text{NH}_3$  and 10 g/L  $\text{F}^-$ . The concentration of LIX 84-I was varied from 0.1 to 0.7 M. The distribution ratio of  $\text{Ni}^{2+}$  was calculated, and slope analysis method of  $\log D$  vs  $\log[\text{LIX}84 - I]$  was applied. Results presented in **Fig. 6** show that a linear relationship with a slope of  $\sim 2$  was obtained. This means that the stoichiometry of the LIX 84-I used in the extraction was 2 with respect nickel. In particular, there was no fluoride extracted into the LIX 84-I. As a result, the extraction reaction can be written as follows (Eq. (5)):

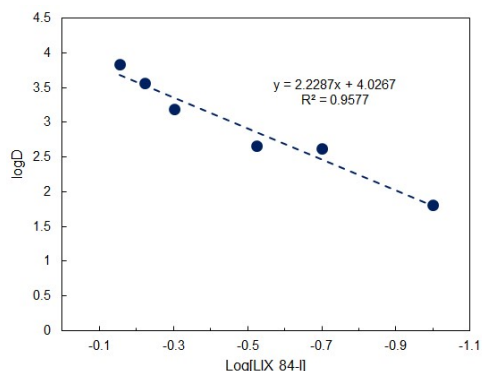


Figure 6. Plot of  $\log D$  as a function of  $\log[\text{LIX}84 - I]$

### Recyclability of the organic extractant

The recyclability of LIX 84-I was investigated through a series of extraction-stripping cycles (six cycles) in which the stripped organic extractants were washed before reuse. Results shown in **Fig. 11** reflect that the LIX 84-I extractant has excellent recyclability without loss of performance when extracting nickel from the ammonium fluoride solutions. This is advantageous in terms of both economics and sustainability.

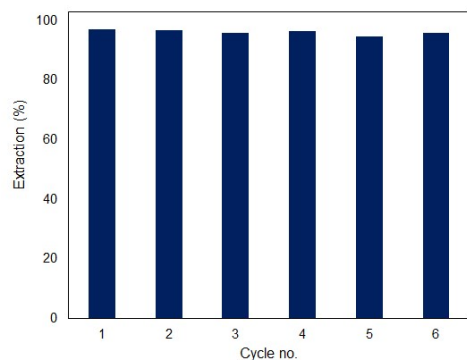


Figure 7. Recyclability of LIX 84-I extractant (extraction: 0.5 M LIX 84-I, 1/1 A/O phase ratio, 5 min shaking time; stripping: 4.0 M  $\text{H}_2\text{SO}_4$ , 1/1 O/A phase ratio; 10 min shaking time)

## Conclusions

The extraction and selective separation of nickel from an ammonium fluoride solution containing 6.9 g/L  $\text{Ni}^{2+}$ , 52 g/L  $\text{F}^-$  and 80 g/L  $\text{NH}_3$  (compositional similarity to the real electroplating wastewater) was performed using LIX 84-I extractant. It was possible to

completely extract and separate nickel from fluoride using LIX 84-I. Operational parameters, including extractant-, fluoride concentration, initial pH, temperature and A/O phase ratio had a significant effect on the nickel extraction, whereas fluoride concentration had no effect. The quantitative extraction of nickel from the solution was accomplished in a two counter-current extraction stages using 0.5 M LIX 84-I at an A/O ratio of 1.3, leaving all fluoride in the raffinate. The nickel-loaded organic phase was stripped with a 2.0 M H<sub>2</sub>SO<sub>4</sub> solution in a three stage counter-current process at O/A = 2, yielding almost 100% stripping efficiency. A strip solution with a Ni<sup>2+</sup> concentration of 17.92 g/L was obtained, resulting in a total enrichment factor of 2.6 times the initial Ni<sup>2+</sup> concentration in the wastewater. The complexation reaction involved two LIX 84-I molecules, and the LIX 84-I extractant can be reused without performance loss or significant pretreatment, which is beneficial for economics and sustainability.

## Acknowledgements

This work was supported by the Korea Institute of Energy Technology Evaluation and Planning (KETEP) grant funded by the Korea government(MOTIE) (20217510100080, Development of critical metal recovery technologies (capacity of 200kg/day) from low grade solid wastes for the foundation of open access recycling platform)

## References

- <sup>1</sup> Kumar, A., Balouch, A., Pathan, A. A., Jagirani, M. S., Mahar, A. M., Zubair, M., & Laghari, B. Remediation of Nickel ion from wastewater by applying various techniques: a review. *Acta Chemica Malaysia*, 2019, 3(1), 1–15.
- <sup>2</sup> Genchi, G., Carocci, A., Lauria, G., Sinicropi, M. S., & Catalano, A. Nickel: Human health and environmental toxicology. *International Journal of Environmental Research and Public Health*, 2020, 17(3), 679–700.
- <sup>3</sup> Świnder, H., & Lejwoda, P. Obtaining nickel concentrates from sludge produced in the process of electrochemical metal surface treatment. *Water, Air, & Soil Pollution*, 2021, 232(12), 1–8.
- <sup>4</sup> Horikawa, K., & Hirasawa, I. Removal and recovery of nickel ion from wastewater of electroless plating by reduction crystallization. *Korean Journal of Chemical Engineering*, 2000, 17(6), 629–632.
- <sup>5</sup> Loza, S. A., Romanyuk, N. A., Korzhov, A. N., & Kovalchuk, N. O. Resource-saving dialysis technology for electroplating wastewater treatment. In *IOP Conference Series: Materials Science and Engineering*, 2021, 1089(1), p. 012028), IOP Publishing.
- <sup>6</sup> Benvenuti, T., Krapf, R. S., Rodrigues, M. A. S., Bernardes, A. M., & Zoppas-Ferreira, J. Recovery of nickel and water from nickel electroplating wastewater by electrodialysis. *Separation and Purification Technology*, 2014, 129, 106–112.
- <sup>7</sup> Duong, H. C., Pham, T. M., Luong, S. T., Nguyen, K. V., Nguyen, D. T., Ansari, A. J., & Nghiem, L. D. A novel application of membrane distillation to facilitate nickel recovery from electroplating wastewater. *Environmental Science and Pollution Research*, 2019, 26(23), 23407–23415.
- <sup>8</sup> Feng, X., Wu, Z., & Chen, X. Removal of metal ions from electroplating effluent by EDI process and recycle of purified water. *Separation and Purification Technology*, 2007, 57(2), 257–263.
- <sup>9</sup> Kul, M., & Oskay, K. O. Separation and recovery of valuable metals from real mix electroplating wastewater by solvent extraction. *Hydrometallurgy*, 2015, 155, 153–160.
- <sup>10</sup> Cheng, C. Y., Barnard, K. R., Zhang, W., & Robinson, D. J. Synergistic solvent extraction of nickel and cobalt: A review of recent developments. *Solvent Extraction and Ion Exchange*, 2011, 29(5–6), 719–754.
- <sup>11</sup> Alviyal-Hein, G., Mahandra, H., & Ghahreman, A. Separation and recovery of cobalt and nickel from end of life products via solvent extraction technique: A review. *Journal of Cleaner Production*, 2021, 297, 126592–126618.

<sup>12</sup> Zuo, Y., Chen, Q., Li, C., Kang, C., & Lei, X. Removal of fluorine from wet-process phosphoric acid using a solvent extraction technique with tributyl phosphate and silicon oil. *ACS omega*, 2019, 4(7), 11593–11601.

<sup>13</sup> Kurniawan, Kim, M. S., Chung, K. W., Kim, R., & Lee, J.-c. Simple and complete separation of copper from nickel in the ammoniacal leach solutions of metal coated ABS plastic waste by antagonistic extraction using a mixture of LIX 84-I and TBP. *Separation and Purification Technology*, 2021, 255, 117712–117723.

# Management of the transfer of manganese impurity from the leach solution to the electrolyte at Ruashi Mining company in the Democratic Republic of Congo.

Godfrey Mitshabu,<sup>a</sup> Daddy Yav,<sup>b</sup> Richard Ngenda,<sup>c</sup> Patty Bwando,<sup>a</sup> Hugues Ngwanza<sup>a</sup> and Bai Faqing.<sup>b</sup>

**Abstract.** Ruashi was the first mining company to successfully commission a hydrometallurgical plant including copper solvent extraction in the Democratic Republic of Congo. Over the past 14 years the company has been one of the many local copper solvent extraction plants which has been fed with a leach solution containing relatively high concentration of manganese. Despite a washing stage in the solvent extraction circuit configuration, the transfer of manganese (II) ion from the leach solution to the electrolyte has been a longstanding issue at Ruashi. So far, the many actions taken at plant scale seem to have not significantly reduced manganese concentration in the electrolyte. Lab tests have shown that for a non-contaminated emulsion, during phase separation, aqueous entrainment is a downward power function of time. According to SX simulation results it is expected that reducing the organic flow in the high-grade section of solvent extraction by 23% would only reduce copper transfer by 2% as copper concentration in the feed is most of the time below design. Differences between Ruashi and other local copper solvent extraction plants running with comparable concentrations of manganese in the leach solution include the relatively higher settler specific flow and the larger electrolyte inventory. Further steps will thus include investigation of the settler specific flow role in mitigating manganese transfer from the leach solution to the electrolyte.

**Keywords:** Democratic Republic of Congo, Ruashi, Manganese, Entrainment

## Introduction

Copper cathodes have been produced at Ruashi mining in the Democratic Republic of Congo (DRC) since 2008 via the Leaching – Solvent Extraction (SX) – Electrowinning (EW) route. The SX circuit of Ruashi has two trains each including 2 extractions, 1 stripping and 1 washing stages. Over time, Mn concentrations in the Pregnant Leach Solution (PLS) and in the electrolyte have been constantly in upward trends at Ruashi: In the PLS, from an average of 2.14 g/L between 2009 and 2013 and 2.61 g/L between 2014 and 2018, the average from 2019 to June 2022 increased to 2.91 g/L. In the electrolyte, averages for the same periods were respectively 0.25 g/L, 0.39 g/L and 1.08 g/L. This paper aims to discuss why the many actions taken at plant scale so far do not seem to reverse this upward trend of Mn concentration in the electrolyte.

## Background

The presence of  $Mn^{2+}$  in the electrolyte has been quoted as a medium to long term threat to the life of lead alloy anodes used in copper electrowinning<sup>i</sup>. On the other hand, when suitable conditions are gathered,  $Mn^{2+}$  ions in the electrolyte may be oxidized to permanganate ( $MnO_4^-$ ) ions within electrowinning cells.<sup>ii</sup> When present in the spent electrolyte returning to

---

<sup>a</sup> BASF South Africa (Pty.) Ltd., 852 16<sup>th</sup> Road, 1685 Midrand, South Africa

<sup>b</sup> Ruashi Mining, 109 Songololo Avenue, Lubumbashi, Democratic Republic of Congo

<sup>c</sup> University of Lubumbashi, Lubumbashi, Democratic Republic of Congo

the stripping mixer(s) of the SX plant,  $\text{MnO}_4^-$  will be oxidizing oximes molecules in the organic phase. SX washing concept is relatively simple<sup>iii</sup>. Together with other impurities physically entrained, Mn in the loaded organic reports to a washing stage. The wash solution dilutes those entrainments carrying over less impurities to the electrowinning<sup>iv</sup>. Typically, the Mn that has accessed the electrolyte is only removed by bleeding, which impacts production cost. One DRC plant running with settlers' specific flows below  $3 \text{ m}^3/\text{m}^2/\text{h}$  proved to experience less entrainment than those running above  $4.5 \text{ m}^3/\text{m}^2/\text{h}$ .<sup>v</sup>

## Theory

Copper is extracted from acidic PLS by oximes based extractants. In this process,  $\text{Mn}^{2+}$  is an example of PLS impurities that reach the electrowinning tank house by aqueous in organic entrainment.

## Experimental

To assess the impact of various working parameters on the transfer of Mn from the PLS to the electrolyte a few actions were attempted, mostly with limited success. At plant scale the increase of the electrolyte bleed was tried but could not be sustained durably because of cost implications incurred (recycling of Cu and acid). The flow of Mn-free water in washing stages was also increased to reduce Mn content in the wash aqueous inventory. Further to these actions, primary mixer tip speeds were reduced from their maximum by 10% in stages likely to produce aqueous in organic entrainment. Due to the adverse impact on emulsion interstage transfer capacity, this action could not be maintained long enough for changes to start showing up. Temporary shutdowns of secondary mixers in “critical” stages were also tried without the significant impact expected on aqueous in organic entrainment. Plans include the upgrade of the primary organic surge tanks into aqueous coalescers. Simulations were carried out using Isocalc™ BASF SX modelling software to assess the impact of reducing the organic flow and/or change of SX flowsheet on metallurgical performance and aqueous entrainment. On the other hand, lab tests were performed to show the impact of clay treatment of the plant organic on phase separation time and thus, on aqueous entrainment.

## Results and Discussion

### Evaluation of the “primary” settling rate of the aqueous phase decanting from a separating non contaminated emulsion

In these tests a “virgin” organic phase was made up at 25% v/v LIX984N in the diluent as available in the plant. The aqueous phase made up at 8.5 g/L with analytical grade  $\text{MnSO}_4$  in tap water. The raise rate of the decanting aqueous phase was measured after the two phases were mixed for 3 minutes. For non-contaminated phases, the « primary break » was quite straightforward in less than 80 seconds. Whilst the primary break results from the coalescing of relatively big size droplets, at a smaller scale, micro droplets of aqueous are likely still scattered within the organic phase several seconds after the primary break. Their total volume might not be “significant”, but the carryover of impurities could be dramatic.

### Evaluation of aqueous entrainment after mixing of non-contaminated phases

Aqueous in organic entrainment was evaluated on samples of organic collected at various times at the same height within the separating organic after mixing for 3 minutes. Aqueous entrainment was evaluated using Mn as a marker.

Table 1: Primary settling rate versus aqueous height

Volume	Aqueous Height, cm	Time, sec			
		Test #1	Test #2	Test #3	Average
50	0.7	23	25	30	26
100	1.4	30	34	41	35
150	2.1	37	40	48	42
200	2.8	40	47	55	47
250	3.5	44	53	62	53
300	4.2	50	59	74	61

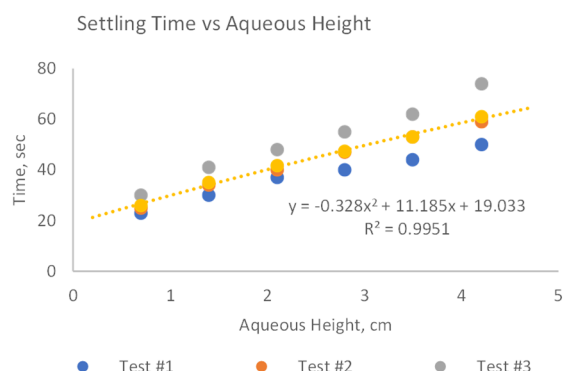


Figure 2: Settling Time versus Aqueous height

Deionized water was used to wash organic samples. Aqueous entrainment was calculated from the quantity of Mn transferred in the deionized water. After 100 sec of separation, aqueous entrainment dropped from 1200 ppm to below 600 ppm. At lab scale, for non-contaminated phases, over the “apparent” settler residence time of 480 sec, aqueous entrainment can be expected to drop below 200 ppm. At plant scale, many factors are likely to affect aqueous entrainment:

1. The presence of interfacial crud and bottom mud in settlers which affect the residence time of phases.
2. The level of contamination of aqueous or/and organic phases.

Table 2: Evaluation of Aqueous Entrainment

Time, sec	Mn concentration in washing water, mg/L				Average Volume of Organic Phase, mL	Aqueous Entrainment, ppm mL Aq/m <sup>3</sup> Org
	Test 1	Test 2	Test 3	Average		
40	5.854	11.98	3.467	7.100	35	1178
80	8.907	1.105	2.405	4.139	28	866
120	1.855	0.792	3.967	2.205	33	396
160	0.381	2.993	2.053	1.809	26	408
200	1.031	1.946	1.412	1.463	25	343

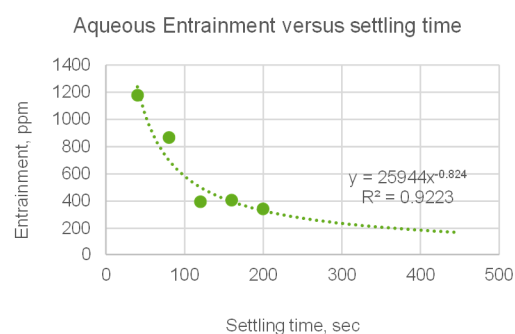


Figure 3: Aqueous Entrainment versus Settling Time

**Evaluation of the “primary” settling rate of the aqueous phase decanting from a separating emulsion where the organic phase is contaminated.**

The organic sample used for these tests was taken from the High-Grade circuit of Ruashi SX plant. For an organic continuous emulsion, the coalescing rate is affected when the organic phase is contaminated.

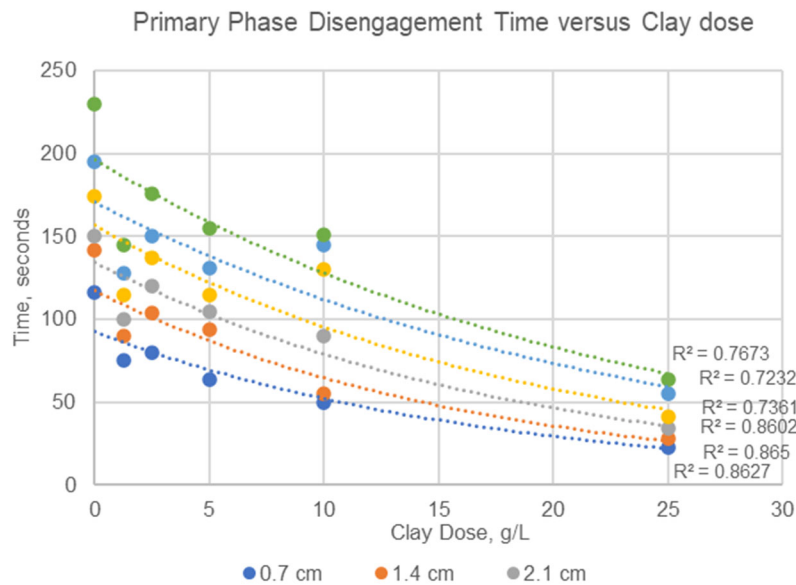


Figure4: Primary Phase Disengagement Time versus Clay Dose

« Primary » phase disengagement times after clay treatment were measured in the lab by measuring the height of « free » aqueous over time for clay doses increasing from 0 to 25 g clay/L organic. Within the clay dose used, the separation rate increases with clay dose.

The « primary separation rate » can be defined here as the ratio of the height of separated aqueous over the time required to reach that height. The average primary separation rate was plotted versus the dose of clay. It increases with the clay dose. Clay treatment of the plant organic does benefit to phase separation time. The impact on the reduction of aqueous entrainment is evident.

Table 3: Rate of Aqueous Phase Separation versus Clay Dose

	Rate of aqueous phase separation versus clay dose, mm/s					
Clay Dose, g/L	25	10	5	2.5	1.25	0
Aqueous. Height, cm						
0.7	0.30	0.14	0.11	0.09	0.09	0.06
1.4	0.50	0.25	0.15	0.13	0.16	0.10
2.1	0.62	0.23	0.20	0.18	0.21	0.14
2.8	0.68	0.22	0.24	0.20	0.24	0.16
3.5	0.64	0.24	0.27	0.23	0.27	0.18
4.2	0.66	0.28	0.27	0.24	0.29	0.18
Average	<b>0.57</b>	<b>0.23</b>	<b>0.21</b>	<b>0.18</b>	<b>0.21</b>	<b>0.14</b>

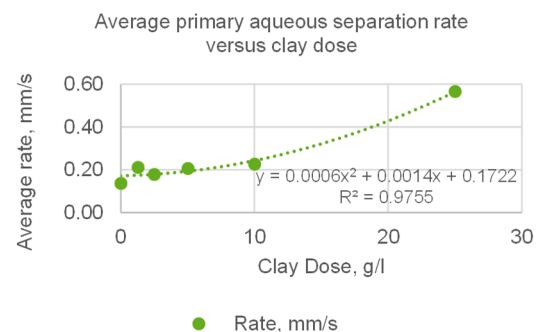


Figure 5: Average Primary Separation Rate versus Clay Dose



## BASF Isocalc™ Software Simulation Results

### Comparison of simulation results for 3 running scenarios.

HG & LG settlers specific flows, annual Cu production and Cu recoveries were compared in 3 cases:

1. “Common” situation: series circuit with 2Es, 1S and 1W as per SX profile of 21 Jan 2022 with higher than designed organic flow.
2. “Optimum” situation: Same as 1, but with designed organic flow (from 840 to 650 m<sup>3</sup>/h or so).
3. Possible situation: parallel circuit with washing stage converted into new E1s, 2Es converted into 2Ps, 1S, with high organic flow.

Table 4: Comparison of simulation results for 3 running scenarios

		Settler specific flow, m <sup>3</sup> /m <sup>2</sup> /h				Aqueous flow, m <sup>3</sup> /h			Org flow	Settler area	Cu	Cu Recovery
		E1	E2	S	W	E	S	W	m <sup>3</sup> /h	m <sup>2</sup>	Tons/year	%
HG SX	series	4.25	4.25	3.51	4.77	385	170	535	840	288	26062	93.5
	series	3.60	3.60	2.85	3.70	385	170	415	651	288	25424	91.3
	parallel	3.73	3.73	3.51	3.44	235	170	150	840	288	24521	77.7
LG SX	series	4.78	4.78	3.67	4.32	300	130	229	430	153	12770	98.2
	series	4.58	4.58	3.47	4.00	300	130	212	399	153	12763	98.1
	parallel	4.13	4.13	3.67	3.47	200	130	100	430	153	12328	87.9

In the HG SX, limiting organic flow within design limits would reduce Cu recovery by 2%, and annual Cu transfer by 6%. But E1 settler specific flow would be reduced by 15% with expected less aqueous entrainment. Running series parallel would highly affect Cu recovery, unless the concentration of extractant is increased significantly... In the LG SX, E1 settler specific flow is relatively high within designs limits of PLS and organic flows. On the other hand, Cu recovery would be significantly affected by the same configuration change a above.

### Impact of some SX parameters on Mn mass Balance

Simulations using Excel were carried out to evaluate the impact of various SX parameters on the mass balance of Mn in the wash aqueous and in the electrolyte.

The quantity of Mn that enters (or leaves) the electrolyte inventory within 24 hours is a balance between the positive contribution from the wash aqueous Mn entrained in the loaded organic advancing from the washing stages of the HG and the LG SX stages into their respective stripping stages, and the negative contribution from the Mn leaving the electrolyte inventory via the electrolyte bleed. The same applies with the PLS Mn entering the wash aqueous via the aqueous entrainment in the loaded organic. The way out for Mn in this loop is via the spent wash aqueous bleed.

To avoid the accumulation of Mn in the wash aqueous inventory, and/or in the electrolyte, the quantity of Mn coming in (aqueous entrainment) must be equal to the quantity of Mn out (bleed). Some of design figures used include:

Electrolyte inventory: 10000 m<sup>3</sup> out of a design of 12000 m<sup>3</sup>, organic flows: 650 m<sup>3</sup>/h in HG SX and 450 m<sup>3</sup>/h in LG SX, wash aqueous inventory: 150 m<sup>3</sup> in HG SX and 110 m<sup>3</sup> in LG SX. To evaluate the mass balance of Mn across the HG wash aqueous inventory on day  $u$

- The flow of PLS entrained in the loaded organic  $m_u$  (m<sup>3</sup>/h) = organic flow (m<sup>3</sup>/h) x Mn conc in HG PLS (g/L) x Aqueous entrainment (ppm) / 10<sup>6</sup>. If  $x_u$  is in kg/day the Mn added to the HG wash aqueous inventory on day  $u$  from aqueous entrainment in HG loaded organic,  $x_u = 24$  (h/d) x  $m_u$ . Likewise for the LG SX wash aqueous inventory.
- The bleed of HG spent wash aqueous out ( $f_u$ ) must include the flow of Mn free aqueous in ( $s_u$ ) and the flow of entrained HG PLS in ( $m_u$ ):  $f_u = s_u + m_u$ . The daily Mn out (kg/d) with the spent wash aqueous bleed  $t_u = 24$  (h/d) x  $f_u$  x  $y_u$ , where  $y_u$  is the starting concentration of Mn in the wash aqueous inventory on day  $u$ . Likewise for the LG wash aqueous inventory.
- The mass (kg) of Mn in the HG wash aqueous inventory  $i_u$  (kg) at the beginning of day  $u$  = HG wash aqueous inventory times its initial concentration ( $y_u$ ) of Mn (g/L):  $i_u = 150 \times y_u$
- The final mass (kg) of Mn in the HG wash aqueous inventory  $i'_u$  (kg) = starting mass of Mn ( $i_u$ ) minus the daily mass of Mn out with the spent wash aqueous bleed ( $t_u$ ) plus the daily mass of Mn ( $x_u$ ) from the aqueous entrainment in the HG loaded organic:  $i'_u = i_u - t_u + x_u$
- The concentration of Mn (g/L) in the HG wash aqueous at the end of day  $u$  is thus  $..._u = i'_u / 150$ .

The starting concentration of Mn in the wash aqueous on day  $u + 1$  is equal to its final concentration in the same on day  $u$

A similar calculation was carried out for daily mass balance of Mn in the electrolyte. Forecasts of Mn in wash aqueous and in electrolyte were calculated with Excel, varying parameters such as organic flow, aqueous entrainment, wash aqueous and electrolyte bleed flows, electrolyte inventory... Many simulations were carried out with the same relatively high starting Mn concentration in the electrolyte. In figure 6 two “extreme” cases are summarized: On one hand, even if Mn concentrations in HG and LG SX wash aqueous are reduced below 200 ppm in 10 days, Mn concentration in the electrolyte would still be dropping very slowly.

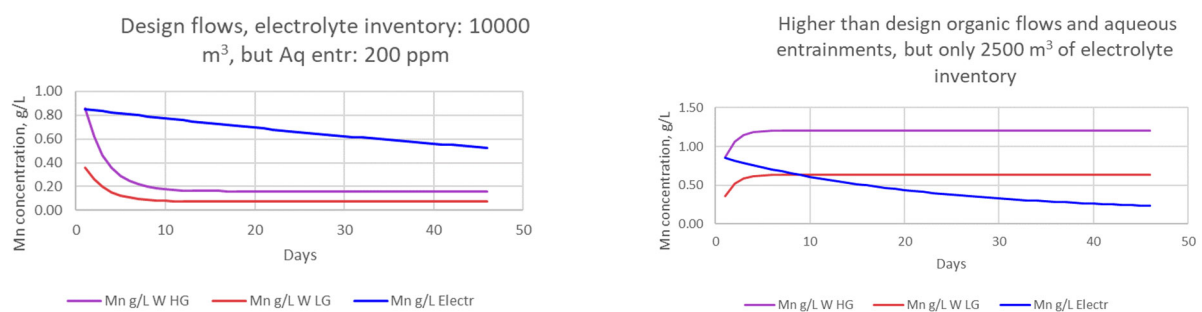


Figure 6: Comparison of 2 “extremes” scenarios, high electrolyte inventory (left) and low electrolyte inventory (right)

On the other hand, if the electrolyte inventory was 2500 m<sup>3</sup>, bleeding would be more effective to bring down Mn concentration in the electrolyte even with relatively high polluted HG and LG wash aqueous.

## Conclusions

Over the last four years, progressive Mn buildup in Ruashi electrolyte was significant. To try reversing this trend, corrective measures were tried, but many of them were difficult to maintain durably. These include many attempts to increase the flow of electrolyte bleed, and/or reduce mixers tip speeds. Compared with other DRC SX-EW plants, Ruashi electrolyte storage capacity is relatively high. This does have advantages, especially owing to power restrictions experienced in the area. On the other hand, pollution of the electrolyte takes long to show up, but the disadvantage is the relatively long time and effort it takes to “decontaminate” the electrolyte inventory once polluted. Lab tests have shown that clay treatment of the plant organic improves phase separation and thus, aqueous entrainment. For a non-contaminated organic, aqueous in organic entrainment is a downward power function of phase separation time. According to BASF Isocalc SX modeling software, it is expected that reducing the organic flow in the high grade SX by 23% would only reduce copper transfer by 2%, but the benefit of incurred reduction of settlers’ specific flows (by 15%) would be significant. On the other hand, the conversion of SX configuration from 2E, 1S & 1W to 1Es, 2Ep & 1S would also benefit settler specific flow, but metallurgical performances would be even more affected, unless the extractant concentration is increased...

## Acknowledgements

Valuable contribution for ISEC2022 conference presentation was received from our colleague Yi Zhou. We would like to thank Zam Tresor and Eric Kitobo for having contributed to the lab work as part of their duty as graduating students. Field discussions at Ruashi with Ajay Modi were very useful.

## References

---

<sup>i</sup> A. Mizra et al., Corrosion of lead anodes in base metals electrowinning, The journal of the Southern African Institute of Mining and Metallurgy, Vol 116, pp533 – 538, 2016.

<sup>ii</sup> G. Miller, Methods of managing manganese effects on copper solvent extraction-electrowinning operations, ALTA copper conference, Perth, Australia, 2010.

<sup>iii</sup> M. Virnig et al., Solvent extraction process for metal recovery, US Patent, 6599414B1, Cognis corporation, 2003.

<sup>iv</sup> H. Hein, Importance of a washing stage in copper solvent extraction, Hydro Copper conference, Santiago, Chile, 2005.

<sup>v</sup> G. Mitshabu, Management of copper solvent extraction plants running at reduced throughput, COM conference, Vancouver, Canada, 2019.

# RECOVERY OF RARE-EARTH METALS FROM NITRATE SOLUTIONS BY EXTRACTION METHOD

Yelena Bochevskaya, <sup>a</sup> Ainash Sharipova and Elmira Sargelova<sup>a</sup>

**Abstract.** The work is devoted to separation from impurities, the extraction and concentration of rare-earth metals (REMs) from nitrate solutions with the use of the extraction processing method. The REMs, Ca, and Fe distribution and separation coefficients were calculated. The optimum parameters of the rare earth metal extraction process with tributyl phosphate were selected, and the choice of reextractant was substantiated. The REMs extraction was 94,81 % at optimum technological parameters of REM re-extraction with water, and the process was characterized by the maximum concentration of  $\Sigma$ REM in an aqueous phase - 5,85 gram per litre.

**Keywords:** Rare-earth metals, Calcium, Iron, Aluminum, Tributylphosphate, Extraction

## Introduction

Steady interest in rare-earth metals is due to a wide range of their consumption in high-tech industries, increasing demand and a rather complicated situation in the world market.

Unique properties of REMs serve as a basis for implementation of advanced technologies in metallurgy, instrument engineering, machine building, radioelectronics, chemical and defense industries, optics, etc. Almost half of REMs is used in production of powerful permanent magnets, catalysts for oil cracking, rubber synthesis, as well as for production of catalytic filters - neutralizers of exhaust gases from motor vehicles. The production of phosphors for monitors and energy-saving lamps is a very promising direction of application of rare earths. In the nearest future, REMs will be widely demanded in production of storage batteries and manufacturing of powders for polishing lenses and microchips. More than 60% of REM is used in the so-called "high-tech" industries<sup>i</sup>.

The total demand for REMs has been steadily increasing over the last decade by 5-7 % per year. The current volume of the global rare earth metals market is estimated at \$1,520 billion<sup>ii</sup>, and the total volume of products where REMs are used is about US\$5 trillion.

## Background

There is a need to find new raw material sources for REMs production due to the steadily growing global demand for rare-earth metals. Currently existing ore dumps, tailings of beneficiated plants, ash and slag dumps of thermal power plants are potential raw materials for rare-earth metal production. Phosphorus production slags also belong to one of such sources.

Phosphorus slag is the most heavy-tonnage waste of yellow phosphorus production stored in the dump fields for many years creating ecological problems in the regions. Rare-earth metals production is one of the relevant and priority directions. Their presence in the phosphorus

---

<sup>a</sup> Sector of rare scattered elements, D.V. Sokolsky Institute of Fuel, Catalysis and Electrochemistry JSC, Almaty, Republic of Kazakhstan

slags allows considering the latter as an acceptable raw material source. At present, a technology has been developed to process phosphorus production slags with the production of a collective concentrate of rare earth metals and precipitated silicon dioxide.

## Experimental

**Methods.** Solutions containing ~0.2 gram per litre of REMs were obtained after leaching of phosphorus production slags under optimal conditions: 7.5 moles per litre of nitric acid  $\text{HNO}_3$  with the solid to liquid ratio equal to 1:2.6, temperature - 60 °C and the duration of the process - 1 hour.

Solutions and cakes produced were analysed for content of  $\text{CaO}$ ,  $\text{Al}_2\text{O}_3$ ,  $\text{Fe}_2\text{O}_3$ , and  $\Sigma\text{REMs}$ . Quantitative content of main components was determined by chemical analysis methods. Quantitative content of  $\Sigma\text{REMs}$  was determined using atomic emission spectrometer with inductively coupled plasma - Optima 8300DV.

X-ray phase analysis of the REMs concentrate was performed using a D8 ADVANCE diffractometer (Bruker AXS GmbH) with a cobalt anode. The diffractograms were decoded, and the interplanar distances were calculated using the EVA software. Sample decoding and phase search were performed with the help of the "Search/match" program using the ASTM card database<sup>iii</sup>.

X-ray fluorescence analysis of the concentrate was performed on the laboratory energy dispersive spectrometer RLP-21T in the Institute of Nuclear Physics RSE of the Ministry of Energy of the Republic of Kazakhstan.

## Results and Discussion

**Leaching.** Under optimal leaching conditions the extraction of  $\Sigma\text{REM}$  is 98 %, iron is extracted by ~19 %, aluminum and calcium by ~99 %.

The concentrations of rare-earth elements (Figure 1) and the degree of extraction in the solution element-by-element during leaching under optimal conditions were determined to study their behavior.

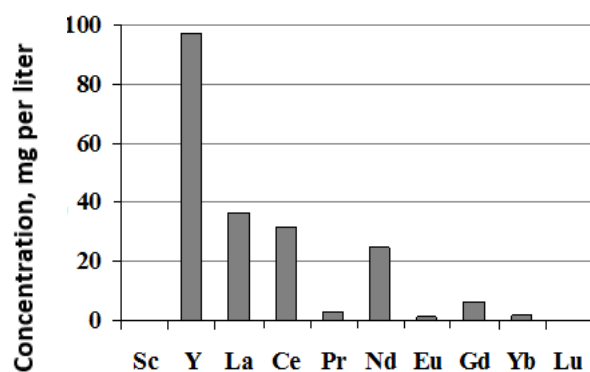


Figure 1. Concentration of rare earth elements in nitric acid solution after phosphorus slag leaching

It has been established that the group of light lanthanides present in phosphorus slag in larger amounts (La, Ce, Pr, Nd, Eu and Gd) is leached better than the group of heavy lanthanides (Yb and Lu).

Almost all of the rare earth elements are quite effectively transferred into solution. From among the most demanded REM, yttrium, neodymium, europium and lutetium are present in phosphorus slag, their recovery rates are ~98, ~99, ~99 and ~28 %, respectively.

**Extraction.** Comparative analysis was performed to use di-2-ethylhexylphosphonic acid (Di-2EHPA), quaternary ammonium salts - chlorides of trialkylbenzylammonium (TABAC) and trialkylmethylammonium (TAMAC), and tributylphosphate (TBP) as extractants for REMs extraction.

Di-2-ethylhexyl phosphoric acid is one of the extractants widely used in REMs extraction. Extraction of  $\Sigma$ REMs, calcium, aluminum and iron by Di-2EHPA with a concentration of 0.39 moles per litre from the solution depending on the ratio of organic and aqueous phases (O:A = 1:1÷10, step 2 and 1:20). It was found that the extraction of  $\Sigma$ REMs decreases from 52 to 19 % with a change in the O:A ratio from 1:1 to 1:20.

When REMs are extracted from nitrate solution by the salts of quaternary ammonium bases: TABAC and TAMAC (or Adogen 464) it was found that REMs extraction is within 10 - 11 % when TABAH is used, and it is slightly higher and makes 12-13 % for TAMAC.

A comparative analysis on the use of TBP, D2EHPA and anion-exchange salts of quaternary ammonium bases was performed for REM extraction from nitrate solutions with TABAC and TAMAC used as example.

The best indicators for the extraction of REMs in the extract of 94.7 % were achieved with the use of a TBP solution with a concentration of 0.73 moles per litre at organic to aqueous phase ratio O:A= 1: 1. The effect of TBP concentration from 0.73 to 3.66 moles per litre on the REMs extraction process was studied depending on the ratio of O:A: 1:1÷10, step 2 and 1:20 (Table 1)<sup>iv</sup>.

The behavior of calcium Ca and iron Fe was studied during the extraction. No data are specified for aluminum since its transition to the organic phase was not observed. The extraction of REMs, calcium, and iron from solutions decreases at all TBP concentrations with an increase in the volume of the aqueous phase from 1 to 20.

The extraction of REMs in the organic phase increases from ~22 to 95% with a ratio 1:20 with an increase in the concentration of TBP from 0.73 to 3.66 moles per litre.

The distribution and separation coefficients for REMs and Ca and Fe were calculated. The distribution coefficients of REMs increase with increase in the extractant concentration. Iron at TBP concentrations from 0.73 to 2.20 moles per litre with O:A ratios of 1:6 to 1:20 was practically not extracted into the organic phase. The separation coefficients of REMs and calcium  $\beta_{\Sigma\text{REMs}/\text{Ca}}$  and REMs and iron  $\beta_{\Sigma\text{REMs}/\text{Fe}}$  increase with increase in the extractant concentration.

Optimal parameters were chosen for the extraction process: TBP concentration of 1.83 moles

Table 1. Effect of TBP concentration on REM extraction in the presence of calcium, aluminum and iron at different ratios of organic and aqueous phases

O:A	Concentration in the equilibrium aqueous phase, gram per litre			Degree of extraction into the organic phase, %			D <sub>Σ REMs</sub> ,	Separation coefficients	
	ΣREMs, mg per litre	Ca	Fe	ΣREMs	Ca	Fe		β <sub>ΣREMs/Ca</sub>	β <sub>ΣREMs/Fe</sub>
TBP concentration - 0.73 moles per litre									
1:1	10.47	117.64	0.14	94.71	6.95	88.24	17.91	239.71	2.39
1:2	28.23	118.94	0.36	85.74	5.92	69.75	12.03	95.50	2.61
1:4	63.94	119.12	0.73	67.71	5.78	38.66	8.39	34.17	3.33
1:6	83.22	120.01	1.19	57.97	5.08	–	8.28	25.78	–
1:8	103.78	120.40	1.19	47.59	4.80	–	7.26	18.13	–
1:10	118.49	120.99	1.19	40.16	4.30	–	6.71	14.92	–
1:20	154.10	123.19	1.19	22.17	2.56	–	5.70	10.83	–
TBP concentration – 1.10 moles per litre									
1:1	6.49	115.67	0.09	96.72	8.51	92.44	29.51	317.22	2.41
1:2	13.19	117.29	0.19	93.34	7.23	84.03	28.02	179.80	2.66
1:4	29.78	118.25	0.46	84.96	6.47	61.34	22.60	81.66	3.56
1:6	44.55	119.00	0.68	77.50	5.88	42.86	20.67	53.60	4.46
1:8	57.44	119.92	0.86	70.99	5.15	27.73	19.58	45.08	6.38
1:10	71.83	120.61	1.19	63.72	4.60	–	17.57	36.40	–
1:20	108.20	122.88	1.19	45.35	2.81	–	16.60	28.73	–
TBP concentration – 1.47 moles per litre									
1:1	5.19	113.81	0.08	97.38	9.98	93.28	37.15	335.03	2.68
1:2	10.12	114.92	0.15	94.89	9.10	87.39	37.13	185.36	2.68
1:4	19.58	116.94	0.36	90.11	7.51	69.75	36.45	112.29	3.95
1:6	34.09	118.15	0.58	82.78	6.55	51.26	28.85	68.61	4.57
1:8	43.12	118.55	0.77	78.22	6.23	35.29	28.73	54.04	6.59
1:10	51.65	119.65	0.90	73.91	5.36	24.37	28.33	50.00	8.79
1:20	86.96	122.52	1.19	56.08	3.09	–	25.54	40.01	–
TBP concentration – 1.83 moles per litre									
1:1	4.89	113.15	0.08	97.53	10.50	93.28	39.49	336.47	2.85
1:2	7.77	113.28	0.14	96.08	10.40	88.24	48.97	210.90	3.26
1:4	16.60	115.05	0.35	91.62	9.00	70.59	43.71	110.48	4.55
1:6	26.60	117.25	0.58	86.57	7.26	51.26	38.66	82.30	6.13
1:8	35.76	117.58	0.76	81.94	7.00	36.13	36.30	60.28	8.02
1:10	42.77	118.92	0.89	78.40	5.94	25.21	36.29	57.47	10.77
1:20	74.23	122.10	1.19	62.51	3.42	–	30.25	47.02	–
TBP concentration – 2.20 moles per litre									
1:1	3.59	109.85	0.06	98.19	13.11	94.96	54.15	358.79	2.88
1:2	6.30	111.70	0.12	96.82	11.65	89.92	60.86	230.74	3.41
1:4	13.68	113.17	0.31	93.09	10.49	73.95	53.89	114.99	4.75
1:6	21.70	115.55	0.55	89.04	8.61	53.36	48.75	86.28	7.10
1:8	33.00	116.25	0.73	83.33	8.05	38.24	40.00	57.10	8.08
1:10	39.60	117.98	0.87	80.00	6.68	26.89	40.00	55.85	10.88
1:20	66.80	121.77	1.19	66.26	3.69	–	39.28	51.32	–
TBP concentration – 3.66 moles per litre									
1:1	1.41	92.29	0.04	99.29	27.00	96.64	139.43	376.91	4.85
1:2	1.60	98.11	0.08	99.19	22.40	93.28	245.50	425.25	8.85
1:4	2.36	106.88	0.15	98.81	15.46	87.39	331.59	453.21	11.96
1:6	2.99	110.07	0.23	98.49	12.94	80.67	391.32	438.80	15.63
1:8	3.78	111.37	0.31	98.09	11.91	73.95	411.05	379.97	18.10
1:10	4.69	112.81	0.39	97.63	10.77	67.23	412.17	341.39	20.09
1:20	9.09	119.00	0.86	95.41	5.88	27.73	415.64	332.85	54.16

per litre at the O:A ratio = 1:6 and 3.66 moles per litre at O:A = 1:20. The recovery of  $\Sigma$ REMs in the extract is  $\sim 87$  and 95 %, respectively, under these conditions.

A representative batch of REM-containing extract in an amount of  $\sim 10 \text{ dm}^3$  was preliminarily produced under the extraction conditions with TBP  $3.66 \text{ mol/dm}^3$ , O:A = 1:20 and phase contact time - 5 min. The concentration of  $\Sigma$ REM in the extract was 1.028 gram per litre.

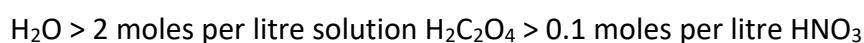
**Stripping.** Further studies were aimed to select the effective reextractant and optimal technological conditions of REM extraction from the rich organic phase

Distilled water, acid solutions,  $\text{mol/dm}^3$ : nitric acid with a concentration of 0.1 and oxalic acid - 2 were used as a re-extractant under the following conditions: O:A = 1:1, temperature  $20 \pm 5^\circ \text{C}$  and process duration - 5 min. The results of the experiments are presented in Table 2.

Table 2. REMs extraction from the rich organic phase into the reextract with different reextractants

Parameter	Reextractants		
	2 moles per litre solution $\text{H}_2\text{C}_2\text{O}_4$	0.1 moles per litre $\text{HNO}_3$	$\text{H}_2\text{O}$
Extraction of $\Sigma$ REMs in the extract, %	95.80	58.47	99.99

As can be seen from Table 2, the reextractants used in descending order of REMs extraction into the reextract can be arranged as follows:



When 0.1 moles per litre  $\text{HNO}_3$  is used as a reextractant, rare-earth metals from the organic phase pass into the solution by only 58.5 %. It was found that iron is co-extracted by 96.6 % during the REM extraction from nitrate solutions of TBP. When  $\text{H}_2\text{C}_2\text{O}_4$  solution is used with a concentration of 2 moles per litre, solid-phase re-extraction occurs with the formation of calcium oxalates as the main impurity and REMs. In this case, the formed metal salts hang in the organic phase in the form of a finely dispersed phase which then complicates their extraction.

The best REMs extraction rates from the extract (99.99 %) were obtained when  $\text{H}_2\text{O}$  was used as a reextractant. Calcium interaction with water forms calcium hydroxide  $\text{Ca}(\text{OH})_2$  which is formed in the reextract and can be further separated from it by filtration. When water is used as a reextractant, the reextraction of nitrate salts of rare earth metals and the subsequent regeneration of the extractant - TBP is not very difficult.

## Conclusions

The parameters of the REMs stripping process with water were established: the O:A ratio = 6:1 and the phase contact time 5 min. The extraction of REMs is 94.8 %, and the process is characterized with a maximum concentration of REMs in the aqueous phase 5.85 gram per litre.

It was established that an increase in the amount of  $\text{H}_2\text{C}_2\text{O}_4$  at the deposition stage from 100 to 240 % of stoichiometry results in an increase in the calcium precipitation degree, and the



concentration of calcium increases in the concentrate from 59.3 to 71.6 %, respectively. It seems more acceptable to precipitate  $\Sigma$ REM oxides without the presence of excess oxalic acid.

It was found that in the concentrate from scandium to lutetium and yttrium, that is, from light REMs to heavy ones, the concentration degree of the latter increases twice.

It is possible to obtain a concentrate with a content of  $\Sigma$ REM oxides 15.0-17.0 % during the processing of phosphorus slag containing about 0.05-0.06 % of  $\Sigma$ REM oxides.

## Acknowledgements

This research was funded by the Science Committee of the Ministry of Science & Higher Education of the Republic of Kazakhstan (Grant No. 1220/GF4).

## References

---

<sup>i</sup> Yushina T.I., Petrov I.M., Grishaev S.I., Chernyi S.A. Mining information and analytical bulletin (scientific and technical journal). 2015, 577-608.

<sup>ii</sup> Dudley Kingsnorth Rare Earths: Is Supply Critical in 2013? AusIMM 2013 Critical Minerals Conference, Perth, Western Australia <http://investorintel.com/wp-content/plugins/google-document-embedder/load.php?d=http://investorintel.com/wp-content/uploads/2013/08/AusIMM-CMC-2013-DJK-Final-InvestorIntel.pdf>

<sup>iii</sup> Powder Diffraction File. Search Manual. Hanawalt Method. / Inorganic. International center for diffraction data. 1987.

<sup>iv</sup> Karshigina Z., Abisheva Z., Bochevskaya Ye., Akcil A., Sharipova A., Sargelova E. *Proceedings of World Multidisciplinary Earth Sciences Symposium (WMESS 2016)*, 5–9 September 2016, Prague, Czech Republic. Published under license by IOP Publishing Ltd. Vol. 44, № 052003. 1-7.

# A process based on Ionic Liquids for tungsten valorization from low grade scheelite concentrates

Javier Nieto<sup>a\*</sup>, Lourdes Yurramendi<sup>a</sup>, José Luis Aldana<sup>a</sup>, Carmen del Río<sup>a</sup>, Amal Siriwardana<sup>a</sup>

**Abstract.** Tungsten is a *Critical Raw Material* with strategic high technological applications and very scarce in Europe. In recent years, an increasing research effort is being dedicated to find innovative routes for the recovery of tungsten from mining wastes, unvalorized at EU level. In this work, a process involving Ionic Liquids for the recovery of tungsten from low grade scheelite concentrates (3.4%) is proposed. Tungsten was recovered in the form of a high purity tungsten oxide (96%) at a high global recovery yield (80%).

**Keywords:** Ionic Liquids, Deep Eutectic Solvents, Tungsten, Critical Raw Material, Scheelite, Leaching, Extraction

## Introduction

Tungsten (W) is a rare metal with a wide range of applications such as rocket engines, aircrafts, magnetic trains, cutting tools, and pacemakers. The EU production (3,200 t) represents only 4% of the global production (2018), while its consumption was 10,000 t. China is the major producer, accounting for 80% of the 81,100 t global production in 2018<sup>i</sup>. Due to its high demand and scarcity in the EU, tungsten has been included among the Critical Raw Materials (CRM) since 2011.

## Background

In the production of tungsten from scheelite ores (~0.3% W) mineral processing is used<sup>ii</sup> to obtain a first low-grade concentrate (LGC ~3% W) and to finally achieve a high-grade concentrate material (HGC ~60% W), together with high amounts of tailings (0.02% W, 7-10 t/t HGC) currently unvalorized. For W metal production, HGC is first processed by acid or alkali digestion to obtain H<sub>2</sub>WO<sub>4</sub>, followed by treatment with NH<sub>4</sub>OH to produce ammonium paratungstate (APT), which is calcinated to WO<sub>3</sub> and finally reduced with hydrogen<sup>iii</sup>.

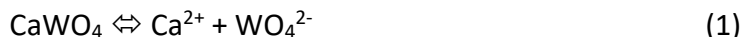
As an alternative to these technologies, involving toxic acids/alkalis and high pressure and temperature, a process based on environmentally-friendly ionic liquids (ILs) is proposed for the obtention of the tungsten oxide. Previous research performed by this team on HGC<sup>iv</sup> showed high W extraction yields (95%) in the leaching when using DES ChCl/OA (choline chloride, oxalic acid). In this work, leaching conditions are optimized for the low-grade scheelite concentrate. Afterwards, W is extracted from the leachate as APT by a two steps process: IL-extraction and stripping. Finally, high purity WO<sub>3</sub> can be produced after evaporation and calcination. In the present work, the global W recovery process from the LGC to the final product in the form of WO<sub>3</sub> is investigated.

---

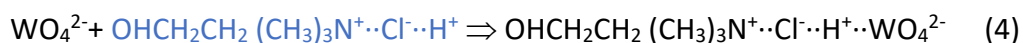
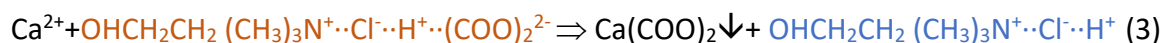
<sup>a</sup> TECNALIA, Basque Research & Technology Alliance (BRTA), Mikeletegi Pasealekua, 2, E-20009 San Sebastian, Spain.

## Theory

In this work, a process for the valorization of tungsten from low grade scheelite concentrates is proposed. Tungsten in scheelite mineral is in the form of calcium tungstate ( $\text{CaWO}_4$ ). This salt is in equilibrium in aqueous medium (1):



However, due to the low solubility of  $\text{CaWO}_4$ , the concentrations of  $\text{Ca}^{2+}$  and  $\text{WO}_4^{2-}$  in equilibrium are very low. In this work, a Brönsted Deep Eutectic Solvent (DES) composed of choline chloride (ChCl) as hydrogen bond (HB) acceptor and oxalic acid (OA) as HB donor is used. ChCl and OA are stabilized by hydrogen bonds (2) in the DES. At some point, an oxalate ion  $(\text{COO})_2^{2-}$  reacts with  $\text{Ca}^{2+}$  ions and the precipitation of calcium oxalate  $\text{Ca}(\text{COO})_2$  takes place (3). Tungstate ions are then stabilized by the remaining choline chloride acceptor by an hydrogen bond (4).



## Experimental

### DES preparation

The DES was made by mixing the individual components (ChCl and OA) and heating the mixture to a temperature above the melting point of the DES (preferably 80 °C).

### Leaching reaction

Low grade concentrate (3.4% W) is used as starting material. However, in some preliminary experiments, high grade concentrate (57% W) was used. The first step in the leaching reaction was the addition of the material (low/high grade concentrate) to the leaching agent under stirring at the selected reaction temperature. Leachate samples were taken during the leaching process at different time intervals. Concentrations of W and some other elements (impurities such as Fe) were measured by ICP-MS to calculate leaching yields.

### IL extraction

Tungsten was recovered from leachate by IL extraction. As oil phase, an IL extractant (dispersed in dodecane with 1-octanol as phase modifier) was used. The leachate was directly used as aqueous phase. For the stripping, a  $\text{NH}_3$  1M solution was put in contact with the oil phase from the previous IL extraction step. The extraction yields were calculated from the difference in the concentrations (measured by ICP) before and after the experiment.

## Characterization

All leachates were characterized by Inductively Coupled Plasma Mass Spectrometry (ICP-MS) using a spectrophotometer mod. 7900 of Agilent.

For solid materials, a representative sample (0.1 g) was digested in 4 mL concentrated HNO<sub>3</sub>, 4 mL HCl, and 2 mL HF in a microwave oven at 220°C. After cooling, the vessel content was diluted to 50 mL and analyzed by ICP-MS.

XRD measurements were performed in a Bruker D8 Advance diffractometer using Cu K $\alpha$  radiation operating at 40 kV and 40 mA.

## Results and Discussion

### Leaching

#### DES screening

The W leaching performance of HGC was evaluated for different DES (Table 1). The conclusions are also valid for W leaching from LGC. The same conditions (T 80°C, L/S 10, t 24h) were used for comparison purposes (Figure 1).

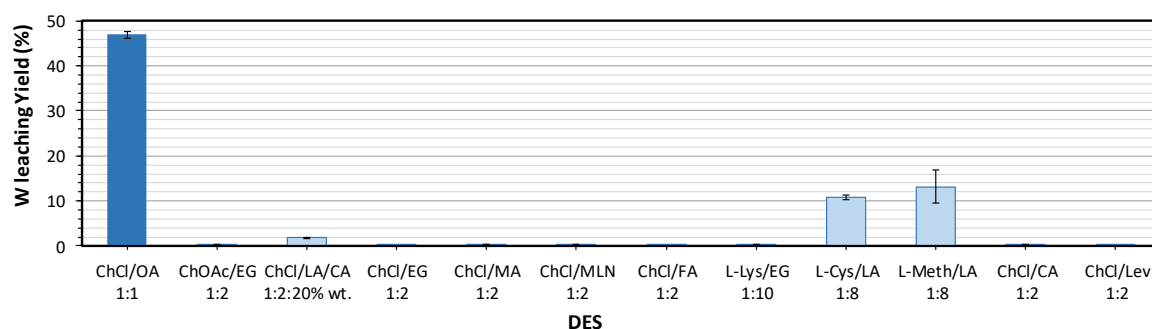


Figure 1. DES screening on W extraction yields. Material: high grade scheelite concentrate 57% W, L/S 10, T 80°C

Table 1. Description of the tested DES for leaching

Formulation	HBA:HBD	HBA	HBD
ChCl/OA	1:1	Choline Chloride	Oxalic Acid
ChOAc/EG	1:2	Choline Acetate	Ethylene Glycol
ChCl/LA/CA	1:2:0.45	Choline Chloride	Lactic/Citric Acids
ChCl/EG	1:2	Choline Chloride	Ethylene Glycol
ChCl/MA	1:2	Choline Chloride	Malic Acid
ChCl/MLN	1:2	Choline Chloride	Malonic Acid
ChCl/FA	1:2	Choline Chloride	Formic Acid
L-Lys/EG	1:10	L-Lysine	Ethylene Glycol
L-Cys/LA	1:8	L-Cysteine	Lactic Acid
L-Meth/LA	1:8	L-Methionine	Lactic Acid
ChCl/CA	1:2	Choline Chloride	Citric Acid
ChCl/Lev	1:2	Choline Chloride	Levulinic Acid

The DES ChCl/OA 1:1 showed the best leaching performance (47%). Very low W leaching yields was observed for the rest of DES (< 15%). The leaching variables were optimized for ChCl/OA DES.

### Effect of leaching variables

The leaching variables (ChCl/OA ratio, T and L/S ratio) were optimized using HGC 57% W as starting material. The best W leaching yield (70%) was achieved with DES ChCl/OA 1:2 at L/S 10 and 60 °C. This DES (ChCl/OA 1:2) was also tested with LGC 3.4% W, achieving W leaching yields higher than 90%.

### Leaching of impurities

The objective of this work is the recovery of W from Low Grade Concentrates in the form of high purity  $\text{WO}_3$ . For this reason, the impurities concentration in all the process steps has to be carefully analyzed. In this chapter, the presence of impurities in the leachate was monitored with time (Figure 2) in the best leaching conditions together with the W leaching yield with the target material, that is, low grade concentrate LGC (3.4% w).

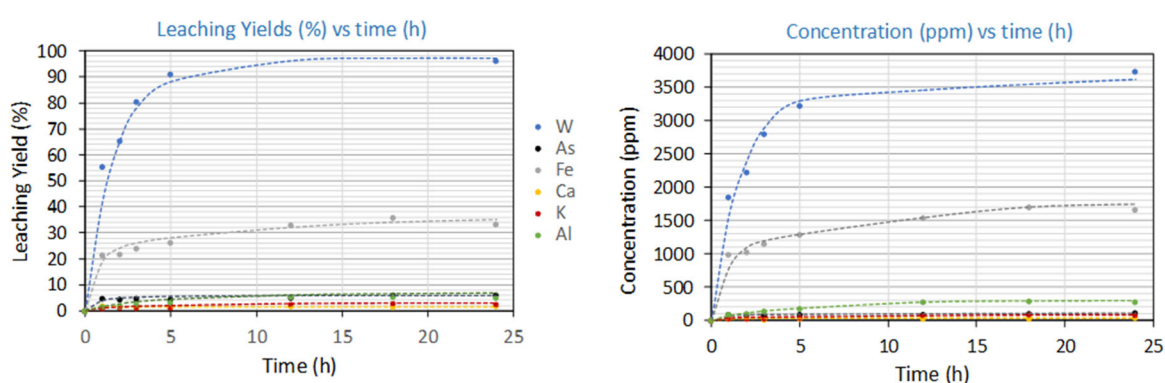


Figure 2. Leaching of impurities and tungsten with time. Left: yields evolution, right: concentrations (ppm) in the leachate vs time. Material: low grade scheelite concentrate 3.4% W, L/S 10, T 60°C

As it can be seen in Figure 2 (Left), near to 100% extraction yields were obtained for W in 24h, but also W leaching yields as high as 90% were achieved in only 5h with a significant reduction of cost which is a key factor for further scale-up of the process. The main impurity in the leachate is iron so its content in the following W recovery steps has to be carefully checked, as high purity  $\text{WO}_3$  is pursued in the global process. The rest of impurities remains lower than 300 ppm in the final leachate.

### Leachate stability: water addition

The main drawback of the selected DES in the previous chapters ChCl/OA 1:2 is that this DES is solid at temperatures lower than 58 °C. After the leaching step, the leachate has to be separated from the residue by filtration and this has to be carried out at temperatures above 60 °C to avoid any possibility of crystallization in the filter, that will often imply stops in the process and higher maintenance costs. Similar problems will also take place in the IL extraction step, where the crud formation in the mixer-settler is a serious inconvenient with

a high economic impact. For these reasons, a liquid leachate at ambient temperature is always desirable.

In order to overcome this problem water was added to this DES. Results (Figure 3) show higher W leaching yields (94% in 1h), and lower presence of impurities (Fe yield < 5%) for the DES-based leaching agent containing water.

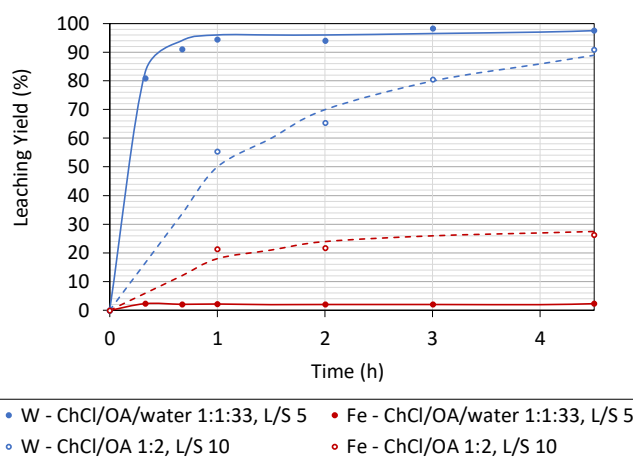


Figure 3. Evolution of W leaching yield vs time. Material: low grade scheelite concentrate 3.4% W, T 60°C

With these results, the selected DES-based leaching agent is ChCl/OA/water 1:1:33. The optimal leaching conditions are L/S 5, T 60°C, time 1h, achieving 94% W leaching yield.

## W recovery from leachates

### IL extraction screening

Different hydrophobic DES and IL extractants (Table 2) were tested for W extraction from the leachate. Results are shown in **Fe! Hittar inte referenskälla..**

Table 2. Description of the tested IL for IL extraction

IL1 TOPO/L_Thymol	IL2 TOPO/Hexanoic Acid	IL3 TOPO/1-Butanol	IL4 TOPO/1-Hexanol	IL5 TOPO/1-Octanol
IL6 Lidocaine/DecA	IL7 Thymol/DecA	IL8 Ali336/DecA	IL9 Ali 336	IL10 Alicy 336
IL11 Cyphos 101	IL12 Cyphos 104	IL13 Cyphos 109	IL14 Cyphos 169	IL15 Cyanex 272
IL16 [C6mim] [BF4]	IL17 [C2mim] [NTf2]	IL18 [C4mim] [NTf2]	IL19 [3C4mN] [NTf2]	

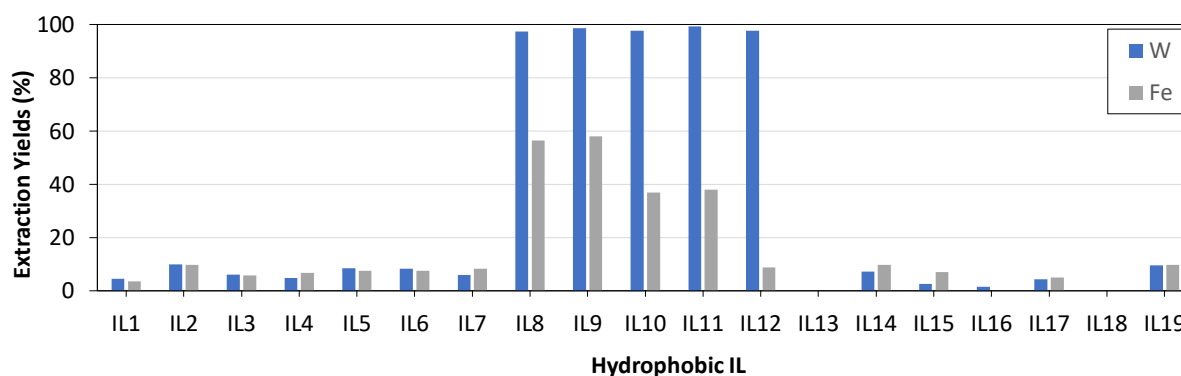


Figure 4. Screening of hydrophobic IL extractants. IL extraction conditions: O/A 1.7 v/v, T 40 °C, time 24h

The best W extraction yields (>90%) were achieved with Cyphos 101 (IL11), Cyphos 104 (IL12) and Ali336-based extractants (IL8, IL9, IL10) (**Fel! Hittar inte referenskölla.**). However, higher selectivity to W was achieved with Cyphos 104. For this extractant, Fe extraction yield was lower than 10%. On the other hand, Cyphos 101 and Ali336 showed 3 phases using dodecane as dispersant. Cyphos 104 was selected as the optimal extractant.

### Stripping

Tungsten was stripped from the oil phase with a  $\text{NH}_4\text{OH}$  1M solution. A very selective reaction takes place between ammonium and tungstate ions ( $\text{WO}_4^{2-}$ ) with the formation of ammonium paratungstate (APT). The global process gave a W yield of 80% with very low Fe extraction yield (< 5%) (Figure 5).

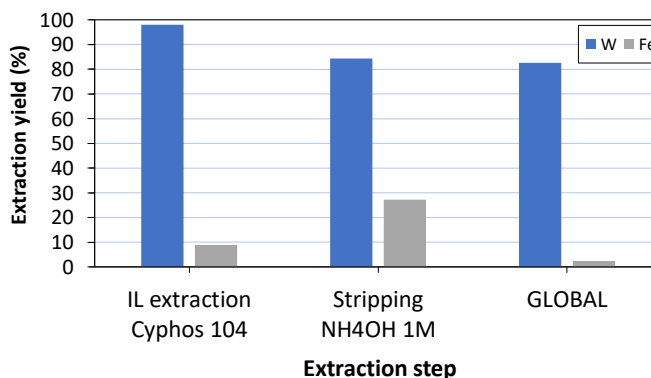


Figure 5. Global process for W recovery from leachates

### Determination of the theoretical number of Mixer-Settlers

The number of MS was determined by the McCabe-Thiele method. This method allows to obtain the number of mixer-settlers required to achieve a given extraction yield, depending on the O/A ratio. A W concentration as low as  $0.01 \text{ g L}^{-1}$  (10 ppm) can be obtained with 2 MS at O/A 1:1, that means 99.85% W extraction yield.

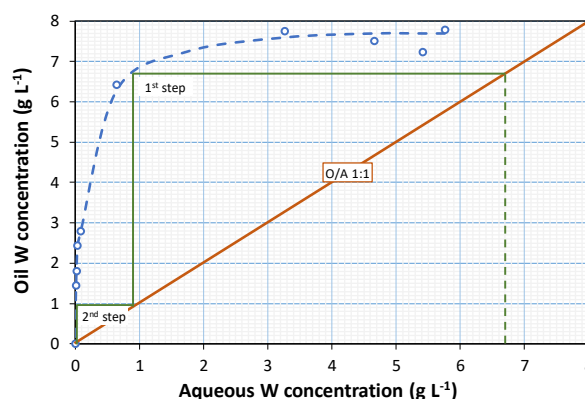


Figure 6. Determination of the number of MS by the McCabe-Thiele method.

### Scale-up of the process

With the aim to demonstrate the feasibility of the process, a certain amount of  $\text{WO}_3$  (26 g) was produced with high purity (96%). The global yield of the process was 80% (Figure 7).

The final product was analyzed by ICP-MS and XRD (

	Conc. %
$\text{WO}_3$	96.2
$\text{MgO}$	0.02
$\text{Al}_2\text{O}_3$	0.27
$\text{SiO}_2$	1.96
$\text{P}_2\text{O}_5$	0.92

K <sub>2</sub> O	0.02
CaO	0.11
TiO <sub>2</sub>	0.38
Others	0.11

Figure 8). ICP results show the high purity grade obtained (96%). The XRD diffractogram fits very well with the WO<sub>3</sub> spectra.

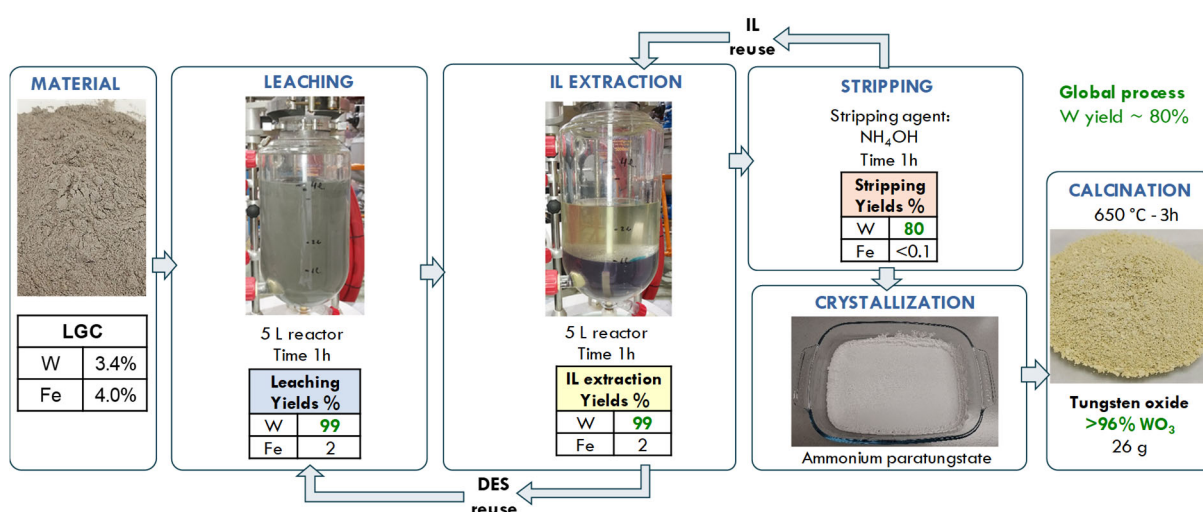


Figure 7. Layout of the process performed at higher scale (5 L reactor)

	Conc. %
WO <sub>3</sub>	96.2
MgO	0.02
Al <sub>2</sub> O <sub>3</sub>	0.27
SiO <sub>2</sub>	1.96
P <sub>2</sub> O <sub>5</sub>	0.92
K <sub>2</sub> O	0.02
CaO	0.11
TiO <sub>2</sub>	0.38
Others	0.11

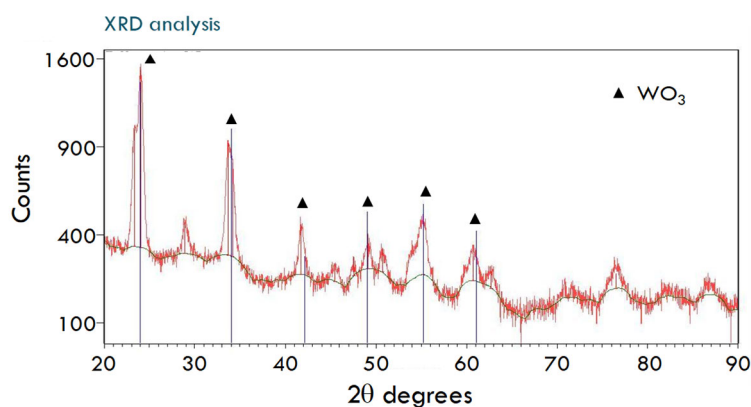


Figure 8. Left: ICP-MS analysis results. Right: XRD diffractogram.

## Conclusion

An environmentally-friendly process based on Ionic Liquids has been developed and tested at TRL4 with a global W recovery yield of 80%. This process is a good alternative to current SoA technologies involving strong acids/alkalis and high temperatures.



## Acknowledgements

This research was funded by the European Union's EU Framework Programme for Research and Innovation Horizon 2020 grant number 821159 (TARANTULA).

## References

- <sup>i</sup> United States Geological Survey (USGS). Tungsten Data Sheet - Mineral Commodity Summaries 2020. s.l. : U.S. Department of the Interior, 2020. <sup>ii</sup> Han, Z. et al. (2021). A review of tungsten resources and potential extraction from mine waste. Minerals, 11 , 701. <https://doi.org/10.3390/min11070701>
- <sup>iii</sup> Bhosale, S. N. et al. (1990) Current Practices in Tungsten Extraction and Recovery. High Temp. Bhosale, S. N. et al. (1990) Current Practices in Tungsten Extraction and Recovery. High Temp.
- <sup>iv</sup> Yurramendi, L et al. (2021). Recovery of Tungsten from Downstream Mineral Processing Fractions by Deep Eutectic Solvents. Mater. Proc., 5, 96. <https://doi.org/10.3390/materproc2021005096>

# ZINC RECOVERY FROM CHLORIDE MEDIA BY APPLYING THE HALOMET™ PROCESS.

Charmain Onoberhie,<sup>a</sup> Enrique Madrigal,<sup>a</sup> Sergio Sanguilinda<sup>a</sup> and Ana Belén Mejías.<sup>a</sup>

**Abstract.** This article describes HALOMET™ process, by Técnicas Reunidas S.A, for recovery of zinc from fly ash residue after incineration of municipal wastes. The process consist in a Solvent Extraction in chloride media, followed by Stripping with sulfuric acid. An economic and technical feasibility study has been conducted to demonstrate the applicability of the process, especially for small-scale operations.

**Keywords:** HALOMET, Zinc, Chloride, DEHPA, Fly Ash, Solid Waste, Incineration

## Introduction

The amount of Municipal Solid Waste (MSW) generated worldwide is ever-increasing. It is expected to rise by 70% to 3.4 billion metric tons by 2050.<sup>i</sup> Incineration is commonly used to reduce the volume of Municipal Solid Waste (MSW), with subsequent coproduction of energy and MSW Incinerator (MSWI) Ash. Bottom Ash is obtained from the base of the incinerator furnace and Fly Ash from the incinerator air pollution control systems.

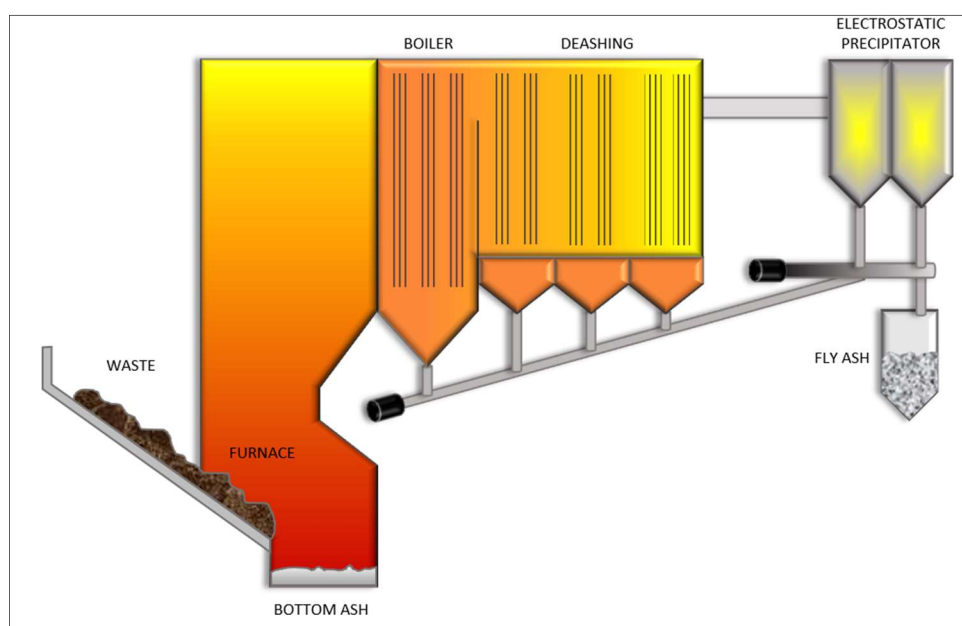


**Figure 1. Municipal Solid Waste Incineration<sup>ii</sup>**

MSWI Fly Ash typically contains high levels of chlorides and heavy metals such as zinc, lead, copper, cadmium, chromium, barium, and tin. Due to the presence of heavy metals, MSWI Ash poses a significant environmental risk and is therefore considered hazardous waste. In many countries, MSWI Fly ash must be treated before disposal.

As natural resources are depleted to meet growing population demands, there is increasing pressure to implement treatment processes that recycle or recover metals contained in waste

<sup>a</sup> TÉCNICAS REUNIDAS S.A. Proprietary Technologies Development Dept. 16 Calle Sierra Nevada, 28830 San Fernando de Henares, Madrid, Spain.

residues such as MSWI Fly ash. The HALOMET™ technology, developed by Técnicas Reunidas, is ideal for achieving this objective.

This paper summarizes the benefits of integrating the Técnicas Reunidas Proprietary HALOMET™ technology into the MSWI Fly Ash residue treatment process. It also includes a description of the HALOMET™ process and estimated CAPEX and OPEX costs associated with the implementation of this technology to recover zinc from a liquor solution obtained from treating MSWI Fly Ash residues. Zinc is recovered as an ultrapure zinc sulfate solution from which SHG zinc can be obtained using conventional zinc electrowinning. Alternatively, crystallization may be used to obtain a high-purity zinc sulfate product.

## **Background: Processing Routes of Incineration Residues**

As MSWI Fly Ash is a potential source of pollution, developing processes to stabilize or recover the heavy metals present is technically challenging.

The treatment methods typically used fall into three main categories: Thermal Treatment, Stabilization/ Solidification and Separation Techniques.

Thermal Treatments: The main objective of thermal treatment is to reduce the toxicity of the MSWI Fly Ash using heat. It achieves this by stabilizing the toxic components, so they are less likely to be leached from the treated residue. Thermal treatments include sintering, melting / vitrification, and thermochemical treatments.

Stabilization/ Solidification: In this case, stabilization processes reduce the toxicity of the fly ash by reducing the solubility of the contaminating components with or without solidification. Solidification processes reduce the leachability of the contaminants by encapsulating them using binders such as cement.

Separation Processes: These includes techniques such as washing, leaching, electrodialytic remediation, magnetic separation, and eddy current separation which are used to separate or recover the metallic components present in the fly ash.

In Switzerland, a large proportion of fly ash is treated using the FLUWA Process.<sup>iii</sup> This involves treating the fly ash with an HCl acid solution and a neutral scrub with lime. The liquor produced from the FLUWA Process can be treated using cementation with zinc dust to remove the lead, copper and cadmium present. The cementation liquor produced can be further treated to recover other contained metals.

This article focuses on the treatment of a chloride media zinc-bearing solution (such as process liquor generated via the FLUWA Process) to produce an Ultrapure Zinc Sulfate Solution using the Técnicas Reunidas HALOMET™ Process. An example of a zinc-bearing solution that may be treated via the HALOMET™ process is the following (all figures in g/l):

Zn 35 – 45, Ca 15 – 25, Mg 5 -15, Na 5 – 10, K 5 – 10, Cl 120 – 140

## HALOMET™ PROCESS

The HALOMET™ Process was originally developed by Técnicas Reunidas as an alternative route to process primary and secondary zinc raw materials in chloride media to produce a high purity zinc sulfate solution from which SHG zinc or other saleable zinc products (i.e. zinc sulfate) can be obtained. This process was derived from Técnicas Reunidas' ZINCEX™ Technology<sup>iv</sup> which is currently being used in three industrial zinc production plants: American Zinc Products (formerly Horsehead, USA), Portovesme Zinc Smelter (Italy), DOWA Metals and Mining (Japan) and Skorpion Zinc (Namibia). The HALOMET™ Process can be used when leaching in chloride media is favored over leaching in sulfate media.

### BLOCK DIAGRAM

Figure 2 below illustrates the use of the HALOMET™ Process to obtain an Ultrapure Zinc Sulfate Solution from a Chloride Media Zinc-Bearing Liquor Solution obtained from treating MSWI Fly Ash residues.

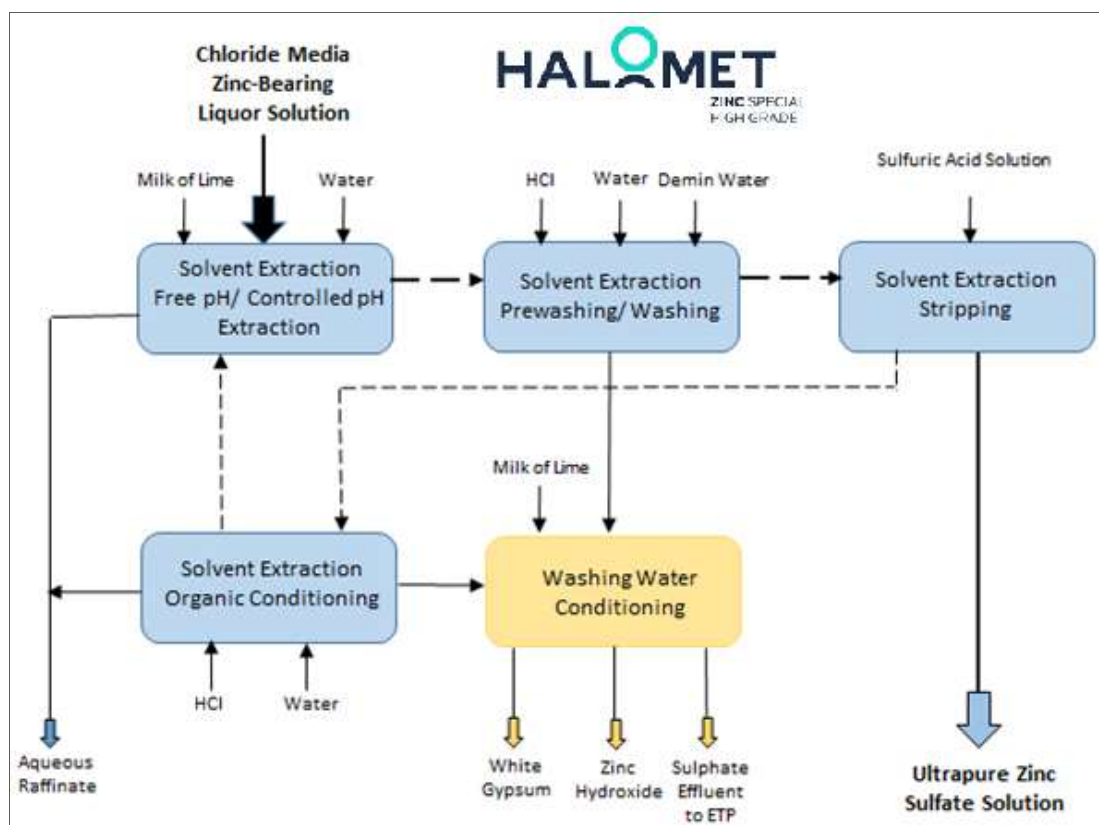


Figure 2. HALOMET™ Process Block Diagram

The solid lines represent the flow of aqueous process solutions throughout the processing circuit. The organic solution associated with the solvent extraction area is represented by dashed lines. The thick lines illustrate the flow of zinc from the raw material to the final zinc product.

As the diagram shows, the HALOMET™ Processing facilities include two major areas: 1) Solvent Extraction, including Controlled pH Extraction, Free pH Extraction, Prewashing, Washing, Stripping, and Organic Conditioning, and 2) Washing Water Conditioning

The Liquor solution is fed to the solvent extraction area where the zinc present is extracted and purified to produce an ultra-pure zinc sulfate solution which can be sent to a Zinc Electrowinning Cell-house to produce SHG Zinc Plates. Alternatively, the purified solution may be crystallized to produce a high-quality Zinc Sulfate product.

Washing liquor generated in the Solvent Extraction Area is sent to the Washing Water Conditioning Unit where it is neutralized and residual zinc is recovered and recycled to the upstream leaching unit.

## PROCESS DESCRIPTION

A more detailed description of the HALOMET™ Process Areas is provided in the following paragraphs.

### Solvent Extraction

The Solvent Extraction Area is comprised of several process units:

Extraction: In this unit, the zinc present in the aqueous PLS is extracted and transferred to an organic solution that contains a zinc-selective extractant. Acidity is generated during the extraction process. To optimize the extraction of zinc from the PLS and to minimize co-extraction of other impurities, the extraction process is carried out in two stages. During the first stage, zinc extraction is carried out at free pH. In the second stage, zinc extraction is carried out under controlled pH conditions. In this case, the acidity generated in the extraction process is neutralized using milk of lime. The Extraction process produces an acidic aqueous raffinate solution containing most of the impurities present in the Zinc-Bearing Liquor Solution. A zinc-loaded organic phase is also produced, and this is sent to the Washing Unit.

The aqueous raffinate, generated by the HALOMET™ Process can be treated using standard water treatment units before disposal. This facilitates the integration of the HALOMET™ Process in existing industrial facilities.

Washing: The washing process is carried out in two steps: prewashing and washing. The zinc-loaded organic phase is first pre-washed using a dilute hydrochloric acid solution to remove co-extracted calcium. In the following washing step, the organic phase is washed with demineralized water and a sulfuric acid solution to remove the remaining co-extracted impurities. The washing process generates a purified zinc-loaded organic phase which is sent to the stripping unit. Washing liquor produced is sent to the Washing Water Conditioning Area.

Stripping: The zinc present in the washed zinc-loaded organic solution is stripped using a high-purity sulfuric acid solution. In the solvent extraction stripping process, the zinc is transferred from the organic solution to the sulfuric acid solution, producing an ultrapure zinc sulfate solution. The stripped organic solution is sent to the organic conditioning unit.

Organic Conditioning: During the solvent extraction process, small quantities of iron are co-extracted from the PLS along with the zinc. Small droplets of sulfate-containing aqueous fluid are also entrained in the organic phase. The organic conditioning unit removes the

sulfates and iron present in the organic phase before it is returned to the main solvent extraction circuit.

#### Wash Water Conditioning

The purpose of the Wash Water Conditioning Unit is to recover sulfates and zinc from the washing liquor solution generated in the Solvent Extraction Area. Sulfate is recovered as gypsum, by partial neutralization of the washing liquor solution with milk of lime. Further neutralization of the washing liquor precipitates the zinc present as zinc hydroxide. The zinc hydroxide produced is recycled to the upstream leaching unit. The conditioned liquid stream is sent to the effluent treatment plant for further treatment prior to disposal.

### **Benefits of HALOMET™ PROCESS**

The HALOMET™ process offers several advantages relative to conventional zinc production processes:

#### Suitability for Leaching in Chloride Media

This process can be used when leaching in chloride media is favored over leaching in sulfate media, as in the case of treatment of MSWI Fly Ash residues. This specifically applies if lead is to be recovered along with zinc.

In chloride media, HALOMET™ Technology permits the interchange of chlorides with sulfates, producing a high-purity sulfate electrolyte that can be processed using conventional electrowinning.

Although many research studies illustrate the technical feasibility of producing zinc from a zinc chloride electrolyte solution using electrowinning, the implementation of such a process at an industrial scale is more problematic than conventional electrowinning in sulfate media.<sup>v</sup>

Electrowinning in chloride media requires more a complex cell design and the use of more expensive construction materials due to the presence of chlorides and wet chlorine gas generated as a by-product. These are some of the reasons why there are no industrial zinc production plants using zinc chloride electrolysis in operation today.

#### Recovery of Zinc From Waste Residues

The most significant benefit of using the HALOMET™ Process is that it can be easily integrated into industrial processes to recover valuable metals from waste residues. Many of these waste residues are currently sent to landfill sites, incurring additional costs and increasing the environmental load. Implementing the HALOMET™ process helps to reduce the production of waste residues and makes a positive contribution to the circular economy.

Given that transportation of residues containing high concentrations of heavy metals can be problematic, integration of the HALOMET™ technology into the industrial facilities where these residues are generated would be highly advantageous.

### Ideal for Small-Scale Zinc Production

Most of the zinc production plants that are currently in operation have production capacities of between 100 000 to 300 000 tons/year. It is rare to find zinc production facilities with capacities of less than 20 000 tons/year.

As an example, taking into account the annual production of MSWI Fly Ash and the quantity of contained zinc, the amount of zinc metal that could potentially be obtained from leaching this waste material would be much less than 20 000 tons/year. Although this zinc production capacity is atypically low, the HALOMET™ process is ideal for this application.

### Versatility and Ease of Operation

The composition of waste residues is highly variable. This especially applies to MSWI Fly Ash residues whose quantity and composition fluctuate on a seasonal or even daily basis. The HALOMET™ process is the perfect candidate for treating these residues, as it is highly versatile and capable of handling fluctuations in raw material composition and throughput to produce an ultrapure zinc sulfate solution.

Regardless of variations in the raw material input, the HALOMET™ process remains easy to operate and maintain.

## **Viability of HALOMET™**

Técnicas Reunidas recently carried out a Preliminary Feasibility Study to evaluate the technical and economic feasibility of implementing the HALOMET™ Process to produce 2 000 t/y SHG zinc from a chloride media zinc-bearing liquor solution obtained from treating MSWI Fly Ash. The study included the Solvent Extraction and Washing Water Conditioning Areas.

### Inlet and Outlet Flows

The principle inlet flows to the HALOMET™ Process are the chloride media zinc-bearing liquor solution and the reagents and utilities required for the process. The main reagents and utilities for the HALOMET™ Process are milk of lime, hydrochloric acid, sulfuric acid, process water, demineralized water and electrical power.

The main outlet flows from the HALOMET™ Process are:

- Ultrapure Zinc Sulfate Solution: This may be used to produce SHG Zinc sheets via electrowinning or a High-Purity Zinc Sulfate product using crystallization.
- Aqueous Raffinate: This consists of a calcium chloride solution that contains all of the impurities present in the zinc-bearing liquor solution, but practically no zinc.
- White Gypsum: This is produced as a by-product that can be used in the construction industry.
- Liquid Effluent: This contains small quantities of metallic sulfates, which must be removed before disposal.

- Zinc Hydroxide: This is recycled to the upstream leaching process to recover the contained zinc.

### Plant Footprint Estimate

The estimated surface footprints for the process areas associated with the HALOMET™ plant are indicated below:

- Solvent Extraction: 1 300 m<sup>2</sup>
- Washing Water Conditioning: 200 m<sup>2</sup>

### Preliminary Economic Estimates

Based on the design prepared during the Feasibility Study, the order of magnitude Investment Cost estimate for the HALOMET™ Plant with a zinc capacity of 2 000 t/year is approximately 12 million Euros. The Operating Cost Expenditure is estimated at 3 million €/year, this equates to 1 500 €/t zinc.

## **Conclusions**

At present, a large proportion of the MSWI Fly Ash residues produced are sent to landfill sites. This incurs disposal costs and is a potential threat to the environment. Given that these residues contain significant quantities of heavy metals such as zinc, lead, copper, and cadmium, integrating the HALOMET™ technology into the fly ash treatment circuit is an effective means of recovering and recycling the contained zinc.

The HALOMET™ process is highly versatile. It can be used for small scale zinc production and is one of the few technologies capable of treating impure zinc chloride liquor solutions generated during MSWI Fly Ash treatment to produce a high-purity zinc sulfate solution. Depending on the market requirements, the final stages of the HALOMET™ process can be adapted to enable the production of SHG zinc sheets via conventional zinc electrowinning or to produce a solid zinc sulfate product using crystallization.

This paper shows the benefits of integrating the HALOMET™ technology into MSWI Fly Ash treatment circuits. It also describes the potential use of this technology for the treatment and revalorization of other waste residues, thus helping to sustain a circular economy.

## **References**

---

<sup>i</sup> Global Waste Generation - Statistics & Facts: <https://www.statista.com/topics/4983/waste-generation-worldwide/>

<sup>ii</sup> Altaf Hussain Kanhar, Shaoqing Chen, and Fei Wan. *Incineration Fly Ash and Its Treatment to Possible Utilization: A Review*. Energies (2020)

<sup>iii</sup> Idem

<sup>iv</sup> G. Díaz, A.B. Mejías, D. Martín, F. Cubeddu. *ZINCET™ Technology: Recent Industrial Operations*. Proceedings of Hydrometallurgy (2014)

<sup>v</sup> Donald J. MacKinnon, John M. Brannen. *Zinc Electrowinning from Chloride Electrolytes*. Journal of Applied Electrochemistry (1983)



# Nickel and Copper Recovery from Sludge Waste Enhancing Circular Economy for the Galvanic Industry

Nuria Ocaña,<sup>a</sup> María Teresa Pinedo,<sup>a</sup> Emilio Pecharroman,<sup>a</sup> María Frades<sup>a</sup>

**Abstract.** This paper describes bench and pilot testwork for recovery of Nickel and Copper from galvanic wastes from automotive industry. Solvent extraction was employed to produce solutions recyclable to galvanic plants.

**Keywords:** Nickel, Copper, Galvanic Sludge, Solvent Extraction, LIX 984N, Cyanex 272, McCabe-Thiele, Pilot Plant.

## Introduction

Presently, the demand for copper and nickel has risen worldwide and alternative sources are needed to meet future demand. On the other hand, galvanic sludge production in EU countries nowadays reaches 150.000 tons per year. These sludges contain high levels of heavy metals, representing a serious hazardous waste. Heavy metals pollution is most harmful due to their high toxicity and persistence. According to EU Directive, galvanic sludge solid residues, must fulfil very strict criteria before landfilled. Overall cost of galvanic sludge disposal is near 230.000 € per ton. The potential recycling of sludges is a potential source of global savings. Finding efficient solutions to recover critical metals from sludges has become a great interest. Various methods have been researched, such as sludge inertisation, stabilization of heavy metals in stable matrices or separation of valuable components for other industries.

For three years, Técnicas Reunidas has worked, in a multidisciplinary team, to develop a purification process based on liquid-liquid solvent extraction, to extract Ni and Cu with high purity standards from galvanic wastes. Wastes provided by a Spanish automotive industry were used as raw material, real solutions were studied, and a wide array of chemical extractants were screened. After a thoughtful study, two process schemes, one for Ni and one for Cu, were defined to be run at pilot scale.

## Testwork

Spent galvanic wastes provided by a Spanish automotive industry were received at the facilities of Técnicas Reunidas' José Lladó Technological Center. The objective of this work was to purify them, obtaining loaded strip solutions with a concentration close to the starting Cu and Ni galvanic baths, so that they can be used in the automotive industry, once purified.

Solvent extraction (SX) is a well-established technique for the removal of Cu and Ni and hydroxyoximes are well-known extractants, which are widely used for copper extraction from dilute acidic sulphate solutions. The choice of diluent is an important aspect of successful SX operation. A diluent reduces the viscosity of the extractants, but sometimes the nature of diluent affects the extraction process. To investigate this, the extraction of copper and nickel was carried out using two different diluents: ShellSol D70 and Escaid 110. The extraction

---

<sup>a</sup> TÉCNICAS REUNIDAS S.A. Proprietary Technologies Development Dept. 16 Calle Sierra Nevada, 28830 San Fernando de Henares, Madrid, Spain. [nocana@trsa.es](mailto:nocana@trsa.es)

efficiency of certain extractants depends significantly on temperature, and therefore the extraction of copper and nickel was studied at different temperatures.

## Copper Solvent Extraction

Copper pregnant liquor solution had the following composition:

Cu: 52 g/L Fe: 29 ppm Zn: 43 ppm  $\text{Cl}^-$ : 69 ppm  $\text{SO}_4^{2-}$ : 153 g/L  $\text{H}_2\text{SO}_4$ : 87.3 g/L

Determined by Inductively Coupled Plasma Optical Emission by spectroscopy (ICP-OES), using PERKIN ELMER equipment.

The extractants selected for copper SX were the following:

- Acorga P5100: 2- hydroxy-5-nonylbenzaldoxime.
- Acorga M5640: 2-hydroxy-5-nonylbenzaldehyde.
- LIX 984 N: a mixture of 5-nonylsalicylaldoxime and 2-hydroxy-5-nonylacetophenone oxime.

These extractants are hydroxyoximes, and they have two active groups: one is the OH of the phenolic group, which has a low acidity, and the other is the oxime group, in which there is a nitrogen atom with a free pair of electrons. As a result, a complex is formed with copper, like the one shown in Figure 01.

Two diluents, at different concentrations and temperatures, were selected for copper SX:

- Shellsol D70 and Escaid 110.
- Extractant concentration: 25% and 40%
- Temperature: 20°C and 40°C.

The tests were carried out keeping the contact time at 5 minutes, with an organic-to-aqueous ratio O:A equal to 1.

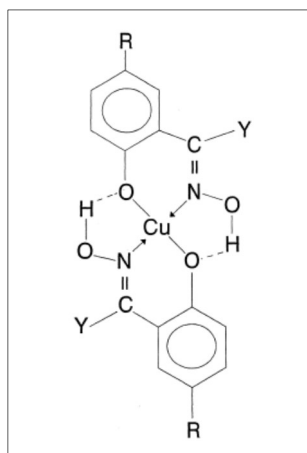


**Figure 01. General structure of the complex formed between copper and hydroxyoximes.**

**Figure 02. Separation of the aqueous and organic phase after copper SX**

**Figure 03. Jacketed funnels for Copper SX.**

The tests were carried out in jacketed glass funnels (figures 02 and 03) agitated and thermally regulated by hot water bath. Experiments were carried out at 20°C and 40°C at two concentrations of extractant 25% (v/v) and 40% (v/v) with two different diluents (Escaid and ShellSol)

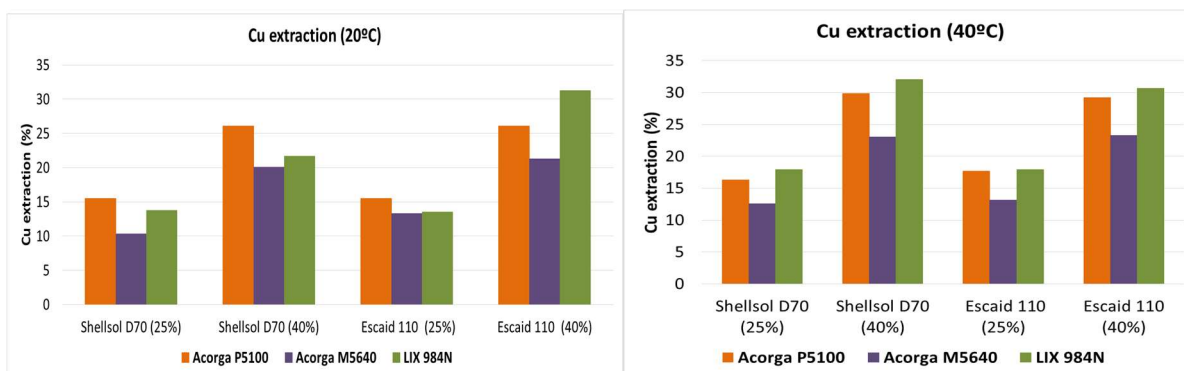


**Figure 04. Results of copper SX at 20°C and 40°C**

After the extraction process, the metal concentration in aqueous raffinate and loaded organic phases were determined by ICP-OES. The results of Cu SX are shown at Figure. Comparing the results above, it was observed that Acorga P5100 and LIX 984N were the extractants that give the highest efficiency. It was also observed that increasing temperature from 20°C to 40°C, copper extraction increases. At 40°C, using Shellsol D70 as a diluent, the extraction efficiency of Cu is slightly higher than using Escaid 110.

To establish a copper extraction isotherm, an aqueous solution containing 52 g/L copper (II) at initial pH of 4, was used for the extraction of copper with 40% (v/v) LIX984 N in Shellsol D70 at 40°C during 5 minutes. The isotherm was obtained by contacting the aqueous solution at O:A phase ratios ranging from 0.5 to 8. The results are shown in Figure 05.

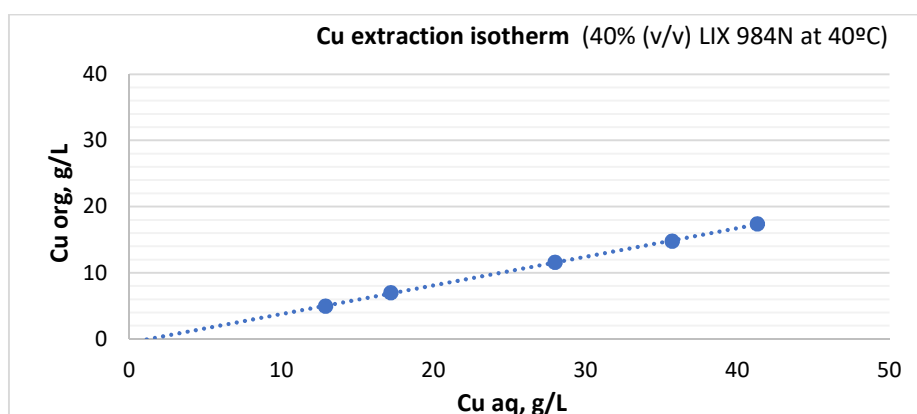


**Figure 05. Extraction isotherm of copper.**

To determine the number of stages required for the extraction of copper, a McCabe-Thiele plot was constructed for O:A ratios from 0.5 to 8, with a constant total volume of the phase. To determine stripping behavior, the copper loaded organic phase was stripped using 155 g/L of sulfuric acid at 40°C, at O:A ratios from 0.5 to 10, for 5 minutes.

With both series of data, A McCabe-Thiele plot was constructed (figure 06). The result is five stages of stripping at an O:A ratio of 5. The analysis show 39.6 g/L Cu in the loaded strip solution, leaving 4.9 g/L copper in the organic phase. The plot shows that < 20 g/L copper will remain in the aqueous raffinate after five extraction stages at O:A ratio equal to 4.4.

The McCabe-Thiele forecast was verified in a copper pilot plant (figure 07) running in continuous during 130 hours to process 300 liters of solution from automotive galvanic

wastes. The remaining Cu in the aqueous raffinate was 15 g/L. Concentration in the stripping loaded solution was 44 g/L Cu, leaving 3.92 g/L Cu in the organic phase. Copper recovery efficiency was 67%.

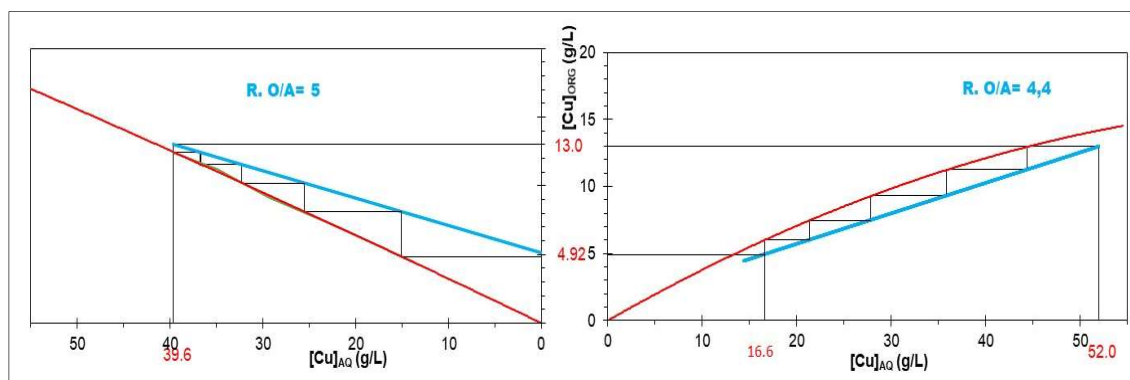


Figure 06. McCabe-Thiele for copper with 40% (v/v) LIX 984 N in Shellsol D70 at 40°C



Figure 07. Copper SX pilot plant

## Nickel Solvent extraction

Nickel pregnant liquor solution (PLS) had the following composition, determined by ICP-OES.:  
Ni: 73.2 g/L Fe: 3.9 ppm Zn: < 1 ppm Cl<sup>-</sup>: 6.3 g/L SO<sub>4</sub><sup>2-</sup>: 106 g/L pH: 4.1.

The extractants selected for Ni are the following:

- D2EHPA: Di-(2- ethylhexyl) phosphoric acid an organophosphorus compound with the formula (C<sub>8</sub>H<sub>17</sub>O)<sub>2</sub>PO<sub>2</sub>H.
- Acorga M5640: 2-hydroxy-5-nonylbenzaldehyde oxime modified with a fatty ester.
- CYANEX 272: bis(2,4,4- trimethylpentyl) phosphinic acid.
- LIX 84 I: 2-hydroxy-5- nonylacetophenone oxime, insoluble in water and contains a hydrocarbon diluent with a high flash point.

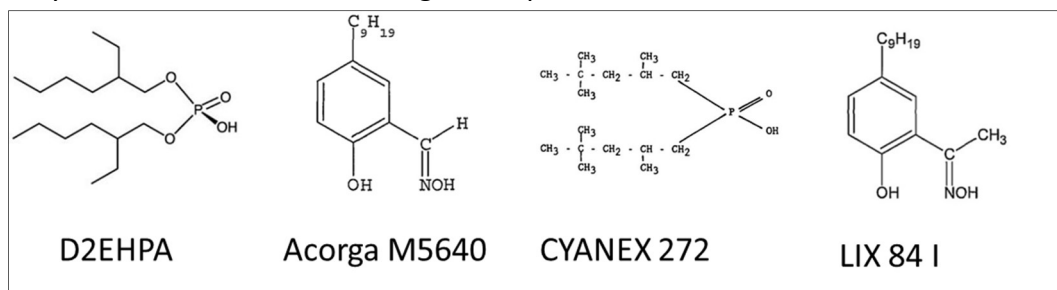


Figure 08. Molecular formulas of nickel extractants.

These extractants were studied with two different diluents, with an extractant concentration of 50% and a temperature of 40°C. The diluents used were Shellsol D70 and Escaid 110. The contacts were made for 5 minutes at O:A ratio 1. No pH control was performed. After the extraction process, the metal concentration in the raffinate and in the loaded organic phase was determined by ICP-OES. The results are shown in Table 1

**Table 1. Results of Ni solvent extraction with free pH**

Organic	LIX84I	LIX84I	D2EHPA	D2EHPA	Acorga M5640	CYANEX 272
Diluent	Shellsol D70 (50%)	Escaid 110 (50%)	Shellsol D70 (50%)	Escaid 110 (50%)	Shellsol D70 (50%)	Shellsol D70 (50%)
pH <sub>aq final</sub>	2.16	2.16	1.68	1.67	1.88	3.25
Extraction efficiency, %	1.1	1.0	2.2	2.2	1.8	0.2

Under the conditions studied, nickel extraction efficiencies were very low.

A new series of experiments was carried out to study the effect of equilibrium pH on the extraction of nickel using Cyanex 272. The tests were carried out using 50% (v/v) Cyanex 272 in Shellsol D70 at 40°C at a controlled pH in a range of 5 to 6.5. The pH was maintained during the test with a 200 g/L NaOH solution. Agitation time was 5 minutes. The results are shown in Table 2.

**Table 2. Results of Ni with 50% (v/v) Cyanex 272 at 40°C and controlled pH.**

pH <sub>aq final</sub>	5	5.5	6	6.5
Extraction efficiency, %	15	21	50	76

The success of these new tests is due to the fact that the extraction were carried out at a controlled pH, keeping it constant during the whole extraction process. At pH 6.5 the highest extraction of nickel is achieved. In a single contact, the nickel extraction efficiency reached 76%. But it was also observed that, above pH 5.5, phase separation is not good under the conditions studied, with a fully emulsified organic phase, as shown in figure 09.

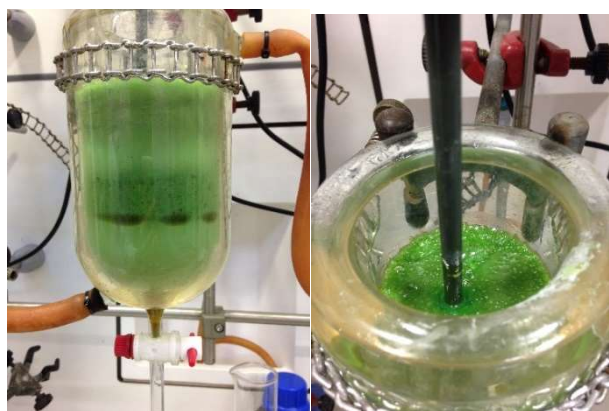


**Figure 1. Emulsion 50% Cyanex 272 at pH 5.5**

Cyanex 272 concentration, %	20	20	20	30
pH	5.0	5.5	6.0	6.0
Phase separation O:A	Fast	Fast	Fast	No separation
Extraction efficiency, %	3	9	25	--

**Table 3. Effect of Cyanex 272 concentration and pH in Ni extraction.**

To avoid the emulsion of the phases, tests were carried out maintaining the temperature at 40°C, with a contact time of 5 minutes. The variables studied were: extractant concentration and pH. The extractant concentration studied was 20% (v/v) and 30% (v/v) Cyanex 272 with Shellsol D70 and working pH 5, 5.5 and 6. The results are shown in

Table 3.A proportion of 20% (v/v) makes the phase separation substantially better than at 30% (v/v). At pH 6, it was not possible to separate the organic and aqueous phases.

To generate isotherms, a solution containing 73 g/L nickel (II) at pH of 4.0 was used for the extraction of nickel with 20% (v/v) Cyanex 272 in Shellsol D70. The isotherm (Figure 20) was obtained at different O:A phase ratios at pH 6 and 5.5 (adjusted by 200 g/l NaOH). Contact time was 5 minutes and temperature 40°C.

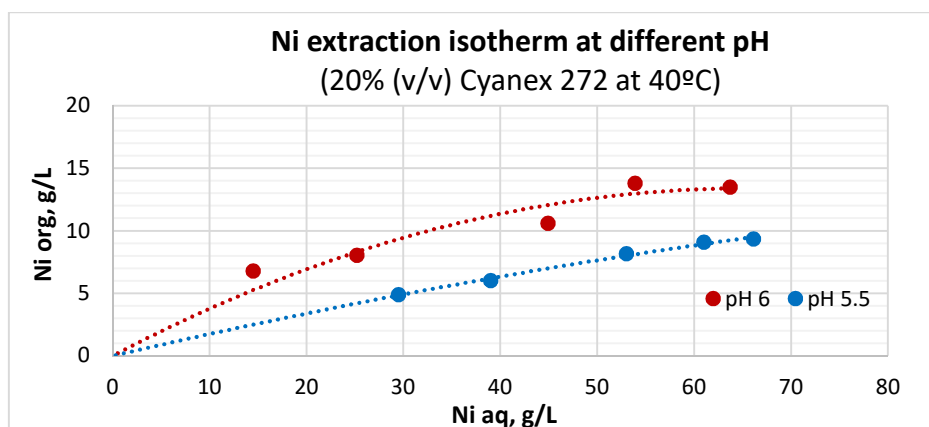


Figure 2. Extraction isotherm of nickel at pH 6 and 5.5

After the isotherms, it was confirmed that Ni extraction efficiency is higher at pH 6 than at 5.5. The phase separation of the different contacts was good and fast.

A McCabe-Thiele plot (figure 11) was constructed for O:A ratios from 0.5 to 8, with the total volume of the phase kept constant. The nickel loaded organic phase was stripped using 120 g/L of sulfuric acid at equal phase ratios for 5 minutes at 40°C. The result is two stages of stripping at an O:A ratio of 7. The analysis show 73 g/L Ni in the loaded strip solution, leaving only 0.1 g/L nickel in the organic phase. The McCabe-Thiele plot shows that < 1.5 g/L nickel will remain in the raffinate after four extraction stages at an O:A ratio of 6.6.

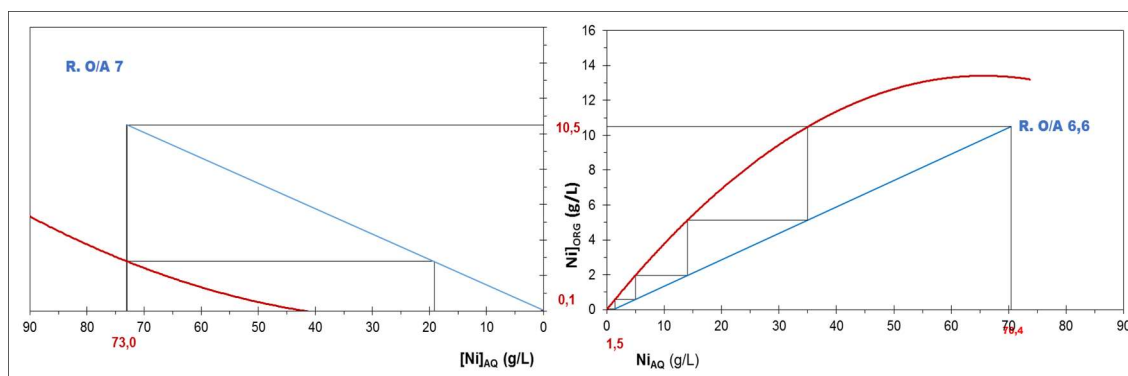


Figure 11. McCabe-Thiele for nickel with 20% (v/v) Cyanex 272 at 40°C and pH 6



McCabe-Thiele forecast was validated in a pilot plant running continuously during 200 hours to process 200 liters of solution from galvanic wastes. Analysis of nickel aqueous and organic were carried out periodically. The remaining Ni in the aqueous raffinate was 0.084 g/L, the content in the loaded electrolyte was 68 g/L Ni, leaving 0.01 g/L Ni in the organic phase, obtaining recovery yields up to 95%. Pilot plant for nickel is shown in Figure 32.



Figure 3. Nickel SX pilot plant

## Conclusions

Effective extraction of copper from an aqueous feed solution containing 52 g/L copper (II) was achieved with 40% (v/v) LIX 984N in Shellsol D70 at 40°C. Piloting of the copper recovery process from galvanic sludges was demonstrated using 300 L of a waste solution, leaching solution with 52 g/L Cu, yielding an overall recovery efficiency of 67%.

Nickel (II) extraction from an aqueous solution containing 73 g/l nickel was performed by 20% (v/v) Cyanex 272 in Shellsol D70 at 40°C. For piloting nickel process, 200 L of galvanic industry waste solution, with 73 g/L Ni was fed to the plant, obtaining recovery yields up to 95%.

Purified Ni and Cu solutions produced under these pilot plants were tested and successfully validated by a galvanic industry partner in their production process, with satisfactory results.

The achieved results have proved that both processes are technically feasible. As a result, these processes could enhance the galvanic industry with a close loop technology to contribute to the implementation of a circular economy strategy. This approach would help fulfilling the Sustainable Development Goal.

## References

---

- [1] A Silva Guimaraes, P. Siquiera da Silva, M. Borges Mansur, *Purification of nickel from multicomponent aqueous sulfuric solutions by synergist solvent extraction using Cyanex 272 and Versatic 10*, Hydrometallurgy 150, December 2014
- [2] Le, H.L., Jeong, J., Lee, J.C., Pandey, B.D., Yoo, J.M., and Huyunh, T.H., *Hydrometallurgical process for copper recovery from waste printed circuit boards (PCBs)*. Mineral Processing & Extractive Metallurgy Review, (32), 2011, pp. 90-104.

[3] R.E. Molnar, N. Verbaan, 2003, *Extraction of copper at elevated feed concentrations*, materials presented at Hydrometallurgy 2003 – Fifth International Conference, Vol. 2: Electrometallurgy and Environmental Hydrometallurgy.

[4] Sole, K.C., and Hiskey, J.B., *Solvent extraction of copper by Cyanex 272, Cyanex 302 and Cyanex 301*. Hydrometallurgy, (37), 1995b, pp.129.

[5] J. Szymanowski, 1993. *Hydroxyoximes and Copper Hydrometallurgy*, CRC Press, Boca Raton, FLG.

[6] P.K. Kuipa, M.A. Hughes, *Diluent effect on the solvent extraction rate of copper*, Sep. Sci. Technol. 37 (2002) 1135–1152.

[7] Y. Marcus, *Diluent effects in solvent extraction*, Solvent Extr. Ion Exch. 7 (1989) 567–575.



# ZINCEX<sup>TM</sup> Process Applied on Manganese Bearing Materials

Emilio Pecharromán,<sup>a</sup> Sergio Sanguilida,<sup>a</sup> Ana Belén Mejías<sup>a</sup> and Nuria Ocaña<sup>a</sup>

**Abstract.** This paper describes testwork results and process alternatives that have been evaluated at laboratory scale to enable recovery of the manganese present in a raw material feed to produce saleable manganese by-products, or as a potential reagent for the cell house at ZINCEX<sup>TM</sup> process.

**Keywords:** Zinc, Manganese, D2EHPA, ZINCEX, Solvent Extraction, Electrowinning, Oxidation, Reduction, Crystallization, Ozone, Hypochlorite, Carbon, Peroxide, Sulfide.

## Introduction

Traditionally zinc production from zinc sulfide concentrates is based on the Roasting, Leaching and Electrowinning (RLE) process. The concentrates containing Zn as zinc sulfide are roasted to give zinc oxide calcine. The gaseous SO<sub>2</sub> outlet requires an annexed sulfuric acid plant. Zinc oxide calcines are leached with sulfuric acid solution generating a Pregnant Leach Solution (PLS). This PLS is purified by Cementation with Zn dust to remove metallic impurities such as Cu Ni and Co, and the purified solution is submitted to Electrowinning (EW), to yield cathodic metallic zinc. In this process, there is one single circuit between Leaching and Electrowinning, therefore a high grade PLS is required for a successful EW. A most careful control on impurities removal stages is performed to avoid impurities passing to the advanced electrolyte to achieve a high-grade zinc product.

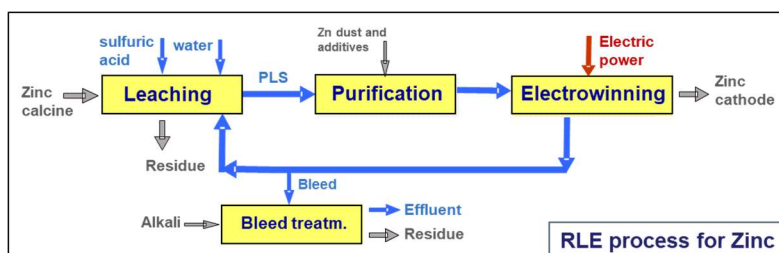


Figure 01. Hydrometallurgical circuit at RLE process.

## Background. The ZINCEX<sup>TM</sup> process

Técnicas Reunidas, S.A. (TR) developed the ZINCEX<sup>TM</sup> Process, the industrial and proven alternative to traditional RLE. Purification of PLS is performed by Solvent Extraction (SX), which constitutes an effective barrier for impurities and a buffer for changes in the composition of the PLS. ZINCEX<sup>TM</sup> process has the ability to treat primary and/or secondary zinc materials for the recovery of zinc in circumstances where significant amounts and a wide variety of impurities are present. These include most of transition metals at higher amounts than Cementation, as well as halides (Cl, F) and alkalines (Mg, Ca, K, Na).<sup>i</sup>

The current version of the process was developed in Spain, in the 1970's and first applied to medium-scale facilities in Spain and Portugal.<sup>ii</sup> On 2000, with Skorpion Zinc Project, in Namibia, the SX technology leaped to a high-scale primary-ore operation. Application of

<sup>a</sup> TÉCNICAS REUNIDAS S.A. Proprietary Technologies Development Dept. 16 Calle Sierra Nevada, 28830 San Fernando de Henares, Madrid, Spain. [epecharroman@trsa.es](mailto:epecharroman@trsa.es)

ZINCEX™ process at Skorpion Zinc has allowed the successful utilization of an ore with composition not regarded as treatable by RLE.<sup>iii</sup> Besides, it has made possible the processing of secondary material with high content in chloride and fluoride, which are harmful impurities that cannot be removed by the traditional Cementation purification. In this way, secondaries have been incorporated into process, as satellite facilities annexed to a pre-existent RLE factory (Akita Zinc in Japan,<sup>iv</sup> Portovesme in Italy)<sup>v</sup> or as a stand-alone facility, devoted 100% to zinc recycling (American Zinc Recycling in the USA)<sup>vi</sup>.

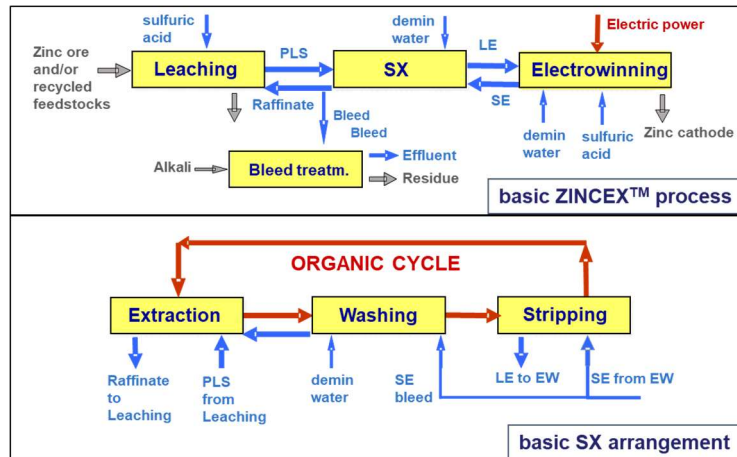


Figure 02. ZINCEX™ basic process arrangement and detail on SX arrangement.

## Manganese at Zn Electrowinning Industry

Manganese is naturally present in zinc sulfide ores, in significant amounts. The usual range is up to 0.8% in the concentrates, but 0.4% is the preferred maximum limit. Manganese is one of the impurities that are not precipitated, either by Neutralization or by Cementation. Except for the bleed, leached manganese is not removed at any extension at RLE purification processes, so all manganese in the PLS reaches the EW unit. An excess of Mn will reduce the capacity of the solution to hold zinc and will raise the density and viscosity of the electrolyte, increasing cell voltage. Cell voltage may increase by 0.05 per cent per 1 g/L Mn.<sup>vii</sup>

When Pb-Ag cathodes are used (which is the standard in industry), Manganese helps protect anodes from corrosion, and some concentration is required in the electrolyte (typically 2 to 5 g/l). Manganese dioxide precipitates, becoming the major constituent of the cell sludge and causes the need to periodically brush the anodes. This sludge may be returned to the process or disposed, providing a way out of the process. It is regarded that the upper limit for Mn concentration in EW is about 15 g/l, because above, brushing frequency required would be excessive, disrupting the cellhouse operation. The other resort to control Mn is the overall volumetric bleed of the circuit. The bleed is submitted to a treatment to recover zinc from it, usually precipitation of Basic Zinc Sulfate (BZS). At this point, Mn co-precipitates with zinc and gets partially returned to the main circuit. Thus, a high Mn concentration hinders the operation, preventing an effective zinc recovery from the bleed.

Thus, manganese constitutes, at the same time, a contaminant in the feedstock and a necessary input to ensure a smooth EW. Standard zinc concentrates contain enough manganese so that no additional input is required for EW in a RLE operation, but a

concentrate with an excess of Mn would attract penalties at market. If a facility specifically devoted to reduce manganese content is to be implemented in a RLE circuit, the point is either the PLS stream or the purified solution entering EW. Due to the one-loop nature of the process, either location needs to be in-line with the rest of the plant. This means that a stop or malfunction of this facility would hinder or stop the zinc production, which becomes a serious risk.

The situation is nearly the opposite in ZINCEX<sup>TM</sup> process. Manganese is effectively removed by the SX, along with the rest of impurities mentioned above. The ability to treat high Mn solutions has been clearly demonstrated both at pilot and at industrial scale. In 1997, a plant near Barcelona, Spain, was commissioned to recover zinc from 2,800 t/y of spent domestic batteries. The feed to Leaching unit was a battery dust containing 26% Mn and 21% Zn, along with high amounts of Ni, Cd, Fe and Cl. The resulting PLS was totalling 22 g/l Zn and 50 g/l Mn that were separated by SX in an arrangement similar to the one shown at figure 02.

At this point, ZINCEX<sup>TM</sup> process allowed the implementation of an innovative pathway to circular economy, yielding, as products, a high purity Zn electrolyte and Mn sulfate salt for agricultural use. This plant did set a benchmark on the zinc solvent extraction technology, and its ability to separate zinc from manganese.<sup>viii</sup> This technology can find new applications, in current mining development projects where the presence of manganese would disrupt the zinc production. Some examples of such ores around the world are Mehdiabad (in Iran)<sup>ix</sup> and Gamsberg (in South Africa),<sup>x</sup> but in a context of continuous zinc demand growth, the interest to benefit new ores is increasing, and ZINCEX<sup>TM</sup> can be the keystone that brings such projects into more favourable numbers.

Once the problem of separating Mn and Zn is solved by application of SX, the issue remains to recover Manganese as a market by-product that adds value to the whole operation. As a starting point, Manganese is recovered from the bleed stream, after all zinc has already been taken away. This means that any upset in Manganese facility will not affect at all the main plant and zinc production. This makes a major difference with RLE, and avoids the risk of unwanted plant stops.

## **Study for Recovery of Manganese at ZINCEX<sup>TM</sup> plants.**

Several technological options are available for this purpose, to render commercial products of manganese. A techno-economical study has to be outlined to determine the best solution for each case. It may not be the same at a plant treating recycled feedstock or primary ore, or at a medium or large size operation. Location of the facility will be also a critical aspect to consider in the economical assessment. Added to this interest on Mn recovery, it has to be stated that Mn is a necessary input to Zinc Electrowinning cellhouses, at least while cathodes of Pb-Ag are the standard in this operation. The concentration of Mn required in EW (2 to 5 g/l) has to be provided into the cellhouse, by means of a controlled addition of Mn, either as metal flakes or as high-purity sulfate salt (MnSO<sub>4</sub>). It is an ironic fact that the high performance of SX purification makes this additive necessary, when it would be naturally provided by the solid feed. Thus, the possibility to treat high-manganese ores by ZINCEX<sup>TM</sup> shows the potential, not only to yield a commercial by-product, but also to re-utilize part of

this manganese into electrowinning, after a proper purification, which will greatly optimize the operating costs.

Therefore, two lines of work are devised for this study, according to Técnicas Reunidas approach: obtaining a commercial by-product and/or recovery of Mn to be used into Electrowinning. In fact, they are not necessarily separate routes. Depending on the amount of Mn in feedstock, the autonomy of supply to EW could be the only objective or, on the other hand, it may be found that purification of Mn to the point required for EW is not economical in the facilities, and only the by-product makes sense. A third scenario would be to employ part of the commercial by-product as starting point for a further process that yields the required additive in EW. A fourth scenario would be to produce the purified solution in excess, so that EW needs are covered, and the rest of solution is employed to manufacture a commercial product with a higher added value.

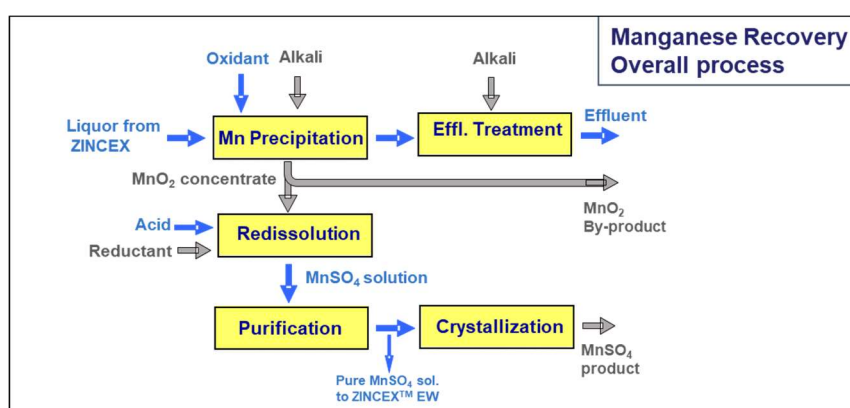


**Figure 03. Overall Flowsheet for Mn Recovery, independent of main Zn production line.**

In an industrial scale hydrometallurgical plant devoted to primary ore treatment, the most logical and synergistic route is to recover a Manganese Dioxide concentrate (MnO<sub>2</sub>). These concentrates, from pyrolusite or similar minerals, are the most prominent share of the manganese worldwide market, used for production of ferro-manganese alloys to be used at steel industry. Thus, Técnicas Reunidas has been performing the required testwork to produce such a concentrate, aiming at a high purity and a content of Mn that would make it comparable to commercial concentrates, or better. As a second activity, purification of the MnO<sub>2</sub> concentrate to be re-used as an EW additive has been studied.

The conversion of purified solution to a valuable commercial product has also been regarded. Crystallization to dry pure MnSO<sub>4</sub> is depicted in the figure, but other alternatives, such as Electrowinning to render metal or oxide are options to explore.

The following points show the testwork description and results of the work.

## Assessed Process Routes

The starting point is the bleed stream from the ZINCEX™ process after zinc recovery. It is a sulfate medium, saturated in calcium, at a pH near neutrality and containing a variable amount of the metals not precipitated. Manganese, as divalent cation (Mn<sup>2+</sup>) is prominent among them, but an expectable concentration is in the range of 5 to 10 g/l.

This solution also contains Cd, Cu, Ni, Co, Pb, Zn, and Al, along with Cl and F, and the alkalines Na, Mg, K. Obviously, the precise composition widely varies depending on the nature of the initial feedstock. Hence, production of Manganese oxide would start by precipitation of a solid from this solution.

### PRECIPITATION OF OXIDES

Screening of technologies has shown that there are two process routes that can be applied to precipitate Mn at this high scale: reaction with NaClO (Sodium Hypochlorite) or reaction with O<sub>3</sub> (Ozone). Both technologies have several points in common:

- The reagent is a strong oxidant that will turn Mn<sup>2+</sup> to a higher oxidation state, rendering solid oxides.
- The reagent can be generated on site, by an annexed facility based on electrolysis: Hypochlorite from NaCl, and Ozone from atmospheric oxygen.
- In both cases, the reaction proceeds by generation of acidity in the medium, in a mole-to-mole ratio, turning the MnSO<sub>4</sub> in solution into H<sub>2</sub>SO<sub>4</sub> (sulfuric acid). This acidity has to be neutralized, during the oxidation or afterwards.

According to TR research, both routes can render a manganese oxide with similar quality with a high reaction efficiency. The choice between them would be based on the specific circumstances of the implementation, related to CAPEX and OPEX. For instance, in a remote desert location, sourcing of the reagents and water required for NaClO would make a disadvantage compared to O<sub>3</sub> generation, which only requires air and electric power.

### REDISSOLUTION IN SULFATE MEDIUM

Opposite to previous step, re-dissolution of solid MnO<sub>2</sub> requires a reductant agent that turns Mn<sup>4+</sup> to Mn<sup>2+</sup>, and acid is consumed in the process. The objective at this step must be to obtain a high concentration of Mn in the solution, because the following steps would be impaired if the Mn is diluted. Thus, a high solid density and a concentrated acid medium are required. Anyway, equipment size and footprint of this area is much smaller, compared to the previous unit.

TR has researched in two process routes: reaction with H<sub>2</sub>O<sub>2</sub> (hydrogen peroxide, which in this medium behaves as a reductant) and reaction with Carbon. These two approaches are rather different, since H<sub>2</sub>O<sub>2</sub> is a liquid reagent, while the use of carbon implies a solid-solid reaction.

The application of one route or another would largely depend on the scale and the circumstances of the project. Hydrogen peroxide is an expensive and dangerous reagent, which cannot be generated on-site. Thus, for a large-scale project or a location with difficult logistics, the advantage of a solid reagent overcomes the additional operation complexity.

### PURIFICATION OF SOLUTION

At this point of the process, the MnSO<sub>4</sub> solution is a concentrated acid liquor that still contains impurities that would make it unsuitable for using it as additive in Electrowinning. Even parts

per million of some heavy metals, such as Cu, Cd, Ni, Co, Pb, As would affect severely the zinc electrowinning performance. If, on the other hand, the objective is to obtain a pure crystallized  $\text{MnSO}_4$  commercial product, Zn also adds to the list of forbidden impurities.

Purification must allow reducing the heavy metals to levels below part-per-million, but it must prevent dilution of the liquor. It is achieved in two consecutive steps:

- Neutralization of the acid
- Final Purification

Neutralization of the acidity would not be strictly needed if the liquor is to be used as EW additive but, actually, it is required to apply a second purification step, whichever it is. Several purification methods have been tested, comprising solvent extraction, ion exchange, and sulfidization. Depending on the final purification method, neutralization has to reach different values of pH. For instance, SX with dithiophosphinic acid, only demanded a pH around 2. On the other hand, an effective sulfidization requires conditions close or beyond neutrality (pH 7 to 9), and the neutralization itself becomes a very effective first step of purification, since heavy metals precipitate as hydroxides in this range of pH.

Neutralization is constrained by the necessity of not diluting the solution. A concentrated solution of NaOH can be used for mild pH adjustments, but economy dictates that a cheap reagent will be required for deeper adjustment. If lime is used as alkali, the reagent has to be added dry, or as milk of lime prepared with the process solution.

For a big industrial scale, the preferred path will always be a neutralization with lime and a scavenging using sodium sulfide ( $\text{Na}_2\text{S}$ ), which is a standard in hydrometallurgy. Purification with SX or IX yields an acid solution, which can be used in EW cellhouse but cannot be readily used for crystallization of a commercial  $\text{MnSO}_4$  product.

Solution returned to EW (either acid or neutral) is aimed to have a sulfate concentration in the same range as ZINCEX<sup>TM</sup> electrolytes (around 2.5 mol/l), a concentration of Mn in the order of 100 g/l and a level of impurities compatible with the strict requirements in a zinc cellhouse operation.

#### CRYSTALLIZATION OF MANGANESE SULFATE

Purified  $\text{MnSO}_4$  solution is submitted to a Crystallization Process, to produce the ultra-pure  $\text{MnSO}_4$  commercial product, removing and recycling the water. Obviously, the higher concentration of the incoming solution, the most efficient and less costly the operation will be. The first challenge that the process has to overcome is the removal of calcium when the solution is saturated. This is why the design consists in two steps and the consequent recycles, to ensure that gypsum and  $\text{MnSO}_4$  are precipitated separately. Although this is not conceived as purification step, the crystallization can tolerate a certain level of impurities and yet produce an ultra-pure  $\text{MnSO}_4$  solid. This final product is dried and packed for market.

## Conclusions

It was demonstrated that zinc sources with high manganese content (not treatable by conventional RLE technologies) can be treated by ZINCEX™ process without any modification of the basic flowsheet.

In order to add potential value to ZINCEX™ process, TR has conducted a development project in which process design and laboratory testwork have been run in parallel, to assess the technical feasibility of a manganese recovery. This is performed from a bleed stream after zinc recovery has been achieved, without any interference with the main facilities, other than the final effluent treatment.

The recovery of manganese can be done by means of three non-excluding alternatives:

- A concentrate of  $\text{MnO}_2$ , comparable, or better, to mining concentrates.
- A purified concentrate  $\text{MnSO}_4$  solution that is consumed internally as ZINCEX™ electrowinning additive, sparing a considerable cost.
- A high added value ultrapure crystallized  $\text{MnSO}_4$  commercial product.

As an alternative to the last, other valuable final products can be considered, such as EMM (electrolytic metal) or EMD (electrolytic manganese oxide).

Several process routes have been successfully researched and evaluated to give a comprehensive network of operations that can be applied. Depending on the specific circumstances of each implementation (type of ore, location, scale, local prices...) the most favourable integrated process would be selected. Summing up TR's know-how and experience with the ZINCEX™ technology, this new development is ready to be implemented in projects where ores and recycled materials with high manganese content are to be exploited.

## References

- 
- <sup>i</sup> D. Martín, G. Díaz, M.A. García, and F. Sánchez. *Extending zinc production possibilities through solvent extraction*. © The South African Institute of Mining and Metallurgy. ISEC 2002 Cape Town (South Africa).
- <sup>ii</sup> G.Díaz, D. Martín, C. Lombera. *Zinc Recycling Through the Modified Zincex® Process*. Third International Symposium Recycling of Metals (TMS, 1995) and Journal of Metals (JOM), 4 (1995) 22-23.
- <sup>iii</sup> C. David, S. Engelbrecht, G. Díaz, F. Sánchez, A.B. Mejías. *Skorpion Zinc: Lessons Learnt in the Operation of the Modified Zincex™ Solvent-Extraction Process*. 19th ISEC Conference 2011 Santiago (Chile).
- <sup>iv</sup> C. Frías, G. Díaz, D. Martín, F. Sánchez. *Implementation of First ZINCEX Commercial Plant Treating Zinc Oxides Secondaries*. Proceedings EMC (2009).
- <sup>v</sup> G. Díaz, A.B. Mejías, D Martín, F. Cubeddu. *ZINCEX Technology, Recent Industrial operations*. Proceedings Hydrometallurgy (2014).
- <sup>vi</sup> G. Díaz, E. Pecharromán, S. Sanguilinda, J. Pusateri, A. Staley. *Mooresboro Zinc Project: First Solvent Extraction Plant in the World to Produce Zinc Entirely from Recycling* ISEC 2014 Würzburg (Germany)
- <sup>vii</sup> R.J. Sinclair. *The Extractive Metallurgy of Zinc*. The Australasian Institute of Mining and Metallurgy. Spectrum Series Volume Number 13. (2005).
- <sup>viii</sup> Martín, D., García, M.A., Díaz, G. and Falgueras J. *A new Zinc Solvent Extraction Application: Spent domestic batteries treatment plant*. ISEC Conference 1999 Barcelona (Spain).
- <sup>ix</sup> S. Maghfouria, M. R. Hosseinzadeha, A. Rajabib, F. Choulet. *A review of major non-sulfide zinc deposits in Iran*. Geoscience Frontiers Volume 9, Issue 1, January 2018, Pages 249-272.
- <sup>x</sup> Mining Weekly "Gamsberg Zinc Manganese options being explored" 31st March 2000

# Assessment of two liquid-liquid extraction systems for Cr(VI) extraction from acidic nitrate media using $^{51}\text{Cr}$ as radiotracer

Deniz Avsar<sup>a\*</sup>, Dag Øistein Eriksen<sup>a</sup> and Jon Petter Omtvedt<sup>a</sup>

The extraction behaviour of Cr(VI) from nitric acid (0.3 M  $\text{HNO}_3$ ) solutions by Aliquat 336 and trioctylamine (TOA) in benzene was investigated using  $^{51}\text{Cr}$ (VI) as radioactive tracer. Extraction of Cr(VI) species were studied for extractant concentrations from 0.01 mM to 0.1 M. The stoichiometry of the extraction mechanisms were determined by slope analysis. Extensive range of D-values were used to achieve superior slope analysis. The main extracted Cr(VI) species were  $\text{HCr}_2\text{O}_7^-$ ,  $\text{HCrO}_4^-$  and  $\text{Cr}_2\text{O}_7^{2-}$  for both extractants. NaOH solutions (0.01 M – 2 M) were used for stripping of the loaded organic phase. The stripping yield was highest for TOA.

**Keywords:** Liquid-liquid extraction, Cr(VI),  $^{51}\text{Cr}$ , Aliquat 336, Trioctylamine, TOA

## Introduction

In aqueous media, chromium exist mainly as Cr(III) and Cr(VI). In comparison to Cr(III), Cr(VI) is 100 times more toxic, a human carcinogen and it has high solubility and mobility.<sup>1</sup> Maximum allowed total chromium concentration in drinking water is 0.05 mg/L.<sup>2</sup> Thus, chromium extraction from industrial solutions is of great interest due to the high toxicity of Cr(VI) species. In this study, we investigated Cr(VI)-extraction mechanisms in acidic nitrate media, using Aliquat 336 (A336) and trioctylamine (TOA) as extraction agents. We used benzene as solvent and  $^{51}\text{Cr}$  as radiotracer. The study showed that Cr(VI) can be extracted in different ionic forms depending on the concentration of the extraction agent. Separation of Cr(VI) from nitric acidic media have not been reported in detail in the literature. Therefore, this study gives beneficial information on how to find and develop an effective low cost and sustainable method to remove and recover Cr(VI) from acidic nitrate media.

## Background

Numerous extraction agents have been used in studies of Cr(VI)-extraction from industrial solutions. Amine extractants such as Aliquat 336<sup>3–7</sup>, TOA<sup>8–10</sup>, and Alamine 336<sup>3,5</sup> are commonly used due to their extraction abilities and chemical stability. El-Hefny<sup>3</sup> investigated the extractable Cr(VI) species from acidic sulphate media and Someda et al.<sup>5</sup> studied Cr(VI) extraction from acidic chloride media by using quaternary amine (Aliquat 336) and tertiary amine (Alamine 336). Both report that the major extractable Cr(VI) species is  $\text{HCrO}_4^-$  and the extraction yield by Aliquat 336 is higher than by Alamine 336 in acidic medium under the same experimental conditions. Deptula<sup>8</sup> investigated the extraction of Cr(VI) by TOA from various mineral acid solutions and found that Cr(VI) is extracted as  $\text{CrO}_3\text{Cl}^-$  from acidic chloride media, and as  $\text{HCrO}_4^-$ ,

---

<sup>a</sup>Department of Chemistry, University of Oslo, Oslo, Norway

\*Sem Sælands vei 26, 0371 Oslo, deniz.avsar@kjemi.uio.no



$\text{Cr}_2\text{O}_7^{2-}$  or  $\text{HCr}_2\text{O}_7^-$  from other mineral acids.<sup>11</sup> Among Cr(VI) extraction studies reported in the literature, extraction from acidic nitrate media has not been investigated in detail and only few of them reported the application of  $^{51}\text{Cr}$  as radiotracer<sup>5,11,12</sup>, even though the implementation of radiotracers is advantageous compared to other analytical methods where in most cases only one phase is measured, e.g. ICP-MS. Furthermore, for all reports, the Cr(VI) extraction mechanism was investigated in a shorter range of extractant concentrations, limiting the validation of the slope analysis.

## Theory

Cr(VI) may exist in different ionic forms in aqueous phase ( $\text{HCrO}_4^-$ ,  $\text{CrO}_4^{2-}$ ,  $\text{Cr}_2\text{O}_7^{2-}$ ,  $\text{HCr}_2\text{O}_7^-$ ), depending on the total amount of chromium and the pH of the solution (Table 1).

Table 1. Published values of equilibrium constants

Equilibrium	Ionic Strength [M]	Equilibrium constant (at 25 °C)	Reference
$\text{H}_2\text{Cr}_2\text{O}_7 \rightleftharpoons \text{H}^+ + \text{HCr}_2\text{O}_7^-$	-	$\sim 10^6$	8
$\text{HCr}_2\text{O}_7^- \rightleftharpoons \text{H}^+ + \text{Cr}_2\text{O}_7^{2-}$	1	0.85	13
$\text{H}_2\text{CrO}_4 \rightleftharpoons \text{H}^+ + \text{HCrO}_4^-$	$\sim 0.16$	0.18	14,15
	1	1.21	13
$\text{HCrO}_4^- \rightleftharpoons \text{H}^+ + \text{CrO}_4^{2-}$	0.33-0.63	$3.2 \cdot 10^{-7}$	13
	1	$1.8 \cdot 10^{-6}$	15
$2\text{HCrO}_4^- \rightleftharpoons \text{Cr}_2\text{O}_7^{2-} + \text{H}_2\text{O}$	$< 0.022$	33.3	13
	1	98	13

For different concentrations of Cr(VI) at pH 0.5 ( $I = 0.3 \text{ M}$ ), the predominant species are listed in Table 2. Extraction of these Cr(VI) species were investigated using anion exchange extractants in order to compare their extraction mechanism. Contributions from  $\text{H}_2\text{Cr}_2\text{O}_7$  and  $\text{CrO}_4^{2-}$  were negligible at these experimental conditions.

Table 2. Adapted calculation of relative concentrations of Cr(VI) species at pH 0.5 (atom%)<sup>14,15</sup>

Cr(VI), ppm	$\text{HCr}_2\text{O}_7^-$	$\text{HCrO}_4^-$	$\text{Cr}_2\text{O}_7^{2-}$	$\text{H}_2\text{CrO}_4$
300	9.88	49.77	28.01	12.34
30	2.16	73.51	6.11	18.22
3	0.25	79.36	0.71	19.68

## Experimental

$\text{K}_2\text{Cr}_2\text{O}_7$  (99.1%) from J.T. Baker,  $\text{HNO}_3$  (69%) from VWR, Benzene (99.8%) from Sigma Aldrich, NaOH (90%) from Merck, TOA ( $\geq 93\%$ ) from Merck, and Aliquat 336 from Thermofisher were used. Type 2 water was used for preparing 3000 ppm Cr(VI) stock solution, equivalent to 57.7 mM, and aqueous phase was prepared by diluting the stock solution in 0.3 M  $\text{HNO}_3$ . 185 MBq  $^{51}\text{Cr}$  as  $\text{NaCrO}_4$  was purchased from Perkin Elmer. 100  $\mu\text{L}$   $^{51}\text{Cr}$  (18 kBq/mL) was added to the aqueous phase for each extraction sample. Organic phases were prepared by weighing out the extracting agent on analytical scale and diluting it in benzene. After preparing the organic phase, TOA was pre-equilibrated

with 1 M HNO<sub>3</sub>, Aliquat 336 was used without further processing. Benzene was used as diluent due to its high purity, which is advantageous for future spectroscopic investigations. A Vortex Genie 2 shaker was used for reaching the equilibrium of the reaction while Heraeus Labofuge 300 centrifuge was used for separation of the two phases. NaI well-detector (2"×2") was used to detect the 320 keV gamma rays from the decay of <sup>51</sup>Cr (T<sub>1/2</sub> = 27.7 d), the counting time was adjusted to give errors below 1%. Ortec Maestro software was used in analysing the gamma spectra.

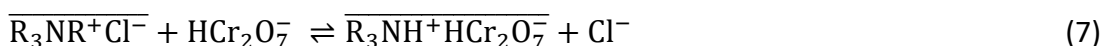
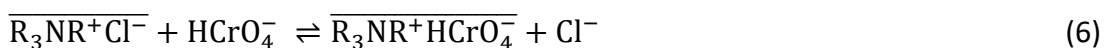
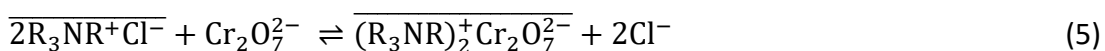
All experiments were performed at ambient temperature (22±2 °C) with a minimum of 2 repetitions. Equal volumes (5 mL) of aqueous phase and organic phase were mixed in a 15 mL centrifuge vial. Initial experimental results showed that the extraction equilibrium for two different systems was reached in less than 5 minutes. Hence, the phases were mixed in the shaker for 5 minutes with the speed rate of 1500 rpm. Afterwards, vials were centrifuged for 2 minutes to achieve total phase separation. The activity distribution in the phases was measured with a NaI well-detector. Distribution ratio (D) of the Cr(VI) was calculated, after the disintegration rate was corrected for radioactive decay. Calculated D-ratios were plotted against varying concentrations of extraction agent in logarithmic scale and conventional slope analysis were performed by least square fitting using OriginLab data analysis and graphing software.

## Results and discussion

### Extraction mechanism of Cr(VI) with Aliquat 336

The stoichiometry of the extracted Cr(VI) species was determined by measuring the distribution ratio of Cr(VI) at varying organic phase concentrations of A336 ranging from 0.022 mM to 0.11 M diluted in benzene. Based on the observed results given in Figure 1, two linear fits were needed in order to fit the data. Linear fit conducted on the concentration from 0.02 mM up to 0.0015 M gave a slope of 1 (R<sup>2</sup>=0.993), and for A336 concentrations higher than 0.0015 M slope of 2 (R<sup>2</sup>=0.999) was obtained. Further increase in A336 concentration lead to deviations from the slope. This deviation can be explained by the increase in the Cl<sup>-</sup> concentration, which may lead to formation of the CrO<sub>3</sub>Cl<sup>-</sup> complex, which has a different extraction mechanism.<sup>5</sup>

The following mechanisms are proposed for Cr(VI) extraction with Aliquat 336 concentrations higher than 0.0015M (Eq. 5) and lower than 0.0015M (Eq. 6 and Eq. 7), where R<sub>3</sub>NR<sup>+</sup>Cl<sup>-</sup> denote to A336 and the upper bar refers to the organic phase:



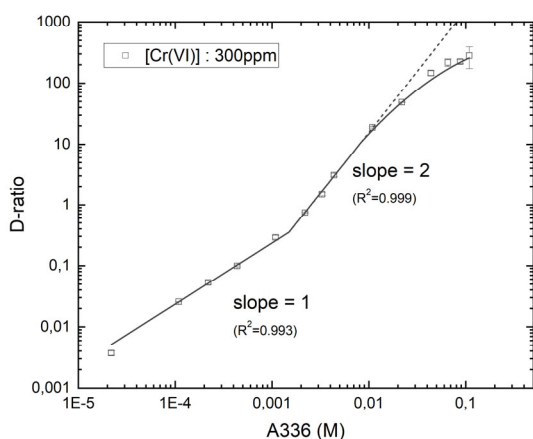


Figure 1. Cr(VI) extraction with varying concentration of A336 in benzene (aqueous phase: 300 ppm Cr(VI) in 0.3 M HNO<sub>3</sub>)

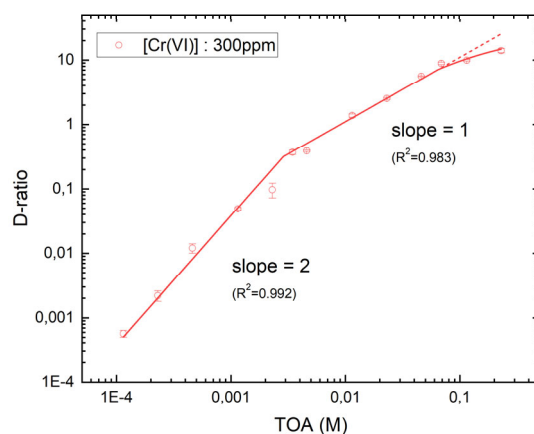


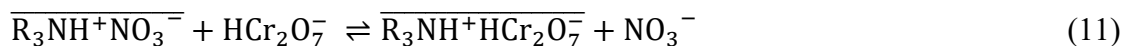
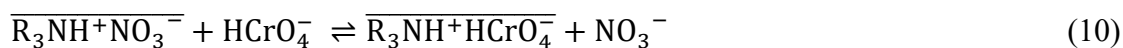
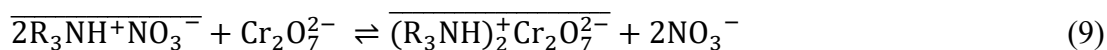
Figure 2. Cr(VI) extraction with varying concentration of TOA in benzene (aqueous phase: 300 ppm Cr(VI) in 0.3 M HNO<sub>3</sub>)

The slope indicates that 2 molecules of A336 is required for the extraction of 1 molecule of  $\text{Cr}_2\text{O}_7^{2-}$  species and that 1 molecule of A336 is required for the extraction of 1 molecule of  $\text{HCrO}_4^-$  or  $\text{HCr}_2\text{O}_7^-$  species. In the previously mentioned literature, the main extracted Cr(VI) species is reported as  $\text{HCrO}_4^-$ , where the extraction mechanism was studied with Cr(VI) concentrations between 5 ppm to 140 ppm. This might explain the differences in the extracted Cr(VI) species, since these are highly depended on the total Cr(VI) concentration and pH of the aqueous solution. Lo and Shiue also proposed two extraction equations where  $\text{HCrO}_4^-$  and  $\text{Cr}_2\text{O}_7^{2-}$  are the main extracted species. However, their slope analysis was closer to  $\text{HCrO}_4^-$  at pH 3.5 and 5 ppm initial Cr(VI) concentration. At pH 0.5 (0.3 M HNO<sub>3</sub>) and initial Cr(VI) concentration of 300 ppm, we observe that with increasing concentration of A336 it is possible to extract  $\text{Cr}_2\text{O}_7^{2-}$ . Furthermore, we studied a wider range of extractant concentrations in order to obtain better understanding of the extraction mechanism.

### Extraction mechanism of Cr(VI) with TOA

The stoichiometry of the extracted Cr(VI) species was determined by measuring the distribution ratio of Cr(VI) at varying organic phase concentrations of TOA ranging from 0.023 mM to 0.23 M diluted in benzene. It can be seen from Figure 2 that the relation between the D-ratio and the increasing concentration of extractant shows two different mechanisms similar to A336. However, for TOA at lower concentrations, a slope of 2 ( $R^2=0.992$ ) and for higher concentrations, a slope of 1 ( $R^2=0.983$ ) were found. This might be explained with a lack of steric effects allowing TOA to extract  $\text{Cr}_2\text{O}_7^{2-}$ . Compared to A336, TOA has only an  $\text{H}^+$  ion between the N-atom and the dichromate, while A336 has a methyl group. At higher concentrations of TOA, the deviations from the slope can be explained by partial or complete aggregation of the amine extractant.<sup>16</sup>

The following extraction mechanisms are proposed for Cr(VI) extraction with TOA concentrations higher than 0.003 M (Eq. 10 and Eq. 11) and lower than 0.003 M (Eq. 9), where  $\text{R}_3\text{N}$  denote to TOA, and upper bar refers to the organic phase:



Saw et al.<sup>10</sup> reported that they extracted Cr(VI) as  $CrO_3Cl^-$  from HCl solutions, and they found a slope of 2 which was similar to extraction experiments that Agrawal<sup>17</sup> performed. This agrees with our results, however not for the higher TOA concentrations. On the other hand, previous work done by Deptula<sup>8</sup>, Huang et al.<sup>9</sup> and Rao and Sastri<sup>18</sup> showed both of these species can be extracted depending on the acidity and the concentration of Cr(VI), which is in agreement with our findings. As explained for the A336 extraction mechanism, using radiotracers allow us to study a wider range of extractant concentrations, hence we could achieve superior slope fitting.

### Comparison of the extraction and stripping systems

To ascertain the nature of the extracted Cr(VI) species, fixed amounts of Cr(VI) were extracted by varying concentrations of A336 and TOA as extracting agents dissolved in benzene, where  $^{51}Cr$  is used to trace the distribution of Cr(VI) in both aqueous and organic phase (Figure 4). As expected, the higher Cr(VI) extraction was observed when the extractant concentration increased. One can conclude that a higher D-ratio was achieved with A336 than TOA. It is noteworthy that at very high/low D-ratios uncertainty increased due to excessive amounts of Cr(VI) in one of the phases making it difficult to detect the trace amounts left in the other phase. Additionally, the entrainment can be limiting the capability to measure very high/low D-ratios.

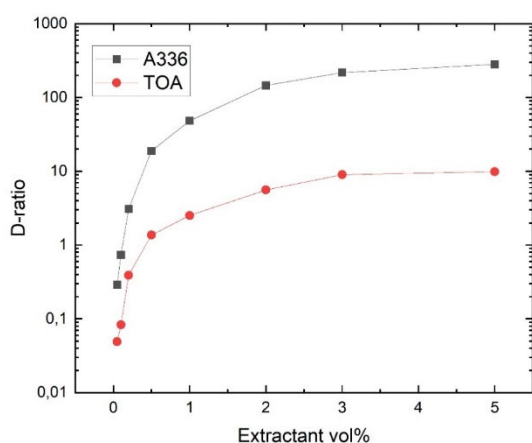


Figure 3. Comparison of two extraction systems (A336, TOA) in benzene for various volume ratios (aqueous phase: 300 ppm Cr(VI) in 0.3 M  $HNO_3$ )

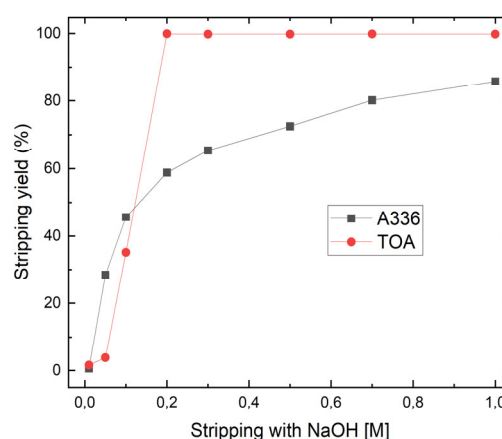


Figure 4. Comparison of two stripping systems for Cr(VI) with various NaOH concentrations (loaded organic phase: A336 5%, TOA 5% in benzene)

Among different types of stripping agents studied in the literature NaOH is reported to give higher stripping yield and a simpler extraction mechanism.<sup>4,6,10,17</sup> Hence, in this study NaOH was used to strip the extracted Cr(VI) species from the organic phase with

varying concentrations ranging from 0.01 M up to 1 M. Extraction was performed with 5 vol% extractant (A336, TOA) in benzene. After extraction, the loaded organic phase was collected for stripping, where  $^{51}\text{Cr}$  was used to trace the distribution of Cr(VI) in both aqueous and organic phase. Comparison of stripping yields for these extractants with varying NaOH concentration is presented in Figure 4. For TOA, >99.8 % of Cr(VI) is stripped from the loaded organic phase with 0.2 M NaOH, and it reached saturation after this concentration. The stripping yield dropped drastically for decreasing NaOH concentrations below 0.2 M. These results suggest that stripping from TOA has a threshold value depending on the pH of the stripping solution, since its extraction mechanism strictly depends on the  $\text{H}^+$  concentration. On the other hand, this trend was not observed with stripping from A336, due to the difference in extraction mechanism. The highest stripping yield was achieved with 1 M NaOH solution, and the stripping yield decreased with decreasing NaOH concentration. One can conclude that complete stripping yield was achieved with TOA but not with A336.

## Conclusions

Cr(VI) in nitric acid media was successfully extracted and stripped at constant ionic strength using two different amine extractants. It can be observed that the total Cr(VI) concentration and aqueous pH value and ionic strength have a great influence on the extracted species. The Cr(VI) species extracted at our experimental conditions were found to be  $\text{HCr}_2\text{O}_7^-$ ,  $\text{HCrO}_4^-$  and  $\text{Cr}_2\text{O}_7^{2-}$  depending on the extractant type and the concentration of the extractant. To understand the extraction mechanism better, varying acid- and Cr(VI)-concentrations need to be studied. Future work will focus on extraction of Cr(VI) species from more complex solutions and/or real industrial solutions.

In conclusion, for many hydrometallurgical processes, it is desirable to have high extraction efficiency and reasonably high D-values as well as high stripping yield and easy stripping mechanism for recovery of heavy metals. Hence, TOA might be a better alternative due to its easy stripping mechanism, adequate D-ratio and lower cost. Slope analysis might be challenging in determination of the stoichiometry of the extracted species unless there are sufficient experimental points to understand the overall mechanism.

## Acknowledgments

This work financially supported by the Research Council of Norway under the contract PRICE – NFR Project 294543 and by the PRICE collaboration.

## References

- (1) Pechova, A.; Pavlata, L. Chromium as an Essential Nutrient: A Review. *Veterinarni Medicina* **2008**, 52 (No. 1), 1–18. <https://doi.org/10.17221/2010-VETMED>.
- (2) World Health Organization. Chromium in Drinking Water. *Guidelines for Drinking-Water Regulations* **2020**.

- (3) El-Hefny, N. E. Comparison of Liquid–Liquid Extraction of Cr(VI) from Acidic and Alkaline Solutions by Two Different Amine Extractants. *Separation and Purification Technology* **2009**, 67 (1), 44–49. <https://doi.org/10.1016/j.seppur.2009.03.004>.
- (4) Kalidhasan, S.; Sricharan, S.; Ganesh, M.; Rajesh, N. Liquid–Liquid Extraction of Chromium(VI) with Tricaprylmethylammonium Chloride Using Isoamylalcohol as the Diluent and Its Application to Industrial Effluents. *J. Chem. Eng. Data* **2010**, 55 (12), 5627–5633. <https://doi.org/10.1021/je100518w>.
- (5) Someda, H. H.; El-Shazly, E. A.; Sheha, R. R. The Role of Some Compounds on Extraction of Chromium(VI) by Amine Extractants. *Journal of Hazardous Materials* **2005**, 117 (2–3), 213–219. <https://doi.org/10.1016/j.jhazmat.2004.09.024>.
- (6) Lo, S. L.; Shiue, S. F. RECOVERY OF Cr(VI) BY QUATERNARY AMMONIUM COMPOUNDS. *Water Research* **1998**, 32 (1), 174–178. [https://doi.org/10.1016/S0043-1354\(97\)00193-0](https://doi.org/10.1016/S0043-1354(97)00193-0).
- (7) Salazar, E.; Ortiz, M. I.; Uriaga, A. M.; Irabien, J. A. Equilibrium and Kinetics of Chromium(VI) Extraction with Aliquat 336. *Ind. Eng. Chem. Res.* **1992**, 31 (6), 1516–1522. <https://doi.org/10.1021/ie00006a014>.
- (8) Deptuła, C. Extraction of Chromium(VI) from Sulphuric Acid Solutions by Means of Tri-n-Octylamine. *Journal of Inorganic and Nuclear Chemistry* **1968**, 30 (5), 1309–1316. [https://doi.org/10.1016/0022-1902\(68\)80560-3](https://doi.org/10.1016/0022-1902(68)80560-3).
- (9) Huang, Y.-H.; Chen, C.-Y.; Kuo, J.-F. Extraction of Chromium(VI) from Acid Solutions by Tri-Iso-Octylamine. *Journal of Chemical Engineering of Japan* **1991**, 24 (2), 149–154. <https://doi.org/10.1252/jcej.24.149>.
- (10) Saw, P. K.; Prajapati, A. K.; Mondal, M. K. The Extraction of Cr (VI) from Aqueous Solution with a Mixture of TEA and TOA as Synergic Extractant by Using Different Diluents. *Journal of Molecular Liquids* **2018**, 269, 101–109. <https://doi.org/10.1016/j.molliq.2018.07.115>.
- (11) Tuck, D. G.; Walters, R. M. 205. The Extraction of Chromium(VI) from Aqueous Solution by Tri-n-Butyl Phosphate. *J. Chem. Soc.* **1963**, No. 0, 1111–1120. <https://doi.org/10.1039/JR9630001111>.
- (12) Iqbal, M.; Ejaz, M. Solvent Extraction of Chromium(VI) from Base Metal Ions with Diphenyl-2-Pyridylmethane as a Liquid Anion Exchanger. *J. Radioanal. Chem.* **1978**, 43 (1), 199–207. <https://doi.org/10.1007/BF02519457>.
- (13) Tong, J. Y.; King, E. L. A Spectrophotometric Investigation of the Equilibria Existing in Acidic Solutions of Chromium(VI) <sup>1-3</sup>. *J. Am. Chem. Soc.* **1953**, 75 (24), 6180–6186. <https://doi.org/10.1021/ja01120a022>.
- (14) Tandon, R. K.; Crisp, P. T.; Ellis, J.; Baker, R. S. Effect of PH on Chromium(VI) Species in Solution. *Talanta* **1984**, 31 (3), 227–228. [https://doi.org/10.1016/0039-9140\(84\)80059-4](https://doi.org/10.1016/0039-9140(84)80059-4).
- (15) Shen-Yang, T.; Ke-An, L. The Distribution of Chromium(VI) Species in Solution as a Function of PH and Concentration. *Talanta* **1986**, 33 (9), 775–777. [https://doi.org/10.1016/0039-9140\(86\)80187-4](https://doi.org/10.1016/0039-9140(86)80187-4).
- (16) Verstegen, J. M. P. J.; Ketelaar, J. A. A. Distribution of Sulphuric Acid between Water and Benzene Solutions of Tri-n-Octyl and Tri-n-Hexyl Amine. *Trans. Faraday Soc.* **1961**, 57 (0), 1527–1533. <https://doi.org/10.1039/TF9615701527>.
- (17) Agrawal, A.; Pal, C.; Sahu, K. K. Extractive Removal of Chromium (VI) from Industrial Waste Solution. *Journal of Hazardous Materials* **2008**, 159 (2–3), 458–464. <https://doi.org/10.1016/j.jhazmat.2008.02.121>.
- (18) Rao, V. M.; Sastri, M. N. Extraction of Cr(VI) from Orthophosphoric Acid Solutions by Trilauryl Amine. *IJC-A Vol.14A(08) [August 1976]* **1976**.

# **An Innovative Process for Simultaneous Production of High Purity Benzene and U.S Grade Gasoline from C6 Heart Cut of FCC Gasoline**

M. Onkarnath Garg<sup>\*a</sup>, Mayuresh Sahasrabudhe<sup>a</sup>, Ajit Sapre<sup>a</sup>, P. Ghosh<sup>b</sup>, S. Kumar<sup>b</sup>, S.M. Nanoti<sup>b</sup>, and B.R. Nautiyal<sup>b</sup>

**Abstract:** The MSAT – II regulations active since January 1, 2011 (“EPA Regulatory Announcement” – EPA420-F-07-017, February 2007), restricts the annual average benzene level in Gasoline sold in U.S (except California), to 0.62 % vol. Currently FCC gasoline comprises nearly 10-20 % of the gasoline pool in a typical refinery. Full range FCC gasoline contains around 15-30 vol. % aromatics with up to 2 vol. % benzene and 1000 – 2000 ppm sulfur. Unprocessed FCC Gasoline contains reactive impurities like oxygenates, metals, chlorides, sulphur compounds, nitrogen compounds, di-olefins and organic peroxides. Complexity of the feedstock has hindered the development of an economic and reliable benzene recovery process in the industry so far. Hydro-processing routes for benzene reduction result in olefin saturation which lowers the octane rating of the final product.

Reliance Industries Ltd (RIL) operates two 220,000 bpsd FCC units at its world class refineries and petrochemical complex at Jamnagar, India. The gasoline from these two FCC units is a major contributor of Benzene in gasoline pool. It thus seemed imperative to remove benzene from this stream in order to meet the forthcoming benzene limit in gasoline pool. CSIR IIP and RIL jointly developed a first of its kind technology for simultaneous production of high purity benzene and U.S grade gasoline from C6 heart cut of FCC gasoline.

The process developed serves a dual role of recovering high purity benzene and producing environmental friendly gasoline from FCC C6 heart cut stream using extractive distillation without the requirement of any prior hydrogenation or pre-processing step to saturate di-olefins in feedstock and reduce impurities. The indigenous technology has been granted patents in several countries including, Russia, China, Japan, European Union and U.S. (US. 8722952 B2). A ~0.7 MMTPA (17.4 KBPSD) plant based on this technology has been commissioned in Reliance Industries’ petrochemical complex at Jamnagar, India in May 2016. The unit has been operating consistently as per expectations even at a throughput of 150% of design.

**Keywords:** Extractive distillation, NMP, benzene, FCC, Sulfur, gasoline, Oldershaw Column

## **Introduction**

Gasoline or petrol is a petroleum-derived transparent liquid. It is primarily used as a fuel in spark-ignited internal combustion engines. It mainly consists of organic compounds derived from the fractional distillation of petroleum. In the pursuit of producing cleaner fuels, benzene has been identified as gasoline component that should be reduced. Benzene being a toxic component, its concentration in gasoline blends is a major health concern and hence placed under environmental regulations worldwide.

---

**a Reliance Industries Limited, Navi Mumbai, India**

**b CSIR-Indian Institute of Petroleum, Dehradun, India**

Current regulations restrict the annual average benzene level in Gasoline sold in U.S to 0.62% vol. effective from 2011. Table 1 provides the norms for benzene in gasoline across the globe. The specification is getting stringent day by day.

**Table1. Gasoline norms for benzene at various parts of the world**

Country	UOM	Max. Limit
US*	Vol.-%	0.62
India**	Vol.-%	1.0
Japan / Europe**	Vol.-%	1.0
South Korea	Vol.-%	0.7

The major contributors of benzene in the gasoline pool, typically, are reformate, hydrogenated pyrolysis gasoline (PG) and catalytically cracked gasoline. Removal or recovery of benzene from reformate and hydrogenated PG is straightforward and is carried out by

- Solvent extraction and/or
- Extractive distillation

using polar solvents such N-Methyl-2-Pyrrolidone (NMP), Sulfolane, N-formylmorpholine (NFM), etc., and several commercial units are currently in operation worldwide.

Unlike reformate and hydrogenated PG, unprocessed cracked gasoline fraction contains olefins along with impurities like oxygenates, metals, chlorides, sulphur compounds, nitrogen compounds, and organic peroxides. Due to the complex nature of this feedstock, an economic and reliable benzene recovery process is difficult to develop and has not been practiced in the industry so far.

## Technical Review of Prior Science and Technology

Both olefins and aromatics in cracked gasoline contribute substantially to the octane number in the gasoline pool. An attempt to reduce benzene by well-known hydro-processing routes would result in saturating the olefins as well, thus lowering the octane of the cracked gasoline fraction. Several other alternative methods have also been developed to reduce benzene in cracked gasoline. Some of these are described below.

One such process removes benzene involving several steps such as:

- Separation of benzene concentrate stream;
- Subjecting this stream to etherification with an alcohol over an etherification catalyst to convert the C6 iso-olefins to ethers;
- Separating the ethers of C6 iso-olefins from benzene concentrate;
- Dissociation of ethers of C6 iso-olefins to recover alcohol and C6 iso-olefins; and
- Hydro treatment of ether removed benzene concentrate to remove olefins and organic impurities.



Removal of benzene from hydro treated benzene concentrate fraction using solvent extraction. The main emphasis is given on the etherification of iso-olefins and their separation from benzene. The process incorporates several steps for benzene removal and no commercial units came out based on the process mentioned. Further, the removal of benzene by solvent extraction from hydro-treated benzene concentrate underlines the difficulty in the recovery of benzene from olefinic feedstock containing substantial impurities.

Another patent, U.S. Pat. No. 8,143,466, discloses a process for removal of benzene from gasoline and involves partial alkylation of benzene in presence of catalyst with alcohol and ether.<sup>4</sup> Alkylated benzene is recovered as bottom stream and the top hydrocarbon stream is water washed to recover the un-reacted alcohol and ether.

The Benzene CDHydro process is another method reported for reducing the benzene content in gasoline which comprises of Hydrotreating followed by Isomerization of Deisohexanizer (DIH) Side cut. In this process benzene is hydrogenated to cyclohexane. The octane loss associated with benzene reduction in gasoline can be trade off by the isomerization of light reformat and light straight run. The hydrogenated C5-C6 cut is from the Benzene CDHydro process is ideal feedstock for isomerization unit. Worldwide there were six commercial Benzene CDHydro units in operation at the end of year 2005. The advantages of Benzene CDHydro process over conventional hydrogenation process includes higher octane product, higher liquid volume yield, and lower expected catalyst replacement rates.<sup>5</sup> The major drawback with this process is high CAPEX, additional OPEX requirements, loss of benzene value, thus loss of opportunity.

The above processes either convert benzene or involve several steps to remove benzene from cracked gasoline fraction. Hence it is clear that there is no commercial unit operating for benzene recovery from unprocessed cracked gasoline fraction (boiling in the range 40 to 90° C.) One of the reasons may be the potential of polymerization of olefins, particularly di-olefins (specially conjugated types) in the presence of reactive organic peroxides. Instances of such polymerization, especially when conjugated olefins are present, have been reported many a time as evident below.

Alkenes are known to undergo polymerization at high reaction temperature in polar medium under acidic conditions. Alkenes with more than 2 carbons have reactive allylic carbon atoms which in turn have allylic hydrogen atoms. Allylic carbon-hydrogen bond dissociation energy is relatively less than other C—H bond energies due to which allylic hydrogen can be substituted relatively easily. The resonance stabilisation of the formed allylic radical/cation/anion is the main factor responsible for substitution of allylic hydrogen. In a free radical substitution reaction the allylic radical formed can be stabilized by resonance. Thus conjugated di-olefins are more susceptible to oxidation. In presence of free radicals at high temperature or even in presence of di-radical oxygen, these allylic carbon-hydrogen bonds generate allylic radicals which are subsequently stabilized by resonance. The allylic radicals attack other olefin molecules and initiate chain growth polymerization. These free radicals may also react with di-radical oxygen to give per-oxy radicals through auto-oxidation reactions. These per-oxy radicals can extract hydrogen from olefin molecules to yield hydroperoxides and generate new allylic free radical giving a chain reaction.

## Present Work

The present work deals with development of a reliable process to produce benzene lean gasoline (benzene content less than 0.4 weight %) by recovery of high purity benzene (purity more than 97 weight %) from benzene concentrated unprocessed catalytically cracked gasoline fraction by Extractive Distillation (ED). The said gasoline fraction is obtained (without any pre-treatment) from a Fluidized Catalytic Cracking (FCC) unit of a petroleum refinery. The said benzene concentrated unprocessed catalytically cracked gasoline fraction, comprises of benzene and close-boiling non-aromatic hydrocarbons like paraffins, iso-paraffins, olefins, di-olefins (including conjugated di-olefins), and naphthenes along with impurities containing but not limited to oxygenates, metals, chlorides, sulphur compounds, nitrogen compounds, and organic peroxides.

Table 2 gives the typical composition of gasoline sample of RIL refinery.

## Experimental

Several solvents typically used in the extraction of aromatics were tested for their stability with

**Table 2. Analysis of gasoline sample of RIL refinery**

Analysis by Gas Chromatography, weight %		
1.	Mono Olefins, %	35.72
	C6 Di-olefins, %	1.18
	Paraffins (Normal + Iso), %	31.54
	Naphthenes, %	17.47
	Benzene, %	14.09
Impurities analysis		
2.	Total Sulfur, ppm	108.1
3.	Total oxygenates (EN-13132) , ppm	208
4.	Total Nitrogen , ppm	6.65
5.	Total Chlorides , ppm	0.1
6.	Metals , ppb	40
7.	Density kg/m <sup>3</sup> , @ 20 oC	725
8.	Research Octane Number (RON)	87.0

the untreated FCC gasoline (composition given above) both under nitrogen and oxygen atmosphere. This helped to identify those solvents which polymerize or decompose in the presence of impurities. NMP along with a proprietary co solvent was found optimally suited. Several extractive distillation runs were carried out to establish the technical feasibility of recovery of benzene without feed treatment. These runs were carried out in a 25 mm dia Oldershaw column containing 50 trays with the provision of regulating reflux and reboiler temperature.

Once the technical feasibility of the solvent was established, many extractive distillation runs were carried out to optimize the operating variables; these are:

1. Reboiler temperature

2. Reflux rate
3. Composition of solvent
4. Column Pressure

Simultaneously, a comprehensive simulation model of the extractive distillation was developed on the ASPEN PLUS platform. The liquid phase non-ideality was modelled with NRTL parameters. These parameters were largely in-house based on a large data bank of both LLE and VLE data generated at CSIR – IIP. These parameters were tuned with additional VLE data and then finally fine-tuned with the extractive distillation runs.

In all the experimental runs as well as in simulations, the benzene and sulfur content of the raffinate was close to zero while the benzene had a purity exceeding 97 % in most cases (Please see Table 3 below).

## Process Design Package Development

A team comprising of scientist, engineers and technologist was formed with team members from both RIL and CSIR-IIP. A Technology Information Package (TIP) was then developed which includes:

- Simplified Process Flow Diagram, please see Figure 1
- Heat and Mass Balance
- Preliminary Data Sheets for Critical Equipment

Table 3 : Experimental and Simulated Composition of Raffinate and Extract

Components	Raffinate (Solvent Free)		Extract (Solvent Free)	
	Lab.	Simu.	Lab.	Simu.
	Mass %	Mass %	Mass %	Mass %
<b>Mono Olefins</b>	41.20	41.19	0.40	0.33
<b>C6 Di-Olefins</b>	0.42	0.39	1.43	1.60
<b>Paraffins (N+I)</b>	38.07	38.11	0.24	0.32
<b>Naphthenes</b>	20.29	20.31	0.01	0.08
<b>Benzene</b>	0.02	0.01	97.92	97.67
<b>Total</b>	100.00	100.0	100.00	100.00
<b>Sulfur (ppm)</b>	3.1		628.6	

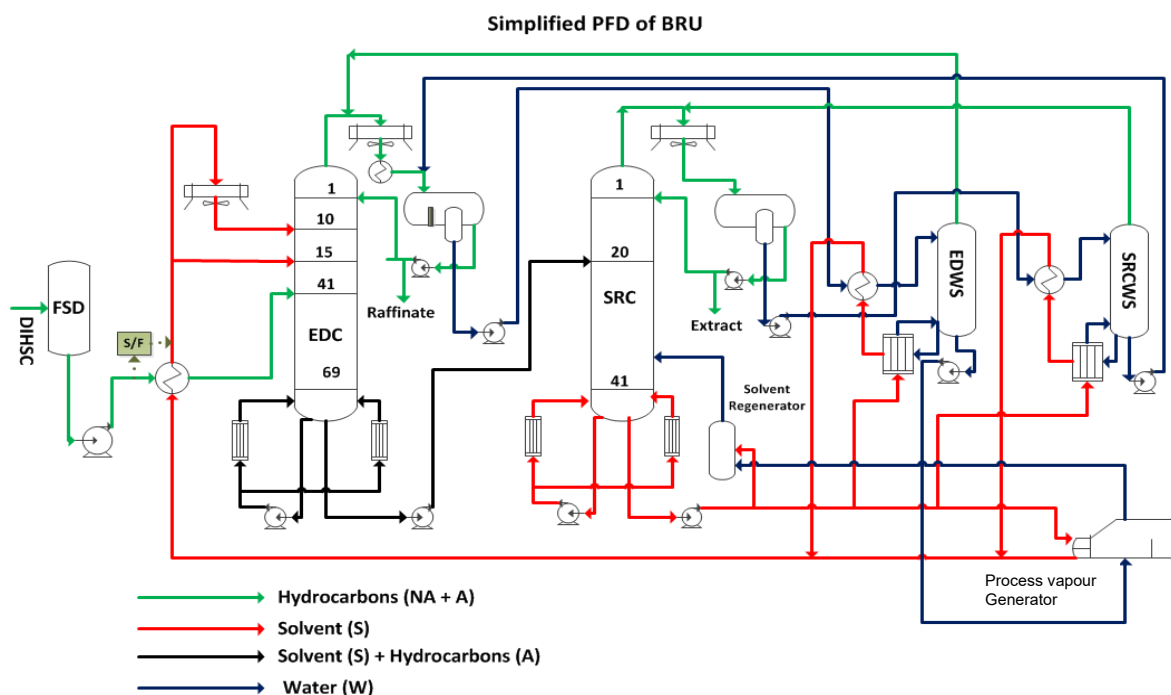


**Figure 1. Simplified Process Flow Diagram (PFD) for Benzene Recovery Unit**

Figure 1 shows the simplified process flow diagram (PFD) for Benzene Recovery Unit. The pre-heated feed consisting of benzene concentrated unprocessed catalytically cracked gasoline fraction containing impurities (typical composition 10-30 weight % benzene, and 70-90 weight % close-boiling non-aromatic hydrocarbons) is charged to extractive distillation column (EDC). The feed material is introduced into the ED column at its middle section and the solvent is introduced into the column at its top section with multiple feed entry locations. The solvent coming out from process vapor generator is cooled using the feed material before entering the EDC. ED re-boiler operates at a temperature range from 140-185°C. Top product i.e. raffinate comprises of gasoline having a benzene content of than 0.4 weight % and bottom product i.e. extract phase contents benzene and solvent mixture. In Solvent Recovery Column (SRC), solvent is separated from extract phase to obtain benzene free solvent from the bottom and benzene having a purity of greater than 97 weight % from the SRC top.

EDWS and SRCWS is water stripper to recover residual gasoline and benzene in co-solvent water coming from respective decanters of EDC and SRC.

## Process Design and Engineering

The team worked together to integrate their technical know-how & operating experience to engineer a highly intensive Process Design, while being robust to provide Reliable & Sustainable Plant Operation. The team worked very closely with Detail Engineering Contractor throughout the Engineering Phase to Evaluate & Integrate design features to achieve above design objectives.

BRU has been designed with state of art engineering and applying various process intensification units to make the process reliable and sustainable.

## Concept to Commercialization: Excellence in Academic – Industry collaboration

The benzene recovery process is an example of excellence in industry-academia collaboration. The team comprising of members from both Council for Scientific Research (CSIR) Indian Institute of Petroleum (IIP) Dehradun and Reliance Industries Limited (RIL) worked passionately & seamlessly as 'One-Team' to combine their strengths in developing Benzene Recovery Process to meet RIL business needs.

## Conclusions

Benzene recovery unit's commercialization is another successful story of excellence in academia-industrial collaboration. It has been designed with an out-of-the box process configuration which minimizes solvent loss, utility requirements, and maximizes yield & purity of products. The process does not require any prior hydrogenation step (Naphtha SHU) to saturate di-olefins which makes it simple, energy efficient, and low-cost operation. The solvent mixture used in the process is highly thermal stable solvent hence suits the process requirements very well. The major distillation columns (EDC and SRC) operates under positive pressure to avoid the possible degradation of solvent due to air oxidation.

RIL-IIP Teamwork resulted in successful Development, Process Design, Engineering, Construction, Commissioning & Operation of "**First Commercial Unit in the World**" to extract benzene from FCC's highly olefinic and contaminants laden stream. The unit was Successfully Commissioned on 23<sup>rd</sup> May 2016. 100% throughput was achieved within a week time and currently plant is operating at design performance at 150% design capacity. Plant has been in operation for more than six years without any shutdown or any safety/reliability/product quality concerns. The molecular value of gasoline was retained by retaining olefins, at the same time benzene content in gasoline brought down to comply with National & International specifications.

This technology, which has now been proved at world scale, is now available for licensing. Also it can give huge benefits to producers who already have an existing benzene recovery unit, which can be re-structured/optimized at very low costs in lines with the said technology to process complex feedstocks like FCC gasoline.

## References:

1. Eckart Muller, Bergen Enkheim, Kamar Percy John, US3591490A, (1971).
2. H Thompson, US3723256A, (1973).
3. Paulino Forte, US5022981A, (1991)
4. Mitchell E. Loescher, Gary G. Podrebarac, Quoc T. Phan, US8143466B2, (2012).
5. Marrten J. Almering, Kerry L. Rock, Arvids Zudjis, NPRA Annual meeting Manchester

## **6. Nuclear Applications**

# Kinetic study of uranium extraction in a microfluidic channel

Hamza Karim<sup>a</sup>, Anne L  lias<sup>a</sup>, Christophe Castel<sup>b</sup>.

**Abstract.** Recent investigations into the kinetics of liquid-liquid extraction have been conducted in microfluidic channels due to the high mass transfer efficiency. In this work, extraction kinetics of uranium (VI) (10-120 g.L<sup>-1</sup>) from aqueous nitric acid solutions (0.1-5 M) by tributyl-phosphate (TBP 5-30 % (v/v)) were investigated using a high-velocity stratified flow Y-Y shaped microfluidic device. Short residence times, around 10 ms, were applied to minimize the diffusional contributions<sup>i</sup>.

Experimental data were modeled using an approach taking into account both diffusional and reactional resistances to examine if the experimentally determined mass transfer coefficient could be considered equal to the chemical rate constant. Modeling results suggest that the mass transfer was under a mixed regime and the forward apparent rate constant ( $k_{app}$ ) is calculated to be  $(7.2 \pm 2) \cdot 10^{-4} \text{ m.s}^{-1}$  under extraction conditions, a value much higher than that predicted by conventional extraction techniques<sup>ii</sup>. Reaction orders with respect to nitrate and TBP were determined and the intrinsic value of the rate constant was then estimated. Furthermore, the reverse rate constant decreased with increasing nitrate and TBP concentration, suggesting the presence of a more complex reaction mechanism.

**Keywords:** Microfluidic, liquid-liquid extraction, extraction kinetics, uranium, modelling

## Introduction

The in-depth understanding of the extraction kinetics in reactive liquid-liquid extraction systems is of high importance for the efficient process design of extractors and accurate modeling of processes<sup>iii</sup>. In such extraction systems, the overall mass transfer is determined by the interfacial kinetics and the diffusion of the reactants and products to the interface. Hence, the mass transfer can be limited by the chemical reaction, the diffusion of the species, or both, under a mixed regime<sup>iv</sup>.

Several methods, such as highly stirred vessels or Lewis cells<sup>v</sup>, are thus employed to investigate the limiting kinetic regime by reducing the boundary layer thickness to a minimum. Nevertheless, for fast chemical reactions, the obtained results often depend on the system's hydrodynamics, which leads to acquire an apparent mass transfer coefficient. The latter brings together diffusional and reactional parts that are difficult to distinguish independently.

Kinetic determinations of fast chemical reactions can thus be complicated using traditional techniques. However, when compared to conventional macroscale systems, microchannels have several advantages. These include short diffusion path lengths and large interfacial area per unit volume, which results in a high mass transfer rate across the interface<sup>vi</sup>. For instance, Hotokezaka *et al.*<sup>vii</sup> found that extracting uranium (VI) with TBP in a parallel flow Y-Y chip generated a yield comparable to batch (95 %) but with a much shorter residence time (1.5 s).

Recently, an experimental methodology for kinetic data acquisition in a reactive liquid-liquid process using parallel flow in a Y-Y microchannel has been proposed. The developed method aims to conduct kinetic experiments at high velocities, reducing thus the diffusion boundary

<sup>a</sup> CEA/DES/ISEC/DMRC/SPTC-LCIS, universit   de Montpellier, Marcoule, France.

<sup>b</sup> Laboratoire de R  action et G  nie des Proc  d  s-CNRS UMR 7274, Nancy, France.

layer as minimum as possible to attain the chemically limited regime. The current work thus intends to answer the following question: can the chemical reaction constant of a fast chemical system be determined using a high velocity parallel flow microfluidic device? For this reason, we chose to study the well-known fast chemical system of uranium (VI) extraction from nitric acid medium using TBP as an organic extractant.

## Theory

Two approaches are used to analyze the kinetic experimental data. In the First, the overall mass transfer resistance ( $R_{aq}$ ) is determined for various operating conditions and then analyzed to determine if a chemical regime is established. In this case, the chemical reaction would solely limits the mass transfer and thus, the chemical kinetic constant could be determined directly from the experimental data. The overall resistance to the mass transfer is determined using the log mean concentration difference as described by Willersinn *et al.*<sup>viii</sup>

However, because the investigated system is extremely fast, the possibility of a mixed or even diffusional limitation should also be considered. As a result, to understand better the chemical system under study and distinguish the limiting regime, a 1-D laminar model with convection in the axial direction and diffusion in the transverse direction is developed (Figure 1). It should be noted that the simulation results were compared with a more sophisticated model taking into account diffusion in the directions perpendicular to the flow and convection in the axial direction. Simulations under current operating conditions and channel geometry demonstrated that the 1-D laminar model is sufficient to predict the same results as those obtained by the more elaborated one.

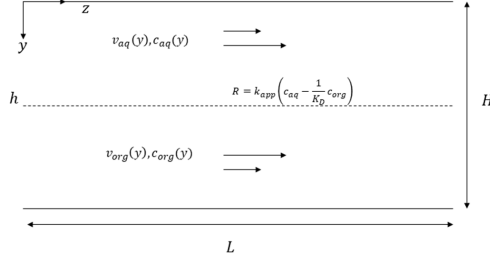


Figure 1 : Schematic representation of parallel flows between two infinite plates

Assuming a flat interface in the channel, negligible gravitational effects, an incompressible fluid and a laminar and fully developed flow over the channel length, an analytical solution for the velocity profile can be obtained. In this work, the analytical solution given by Malengier *et al.*<sup>ix</sup> is used.

For the mass transfer, the following characteristic scales are used to obtain the non-dimensional form of the governing equations:

$$y_{ch} = H, \quad x_{ch} = D, \quad v_{aq,ch} = \frac{\widetilde{Q}_{aq}}{H}, \quad v_{org,ch} = \frac{\widetilde{Q}_{org}}{H}, \quad C_{i,ch} = C_{aq,0} \quad (1)$$

with  $\widetilde{Q}_i$  representing the flow rate of phase  $i$  per unit depth of the channel.

The dimensionless convection diffusion equations describing the transfer of U(VI) from the aqueous phase to the organic phase are given by:



$$\begin{cases} \frac{\partial c_{aq}}{\partial z} = \left( \frac{1}{v_{aq}(y)} \right) \left( \frac{1}{Pe_{aq}} \right) \left[ \frac{\partial^2 c_{aq}}{\partial y^2} \right] & 0 \leq y \leq \alpha \\ \frac{\partial c_{org}}{\partial z} = \left( \frac{1}{v_{org}(y)} \right) \left( \frac{1}{Pe_{org}} \right) \left[ \frac{\partial^2 c_{org}}{\partial y^2} \right] & \alpha \leq y \leq 1 \end{cases} \quad (2)$$

where  $\alpha$  is the holdup of the aqueous phase ( $\alpha = h/H$ ), and  $Pe_i$  is the Peclet number of the phase  $i$  given by:

$$Pe_i = \frac{\tilde{Q}_i H}{\mathcal{D}_i L} \quad (3)$$

with  $\mathcal{D}_i$  being the diffusion coefficient in the phase  $i$ .

The governing mass transfer equations are subject to the no flux conditions at the walls of the channel ( $y = 0$  &  $y = 1$ ) and a reversible first order reaction at the interface ( $y = \alpha$ ):

$$\begin{cases} \frac{\partial c_{aq}}{\partial y} = -Bi_{aq} \left( c_{aq} - \frac{1}{K_D} c_{org} \right) \\ \frac{\partial c_{org}}{\partial y} = -Bi_{org} \left( c_{aq} - \frac{1}{K_D} c_{org} \right) \end{cases} \quad (4)$$

where  $Bi_{aq}$  and  $Bi_{org}$  are the Biot numbers for the metal and the complex respectively. The Biot number represents the ratio of the diffusion time scale to the reaction time scale and is given by:

$$Bi_i = \frac{k_{app} H}{\mathcal{D}_i} \quad (5)$$

The system of equations is solved numerically using the Method of Lines. Briefly, the  $y$ -direction is discretized using second-order differences, and the resulting set of ordinary differential equations is integrated along the axial direction  $z$  using ode15s in MATLAB.

## Experimental

Kinetic experiments were performed in a Y-Y geometry glass microchip from Dolomite® (part No. 3200008). Microchannel dimensions ( $D \times H \times L$ ) were  $100 \mu\text{m} \times 205 \mu\text{m} \times 12.5 \text{ mm}$  with a semicircular cross-sectional area. The extraction procedure and experimental setup have been described previously<sup>1</sup>: briefly, two inlet vessels (100-mL glass vials) containing respectively an aqueous solution of uranium (VI) (10-120  $\text{g.L}^{-1}$ ) in nitric acid (0.1-5 M) and TPH solution of TBP (5-30 % (v/v)) were connected to a Fluigent MFCS-EX pressure pump. The flow rates were set using the same entrance pressure to ensure a 50/50 phase proportion inside the microchannel. In addition, a compensation pressure ranging from 0 to 20 mbar was used at the organic outlets to ensure its purity. Uranium (VI) was stripped from the organic phase by contacting it with ten times its volume of 0.3 M  $\text{HNO}_3$  for 30 min under strong stirring. The obtained aqueous phase was then analyzed by ICP-OES.

## Results and Discussion

Experimental results of the extraction of U(VI) from a 3 M nitric acid solution by TBP 30% in TPH are summarized in Figure 2. The observed mass transfer resistance from the aqueous phase to the organic one ( $R_{aq}$ ) is almost independent of the residence time in the

microchannel. This implies that the applied velocities may have been sufficiently high to reduce the thickness of the diffusion boundary layer, resulting in a chemically limited regime. In such case, the overall resistance would equal the reactional resistance ( $R_{aq} = 1/k_{app}$ ) and the apparent rate constant could be determined experimentally. However, a key future of a chemical control regime is that the obtained kinetic rate constant is independent of the reactant concentration<sup>x</sup>.

Nevertheless, it is clear from Figure 2, that  $R_{aq}$  varies with the initial concentration of U(VI) which means that the assumption of a chemically limited regime is not valid under the current operating conditions.

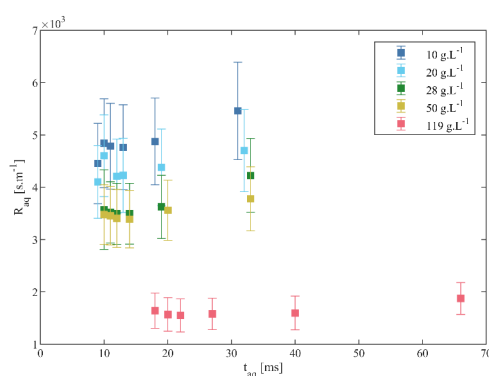


Figure 2 : Variation of the overall resistance with the residence time in the aqueous phase for different initial concentration of U(VI) ([HNO<sub>3</sub>] = 3 M, % TBP = 30 % (v/v))

The observation of constant  $R_{aq}$  with respect to the residence time is most likely due to the “slip effect” encountered most often in constant interfacial area stirred cells. In fact, despite the increase of the velocity, the thickness of the diffusion films may never fall below a sufficiently low value to make diffusion so fast that it can be completely ignored relative to the chemical reaction. Hence, most probably a diffusional contribution is still present in the current system and needs to be accounted for.

Moreover, as the initial concentration of the metal increases, the diffusive mass transfer usually contributes an added proportion to the overall mass transfer, thus increasing the overall resistance to mass transfer. However, Figure 2 depicts that  $R_{aq}$  is decreasing with increasing initial concentration of U(VI) indicating that mass transfer is accelerated at these conditions.

To understand better this last observation, the 1-D model is used to investigate the behavior of the system under consideration at different values of the apparent rate constant. This is illustrated in Figure 3 where the relative error between the simulated and experimental extraction ratios (ER) is plotted against the base-10 logarithmic of  $k_{app}$  for different residence times and initial concentration of U(VI) allowing to represent the three different extraction regimes on a single graph.

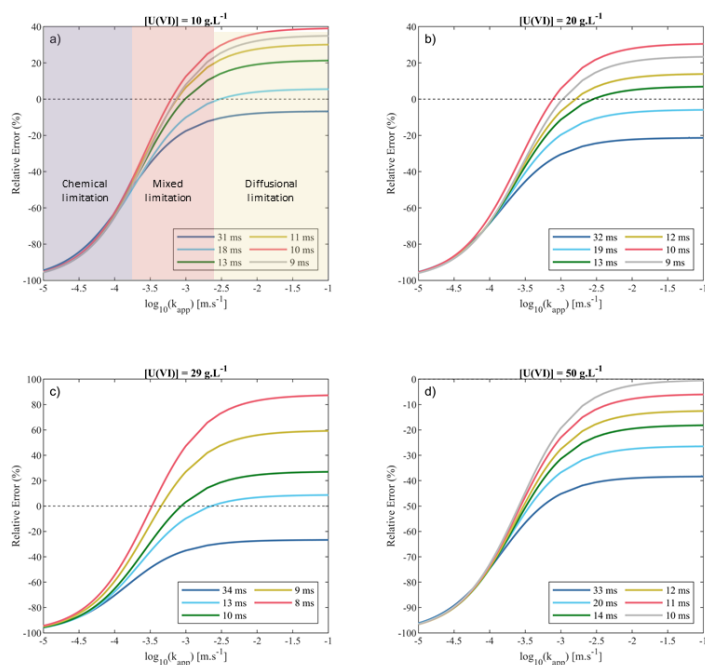


Figure 3 : Relative error between simulated and experimental extraction ratios vs  $k_{app}$  for different values of residence times in the aqueous phase ([HNO<sub>3</sub>] = 3 M, % TBP = 30 % (v/v))

Figure 3 reveals that a mixed regime is observed for low initial concentration of U(VI) (10-30 g.l<sup>-1</sup>) and short residence times ( $t_{aq} \leq 13$  ms), where the same value of  $k_{app}$  reproduces the experimental ER. Nevertheless, for high initial concentration of U(VI) and high residence times, the model always underestimates the extraction ratio even after removing the reactional resistance ( $k_{app} \geq 10^{-2}$  m.s<sup>-1</sup>). The experimental extraction ratio stays accelerated with respect to the simulated one. These observations are in coherence with those of the overall mass transfer resistance analysis, where an acceleration of the mass transfer is observed at higher [U(VI)]. To verify the analysis, the apparent rate constant is determined using the 1-D model by fitting the operating conditions where a mixed regime is most probably present. Then, the value of the overall mass transfer coefficient  $K_{aq}$  is obtained at the highest value of [U(VI)], where the accelerating phenomena might have completely eliminated the diffusional contribution. The obtained value of  $k_{app}$  is equal to  $(7.2 \pm 2) \cdot 10^{-4}$  m.s<sup>-1</sup> and the overall mass transfer coefficient at [U(VI)] of 119 g.l<sup>-1</sup> is  $K_{aq} = (6.2 \pm 0.5) \cdot 10^{-4}$  m.s<sup>-1</sup>. The latter being equivalent to the former (within the error), the assumptions of a mixed regime at low [U(VI)] and short residence times and a chemical regime at [U(VI)] = 119 g.l<sup>-1</sup> are reinforced.

Next, the variation of the apparent rate constant with respect to NO<sub>3</sub><sup>-</sup> and TBP is examined. Note that for each initial condition, a scan was performed over a wide range of  $k_{app}$  values for the different residence times to determine the appropriate operating conditions where the 1-D model is suitable, as illustrated in Figure 3. Once the operating conditions are chosen, the value of the  $k_{app}$  was obtained by a fitting procedure to the experimental data.

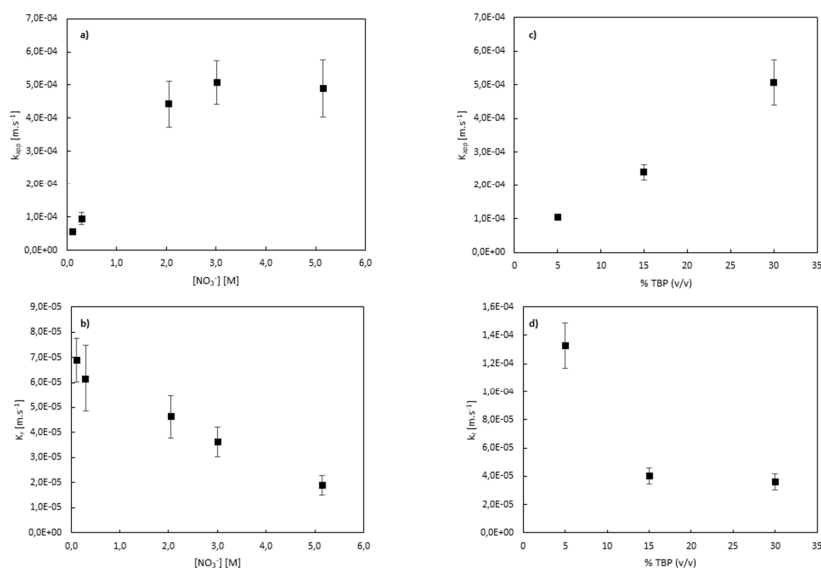


Figure 4 : a & b) Variation of the apparent and reverse reaction rates with respect to  $[\text{NO}_3^-]$  ( $[\text{U(VI)}] = 30 \text{ g.l}^{-1}$ , 30 % TBP (v/v)); c & d) with respect to % TBP (v/v) ( $[\text{U(VI)}] = 30 \text{ g.l}^{-1}$ ,  $[\text{NO}_3^-] = 3 \text{ M}$ )

The forward apparent reaction constant increases with the initial concentration of nitrate and TBP. In the case of increased nitrate concentrations,  $k_{app}$  reaches an asymptotic value at 2 M of  $\text{NO}_3^-$ . This tendency has also been observed by Moszkowicz<sup>xi</sup> and might be due to the increased fraction of the metal ion present as nitrate complexes as the nitrate concentration is increased.

The partial orders with respect to both nitrate ions and TBP were determined by plotting the log-log variation of the apparent constant with respect to both species. The obtained values were respectively of  $0.73 \pm 0.06$  and  $0.9 \pm 0.1$  for nitrate and TBP. Hence, based on the proposed mechanism (the complexation of the neutral metal with the extractant) the partial orders with respect to nitrate and TBP can be approximated as one. This means that the forward reaction rate for the proposed mechanism increases linearly with the concentrations of nitrate, TBP and U(VI):

$$R = (3.31 \pm 0.9) \cdot 10^{-9} [\text{NO}_3^-] [\text{TBP}] [\text{U(VI)}] \quad (6)$$

Nevertheless, the increased concentrations of nitrate and TBP have a negative influence on the reverse rate constant. It should be mentioned that Baumgärtner *et al.*<sup>xii</sup> and Horner *et al.*<sup>xiii</sup> observed the same tendency using the single drop technique. This negative dependency is evidence of a complex reaction involving not only the neutral metal, but also ionic species, which could be the limiting step in the reaction mechanism. Furthermore, a molecular dynamic study conducted by Sahu *et al.*<sup>xiv</sup> suggested that the  $\text{UO}_2^{2+}$  ions were found to complex with 1-3 TBPs at the interface and that the final experimentally observed complex  $(\text{UO}_2(\text{NO}_3)_2 \cdot 2\text{TBP})$  is formed *via* reorganization of these intermediate interfacial complexes, reinforcing the assumption of a more complex reaction mechanism.

## Conclusion

This study sought to determine whether a fast chemical system's reaction rate constant could be experimentally determined using a high velocity parallel flow microfluidic setup. For this purpose, a

**Kommenterad [LA1]:** ta conclusion résonne un peu avec la question de Christian dans ta NT : est-ce que les nitrates ne joueraient pas un rôle particulier avec des espèces qu'on n'aurait pas envisagées ? ce que tu dis d'ailleurs dans la phrase suivante.

combination of overall mass transfer resistance ( $R_{aq}$ ) calculations for the aqueous phase and advection diffusion-reaction simulations were used to model experimental kinetic data for Uranium (VI) extraction by TBP 30% in TPH.

The analysis suggested that a mixed regime was established for low initial concentration of uranium (VI) ( $10\text{--}30\text{ g.l}^{-1}$ ) and short residence times ( $t_{aq} \leq 13\text{ ms}$ ). Under these conditions, the apparent rate constant cannot be determined experimentally and a numerical model is instead needed. Furthermore, an acceleration of mass transfer was observed at increasing initial concentration of U(VI). This has been confirmed by the equivalence between the fitted value of  $k_{app}$  (mixed regime) with that obtained experimentally at  $[U(VI)]_0 = 119\text{ g.l}^{-1}$  (chemical regime).

Furthermore, it has been shown that the forward reaction rate varied linearly with nitrate and TBP concentrations if the neutral metal complexation with the extractant was considered as the limiting step. However, the negative dependence of the reverse rate constant on nitrate and TBP concentrations suggests that a more complex reaction mechanism involving ionic species complexation should be proposed.

## References

- 
- <sup>i</sup> Corne, F. (2019). Experimental Methodology for Kinetic Acquisitions Using High Velocities in a Microfluidic Device. *CET*, 42(10).
- <sup>ii</sup> Dinh, B. (1987). Investigation of the extraction kinetics of uranyl nitrate by tributyl phosphate: application of the single drop method in pulsed medium. (PhD thesis), Ecole Centrale des Arts et Manufactures, France.
- <sup>iii</sup> Stefan Willersinn and Hans-Jörg Bart. Kinetics of Ge(IV) extraction using a microstructured membrane contactor. *International Journal of Chemical Kinetics*, 48(10):609–621, 2016.
- <sup>iv</sup> Pier Roberto Danesi. Solvent extraction kinetics. In *Solvent Extraction Principles and Practice, Revised and Expanded*, pages 218–268. CRC Press, 2004.
- <sup>v</sup> Anne Lélías, Romain Berlemont, Manuel Miguiditchian, and Jean Pierre Simonin. Determination of U (VI) and Pu (IV) mass transfer constants with n, n-dialkylamides in liquid-liquid extraction. *ISEC, Prague, Czech Republic–April*, pages 4–5, 2016.
- <sup>vi</sup> Davide Ciceri, Jilksa M. Perera, and Geoffrey W. Stevens. The use of microfluidic devices in solvent extraction. *Journal of Chemical Technology & Biotechnology*, 89(6):771–786, 2014.
- <sup>vii</sup> Hiroyasu Hotokezaka, Manabu Tokeshi, Masayuki Harada, Takehiko Kitamori, and Yasuhisa Ikeda. Development of the innovative nuclide separation system for high-level radioactive waste using microchannel chip. *Bull. Res. Lab. Nucl. React*, 30:263–264, 2006.
- <sup>viii</sup> Stefan Willersinn and Hans-Jörg Bart. Reactive mass transfer in a membrane-based microcontactor. *Chemical Engineering and Processing: Process Intensification*, 95:186–194, 2015.
- <sup>ix</sup> Benny Malengier, JL Tamalapakula, and S Pushpavanam. Comparison of laminar and plug flow-fields on extraction performance in micro-channels. *Chemical engineering science*, 83:2–11, 2012.
- <sup>x</sup> Dong Zhang, Longyang Fu, Guangze Xu, and Yadong Zhang. Segmented flow capillary microreactors for determination of kinetic rate constants of reactive zinc extraction system. *Chemical Engineering Science*, 247:117037, 2022.
- <sup>xi</sup> Pierre Moszkowicz. Contribution to the study of interfacial mass transfers: extraction of U and Pu. Technical report, CEA Centre d'Etudes Nucleaires de Fontenay-aux-Roses, 1976.
- <sup>xii</sup> Franz Baumgärtner and L Finsterwalder. On the transfer mechanism of uranium (VI) and plutonium (IV) nitrate in the system nitric acid-water/tributylphosphate-dodecane. *The Journal of Physical Chemistry*, 74(1):108–112, 1970.
- <sup>xiii</sup> D Horner, J Mailen, S Thiel, T Scott, and R Yates. Interphase transfer kinetics of uranium using the drop method, lewis cell, and kenics mixer. *Industrial & Engineering Chemistry Fundamentals*, 19(1):103–109, 1980.
- <sup>xiv</sup> Sahu, P., et al., Does uranyl-TBP complex formation happen at the aqueous-organic interface? Revelation by molecular dynamics simulations. *Journal of Molecular Liquids*, 330:115621, 2021.

# CFD Simulations of Pulsatile Two-phase Flow in Columnar Contactors: Effect of the Shape of the Internals on Dispersed Phase Holdup and Axial Dispersion

Sourav Sarkar,<sup>a,b,\*</sup> K.K. Singh,<sup>a,b</sup> S. Mukhopadhyay,<sup>a,b</sup> K. T. Shenoy<sup>c</sup>

## Abstract

*Two-phase Euler-Euler based Computational Fluid Dynamics (CFD) simulations of pulsed disc and doughnut columns are performed to understand the effects of shapes of the internals on the dispersed phase holdup and axial dispersion coefficient. Flow field is obtained by solving continuity and momentum equations and turbulence is modeled using standard  $k-\varepsilon$  mixture model of turbulence. Species transport equation is solved to carry out virtual tracer study for the estimation of axial dispersion of continuous phase. Four different shapes of disc and doughnut internals are analyzed in terms of dispersed phase holdup and axial dispersion. Novel disc and doughnut designs show considerable decrease in axial dispersion with insignificant change in dispersed phase holdup compared to conventional design for identical operating conditions.*

**Keywords:** axial dispersion, pulsed disc and doughnut column, numerical simulation, holdup, two-phase flow

## Introduction

Liquid-liquid extraction is one of the major separation processes which is widely used in chemical, hydrometallurgical and nuclear industry. In nuclear industry solvent extraction is widely used in both front and back-end<sup>i,ii,iii</sup>. There are several solvent extraction equipments which are used for separation of nuclear materials but pulsed column is most commonly used in nuclear fuel cycle as it provides high throughput and high separation efficiency along with the advantages like low maintenance, no moving part in contact with the working fluid<sup>iv,v,vi,vii,viii</sup>. Conventionally sieve plate internal is widely used in pulsed column but further it is modified to disc and doughnut internal for several advantages like low channelling, better solid handling capabilities<sup>ix,x</sup>.

Several experimental and numerical studies are reported on pulsed disc and doughnut column. These studies aim to estimate axial dispersion in single-phase flow<sup>xi,xii,xiii,xiv</sup> as well as in two-phase flow<sup>xv,xvi</sup>. There are also studies which estimate drop size distribution<sup>xvii,xviii</sup>, slip velocity<sup>xix</sup>, flooding<sup>xx</sup>, mass transfer<sup>xxi</sup> and dispersed phase holdup<sup>xxii,xxiii,xxiv</sup> both experimentally and numerically.

In the present work, Euler-Euler based two-phase CFD model is used to estimate dispersed phase holdup and extent of axial dispersion in pulsed disc and doughnut column. A validated CFD model is used to evaluate the performance of novel conceptual design which are

---

<sup>a</sup>Chemical Engineering Division, Bhabha Atomic Research Centre, Trombay, Mumbai, INDIA-400085

<sup>b</sup>Homi Bhabha National Institute, Anushaktinagar, Mumbai, INDIA-400094

<sup>c</sup>Chemical Engineering Group, Bhabha Atomic Research Centre, Trombay, Mumbai, INDIA-400085

\*[souravs@barc.gov.in](mailto:souravs@barc.gov.in)

obtained by changing the shape of conventionally used disc and doughnut internals. The new designs are evaluated computationally in terms of dispersed phase holdup and axial dispersion. It is found that novel conceptual designs show encouraging results in terms of axial dispersion. It is also found that dispersed phase holdup is nearly remain same in all the designs.

## Mathematical model and validation

Simulations are carried in two steps. In the first step of the simulation, CFD model solves the conservation equations of mass and momentum for both phases using Euler-Euler method which assumes that both phases can be present in each cell of the computational domain. Momentum exchange between the two phases is modelled using interphase exchange coefficients. Drag coefficient is estimated from Schiller-Naumann drag model. Turbulence is modelled using the mixture  $k-\varepsilon$  model in which the turbulence equations are solved for the mixed phase. To take care of droplet-droplet collision effect in the zone where dispersed phase holdup is high, the collision model based on the kinetic theory of granular flows is incorporated. Uniform drop size is considered and it is estimated from the correlation reported by Sarkar and co-workers<sup>xvii</sup>. For the simulations 3N nitric acid is kept as continuous phase and 30% TBP in dodecane is kept as dispersed phase (corresponding material properties are used in simulations). Once the two-phase flow field is reached steady state (dispersed holdup averaged over the pulsing cycle is nearly constant) species transport equation is also solved along with the conservation equations of mass and momentum. Virtual tracer study is carried out by solving species transport equation. From the virtual tracer study, Peclet number is estimated. For efficient computation only a few discs and doughnuts are simulated and the details of the computation technique may be found in our previous work<sup>xv</sup>. CFD model is extensively validated by varying different operating and geometric parameters with the inhouse experimental data. Details of the validation are published in our previous works<sup>xv,xxiv</sup>.

## Results and discussion

### Novel designs

Axial dispersion depends primarily on flow field in the column. Geometry of the column and internals play an important role in determining the flow field in the column. It is reported in literature that with the change in disc spacing to column diameter ratio ( $h/D$ ) circular recirculation pattern changes which changes the axial dispersion<sup>xiv</sup>. It is also reported that with the decrease of  $h/D$  ratio, axial dispersion reduces significantly but the accumulation of dispersed phase under the plate increases so possibility of flooding also increases<sup>xxiv</sup>. Therefore, it is desired to have design of internals which reduce the size of recirculation zone and squeezes the circular recirculation pattern to elliptical recirculation pattern keeping

dispersed phase holdup nearly same. To achieve this goal design of disc and doughnut column internals is modified. Novel conceptual and conventional designs tested in this study are shown in Fig. 1.

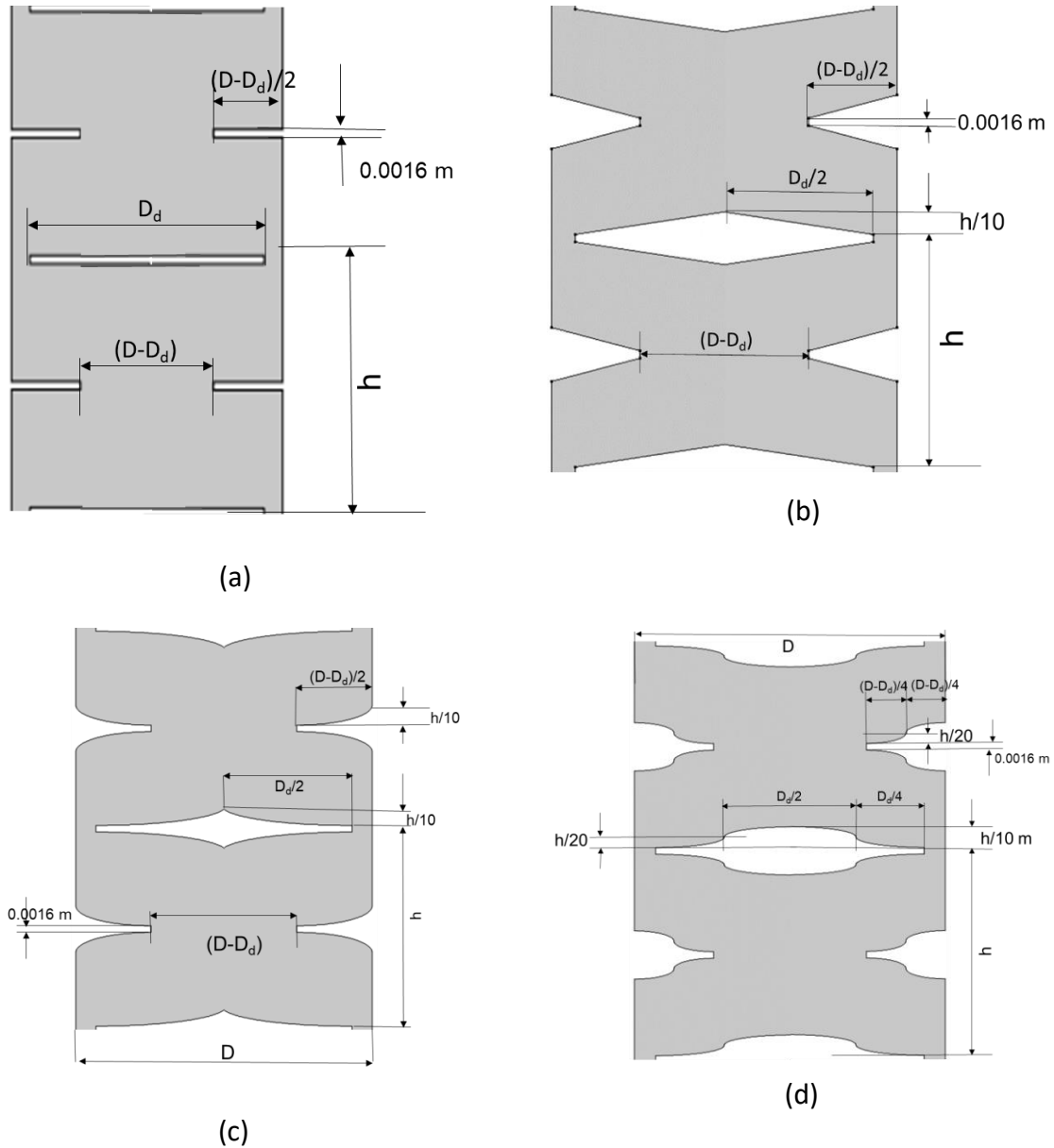


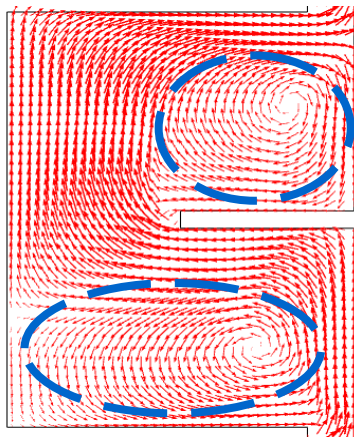
**Figure 1:** Front view of (a) conventional, (b) Slanted, (c) Convex and (d) Inflected disc and doughnut column

## Flow field

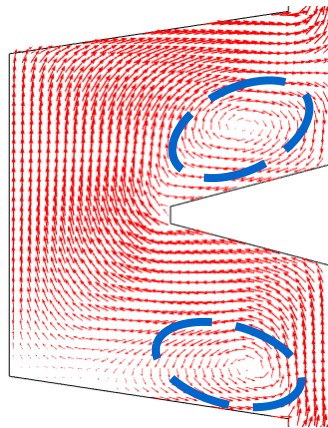
Velocity vector plots and recirculation zones for different internals are shown in Fig. 2(a)-(d). Spatial variations of velocity magnitude alongwith stream lines are shown in Fig. 2(e)-(h) for different internals. It may be noted that recirculation zone in slanted, convex and inflected disc and doughnut is smaller and elliptical in shape compared to conventional disc and doughnut



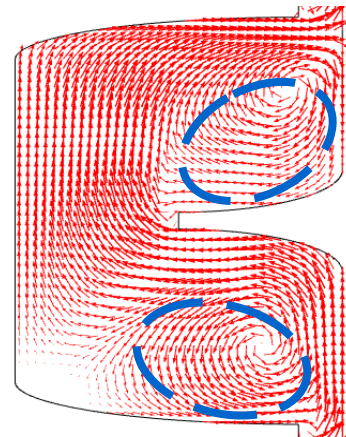
internal which has larger recirculation zones. This reduces the strength of recirculation resulting in lower axial mixing.



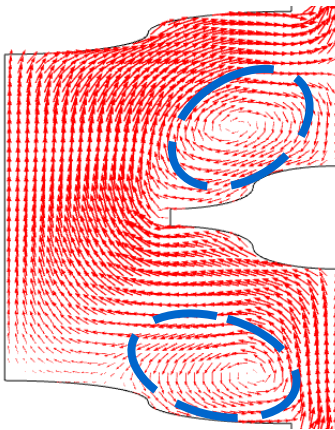
(a)



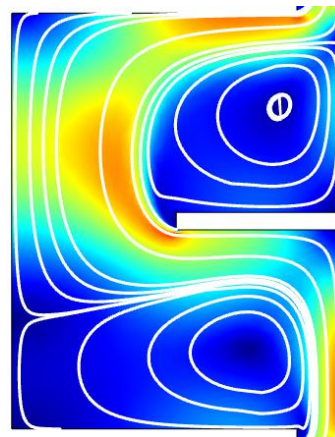
(b)



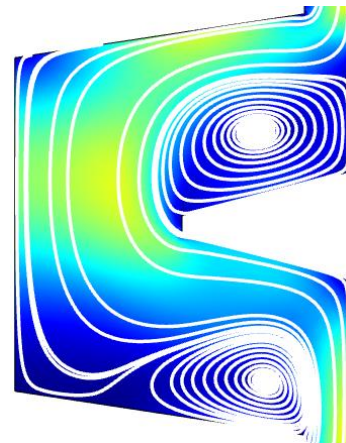
(c)



(d)



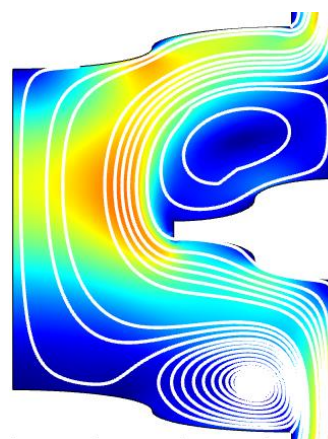
(e)



(f)



(g)



(h)



**Figure 2:** Velocity vector plot for (a) Conventional, (b) Slanted, (c) Convex and (d) Inflexed disc and doughnut column and velocity magnitude and streamlines of (e) Conventional (f) Slanted, (g) Convex and (h) Inflexed disc and doughnut column

## Dispersed phase holdup and axial dispersion

Simulations are carried out for the same operating conditions with different internals and it is found that dispersed phase holdup remains nearly same for all the internals. Maximum change of dispersed phase holdup with respect to conventional disc and doughnut internals is 3.8%. On the other hand, continuous phase Peclet number changes significantly with the change in internals. Peclet number increases by 112% in inflexed disc and doughnut column compared to conventional disc and doughnut column. This significant increase in Peclet number shows significant reduction of axial mixing in the inflexed disc and doughnut design. Other novel designs are also found to have lower axial mixing compared to conventional disc and doughnut column. Fig. 3 shows dispersed phase holdup and Peclet number for different internals for the same operating condition (continuous phase velocity and dispersed phase velocity are 0.0055 m/s, O:A=1:1, and pulsing velocity is 0.0277 m/s). Fig. 3 also shows corresponding spatial variation of dispersed phase holdup in between two discs for different types of internals.

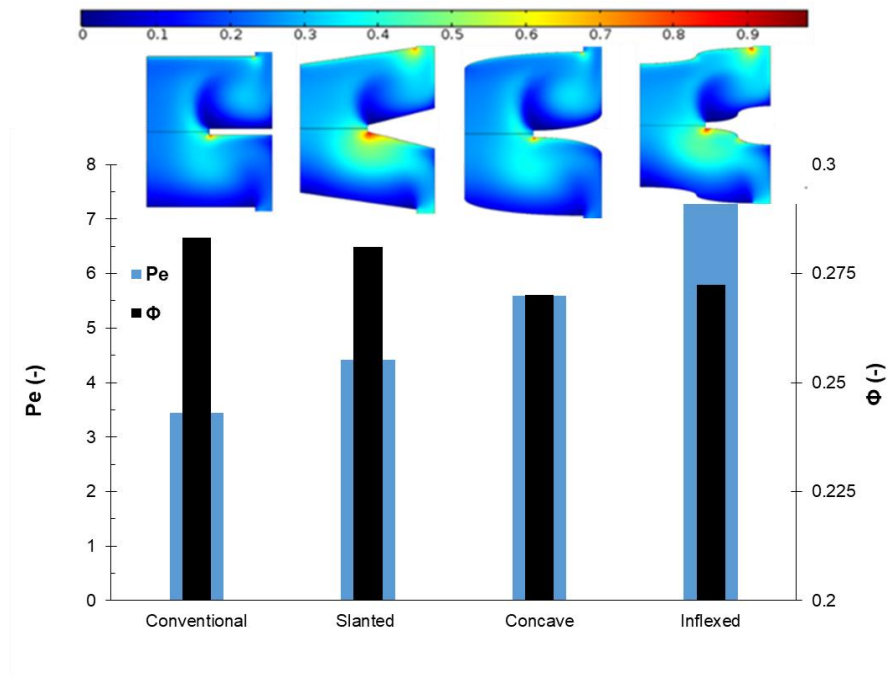


**Figure 3:** Comparison of dispersed phase holdup and Peclet number along with spatial variation of the dispersed phase holdup for different internals

## Conclusion

Axial dispersion and dispersed phase holdup are two important parameters for the estimation of height required for a columnar contactor. In present work, a validated two-phase Euler-Euler CFD model is used to estimate dispersed phase holdup and Peclet number in pulsed disc and doughnut column. A few novel conceptual designs of disc and doughnuts (slanted, convex, inflexed disc and doughnut) are evaluated by using the CFD model. The evaluation is done on the basis of dispersed phase holdup and Peclet number obtained for different types of designs for the same operating conditions. It is found that all the novel designs show lower axial mixing compared to conventional disc and doughnut column for identical operating conditions. It is also found that dispersed phase holdup hardly changes with the change in the design of internals (maximum change is 3.8%). Peclet number changes significantly (112%) in inflexed disc and doughnut design. Thus the work reported here shows the possibility of intensification of solvent extraction process (reduction in HETP) by altering the shape of the disc and doughnut in a pulsed disc and doughnut column. In the present study drop diameter is assumed uniform and obtained from an empirical correlation to reduce the computational time. In future, CFD-PB simulations may be used to estimate droplet size directly from the simulation instead of using correlation.

## References

- 
- <sup>i</sup>R. A. Leonard, *Separation Science and Technology*, 1988, 23(12-13), 1473.
- <sup>ii</sup> J. N. Sharma, A. Kumar, V. Kumar, S. Pahan, C. Janardanan, V. Tessi and P. Wattal *Separation and Purification Technology*, 2014, 35, 176.
- <sup>iii</sup> M. Zhao, S. Cao and W. Duan, *Progress in Nuclear Energy*, 2014, 74, 154.
- <sup>iv</sup> S. Chaturabul, P. Wannachod, B. Rojanasiraprapa, S. Summakasipong, A. W. Lothongkum and U. Pancharoen, *Separation Science and technology*, 2012, 47(3), 432.
- <sup>v</sup> E. Ferreira, S. Ana, R. Agarwal, M. Machado, M. L. F. Gameiro, S. M. Santos, M. T. A. Reis, M. R. C. Ismael, M. J. N. Correia and J. M. Carvalho, *Hydrometallurgy*, 2010, 104(1), 66.
- <sup>vi</sup> M.L.F. Gameiro, R. M. Machado, M. R. C. Ismael, M. T. A. Reis and J. M. Carvalho, *Journal of Hazardous Materials*, 2010, 183(1), 165.
- <sup>vii</sup> E. Liebermann and A. C. Jealous, 1953, ORNL-1543. Oak Ridge National Lab., Tenn.
- <sup>viii</sup> J. Schön, H. Schmieder and B. Kanellakopoulos., *Separation Science and Technology*, 1990, 25 (13-15), 1737.
- <sup>ix</sup> R. L. Movsowitz, R. Kleinberger, E. M. Buchalter and B. Grinbaum, in *Uranium 2000: International symposium on the process metallurgy of uranium*, 2000.
- <sup>x</sup> A. B. Jahya, G. W. Stevens and H. R. Pratt, *Solvent Extraction and Ion Exchange*, 2009, 27(1), 63.
- <sup>xi</sup> G. H. Jeong and C. Kim, *Korean Journal of Chemical Engineering*, 1984, 1(2), 111.
- <sup>xii</sup> M. F. Buratti, INPL, 1988.
- <sup>xiii</sup> S. Sarkar, K. K. Singh and K. T. Shenoy, *Progress in Nuclear Energy*, 2018, 106, 335-344.
- <sup>xiv</sup> Sarkar, S., Singh, K.K. and Shenoy, K.T., *Separation Science and Technology*, 2017, 52(18), 2863.
- <sup>xv</sup> S. Sarkar, K. K. Singh and K. T. Shenoy, *Industrial & Engineering Chemistry Research*, 2019, 58(33), 15307.
- <sup>xvi</sup> N. Sen, S. Sarkar, K. K. Singh and K. T. Shenoy, *Progress in Nuclear Energy*, 2021, 142, 103987.
- <sup>xvii</sup> S. Sarkar, K. K. Singh and K. T. Shenoy, *Progress in Nuclear Energy*, 2019, 106, 76.
- <sup>xviii</sup> S. Sarkar, K. K. Singh, S. M. Mahajani and K. T. Shenoy, *Solvent Extraction and Ion Exchange*, 2020, 38(5) 536.

- 
- <sup>xix</sup>M. Torab-Mostaedi, H. Jalilvand and M. Outokesh, *Chemical Industry and Chemical Engineering Quarterly*, 2011, 17(3), 333.
- <sup>xx</sup>M. Torab-Mostaedi, A. Ghaemi and M. Asadollahzadeh, *Chemical Engineering Research and Design*, 2011, 89(12), 2742.
- <sup>xxi</sup>M. Torab-Mostaedi, A. Ghaemi, M. Asadollahzadeh and P. Pejmanzad, *Brazilian Journal of Chemical Engineering*, 2011, 28(3), no. 3, 447.
- <sup>xxii</sup>J. F. Milot, J. Duhamet, C. Gourdon and G. Casamatta, *The Chemical Engineering Journal*, 1990, 45(2), 111.
- <sup>xxiii</sup>S. Sarkar, N. Sen, K. K. Singh, S. Mukhopadhyay and K. T. Shenoy, *Chemical Engineering and Processing: Process Intensification*, 2017, 118, 131.
- <sup>xxiv</sup>S. Sarkar, K. K. Singh and K. T. Shenoy, *Separation and Purification Technology*, 2018, 209, 608.

# Distribution data for the extraction of Am(III), Ln(III) and HNO<sub>3</sub> with 2,6-bis(1-(2-ethylhexyl)-1H-1,2,3-triazol-4-yl)pyridine

Andreas Geist<sup>1</sup>

**Abstract.** 2,6-bis(1-(2-ethylhexyl)-1H-1,2,3-triazol-4-yl)pyridine (PTEH) is a promising extracting agent for the separation of chemically similar trivalent actinides, An(III) and lanthanide, Ln(III). Distribution data for the extraction of An(III), Ln(III) and HNO<sub>3</sub> from 0.1–5 mol/L HNO<sub>3</sub> into solutions of 0.1–0.3 mol/L PTEH + 10%<sub>vol.</sub> 1-octanol in kerosene were determined. A simple equilibrium model for HNO<sub>3</sub> extraction was established.

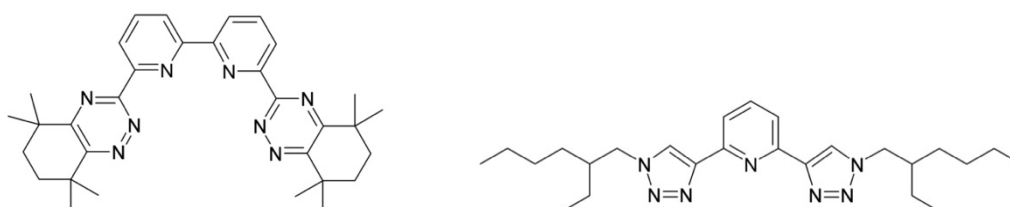
**Keywords:** Nuclear fuel cycle, americium, lanthanides, separation, PTEH

## Introduction

The recycling of irradiated nuclear fuels offers advantages with respect to the sustainability of nuclear power production. On one hand, recycling uranium and plutonium substantially reduces the amount of natural uranium to be mined, with uranium mining dominating the environmental footprint of nuclear energy production. On the other hand, additionally recycling americium would reduce the thermal burden on a final geological disposal for highly radioactive wastes, thus increasing the capacity of such a disposal facility.<sup>1–2</sup>

While uranium and plutonium recycling is addressed by the PUREX process, innovative separations are under development to separate americium from irradiated fuel.<sup>3</sup> Such separation schemes, at some point, require separating trivalent actinides, An(III) (= Am(III) and Cm(III)), from the chemically similar lanthanides, Ln(III), including Y(III). Some of the schemes developed in Europe<sup>4</sup> employ CyMe<sub>4</sub>-BTBP<sup>5–8</sup> (Scheme 1 left) to achieve this separation. Despite its otherwise good performance, CyMe<sub>4</sub>-BTBP has rather slow kinetics<sup>9</sup> and a limited solubility in the diluent used, 1-octanol.<sup>10</sup>

Recently, 2,6-bis(1-(2-ethylhexyl)-1H-1,2,3-triazol-4-yl)pyridine (PTEH, Scheme 1 right) was developed and screened for An(III)/Ln(III) separation. PTEH exhibits an An(III)/Ln(III) selectivity and stability against radiolytic degradation comparable to CyMe<sub>4</sub>-BTBP but has much better solubility and faster kinetics. Furthermore, it is better soluble even in kerosene containing a small volume fraction of 1-octanol.<sup>11–12</sup>



Scheme 1. CyMe<sub>4</sub>-BTBP(left) and PTEH (right).

<sup>1</sup> Karlsruhe Institute of Technology (KIT), Institute for Nuclear Waste Disposal (INE), 76021 Karlsruhe, Germany

Augmenting data available in the literature, distribution data for the extraction of Am(III) and Ln(III) into a solvent comprising PTEH + 10%<sub>vol.</sub> 1-octanol in kerosene were determined over a wide range of nitric acid concentrations (0.1–5 mol/L) and for three different PTEH concentrations (0.1, 0.2 and 0.3 mol/L). Furthermore, nitric acid extraction into this solvent was determined, and a simple equilibrium model for nitric acid extraction was established.

## Experimental

PTEH was synthesised according to the literature.<sup>11</sup> Organic phases were prepared by adding weighed amounts of PTEH and 1-octanol into volumetric flasks and making up with kerosene (TPH) to obtain 0.1, 0.2, and 0.3 mol/L PTEH + 10%<sub>vol.</sub> 1-octanol.

*Am(III) and Ln(III) extraction:* Aqueous phases were prepared by adding 5 µL of a spike solution (<sup>243</sup>Am(III), Y(III), La(III)–Lu(III) except Pm(III), 100 mg/L each) to 495 µL HNO<sub>3</sub> (0.1–5 mol/L) in 2 mL screw-cap glass vials. After adding each 500 µL of organic phase (0.1–0.3 mol/L PTEH), the vials were shaken on a temperature-controlled vortex mixer (40 Hz) for 45 min at 20°C. After centrifugation, organic samples were stripped into 0.5 mol/L ammonium glycolate, pH = 4, A/O = 5. Aqueous samples were diluted to 1/5 with 0.5 mol/L ammonium glycolate, pH = 4. Following further dilution to 1/40, samples were measured by ICP-MS. Several experiments were performed analogously with 0.2 mol/L PTEH using <sup>241</sup>Am(III) and <sup>154</sup>Eu(III) (2 kBq/mL each) only, and were directly measured by gamma counting.

*Nitric acid extraction:* Nitric acid (0.5–1 mol/L, 800 µL and 2–5 mol/L, 500 µL) and equal volumes of organic phase (0.1–0.3 mol/L PTEH) were added into 2 mL screw-cap glass vials and shaken (40 Hz) for 30 min at 20°C. After centrifugation, organic phase aliquots (700 µL or 400 µL) were stripped into (700 µL or 800 µL) water. Initial and equilibrium nitric acid concentrations were determined by duplicate titration with 0.1 mol/L NaOH on a Metrohm Titroprocessor.

## Results and Discussion

It was observed that at a PTEH concentration of 0.3 mol/L, a third phase formed upon contacting with aqueous phases containing 4–5 mol/L HNO<sub>3</sub>. However, no such issues were observed with 0.1 mol/L and 0.2 mol/L PTEH.

### Nitric acid extraction

Equilibrium organic phase nitric acid concentrations as a function of initial aqueous phase nitric acid concentrations for extraction into 0.1–0.3 mol/L PTEH + 10%<sub>vol.</sub> 1-octanol in kerosene are shown in Figure 1.

It is evident that the solvent extracts significant concentrations of nitric acid, which cannot be attributed to the rather low volume fraction of 1-octanol: 10%<sub>vol.</sub> 1-octanol in kerosene extracts approximately 0.1 mol/L HNO<sub>3</sub> from initially 5 mol/L HNO<sub>3</sub>, under otherwise identic experimental conditions.<sup>13</sup> Surplus nitric acid extraction hence is due to PTEH.

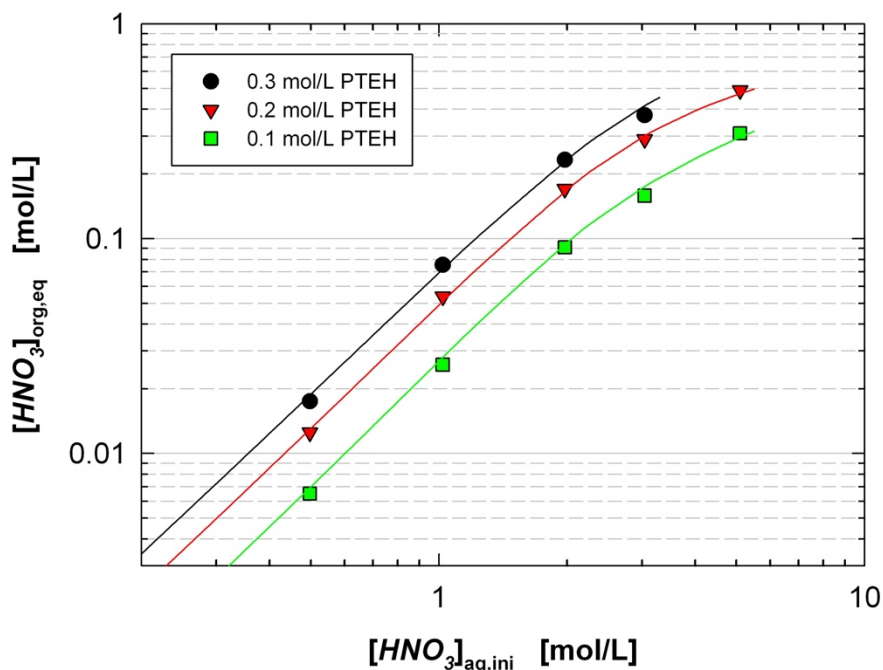
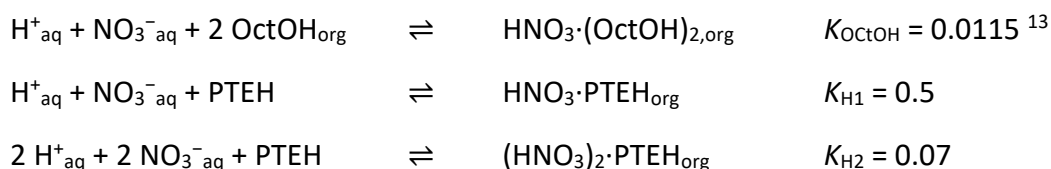


Figure 1. Extraction of nitric acid by PTEH. Organic phase, 0.1–0.3 mol/L PTEH + 10%<sub>vol.</sub> 1-octanol in kerosene. Aqueous phase, HNO<sub>3</sub>.  $T = 293\text{ K}$ ,  $A/O = 1$ .

The equilibrium model describing nitric acid extraction into 1-octanol-kerosene diluents<sup>13</sup> was extended to account for nitric acid extraction by PTEH. The following equilibria with the respective extraction constants were considered:



This rather simple model is in excellent agreement with the experimental data (see Figure 1), hinting that additional synergistic or antagonistic adducts<sup>14</sup> do not contribute significantly.

### Am(III) and Ln(III) extraction

Distribution data for the extraction of Am(III), Ln(III) and Y(III) into 0.1–0.3 mol/L PTEH + 10%<sub>vol.</sub> 1-octanol in kerosene are shown in Figures 2–4. Further to the data determined by ICP-MS analysis, four experiments were performed which were analysed by gamma counting (see Figure 3). The excellent agreement is proof of a sufficiently efficient back-extraction of the organic phase samples prior to ICP-MS analysis; incomplete back-extraction would have produced falsely low distribution ratios.

The Am(III)/Eu(III) selectivity is  $SF_{\text{Am/Eu}} = 105 \pm 10$ . With a PTEH concentration of 0.2 mol/L, separation of Am(III) from all Ln(III) and Y(III) (i. e.  $D_{\text{Am}} > 1$  and  $D_{\text{Ln,Y}} < 1$ ) is feasible for 1–2 mol/L HNO<sub>3</sub>. However, considering that irradiated fuel does not contain lanthanides heavier than dysprosium, this range extends to 1–3 mol/L HNO<sub>3</sub>. Alternatively, with 0.1 mol/L PTEH, the usable range is 2–5 mol/L HNO<sub>3</sub>.



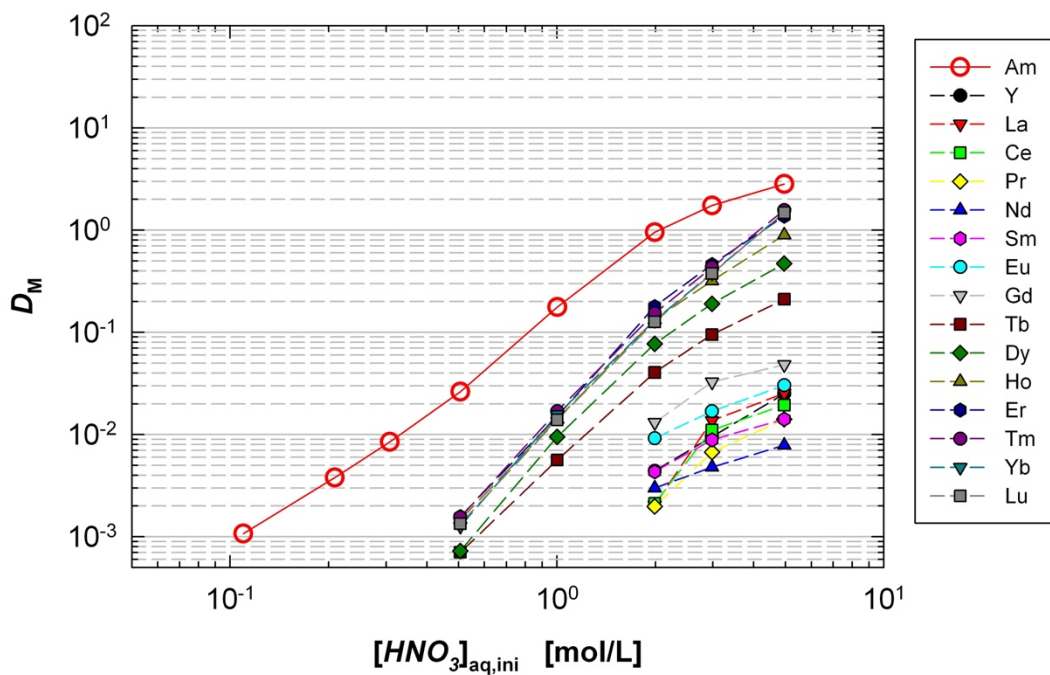


Figure 2. Extraction of Am(III) and Ln(III) by PTEH. Organic phase, **0.1 mol/L PTEH** + 10%<sub>vol.</sub> 1-octanol in kerosene. Aqueous phase,  $^{243}\text{Am(III)}$ , Y(III), La(III)–Lu(III) except Pm(III) (1 mg/L each) in  $\text{HNO}_3$ .  $T = 293 \text{ K}$ ,  $A/O = 1$ .

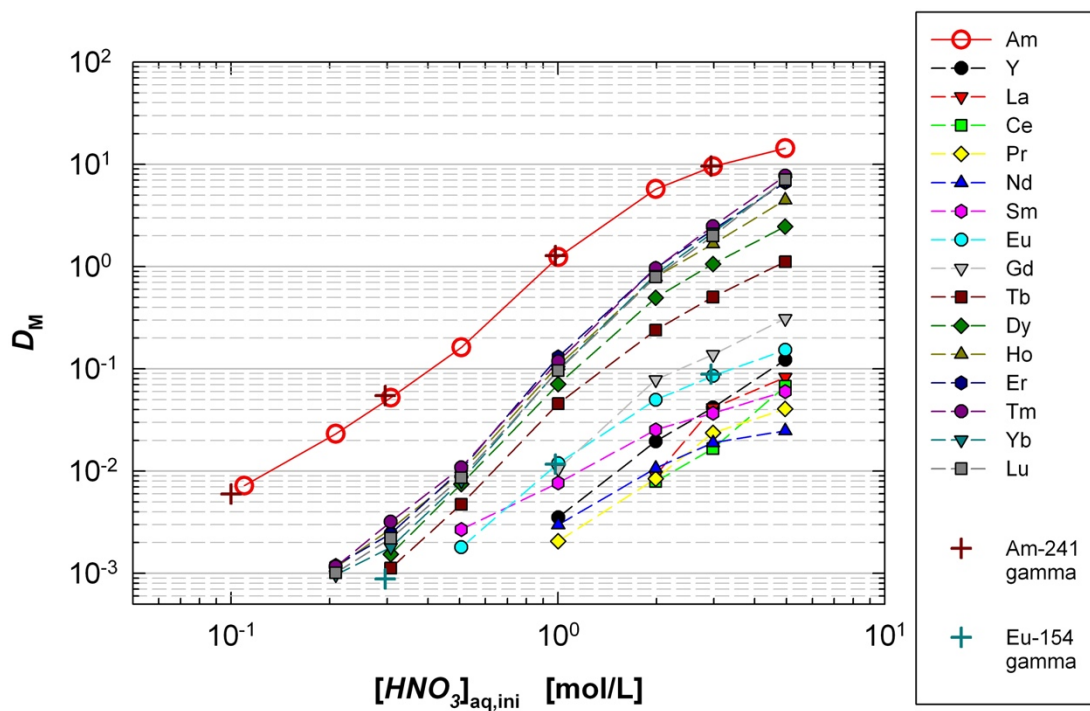


Figure 3. Extraction of Am(III) and Ln(III) by PTEH. Organic phase, **0.2 mol/L PTEH** + 10%<sub>vol.</sub> 1-octanol in kerosene. Aqueous phase,  $^{243}\text{Am(III)}$ , Y(III), La(III)–Lu(III) except Pm(III) (1 mg/L each) or  $^{241}\text{Am(III)}$  +  $^{154}\text{Eu(III)}$  (2 kBq/mL each) in  $\text{HNO}_3$ .  $T = 293 \text{ K}$ ,  $A/O = 1$ .



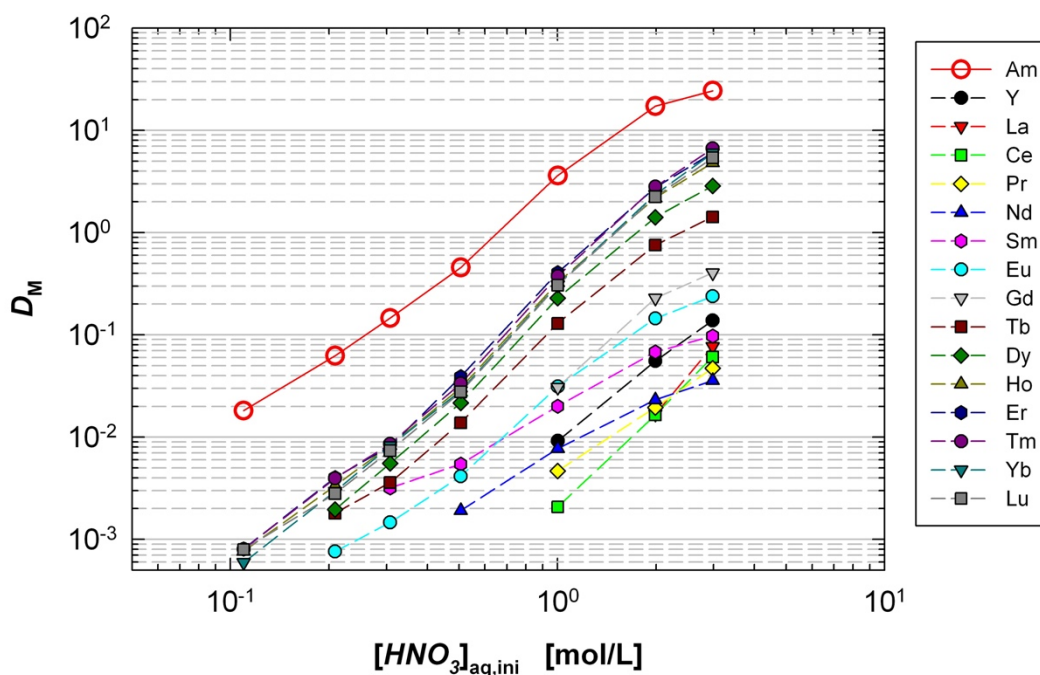


Figure 4. Extraction of Am(III) and Ln(III) by PTEH. Organic phase, **0.3 mol/L PTEH** + 10%<sub>vol.</sub> 1-octanol in kerosene. Aqueous phase,  $^{243}\text{Am(III)}$ , Y(III), La(III)–Lu(III) except Pm(III) (1 mg/L each) in  $\text{HNO}_3$ .  $T = 293 \text{ K}$ ,  $A/O = 1$ .

Agreement with distribution data published earlier<sup>12</sup> is reasonably good for 2–3 mol/L  $\text{HNO}_3$ , the latter being lower approximately by a factor of 1.5. However, distribution data for 1 mol/L  $\text{HNO}_3$  differ by a factor of approximately 5.

Plotting  $\log D_{\text{Am(III)}}$  vs.  $\log[\text{PTEH}]$  at constant nitric acid concentrations results in slopes of  $2.65 \pm 0.1$ , hinting to the formation of 1:3 complexes,  $[\text{Am}(\text{PTEH})_3]^{3+}$ . A slightly lower slope, 2.1, is reported in the literature.<sup>12</sup> Indeed, the formation of the 1:3 Am(III) complex was proven by NMR, as was the formation of the respective  $[\text{Cm}(\text{PTEH})_3]^{3+}$  and  $[\text{Eu}(\text{PTEH})_3]^{3+}$  complexes by TRLFS.<sup>15</sup>

## Conclusions

A set of distribution data for the extraction of Am(III), Ln(III) and  $\text{HNO}_3$  into PTEH solvents is reported. A slight disagreement between data reported herein and literature data<sup>12</sup> calls for further investigations on the topic.

## Acknowledgements

This work has received funding from the European Research Council (ERC) under the European Union's Horizon 2020 research and innovation programme [project GENIORS, grant agreement N° 755171]. Jasmin Schießl, Heidelberg University, is acknowledged for providing the PTEH.

## References

1. Poinssot, C.; Bourg, S.; Boullis, B., Improving the nuclear energy sustainability by decreasing its environmental footprint. Guidelines from life cycle assessment simulations. *Progr. Nucl. Energy* **2016**, *92*, 234–241.
2. Taylor, R.; Bodel, W.; Stamford, L.; Butler, G., A review of environmental and economic implications of closing the nuclear fuel cycle—part one: wastes and environmental impacts. *Energies* **2022**, *15* (4), 1433.
3. OECD-NEA *State-of-the-art report on the progress of nuclear fuel cycle chemistry*; NEA No. 7267, OECD, Nuclear Energy Agency (NEA), Paris: 2018.
4. Geist, A.; Adnet, J.-M.; Bourg, S.; Ekberg, C.; Galán, H.; Guilbaud, P.; Miguirditchian, M.; Modolo, G.; Rhodes, C.; Taylor, R., An overview of solvent extraction processes developed in Europe for advanced nuclear fuel recycling, part 1 — heterogeneous recycling. *Separ. Sci. Technol.* **2021**, *56* (11), 1866–1881.
5. Foreman, M. R. S.; Hudson, M. J.; Drew, M. G. B.; Hill, C.; Madic, C., Complexes formed between the quadridentate, heterocyclic molecules 6,6'-bis-(5,6-dialkyl-1,2,4-triazin-3-yl)-2,2'-bipyridine (BTBP) and lanthanides(III): implications for the partitioning of actinides(III) and lanthanides(III). *Dalton Trans.* **2006**, (13), 1645–1653.
6. Geist, A.; Hill, C.; Modolo, G.; Foreman, M. R. S. J.; Weigl, M.; Gompper, K.; Hudson, M. J.; Madic, C., 6,6'-bis (5,5,8,8-tetramethyl-5,6,7,8-tetrahydro-benzo[1,2,4]triazin-3-yl) [2,2']bipyridine, an effective extracting agent for the separation of americium(III) and curium(III) from the lanthanides. *Solvent Extr. Ion Exch.* **2006**, *24* (4), 463–483.
7. Modolo, G.; Wilden, A.; Daniels, H.; Geist, A.; Magnusson, D.; Malmbeck, R., Development and demonstration of a new SANEX partitioning process for selective actinide(III)/lanthanide(III) separation using a mixture of CyMe<sub>4</sub>-BTBP and TODGA. *Radiochim. Acta* **2013**, *101* (3), 155–162.
8. Magnusson, D.; Christiansen, B.; Foreman, M. R. S.; Geist, A.; Glatz, J. P.; Malmbeck, R.; Modolo, G.; Serrano-Purroy, D.; Sorel, C., Demonstration of a SANEX process in centrifugal contactors using the CyMe<sub>4</sub>-BTBP molecule on a genuine fuel solution. *Solvent Extr. Ion Exch.* **2009**, *27* (2), 97–106.
9. Geist, A.; Magnusson, D.; Müllich, U., A kinetic study on the extraction of Am(III) into CyMe<sub>4</sub>-BTBP. In *Actinide and Fission Product Partitioning and Transmutation, 12th Information Exchange Meeting. Prague, Czech Republic, 24–27 September 2012*, OECD-NEA: 2013.
10. Ekberg, C.; Aneheim, E.; Fermvik, A.; Foreman, M.; Löfström-Engdahl, E.; Retegan, T.; Spendlikova, I., Thermodynamics of dissolution for bis(triazine)-bipyridine-class ligands in different diluents and its reflection on extraction. *J. Chem. Eng. Data* **2010**, *55* (11), 5133–5137.
11. Ossola, A.; Macerata, E.; Mossini, E.; Giola, M.; Gullo, M. C.; Arduini, A.; Casnati, A.; Mariani, M., 2,6-Bis(1-alkyl-1H-1,2,3-triazol-4-yl)-pyridines: selective lipophilic chelating ligands for minor actinides. *J. Radioanal. Nucl. Chem.* **2018**, *318* (3), 2013–2022.
12. Ossola, A.; Mossini, E.; Macerata, E.; Panzeri, W.; Mele, A.; Mariani, M., Promising lipophilic PyTri extractant for selective trivalent actinide separation from high active raffinate. *Ind. Eng. Chem. Res.* **2022**, *61* (12), 4436–4444.
13. Geist, A., Extraction of nitric acid into alcohol:kerosene mixtures. *Solvent Extr. Ion Exch.* **2010**, *28* (5), 596–607.
14. Woodhead, D.; McLachlan, F.; Taylor, R.; Müllich, U.; Geist, A.; Wilden, A.; Modolo, G., Nitric acid extraction into a TODGA solvent modified with 1-octanol. *Solvent Extr. Ion Exch.* **2019**, *37* (2), 173–190.
15. Galluccio, F.; Macerata, E.; Weßling, P.; Adam, C.; Mossini, E.; Panzeri, W.; Mariani, M.; Mele, A.; Geist, A.; Panak, P. J., Insights into the complexation mechanism of a promising lipophilic PyTri ligand for actinide partitioning from spent nuclear fuel. *Inorg. Chem.* **2022**, (accepted).

# Development of the Co-processing process with the centrifugal contactor.

Atsushi Sakamoto<sup>\*a</sup>, Takehiko Sato<sup>a</sup>, Yuichi Sano<sup>a</sup> and Masayuki Takeuchi<sup>a</sup>.

**Abstract.** The Japan Atomic Energy Agency has been developing a new reprocessing flowsheet, call “Co-Processing”, to apply to the future spent nuclear fuel reprocessing plant for nuclear proliferation resistance. In this study, for constructing the Co-processing flowsheet, Uranium extraction, and Zirconium and Rhenium decontamination performances by using the centrifugal contactors were carried out.

**Keywords:** Co-processing, Centrifugal contactor, Uranium extraction, Decontamination performance, Zirconium, Rhenium

## Introduction

In the present reprocessing plants, the PUREX process<sup>i</sup> has widely been used to extract Uranium (U) and Plutonium (Pu) from the spent nuclear fuel for recycling. In the PUREX process, Pu is isolated by in its partitioning stage, which would be a concern material for nuclear non-proliferation.

In order to enhance the nuclear proliferation resistance, the Japan Atomic Energy Agency has been developing a new process, named Co-processing<sup>ii,iii</sup>. The comparison of the flowsheets between the PUREX and the Co-processing is shown in Fig. 1.

PUREX	Co-Processing
• Solvent : TBP	• Solvent : TBP
• Acid: HNO <sub>3</sub>	• Acid: HNO <sub>3</sub>
• Flow part	• Flow part
Extraction(U,Pu)	Extraction(U,Pu)
Partitioning → <u>separate Pu &amp; U</u>	Partitioning → <u>recover Pu with U</u>
Back extraction(U)	Back extraction(U)
Purification(Pu)	
Purification(U)	None

Fig. 1. Flowsheet comparison

In the both processes, TBP as the solvent and HNO<sub>3</sub> as the acid are used. The PUREX consists of five flow parts (the extraction, the partitioning, the back extraction and two purification stages). On the other hand, the Co-processing consists of three flow parts (the extraction, the partitioning and the back extraction). In the partitioning stage of the Co-processing, Pu is recovered with U in the partitioning stage for no Pu isolation. However, prior to recover Pu with U, sufficient decontamination performance of the fission products is needed in the extraction stage for reducing the purification stages.

<sup>a</sup> Japan Atomic Energy Agency, 4-33 Muramatsu, Tokai-village, Naka-gun, Ibaraki-prefecture, Japan

In this study, to make sure the extraction stage of Co-processing flowsheet, extraction performance by using U and decontamination performance by using Zirconium (Zr) and Rhenium (Re), substitute for Technetium (Tc), were investigated.

## Experimental

The centrifugal contactors used in this study is shown in Fig. 2. It consists of 16 stages of  $\phi 25$  mm inner diameter rotor in each bank. During the operation, the rotor speed was controlled at 3,500 rpm.

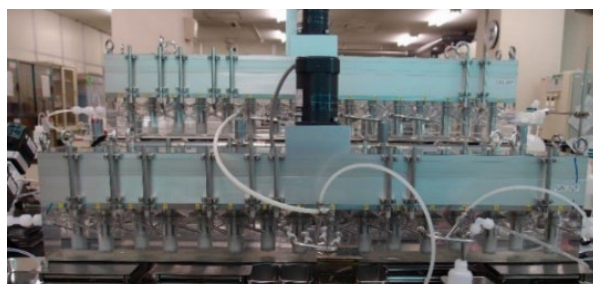


Fig. 2. The centrifugal contactors

In the U extraction tests, 220 g/L natural uranium nitrate solution, which  $H^+$  was 3.0 mol/L, was used as the feed solution of the aqueous phase. Also, 2.0 and 4.7 mol/L  $HNO_3$  were used as the scrubbing solutions of the aqueous phases. 30% TBP-n-dodecane was used for extracting U as the organic phase.

These solutions were fed into the centrifugal contactors in 3 hours by the Co-processing extraction stage flowsheet shown in Fig. 3.

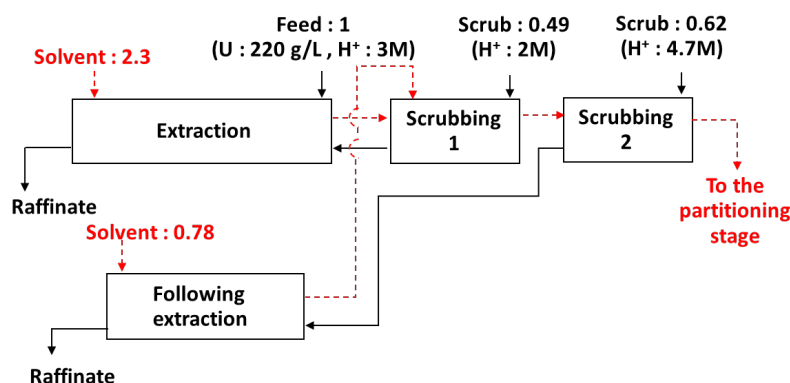


Fig. 3. “Co-processing” extraction stage flowsheet

The U concentrations in the centrifugal contactors were measured by the spectroscopy. Also, the results were compared with the simulation results, which were calculated by the MIXSET- $X^{iv}$ . In this study each simulation was performed at the 100 % mass transfer efficiency.

In addition to the test performed by the flowrate condition of Fig. 3, 10 % higher flow rate of the feed solution test was performed to ensure the robustness of the Co-recovery process flowsheet.

In the Zr and Re decontamination test, 1 g/L Re and 3 g/L Zr dissolved in 3 mol/L  $HNO_3$  was used as the feed solution of the aqueous phase. The scrubbing solutions as the aqueous

phases and the extractant of 30% TBP-n-dodecane as the organic phase were same as the U extraction tests shown in Fig. 3. These solutions were fed into the centrifugal contactors in 2 hours.

In addition to perform the decontamination test by the flowsheet shown in Fig. 3, the effect of an improved flowsheet, in which the scrubbing 2 was changed as shown in Fig. 4, was carried out. In the improved flowsheet, two different concentrations of  $\text{HNO}_3$  were fed into the scrubbing 2 for enhancing the decontamination performance of fission products and for reducing the  $\text{H}^+$  concentration in the discharged organic phase to decrease the deterioration of back extraction performance in the partitioning stage.

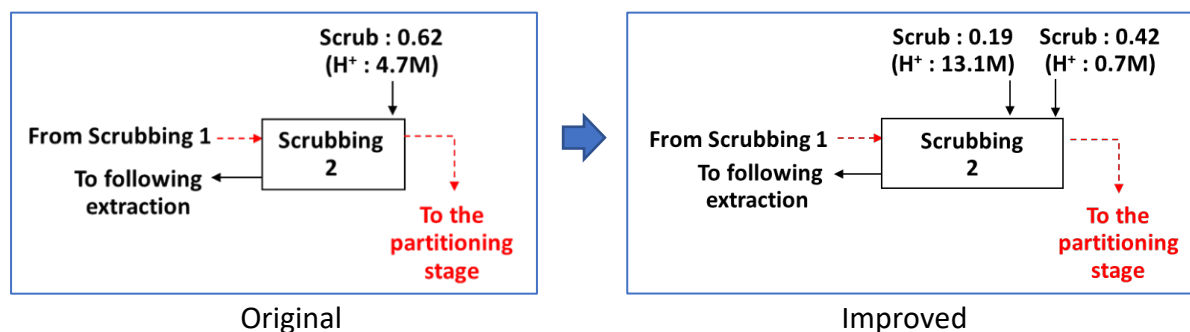


Fig. 4. Changes of the flowsheet at scrubbing 2 part

The concentrations of Zr, Re and  $\text{H}^+$  were measured by the Inductivity Coupled Plasma – Atomic Emission Spectroscopy (ICP-AES) and the titrator, respectively. Also, the  $\text{H}^+$  profiles in the centrifugal contactors were compared with the simulation results by the MIXSET-X.

## Results and Discussion

### Extraction performance by using Uranium

The U concentration profiles in the centrifugal contactors were shown in Fig. 5. U was immediately extracted from the aqueous phase after fed into the centrifugal contactor, as well as the U concentration in the organic phase was highly increased along with its flow.

This tendency was also confirmed at the 10 % higher flowrate of feed solution. In addition, both profiles showed good correspondence to the simulation results. (The condition of 20% increment was not confirmed by the experiment, due to the too much U leakage was estimated by the simulation.)

Also, since the each simulation result was performed at 100 % mass transfer efficiency, the extraction process of the Co-processing will be achieved efficiently by the centrifugal contactors in the acceptable flowrate condition by the simulation.

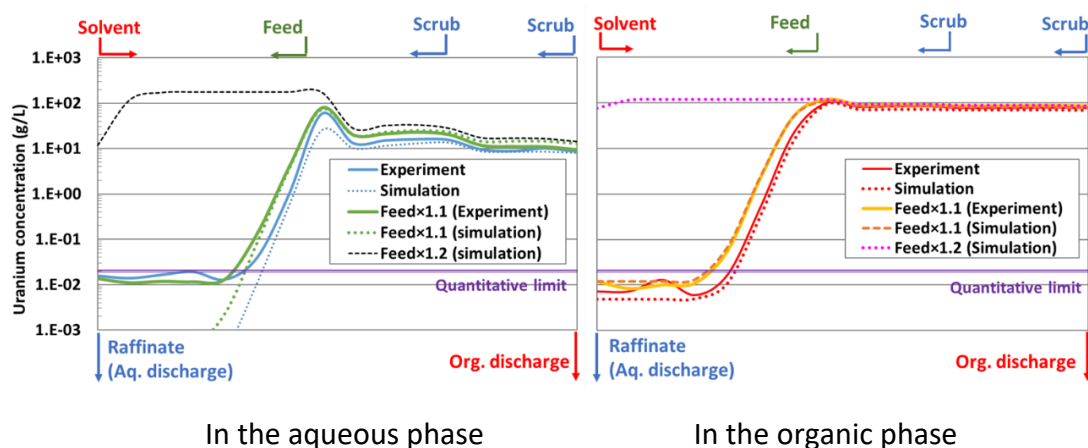


Fig. 5. Uranium concentration profiles

### Decontamination performance by using Zirconium and Rhenium

Changes of Zr & Re concentration profiles in the aqueous and the organic phases between the original and the improved flowsheets are shown in Fig. 6 and Fig. 7, respectively. As shown in the figures, both elements in the organic phases are scrubbed along with the flow of the solvent. The concentrations of Zr & Re in the organic discharge solution could be decreased by improving the flowsheet.

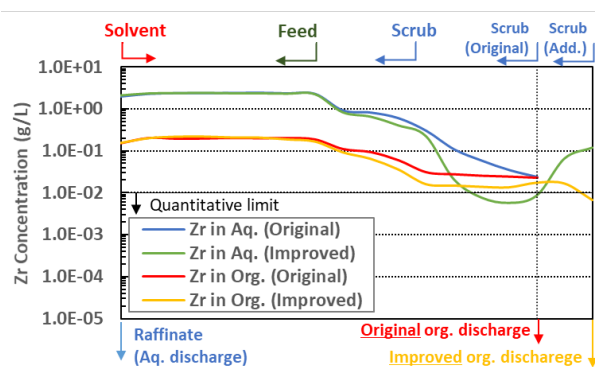


Fig. 6. Zr concentration profiles

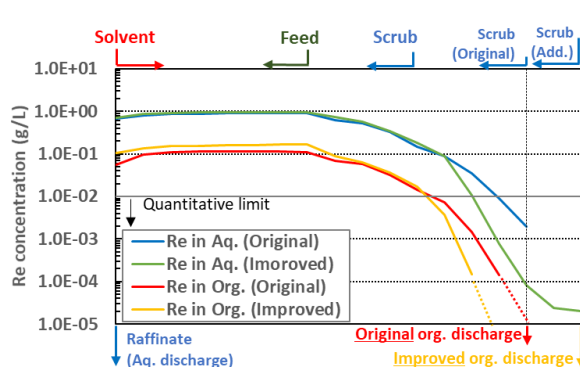


Fig. 7. Re concentration profiles

Also, the changes of  $H^+$  concentration profiles in the organic phases with the simulation results are shown in Fig. 8. By improving the flowsheet,  $H^+$  concentration in the organic discharge solution could be decreased.

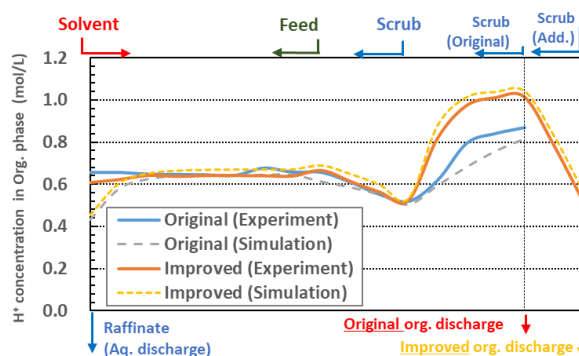


Fig. 8.  $H^+$  concentration profiles in the organic phases

## Conclusions

A new reprocessing flowsheet, named “Co- Processing”, has been developing to apply to the future reprocessing plant for enhancing nuclear non-proliferation. For realizing the flowsheet of the extraction stage in the Co-processing, U extraction, and Zr and Re decontamination tests were performed by the centrifugal contactors. The results indicated that U could be extracted as the simulation calculated by 100% mass transfer efficiency. Also, it was indicated that the sufficient decontamination of fission products for reducing the purification stages and decrease the  $H^+$  concentration in the organic discharge solution for reducing its influence to the next (partitioning) stage will be achieved by improving the flowsheet.

## Acknowledgements

This study includes the result of “Technology development program of fast breeder reactor international cooperation, etc.” entrusted to Japan Atomic Energy Agency (JAEA) by the Ministry of Economy, Trade and Industry (METI).

## References

---

<sup>i</sup> E. R. Irish and W. E. Reas, “The PUREX Process – A Solvent Extraction Reprocessing Method for Irradiated Uranium.”, AEC Research and Development Report, HW-49483A (1957).

<sup>ii</sup> K. Yamamoto, F. Yanagibashi, I. Fujimoto, T. Sato, T. Ohbu, K. Taki and S. Hayashi, “Development of U and Pu Co-Recovery Process (Co-Processing) for Future Reprocessing”, Proceedings of Global 2013, Salt Lake City, Utah, USA (2013)

<sup>iii</sup> A. Kudo, K. Kurabayashi, F. Yanagibashi, S. Sasaki, T. Sato, I. Fujimoto and T. Ohbu, “Development of U and Pu Co-processing process demonstration of U, Pu and Np Co-recovery with centrifugal contactors” , Proceedings of ICAPP 2017, Fukui and Kyoto, Japan (2017).

<sup>iv</sup> M. Naito, T. Suto, K. Asakawa and E. Kashiwagi, “MIXSET-X : A Computer Code for Simulationg the PUREX Solvent Exctraction Process” , JNC T8400 99-005, JNC (1990) in Japanese.

## **7. Plant equipment and Design**



# Mask R-CNN based droplet detection in liquid-liquid systems.

## Part 1: A proof of concept.

Stepan Sibirtsev<sup>a,b</sup>, Song Zhai<sup>a,b</sup>, Mathias Neufang<sup>a</sup>, Jakob Seiler<sup>a</sup> and Andreas Jupke<sup>a</sup>.

The droplet size distribution (DSD) in liquid-liquid systems highly affects fluid dynamics, mass transfer, and reaction kinetics. Photo-optic measurement with subsequent image processing is the most trusted method of accessing the DSD. Since manual image processing is elaborate work, methods for automated processing have been developed. However, in most cases, these methods are not publicly accessible, or their droplet detection performance has not been tested on different image qualities. In this work, we modified and trained a state-of-the-art and open-source method for image processing, Mask R-CNN (MRCNN), to detect droplets on images of four different image qualities. We defined DSD characteristic rating metrics for the testing, e.g., the relative error in Sauter mean diameter. Our MRCNN implementation shows high detection accuracy, e.g., relative errors in Sauter mean diameters less than 5 %. Due to the high accuracy, our MRCNN implementation is a competitive, publicly accessible, and fast image processing method enabling further progress in process analysis and process control in liquid-liquid systems.

**Keywords:** Convolutional neural networks, Image processing, Object detection, Droplet size distribution, Sauter mean diameter

## Introduction

The droplet size distribution (DSD) in liquid-liquid systems is a fundamental design and operating parameter for extraction and reaction plant equipment as it affects fluid dynamics, mass transfer, and reaction kinetics. Several measuring and object detection techniques exist to determine the droplet size distribution<sup>1</sup>. The most common technique is a photo-optic measurement of the liquid-liquid system with subsequent image processing. The photo-optic measurement can be performed with an internal probe or an external camera, and the image processing can be performed manually or automated. Since the manual processing of images is elaborate work, methods for automated processing have been developed.

A method for automated processing should meet the following requirements to enable the broadest possible application for droplet detection in liquid-liquid systems: public accessibility, fast processing speed, and high detection accuracy independent of the image quality, droplet diameter, or hold-up. These requirements eliminate methods charged by providers, and thus open-source, and state-of-the-art methods for automated image processing based on convolutional neural networks (CNN) remain potential candidates.

The open-source method U-Net<sup>2</sup>, initially developed for biological image processing, was combined with an algorithm for droplet detection to measure DSDs in liquid-liquid flows<sup>3</sup>. The U-Net implementation was trained on artificially generated images and is customized for specific image quality from optical multimode online probe<sup>4</sup> images. Images with Sauter mean diameter range of 0.3-0.8 mm and hold-up range of 1-20 Vol % were used to test this image processing method. The average relative error between the manual and automated

---

<sup>a</sup> RWTH Aachen University, Fluid Process Engineering (AVT.FVT), Forckenbeckstraße 51, 52074 Aachen, Germany

<sup>b</sup> These authors contributed equally

processing for the Sauter mean diameter is less than 4.5 %. However, the U-Net implementation for droplet detection is not publicly accessible and was only shown for one specific hardware setup.

Faster R-CNN<sup>5</sup> (FRCNN), which can be used for real-time detection due to its fast image processing performance, detects bounding boxes of multiple objects in an image. BubCNN<sup>6</sup>, a combination of an FRCNN and a shape regression CNN, detects bubbles in an image and approximates the bubble shapes by ellipses. BubCNN was trained on artificially generated images and images from different camera systems. Artificially generated images with unspecified bubble size range and hold-up range of 2.5-15 Vol-% were used to test this image processing method. Depending on the hold-up, the mean average precision  $mAP$ <sup>7</sup> is between 75 % for high and 100 % for low hold-ups. BubCNN is publicly accessible, but its droplet detection application has not yet been shown.

Mask R-CNN<sup>8</sup> (MRCNN), a further development of FRCNN, detects object segmentation masks in addition to bounding boxes. Moreover, MRCNN achieves higher detection accuracy than FRCNN at a similar processing speed<sup>8</sup> and is easy to implement and adapt to the required application since the source code of MRCNN is publicly accessible<sup>9</sup>. A detailed application of MRCNN to droplet detection, including an error estimation in terms of mAP or relative error of Sauter mean diameter, has yet to be shown.

In summary, several automated image processing methods exist. However, none of these methods meets all the defined requirements because they are either not publicly accessible or were not applied to droplet detection in liquid-liquid systems. In this work, we aim to specialize the MRCNN in droplet detection. Moreover, we intend to show that it is an accurate image processing method that can be applied in a wide droplet diameter and hold-up range, regardless of the photo-optical measurement equipment. Therefore, we modify and train MRCNN to detect droplets on images of four different image qualities in a droplet diameter range of 0.2-3.6 mm and a hold-up range of 5-35 Vol-%.

## Modifications of MRCNN

We extended the publicly accessible implementation of MRCNN<sup>9</sup> by several modifications dealing with droplet diameter determination and filter to specialize MRCNN in droplet detection. First, we extended the MRCNN implementation<sup>9</sup> with the FRCNN mode<sup>10</sup>. The FRCNN mode allows us to use MRCNN without generating object segmentation masks, resulting in faster training and detection performance. For our application, the information from the bounding boxes suffices to determine the droplet diameter. The bounding boxes of detected droplets must be transformed to a droplet diameter  $d_i$ . For this purpose, the droplet diameters were determined by  $d_i = 0.5 \cdot (h_{box} + w_{box})$  (Eq.1), whereby  $h_{box}$  is the height and  $w_{box}$  is the width of a bounding box.

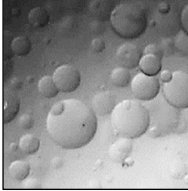
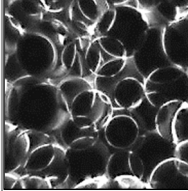
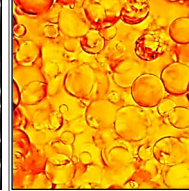
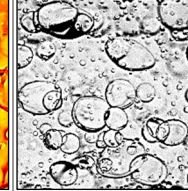
Second, we implemented three filters for the post-processing of detected droplets. The material system, the operating conditions, and the droplet diameter determine the shape of a droplet<sup>11</sup>. The first filter utilizes the fact that droplets below a diameter of 1 mm can be treated as spherical<sup>12</sup>. If the diameter range of a DSD is known or can be assumed to be

smaller than 1 mm, the detection of elliptical shapes indicates most probably two overlapping droplets. Therefore, we implemented an algorithm that filters detections of elliptical shapes allowing only droplets with a defined degree of deformation to be detected. The second filter deals with partly captured droplets located at the image edges. We implemented an algorithm that sorts out droplets whose bounding boxes intersect a defined border area of the image. The third filter treats adhering droplets. Droplets may adhere, e.g., to the lens of the internal probe. In this case, the adhering droplets must be determined in the recorded image to avoid multiple counting of the same droplets in successive images. For this purpose, we implemented an algorithm that sorts out adhering droplets. All three filters can be adjusted with the corresponding parameters described in the documentation on GitHub<sup>13</sup>.

## Equipment and data base

We obtained the image sets for training and testing of MRCNN from four different experimental setups, which differ of technical and photo-optical measurement equipment. Table 1 shows the equipment used to obtain the image sets, the hold-up, and image specifications. Every image set consists of 100 manually processed images. For the manual processing, we used the Visual Geometry Group Image Annotator<sup>14</sup>.

*Table 1: Equipment and image specifications.*

Image set	Nr.1	Nr.2	Nr.3	Nr.4
Sample image				
Technical equipment	Centrifugal pump	Stirring tank	Kühni column	Packed column <sup>c</sup>
Hold-up (Vol.-%)	5	33	10-15	25-35
Measurement equipment <sup>d</sup>	Internal	Internal	External	External
Camera resolution (MP)	5	5	10	5
Pixel size (μm/px)	3.45	1	6	15
Number of droplets <sup>e</sup> (-)	603	188	79	1454
Min. diameter <sup>d</sup> (mm)	0.18	0.18	1.72	0.89
Sauter mean diameter <sup>d</sup> (mm)	0.29	0.26	2.44	1.80
Max. diameter <sup>d</sup> (mm)	0.63	0.49	3.31	3.61
Mean average precision (%)	64	3	72	31

## MRCNN training and testing procedure

<sup>c</sup> Spacers of 30mm height were placed between the packing elements.

<sup>d</sup> Nr.1: endoscope type ENDO R100 038 000 50 (Olympus DE GmbH, Hamburg, DE) with high-speed camera type JAI GO-5100M-USB (Stemmer Imaging AG, Puchheim, DE). Nr.2: endoscope with an integrated high-speed camera type Sc-VR420-C22 (Sopat GmbH, Berlin, DE). Nr.3: high-speed camera type Alpha 6000 with camera lens type E 3.5/30 Macro (Sony, Tokyo, JP). Nr.4: high-speed camera type MV-CH050-10UM/UC (Hangzhou Hikrobot Technology Co., Ltd., Hangzhou, CH) with camera lens type MGTLO23H (MYUTRON INC., Tokyo, JP).

<sup>e</sup> Resulting from manual image processing of the testing image sets

Training and testing MRNN require splitting the data set and defining training and testing parameter values. We randomly divided each manually processed image set into a training and a testing set of 75 and 25 images, respectively. We used the training sets for the MRCNN training and the testing sets to test the detection performance of the trained MRCNN models on unseen images of the same image quality. Several training and processing parameters can significantly influence the training and detection performance of MRCNN<sup>9,13,15,16</sup>. We set their values based on recommendations from the literature<sup>9,17</sup> to avoid a computationally expensive parameter search. Since we used only one GPU, which can process a maximum of two images simultaneously, we set the batch size to two. Moreover, we assumed that training for 50 epochs is sufficient to reach overfitting<sup>15</sup> and thus the epoch of best performance. Table 2 summarizes the most influencing parameters and their values. The values of the filter parameters correspond to the default values of our MRCNN implementation<sup>13</sup>.

*Table 2: Parameter values for MRCNN training and processing\*.*

Parameter	Value	Parameter	Value
<b>Backbone</b>	Resnet50 <sup>18</sup>	<b>Learning rate</b>	0.001
<b>Base weights</b>	COCO <sup>19</sup>	<b>Momentum</b>	0.9
<b>Train layers</b>	heads	<b>Weight decay</b>	0.0001
<b>Train epochs</b>	50	<b>Gradient clipping</b>	5
<b>Batch size</b>	2	<b>Image resolution*</b>	1024px
<b>Resizing mode</b>	square	<b>Pixel size*</b>	see Table 1
<b>Image resolution</b>	1024px	<b>Detection confidence*</b>	90 %

After training, we tested the resulting 50 models per image set for their detection performance. First, the mean average precision  $mAP^7$  of bounding boxes at an intersection-over-union value of 50 % was determined. The  $mAP$  allows us to assess the matching precision of bounding boxes resulting from manual and automated processing. Second, we specified rating parameters as characteristic diameters of the DSD<sup>20,21</sup>: *Sauter mean diameter*  $d_{32}$ , *minimum droplet diameter*  $d_{10}$ , and *maximum droplet diameter*  $d_{95}$ , as well as the *number of detected droplets*  $n_d$ . We defined the relative errors between the manual and automated determined values of these parameters as rating metrics to quantify and compare the detection performance of the MRCNN models. We used the curves of the cumulative volume distributions resulting from image processing to determine the parameters  $d_{10}$  and  $d_{95}$ <sup>20,21</sup>. Since the progression of the curves is not continuous,  $d_{10}$  and  $d_{95}$  are determined to be the following largest diameters of the corresponding 10 % and 95 % boundaries. Finally, we summed up the absolute values of the relative errors in these four parameters. We defined the epoch with the lowest sum as the model with the best detection performance.

We performed all simulations on an NVIDIA Volta V100-SXM2 GPU with 16 GB VRAM provided by the RWTH Aachen University Compute Cluster as a part of project thes1173.

## Results and Discussion

To illustrate the visual result of the MRCNN testing, Figure 1 shows an exemplary image of the testing image set Nr.1 before and after the image processing with the MRCNN model of the 47<sup>th</sup> epoch trained on the training image set Nr.1.

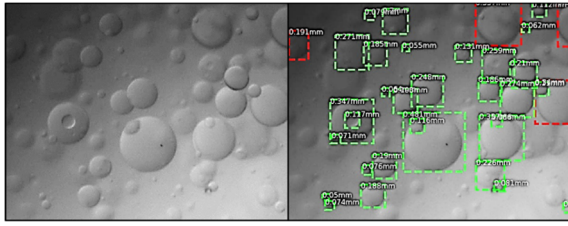


Figure 1: Exemplary image of testing image set Nr.1 before and after the image processing.

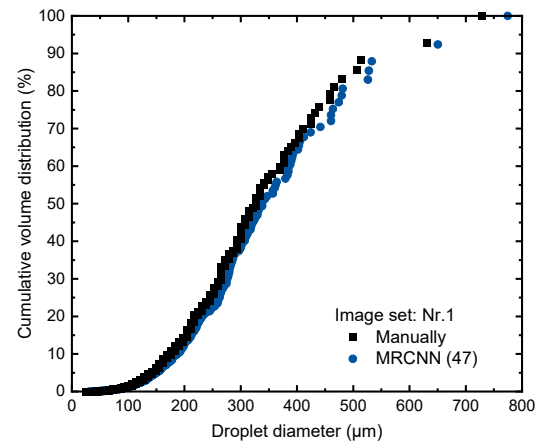


Figure 2: Cumulative volume distribution.

The red-colored bounding boxes represent filtered droplets whose bounding boxes intersect the image edge. The green-colored bounding boxes represent droplets, which MRCNN takes into account to determine the cumulative volume distribution. MRCNN labels each box by its droplet diameter calculated by Equation 1. The  $mAP$  values of the final models determined in the next step are summarized in Table 1. Comparing the  $mAP$  values with literature<sup>6</sup> shows an adequate precision for image sets Nr.1 and Nr.3 with hold-up values up to 15 Vol.-%. For image sets Nr.2 and Nr.4, the  $mAP$  values are significantly lower, which can be explained by the high hold-up values<sup>6</sup>.

Figure 2 shows the cumulative volume distributions of the manual and automated processing performed with the MRCNN model of the 47<sup>th</sup> epoch trained on the image set Nr.1.

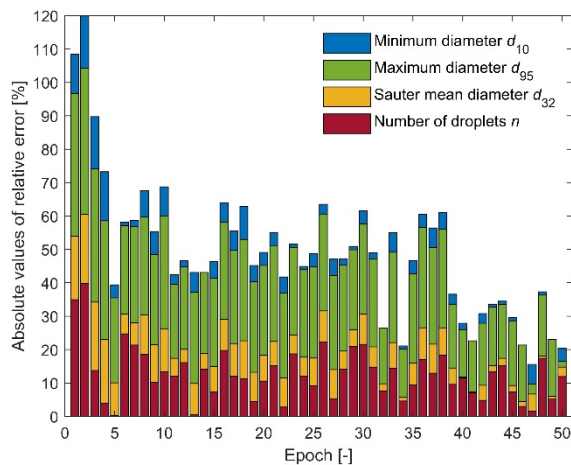


Figure 3: Rating metrics of MRCNN models trained on image set Nr.1.

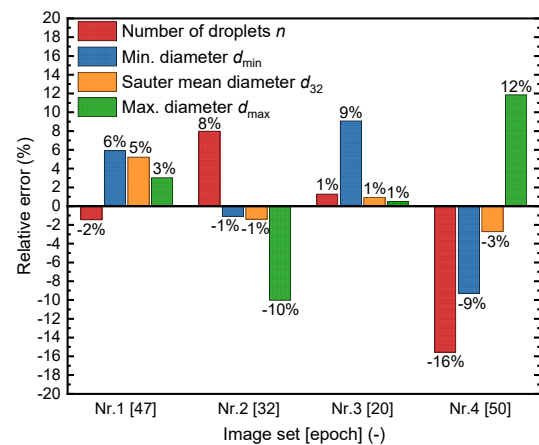


Figure 4: Rating metrics of the final MRCNN models.

The curves of the manual and automated processing are in good agreement. The deviation increases with larger droplet diameters. However, the absolute number of detected droplets with a diameter between 0.4-0.8 mm is comparatively slight for both manual and automated processing, which could explain the higher deviation in this range. Table 1 lists the rating parameters determined from manual processing.

Figure 3 shows the rating metrics of the testing image set Nr.1 as a function of the epoch for the MRCNN models trained on the image set Nr.1. In the shown example, the model at the 47<sup>th</sup> epoch has the lowest sum of the four rating metrics. Therefore, we choose this model as the final model of the image set Nr.1. Figure 4 summarizes the rating metrics of the final models for each image set. The corresponding epoch of each model is noted in the brackets. Positive values of the relative error represent overestimations and negative values underestimations of the MRCNN models. We attribute the difference in detection performance depending on the image quality to the chosen parameter values for MRCNN training and testing. Except for image set Nr.4, a training length of 50 epochs is sufficient, as the epochs of the final models are below 50. The relative errors in  $d_{32}$  are less than 5 % for all image sets, comparable to the literature<sup>3</sup>. With a relative error in all characteristic diameters of DSD less than 12 %, the determination accuracy of the DSD is generally adequate.

However, we observe a high relative error in  $n_d$  for image sets Nr.2 and Nr.4, which agrees with the determined  $mAP$  values (Table 1). In the case of the image set Nr.2, the MRCNN model overestimates  $n_d$  and underestimates  $d_{95}$ , while relative errors in  $d_{10}$  and  $d_{32}$  are comparably low. Thus, compared to manual processing, the MRCNN model detects more droplets, especially between the diameters  $d_{10}$  and  $d_{95}$ . This result could mean that the model is accurate but that the manual processing must be more systematic. For image set Nr. 4, the MRCNN model underestimates  $n_d$  and  $d_{10}$ , overestimates  $d_{95}$ , and matches  $d_{32}$  well. Thus, compared to the manual processing, the model detects more small and large droplet diameters but fewer middle droplet diameters relative to all detected droplets, making the DSD spread higher. Nevertheless, since MRCNN matches  $d_{32}$  well, the underestimation in  $n_d$  is not critical. Training over 50 epochs could improve the results.

## Conclusions

In this work, a state-of-the-art and open-source method for image processing, MRCNN, is modified and trained to detect droplets on images of four different image qualities. We showed the first proof of concept for our MRCNN implementation for droplet detection for a wide range of droplet diameters and hold-ups. our MRCNN implementation usually shows a high detection accuracy comparable to other automated image processing methods. Therefore, our MRCNN implementation is a competitive, publicly accessible<sup>13</sup>, and fast image processing method enabling further progress in process analysis and process control in liquid-liquid systems. We attribute uncertainties in detection performance to the subjectivity of the manual processing and the chosen parameter values for MRCNN training and testing. In future work, we will apply augmentation methods to reduce the subjectivity of manual processing. Furthermore, we will investigate MRCNN training and detection performance in more detail. For example, we will perform a hyperparameter study to identify the most suitable hyperparameter values.

## Literature Cited

1. Hlawitschka MW, Schulz J, Wirz D, Schäfer J, Keller A, Bart H-J. Digital Extraction Column: Measurement and Modeling Techniques. *Chemie Ingenieur Technik*. 2020;92(7):914–925.
2. Ronneberger O, Fischer P, Brox T. *U-Net: Convolutional Networks for Biomedical Image Segmentation*. arXiv, 2015.
3. Schäfer J, Schmitt P, Hlawitschka MW, Bart H-J. Measuring Particle Size Distributions in Multiphase Flows Using a Convolutional Neural Network. *Chemie Ingenieur Technik*. 2019;91(11):1688–1695.
4. Mickler M, Bart H-J. Optical Multimode Online Probe: Erfassung und Analyse von Partikelkollektiven. *Chemie Ingenieur Technik*. 2013;85(6):901–906.
5. Ren S, He K, Girshick R, Sun J. *Faster R-CNN: Towards Real-Time Object Detection with Region Proposal Networks*. arXiv, 2015.
6. Haas T, Schubert C, Eickhoff M, Pfeifer H. BubCNN: Bubble detection using Faster RCNN and shape regression network. *Chemical Engineering Science*. 2020;216:115467.
7. Wood L, Chollet F. *Efficient Graph-Friendly COCO Metric Computation for Train-Time Model Evaluation*. arXiv, 2022.
8. He K, Gkioxari G, Dollár P, Girshick R. *Mask R-CNN*. arXiv, 2017.
9. Abdulla W. Mask R-CNN for object detection and instance segmentation on Keras and TensorFlow. *GitHub repository*. Github, 2017. [https://github.com/matterport/Mask\\_RCNN](https://github.com/matterport/Mask_RCNN). [Accessed 15.11.22].
10. Knapik M. Added FRCNN-like mode where only bboxes are generated. *GitHub repository*. Github, 2020. [https://github.com/mat02/Mask\\_RCNN](https://github.com/mat02/Mask_RCNN). [Accessed 15.11.22].
11. Clift R, Grace JR, Weber ME. *Bubbles, drops, and particles* (3rd edition). New York, NY: Acad. Press, 1992.
12. Simon M. *Koaleszenz von Tropfen und Tropfenschwärmen*. Doctoralthesis. Technische Universität Kaiserslautern, 2005.
13. Sibirtsev S. Mask R-CNN implementation for particle detection in multiphase systems. *GitHub repository*. Github, 2022. <https://git.rwth-aachen.de/avt-fvt/public/mrcnn-particle-detection>.
14. Dutta A, Zisserman A. The VIA Annotation Software for Images, Audio and Video. In: Amsaleg L, Huet B, Larson M, Gravier G, Hung H, Ngo C-W, Tsang Ooi W, editors. *Proceedings of the 27th ACM International Conference on Multimedia*. New York, NY, USA: ACM, 2019:2276–2279.
15. Jia Wu, Xiu-Yun Chen, Hao Zhang, Li-Dong Xiong, Hang Lei, Si-Hao Deng. Hyperparameter Optimization for Machine Learning Models Based on Bayesian Optimization. *Journal of Electronic Science and Technology*. 2019;17(1):26–40.
16. Rukundo O. *Effects of Image Size on Deep Learning*. arXiv, 2021.
17. Abdulla W. Splash of Color: Instance Segmentation with Mask R-CNN and TensorFlow., 2018. <https://engineering.matterport.com/splash-of-color-instance-segmentation-with-mask-r-cnn-and-tensorflow-7c761e238b46>. [Accessed 15.11.22].
18. Serte S, Serener A, Al-Turjman F. Deep learning in medical imaging: A brief review. *Trans Emerging Tel Tech*. 2022;33(10).
19. Lin T-Y, Maire M, Belongie S, Bourdev L, Girshick R, Hays J, Perona P, Ramanan D, Zitnick CL, Dollár P. *Microsoft COCO: Common Objects in Context*. arXiv, 2014.
20. Kwakernaak PJ, van den Broek WMGT, Currie PK, editors. *Reduction of Oil Droplet Breakup in a Choke*. SPE Oklahoma City Oil and Gas Symposium / Production and Operations Symposium. All Days., 2007.
21. Schmitt P, Sibirtsev S, Hlawitschka MW, Styn R, Jupke A, Bart H-J. Droplet Size Distributions of Liquid-Liquid Dispersions in Centrifugal Pumps. *Chemie Ingenieur Technik*. 2021;93(1-2):129–142.

# Optimal Mixing in Agitated Extraction Columns.

Donald J. Glatz<sup>a</sup> and Brendan Cross<sup>a</sup>

**Abstract:** Liquid-liquid extraction columns are designed to increase the interfacial surface area between two immiscible phases so that the solute to be removed can be efficiently transferred between phases. The optimal efficiency of an extraction column is generally obtained by minimizing the dispersed-phase droplet size and maximizing the contact time. In agitated extraction columns, greater agitation generally increases the efficiency (theoretical plates per unit height of the column). However, an excessively high agitation speed can decrease the extraction performance due to back-mixing of the continuous phase or flooding in which the dispersed phase stops flowing counter-currently to the continuous phase. When designing an agitated column, the goal is to find the optimal speed that will produce the highest efficiency. However, the type of mixing also plays an important role in designing an optimal agitated extraction column. Typically, there are two methods for providing mixing in agitated columns: rotating-type impellers and reciprocating plates. Experience has demonstrated that rotating internals work best for systems that require a high amount of agitation, typically those with high interfacial tension and/or a large density difference between phases. Conversely, reciprocating internals are the better choice for systems with low interfacial tension and/or a small density difference between phases. The focus of this paper will be to investigate these two types of mixing and how each can be used to provide the best column design for different types of two-phase systems for liquid-liquid extraction.

**Keywords:** Solvent Extraction, Extraction Columns, Phase Continuity, Extraction Pilot Testing, Mixing Dynamics

## Introduction

Typically, there are two types of mixing used for agitated extraction columns: rotational mixing and reciprocating mixing. Rotational mixing is generally supplied by rotating discs or turbine-type impellers. Reciprocating mixing is supplied by perforated plates that reciprocate up and down inside a column. Rotational mixing requires less power and can produce very small (1–2 mm) dispersed phase droplets and is generally the best type of mixing for systems with high interfacial tension and large density differences between phases. A reciprocating plate stack provides uniform cross-sectional shear and generates a more uniform dispersed phase droplet size. The high open area on the perforated plates provides a greater capacity for the column. Experience has shown that this type of mixing is optimal for systems with low interfacial tension and/or a small density difference between phases.

---

<sup>a</sup> Koch Modular Process Systems LLC, Paramus, New Jersey, USA



When operating an extraction column, the continuous phase must preferentially wet internal surfaces to minimize coalescence of the dispersed phase and, therefore, maximize the interfacial area. The general rule of thumb for aqueous-organic systems is: if water is the continuous phase, metal internals should be used; if an organic solvent is the continuous phase, plastic internals should be used.

## Experimental

The first step for determining which type of agitated extraction column to use is to perform laboratory tests<sup>i</sup> to generate liquid-liquid equilibrium data. It is equally important to observe the mixing and settling behavior of a system. Generally, if the separation time is quick ( $< 60$  s), no emulsion formation is observed, and the interface is relatively sharp and easy to discern, then a column with rotating impellers should be selected for scale-up. However, if the separation time is long ( $> 1$  min) and/or emulsification occurs, then a column with reciprocating internals is a better choice for scale-up.

After performing laboratory tests, pilot testing using the column selected for scale-up can proceed. The criteria for this selection are generalized as follows. Rotating internals are optimal for systems with  $> 0.1$  difference in specific gravity between the phases and when laboratory tests have shown fast phase separation and no emulsification tendency. Reciprocating internals are optimal for systems with  $< 0.1$  specific gravity difference and when laboratory tests have shown slow phase separation and/or an emulsification tendency.

Once the pilot column has been selected, the test procedure is as follows:

- For start-up each day, the column must be filled with the continuous phase. Once full, the agitator is turned on at a low speed, and the dispersed phase is added.
- Inlet flows are adjusted to the desired rates, and the interface level is controlled by adjusting the bottom take-off pump, as required.
- The agitator speed is adjusted to the specified rate.
- The test supervisor specifies the conditions for each run. The feed and solvent rates are confirmed on a regular basis. The temperature is adjusted as required using heat exchanges for the feed and solvent streams. At the completion of the run, the raffinate and extract flow rates are measured, and samples of each phase are taken for analysis.
- During start-up each day, a total of five column turnovers are performed before the initial samples are taken. (A column turnover is defined as the total column volume, divided by the combined flow of feed and solvents.) After the first run, and following adjustments of the variables, a total of three turnovers are performed before additional sampling.

The authors suggest using step-by-step optimization during pilot plant testing. Details for this test method are well documented in another paper.<sup>ii</sup> Testing continues until the process conditions are optimized and desired results are achieved. Data from the runs with optimal performance are used for empirical scale-up to the production column using proven design correlations.

## Results and Discussion

Four case studies are presented here, which demonstrate the selection of the best agitated extraction column based on the type and amount of mixing.

### Application 1 – Fermentation broth

This application involved the extraction of carboxylic acids from an aqueous fermentation broth generated during a cellulosic ethanol process. Ethyl acetate was the selected solvent. The desired outcome was > 95% acetic acid recovery and a solvent-to-feed ratio (S:F)  $\leq$  1.7. Laboratory tests showed that moderate mixing resulted in emulsification and slow phase separation. Preliminary tests in a rotating disc column (RDC) demonstrated poor performance due to emulsification and flooding. Subsequently, the process was tested in a 25 mm-diameter KARR<sup>®</sup> Column<sup>iii</sup> with a reciprocating plate stack. The KARR<sup>®</sup> Column demonstrated excellent operability and generated a fine dispersion of the solvent phase. Results from pilot runs are shown in Table 1. A review of the data shows: (1) a S:F ratio of 1.5 was acceptable; (2) > 98% acetic acid extraction at 40–45 °C and a plate stack height of 3660 mm; (3) successful operation at a capacity of 26.5 – 28.5 m<sup>3</sup>/m<sup>2</sup>h.

RUN #	Plate Stack Ht. (mm)	Capacity m <sup>3</sup> /m <sup>2</sup> hr	Temp. C	S:F Ratio	Agitation SPM	Acid Recovery %
1	3660	28.5	23	1.7	30	95.0
2	3660	28.5	23	1.7	40	97.5
3	3660	28.5	23	1.7	50	Flooded
4	2438	28.5	23	1.7	30	93.3
5	2438	28.5	23	1.7	40	Flooded
6	3050	28.5	23	1.7	30	96.3
7	3660	26.5	23	1.5	30	96.5
8	3660	20.4	23	1.5	40	97.6
9	3660	28.5	23	1.5	30	94.3
10	3660	26.5	45	1.5	30	98.3
11	3660	26.5	45	1.5	50	98.7
12	3660	26.5	45	1.5	60	Flooded

Table 1. Pilot plant data for fermentation broth extraction in a 25 mm-diameter KARR<sup>®</sup> column

Based upon these results, a 0.56m diameter x 11.6m plate stack height KARR Column was designed, supplied, and has operated successfully, meeting the design requirements.

## Application 2 – C5 Acid Extraction

This process involved the extraction of C5 acids from an aqueous feed stream using an alkane solvent. The feed contained 4% C5 acids and the target raffinate concentration was < 1000 ppm. The density difference was large ( $SG_{\text{feed}} = 1.02$ ,  $SG_{\text{solvent}} = 0.68$ ), and the interfacial tension was high (> 30 dynes/cm). Laboratory settling occurred within seconds with a clear, sharp interface. The number of required theoretical stages was > 8 at the desired S:F ratio. Thus, this process was an ideal candidate for a SCHEIBEL® Column<sup>iii</sup> with rotating turbine-type impellers.

Pilot plant testing in a 3" diameter x 60-stage SCHEIBEL® Column was successful. The results from pilot testing are shown in Figure 1. The process was optimized at a capacity of 26.5 m<sup>3</sup>/m<sup>2</sup>hr, with an S:F of 3.5, and at least 40 agitated stages. The optimal agitation speed was 850 rpm. Although flooding did not occur at higher speeds, there was a slight reduction in efficiency, probably due to back-mixing of the continuous phase. Based on the data generated in the pilot plant, a 1219 mm-diameter production column with 60 agitated stages was designed and supplied to the production plant. This column started up successfully and has been operating since.

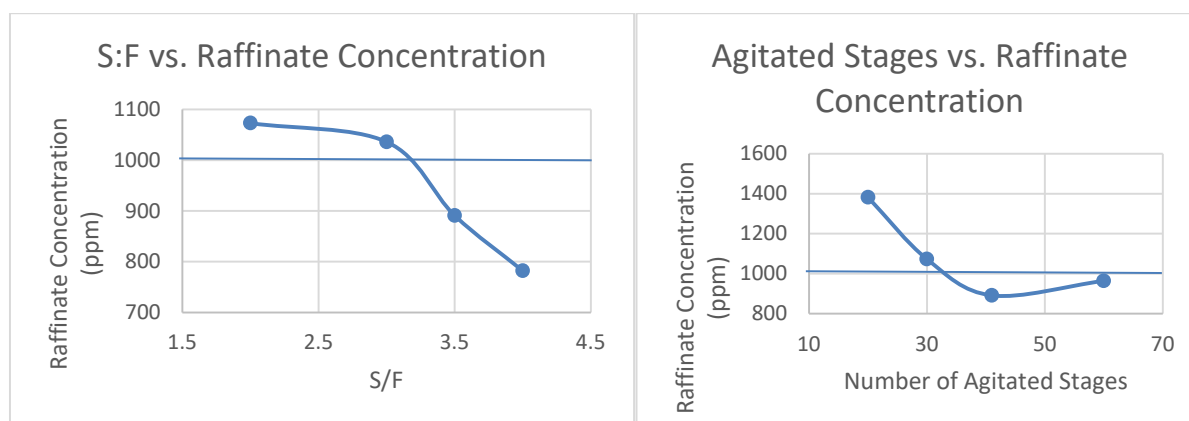


Figure 1. Pilot plant testing to determine the optimal S:F (left) and the number of agitated stages (right) using a SCHEIBEL® Column to extract C5 acids from an aqueous stream.

## Application 3 – Aromatic Purification by Fractional Extraction

The process involved a light tar feed in a petrochemical plant that contained polar aromatics (product) and non-aromatic impurities. A fractional extraction process<sup>iv</sup> was identified in which

a glycol was used as the polar solvent and an immiscible alkane as the non-polar solvent. Although no laboratory work was performed for this process, the density of the alkane (SG = 0.66) was much lower than either the feed (SG = 0.96) or polar solvent (SG = 1.11). The solubility between the polar and non-polar solvent was very low, indicating a high interfacial tension. Thus, a SCHEIBEL® Column (rotational mixing) was selected for this process.

A 3" diameter, pilot SCHEIBEL® Column was used for testing this application using actual plant feed material. All runs demonstrated that the process required a high agitation speed and produced a clear, sharp interface. Thus, the SCHEIBEL® Column was the optimal selection for this application. Table 2 shows data for significant test runs performed for this process.

Run #	Number of Stages			Feed Rate (cc/min)			Ratio by Weight			Capacity (m <sup>3</sup> /m <sup>2</sup> hr)	Feed Point	Agit. RPM	% Extract Recovery	Impurities Total
	Total	Above	Below	Feed	Polar	N.P.	Feed	Polar	NP					
A	99	34	65	140	120	470	1	1	2.3	25.7	2	750	94.9	0.46
B	99	57	42	135	100	390	1	0.87	2	24.4	4	700	95.0	0.99
C	99	34	65	165	100	360	1	0.7	1.5	24.4	2	800	93.3	1.10
D	77	24	53	75	90	330	1	1.4	3	21.0	2	850	95.8	0.58
E	65	12	53	165	100	360	1	0.7	1.5	25.5	3	625	92.1	1.38
F	65	12	53	150	90	385	1	0.7	1.8	25.5	3	625	94.2	0.59
G	65	23	42	150	90	385	1	0.7	1.8	25.5	4	625	93.9	1.18

Table 2. Pilot plant data for aromatic purification via fractional extraction in an 80 mm diameter SCHEIBEL® Column.

Run F was the optimal run. Thus, based on this run, the designed capacity was 25.5 m<sup>3</sup>/m<sup>2</sup>h, and 65 agitated stages were required. The feed location was 13 stages down from the top of the column. The polar S:F ratio was 0.7, and the non-polar S:F ratio was 1.8. Tests also demonstrated that a variable mixing intensity was required to optimize the process. Smaller-diameter impellers were used immediately above and below the feed location, and the impeller diameters increased moving up and down from the feed location. The production column design for the operating plant had a diameter of 1778 mm with 65 agitated stages. This column started up successfully and has been operating as designed for more than 10 years.

#### Application 4 – Amine Extraction

This process involved the extraction of an amine from a toluene feed using acidic water as the solvent. The density difference was relatively high, with a specific gravity of 0.9 for the feed and 1.05 for the acidic water. Laboratory work showed that phase separation occurred rapidly and produced a sharp interface. Thus, a SCHEIBEL® Column was initially selected for this process.

A 3" diameter pilot SCHEIBEL® Column was used to test actual plant toluene feed and acidic water. Initial tests with the toluene phase as the continuous phase and aqueous phase dispersed resulted in poor performance due to excessive coalescence of water droplets onto the metal internal surfaces. Reversing the phases with the aqueous continuous phase provided good hydraulic performance for the column (no dispersed phase coalescence), but the stage efficiency was very low, possibly due to the Marangoni Effect.<sup>v</sup>

The decision was made to switch to a 25 mm-diameter KARR® Column using PTFE perforated plates and spacers so that the organic phase could be tested as the continuous phase. The operation was successful because the aqueous droplets dispersed without coalescing on the PTFE surfaces. The target raffinate of < 1 ppm amine was achieved using a 3660 mm plate stack height and S:F of 0.67. This result was achieved for capacities of 22.0 and 26.5 m<sup>3</sup>/m<sup>2</sup>h and an agitation speed of 100 strokes per minute, which is a moderate agitation speed for a KARR® column. This result confirmed that the KARR® Column with a reciprocating plate stack was a better choice than a column with rotating impellers for this application.

## Conclusions

For agitated extraction columns, both the type of agitation (rotational vs reciprocating) and the amount of agitation are important for optimizing the extractor design. The design must also utilize proper materials of construction for the internals to avoid coalescing dispersed phase droplets on internal surfaces, which could degrade the performance. Finally, in some processes with significantly different hydraulic behavior throughout the column, a variable mixing intensity should be considered by changing the design of the internals.

## References

- 
- i. B. Cross, D. Glatz, and T. Lightfoot, "Liquid-Liquid Extraction: Generating Equilibrium Data", *Chemical Engineering*, October 2018
  - ii. B. Cross, D. Glatz, and T. Lightfoot, "Pilot Plant Testing for Liquid-Liquid Extraction", *Chemical Engineering Progress*, February 2018
  - iii. R. Cusack, and P. Frameaux, "A Fresh Look at Liquid-Liquid Extraction, Inside the Extractor", *Chemical Engineering*, March 1991
  - iv. D. Glatz, T. Lightfoot, "Designing Columns for Fractional Liquid-Liquid Extraction", *AIChE National Meeting*, November 2010
  - v. R. Cusack, D. Glatz, and A. Karr, "A Fresh Look at Liquid-Liquid Extraction, Extraction Systems", *Chemical Engineering*, February 1991

## 8. Posters

# Electrical Separation Process for Biodiesel-Glycerol Product Mixture.

Ajalaya Boripun,<sup>a</sup> Rossarin Ampairojanawong,<sup>a</sup> Sayan Ruankon,<sup>b</sup> Thanapong Suwanasri,<sup>b</sup> Kraipat Cheenkachorn,<sup>c</sup> Andreas Pfennig,<sup>d</sup> and Tawiwan Kangsadan.<sup>\*a</sup>

Electroseparation technology has potential for the separation of multicomponent mixtures in wastewater treatment, the water separation from water-in-oil emulsion, the petroleum-demulsification and the recycling of waste. However, its application in the separation of biodiesel and glycerol has hardly been investigated. In this study, the electrical separation process with applied AC voltage was used to separate glycerol and other impurities from the biodiesel product mixture. AC was preferred due to its shorter separation time, high separation efficiency, effective energy consumption, and low corrosion rate of the electrodes. The transesterification reaction of refined palm oil with excess methanol in the presence of sodium methoxide was carried out at 60 °C. At the end of the reaction, the product mixture containing biodiesel, glycerol, methanol, residual catalyst, and unreacted reactants was transferred to the separation chamber. The separation process was then carried out at 60 °C, varying the applied voltages and the distances between the electrodes. The high voltage ranged from 1 to 9 kV, and the low voltage ranged from 72 to 168 V. The distance between the electrodes varied between 0.5 and 3 cm for the high voltage experiments and between 0.1 and 0.5 cm for the low voltage. An iron point-to-point electrode configuration was used because a non-uniform electric field distribution was produced, and the electric field strength was intensified near the electrode tips. The separation efficiency of 99.9% was achieved with an applied AC high voltage of 3 kV at a distance between the electrodes of 3 cm and with an applied AC low voltage of 168 V at a distance between the electrodes of 0.1 cm. The separation time to observe the clear interphase between biodiesel and glycerol phases was reduced from 2 h for gravity separation to 225 s for low voltage and further reduced to 40 s for high voltage. As the voltage increased, the electric potential between the electrodes increased and so did the surface charge of glycerol droplets. Under this high electric field strength, the dispersed glycerol droplets moved toward the point electrodes and aligned along the electrical field streamlines. As droplets approached each other, they merged to form larger droplets. These larger glycerol droplets easily settled to the bottom of the chamber due to gravity. The remaining catalyst was removed from the biodiesel via the settling glycerol droplets. Reducing the distance between the electrodes also increases the strength of the electric field. Therefore, the separation efficiency was directly proportional to the applied voltage and inversely proportional to the distance between the electrodes. The high voltage process completely removed the residual catalyst in the product mixture without further purification, usually realized by washing with warm water, but the soap content was still high (approximately less than 900 ppm). Therefore, three washing steps were required to reduce the soap content to less than 41 ppm. In contrast, the remaining catalyst and

---

<sup>a</sup> Chemical and Process Engineering Program, The Sirindhorn International Thai-German Graduate School of Engineering, King Mongkut's University of Technology North Bangkok, 1518 Pracharat 1 Road, Bangsue District, Bangkok, Thailand

<sup>b</sup> Electrical and Power Energy Engineering Program, The Sirindhorn International Thai-German Graduate School of Engineering, King Mongkut's University of Technology North Bangkok, 1518 Pracharat 1 Road, Bangsue District, Bangkok, Thailand

<sup>c</sup> Department of Chemical Engineering, Faculty of Engineering, King Mongkut's University of Technology North Bangkok, 1518 Pracharat 1 Road, Bangsue District, Bangkok, Thailand

<sup>d</sup> PEPs - Products, Environment, and Processes, Department of Chemical Engineering, University of Liège, Sart-Tilman, Quartier Agora, Allée du Six Août 11, 4000 Liège, Belgium

soap content were higher for the low-voltage process and required more washing steps. The final biodiesel product met all specifications of ASTM D6751 and EN 14214 standards.

**Keywords:** Electroseparation, High and Low Voltage, Biodiesel-Glycerol Mixture

## Introduction

Biodiesel is one of the renewable energy sources which is commercially produced by transesterification of triglycerides<sup>i</sup> and short-chain alcohol<sup>ii</sup> (e.g., methanol or ethanol) in the presence of homogenous alkali-catalysts at low temperature and pressure, allowing conversion up to 98%<sup>iii</sup>. After completion of the reaction, the main product, biodiesel, must be separated from other by-products using the conventional separation process such as the gravitational settling. However, the desired biodiesel product from this process is contaminated with impurities such as excess amounts of unreacted reactants (e.g., alcohol, catalyst, saturated or unsaturated glycerides) and glycerol. Because this process takes a long time (more than 24 h) to separate biodiesel from other products, the long settling time leads to a back reaction and thus a decrease in product yield. Additional process with hot water washing or acid washing is required to purify biodiesel to meet standard requirements. Water washing is a time-consuming process and uses substantial amounts of water, leading to controversy over wastewater treatment and environmental sustainability. In addition, the water wash must be followed by a high temperature evaporation process to remove the remaining water in the biodiesel phase, resulting in high capital and operating costs.

Biodiesel purification also involves neutralizing the biodiesel with acidified water to remove soap, free glycerin, and catalyst residues<sup>iv</sup>. This neutralization method can result in residual acid, and it is possible to obtain a total acid number higher than the EN 14214 limit<sup>v</sup>. This also leads to environmental problems in terms of wastewater generation. It is a challenge to find a separation process that is effective and less harmful to the environment.

## Background

Electro-separation technique has a potential in the separation of multicomponent mixture for various applications such as the wastewater treatment<sup>vi</sup>, the water separation from water-in-oil emulsion<sup>vii</sup>, the petroleum-demulsification<sup>viii</sup> and the recycling of waste<sup>ix</sup>. However, the application in the biodiesel-glycerol separation has been rarely investigated. In this study, the electrical separation process with applied AC voltages was utilized to separate glycerol and other contaminants from the biodiesel product mixture. AC was preferred due to shorter separation time, high removal efficiency as well as effective energy consumption, and low corrosion rate of electrodes.

## Theory

Under the influence of electric field, the small drops approach each other and eventually merge to form larger drops (coalescence)<sup>x</sup>. After that the larger drops have formed, they can easily settle and be precipitated by gravity at higher sedimentation rate. Increasing the electric field can also accelerate the coalescence rate and increase the speed of migration



droplets, which facilitates phase separation. Therefore, the application of electrical separation offers enormous potential for separating products, by-products, and impurities in the multi-component mixtures with less complexity and high separation performance due to the increase of coalescence rate, improvement of migration rate of droplets and shortening of the process.

The electrical separation technique can be operated by direct current (DC)<sup>xi</sup>, alternating current (AC)<sup>xii,xiii</sup> and the pulsed electric field (PEF)<sup>xiv</sup>. Although the DC mode is widely used for electrical separation processes such as electrocoagulation process and electrostatic phase separation, there are some disadvantages in terms of electrode passivation and corrosion. An impermeable oxide film or layer may form on the cathode electrode, while the corrosion layer on the anode is formed by the oxidation reaction. For this reason, the deposition efficiency decreases. These problems are impressively reduced by using the AC process. In the AC process, there is a continuous change in polarity and direction of electron flow between the negative and positive terminals, which reduces and avoids the formation of electrode passivation during the process and consequently extends the life of the sacrificed anode electrode. In addition, low voltage<sup>xii</sup> and high voltage<sup>xiii</sup> AC sources can be used. These depend on the electrical conductivity of chemical species in the solution. At high concentrations of dissolved ions, they are good conductors, suggesting that the electrical separation can be adequately operated with the low voltage. Otherwise, the AC high voltage would be more suitable.

The aim for this study was to design and investigate the optimum conditions of the electrical separation process by comparing between the applied AC low and high voltages for the separation of biodiesel mixture (refined palm oil as a raw material) from crude glycerol using the iron (Fe) electrode material with the vertical point-to-point electrode configuration. Separation efficiencies were obtained for varying electrical voltages (low and high) and vertical distance between electrodes (cm). The final biodiesel product was analyzed for the remaining soap and catalyst contents, the methyl ester content, and the quality according to EN14214 and ASTM D675 standards.

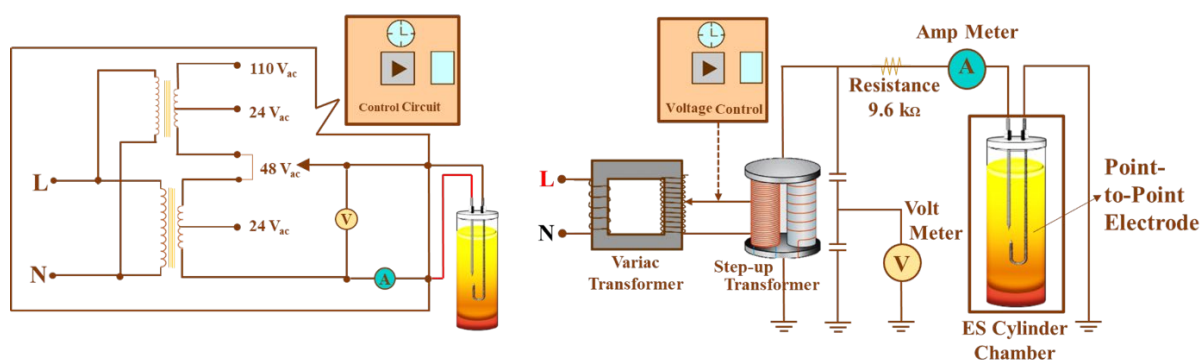
## Experimental

The experiment is divided into two parts: Biodiesel Production and Electrical Separation Process. In the biodiesel production, the transesterification reaction of refined palm oil with methanol in the presence of sodium methoxide as a homogeneous catalyst was carried out to produce high ester content of biodiesel. The reaction operated at the optimum conditions with a methanol to oil molar ratio of 6:1 and a catalyst concentration of 2.16 wt% of oil at the reaction temperature of 60°C for the reaction time of 1 h in a batch reactor with the stirrer speed of 480 rpm. At the end of the reaction, the product mixture containing biodiesel, glycerol, methanol, remaining catalyst, and unreacted reactants was transferred to the separation chamber. The product mixture of 785 mL was required for the separation process.

The electrical separation setup for the high voltage (Figure 1b) consists of a test separation chamber, an auto-transformer unit, and a control unit. An AC power source of 50 Hz and 220 V from the electrical system line in the laboratory was initially transmitted to the variable-ac-voltage transformer to adjust the AC power to the desired AC voltage. Then, a step-up

transformer was used to increase the voltage from the primary side (0-220 V) to the secondary side (0-100 kV). Finally, the desired high voltage (kV) was applied to the test chamber. The straight electrode was connected to the terminal of the high-voltage step-up transformer whereas the curve electrode was connected to the earthed terminal of the transformer. The current was measured and at the end of the separation, the current would be zero as no more conducting glycerol molecules dispersed in the mixture. In the test chamber, two different layers were observed at the end of separation: the upper layer of biodiesel phase (non-polar phase) and the bottom layer of glycerol-catalyst phase (polar phase). The electrical separation experiments were conducted in a Faraday cage for safety. For the applied AC low voltage (Figure 1a), the instrument set-up was mainly in a control box which consists of two transformers input 220 V<sub>AC</sub> Output 12 V<sub>AC</sub>; 1 A, and one transformer 220 V<sub>AC</sub> to 110 V<sub>AC</sub>; 100 W, Digital AC amp meter and voltmeter measurement, cable connector, and resistors.

The test chamber was made of glass with a PTFE Teflon lid to reduce interference and conduction. Iron electrodes (Fe) with sharp tips were used in the point-to-point electrode arrangement<sup>xiii</sup>. As presented in the previous study<sup>xiii</sup>, this point-to-point electrodes configuration can produce a non-uniform electric field distribution that generates strong electrical field strength near the electrode tips. The experiments were carried out by varying the high voltages of 1, 3, 5, 7, and 9 kV and the low voltages of 72, 96, 120, 144, and 168 V.



(a) ES Set-up with applied AC Low Voltage (LV) (b) ES Set-up with applied AC High Voltage (HV)

Figure 1. Electrical Separation Set-up

## Results and Discussion

Since the performance of the electrical separation process depends on the applied voltage and the distance between electrodes, the effect of these two parameters was investigated for the high voltage system and compared with the low voltage system. The separation efficiency and the separation time were evaluated, and the final biodiesel products were analyzed for the methyl ester content as well as the remaining catalyst and soap contents.

### I. Effect of Fe electrode configuration and vertical distance between electrodes on separation efficiency of electrical separation (ES) with applied AC high voltage and separation time

The highest separation efficiency of 99.9% was achieved with the point-to-point electrode configuration (Figure 2), as it generated the strongest electrical field strength compared to the other two electrode configurations. The experimental results were confirmed by the

simulation results of electric field intensity and magnetic field flux using Finite Element Method Magnetics (FEMM 4.2) as illustrated in Figure 3.

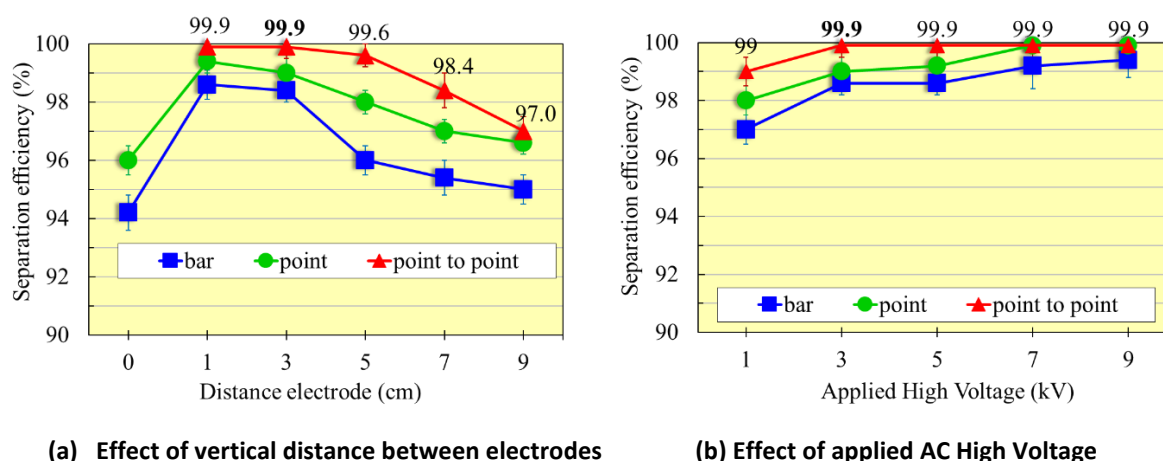


**Figure 2. Effect of Fe electrode configuration and vertical distance between electrodes on separation efficiency of ES with applied AC high voltage**

By applying an AC high voltage, a strong electric field strength was generated between two sharp-edged electrode tips, as shown in pink color (Figure 3). In addition, this point-to-point electrode configuration formed the non-uniform electrical field, as shown in curved lines. In contrast, a uniform electrical field was generated by the bar or point electrode configuration.

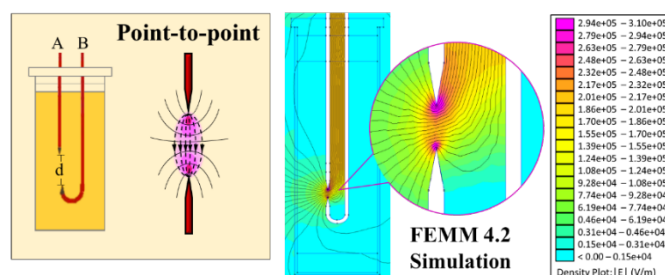


**Figure 3. Simulation results of electric field intensity and magnetic field flux for the point-to-point electrode configuration using Finite Element Method Magnetics (FEMM 4.2)**

Separation efficiency of 99.9% was achieved with an applied AC high voltage of 3 kV at a distance between the electrodes of 3 cm and with an applied AC low voltage of 168 V at a distance between the electrodes of 0.1 cm. The following chemical analysis performed at these optimal operating conditions. The separation time was significantly reduced by approx. 360 times with the applied AC high voltage and by approx. 20 times with the low voltage.

## II. Comparison of electrical separation (ES) with applied AC high voltage (AC-HV) and low voltage (AC-LV) with gravitational settling (GS) for remaining catalyst

All catalysts were completely removed from the biodiesel product by the shortest time of 240 s with the used of electrical separation with applied AC high voltage as shown in Figure 4a. This is a significant improvement over the gravitational settling (no electrical field), which required more than 24 h to completely remove all remaining catalyst. With applied AC low voltage, the removal efficiency for the remaining catalyst was still better than the gravitational settling, even though more than 1 h was required.

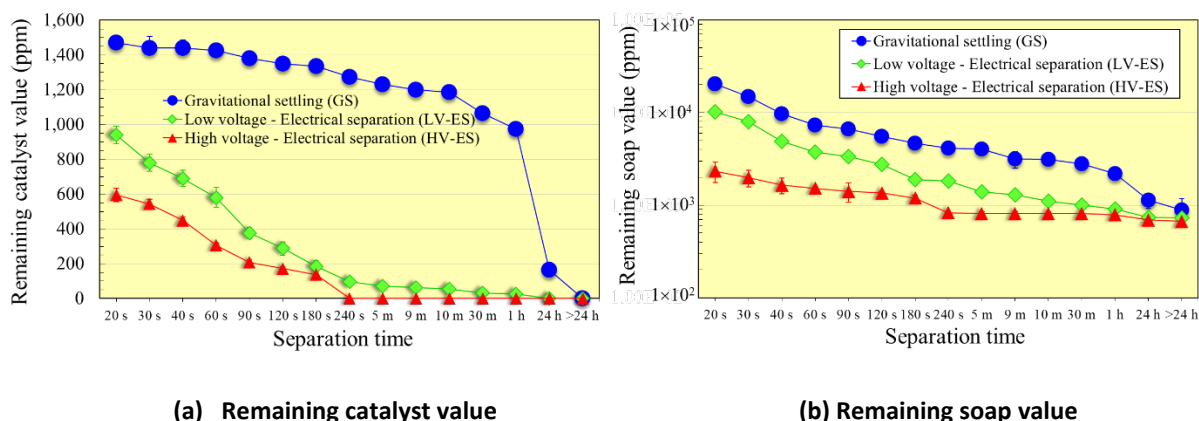


**Figure 4. Remaining catalyst and soap values in the biodiesel final product from the gravitational settling (GS) and the electrical separation (ES) with an applied AC high voltage of 3 kV at a distance between the electrodes of 3 cm (HV-ES) and with an applied AC low voltage of 168 V at a distance between the electrodes of 0.1 cm (LV-ES)**

### III. Comparison of electrical separation (ES) with applied AC high voltage (AC-HV) and low voltage (AC-LV) with gravitational settling (GS) for remaining soap

In addition, the remaining soap in the biodiesel final product was less than 900 ppm with the applied AC high voltage after the separation time of 240 s as shown in Figure 4b. However, according to the ASTM limit, the remaining soap in the biodiesel product must be less than 41 ppm. Therefore, a further purification process with warm water washing was necessary. The same removal efficiency was observed with the applied AC low voltage after the separation time of 1 h, while the gravitational settling required more than 24 h.

### IV. Content of the acylglycerols (TG, DG, and MG) and total glycerol in biodiesel product

After separation, the applied AC high voltage required only three times of washing to achieve an ester content higher than 96.5 wt% with the content of mono-, di-, tri-glycerides, free glycerol and total glycerol within the EN14105 limits. Gravitational settling (GS), on the other hand, required washing with water at least five times to achieve the same quality of final biodiesel product. Importantly, the soap content was less than 41 ppm (the standard limit). Figure 5 shows the diglyceride and total glycerol concentrations in the biodiesel final product.

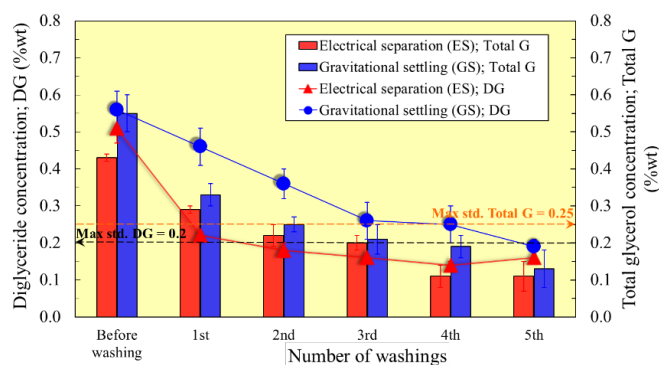


**Figure 5. Diglyceride (DG) and total glycerol (Total G) concentrations in the biodiesel final product from the gravitational settling (GS) and the electrical separation (ES) with an applied AC high voltage of 3 kV at a distance between the electrodes of 3 cm (HV-ES) before and after water washing process**

## Conclusions

This current research has demonstrated that the separation process with applied low and high electrical voltage performed better than gravitational settling (without applied electrical field) in separating glycerol and other impurities from biodiesel. As observed in the experiments, the glycerol droplets moved toward the electrode tips where the electrical field was generated, while the charge on the surface of the glycerol droplet changed. The more droplets were in the electrical field, these droplets would align along the streamlines and the coalescence of droplets were occurred. This phenomenon took place in a shorter time than the gravitational settling. Therefore, the electroseparation technology has potential to be applied to other multi-components and emulsion mixtures.

## References

- 
- <sup>i</sup> Fukuda, H., Kondo, A., & Noda H. (2001). Biodiesel fuel production by transesterification of oils. *Journal of Bioscience and Bioengineering*, 92(5), 405–416.
- <sup>ii</sup> Musa, I.A. (2016). The effects of alcohol to oil molar ratios and the type of alcohol on biodiesel production using transesterification process. *Egyptian Journal of Petroleum*, 25 (1), 21-31.
- <sup>iii</sup> Barnwal, B.K. and Sharma, M.P. (2005). Prospects of biodiesel production from vegetable oils in India. *Renewable and Sustainable Energy Reviews*, 9(4), 363-378.
- <sup>iv</sup> Mendow, G., & Querini, C. A. (2013). High performance purification process of methyl and ethyl esters produced by transesterification. *Chemical Engineering Journal*, 228, 93–101.
- <sup>v</sup> EN 14214, Liquid petroleum products - Fatty acid methyl esters (FAME) for use in diesel engines and heating applications - Requirements and test methods. European Committee for Standardization, Brussels, 2012
- <sup>vi</sup> Ehsani, H., Mehrdadi, N., Asadollahfardi, G., Bidhendi, G. N., & Azarian, G. (2020). A new combined electrocoagulation-electroflotation process for pretreatment of synthetic and real Moquette-manufacturing industry wastewater: Optimization of operating conditions. *Journal of Environmental Chemical Engineering*, 104263.
- <sup>vii</sup> Lee, H. S., Zheng, C., & Yang, B. (2018). Separation of Water-in-Oil Emulsions by Electrostatic Field at the Elevated Temperature. *Journal of Applied Mechanical Engineering*, 07(04).
- <sup>viii</sup> Noik, C., Chen, J., & Dalmazzone, C. S. H. (2006). Electrostatic Demulsification on Crude Oil: A State-of-the-Art Review. International Oil & Gas Conference and Exhibition in China.
- <sup>ix</sup> Eow, J. S., Ghadiri, M., Sharif, A. O., & Williams, T. J. (2001). Electrostatic enhancement of coalescence of water droplets in oil: a review of the current understanding. *Chemical Engineering Journal*, 84(3), 173–192.
- <sup>x</sup> Sadeghi, H. M., Sadri, B., Kazemi, M. A., & Jafari, M. (2018). Coalescence of charged droplets in outer fluids. *Journal of Colloid and Interface Science*, 532, 363–374.
- <sup>xi</sup> Kwon, W.-T., Park, K., Han, S. D., Yoon, S. M., Kim, J. Y., Bae, W., & Rhee, Y. W. (2010). Investigation of water separation from water-in-oil emulsion using electric field. *Journal of Industrial and Engineering Chemistry*, 16(5), 684–687.
- <sup>xii</sup> Sakkamas, W., Boripun, A., Ampairojanawong, R., Ruankon, S., Suwanasri, T., & Kangsadan, T. (2020). Electrocoagulation with AC Electrical Current at Low Voltage for Separation of Crude Glycerol from Biodiesel Product Mixture. *E3S Web of Conferences*, 141, 01011.
- <sup>xiii</sup> Ampairojanawong, R., Boripun, A., Ruankon, S., Suwanasri, T., & Kangsadan, T. (2020). Development of Purification Process Using Electrocoagulation Technique for Biodiesel Produced via Homogeneous Catalyzed Transesterification Process of Refined Palm Oil. *E3S Web of Conferences*, 141, 01010.
- <sup>xiv</sup> Guderjan, M., Elez-Martínez, P., & Knorr, D. (2007). Application of pulsed electric fields at oil yield and content of functional food ingredients at the production of rapeseed oil. *Innovative Food Science & Emerging Technologies*, 8(1), 55–62.